

Erweiterung der zellbasierten Calcium-Imaging-Methode im eukaryotischen zellfreien Proteinsynthese-System für die *transient-receptor-potential (TRP)*-Ionenkanäle

**Priyavathi Sureshkumar
(geb. Dhandapani)**



**zur Erlangung des akademischen
Degrees "doctor rerum naturalium"
(Dr. rer. nat.)
in der Wissenschaftsdisziplin "Molekulare Biologie"**

Dissertation

**eingereicht an der
Mathematisch-Naturwissenschaftlichen
Fakultät Institut für Institut für Biochemie
und Biologie der Universität Potsdam**

Tag und Ort der Disputation: 25.9.2023, Potsdam

This work is protected by copyright and/or related rights. You are free to use this work in any way that is permitted by the copyright and related rights legislation that applies to your use. For other uses you need to obtain permission from the rights-holder(s).
<https://rightsstatements.org/page/InC/1.0/?language=en>

Hauptbetreuer:

Prof. Dr. Frank Bier
AG Molekulare Bioanalytik und Bioelektronik
Universität Potsdam, Institut für Biochemie und
Biologie
Karl-Liebknecht-Straße 24/25, 14476 Potsdam (OT-Golm).

Betreuer:

1. Dr. Stefan Kubick, Abteilung -Zellfreie und Zellbasierte Bioproduktion, Fraunhofer-Institut für Zelltherapie und Immunologie, Institutsteil Bioanalytik und Bioprozesse IZI-BB, Am Mühlenberg 13, 14476 Potsdam.
2. Prof. Dr. Michael Bader, Max-Delbrück Center für Molekulare Medizin, Berlin - Buch Haus 31.1, Raum 1062.1 Robert-Rössle-Straße 10 13125 Berlin-Buch.
3. PD. Dr. Stefan Mergler, Charité - Universitätsmedizin Berlin, Campus Virchow-Klinikum- *Mittelallee 4, Experimentelle Ophthalmologie, Augustenburger Platz 1, 13353 Berlin.*

Gutachter:

1. Prof. Dr. Frank Bier
AG Molekulare Bioanalytik und Bioelektronik
Universität Potsdam, Institut für Biochemie und
Biologie
Karl-Liebknecht-Straße 24/25, 14476 Potsdam (OT-Golm), Germany
2. PD. Dr. Stefan Mergler, Charité - Universitätsmedizin Berlin, Campus Virchow-Klinikum- *Mittelallee 4, Experimentelle Ophthalmologie, Augustenburger Platz 1, 13353 Berlin.*
3. Prof. Dr. Otto Baumann, AG Mikroskopie,
Universität Potsdam, Institut für Biochemie und
Biologie Karl-Liebknecht-Str. 24-25, Haus 26, 14476
Potsdam.
4. Prof. Dr. Stephan Hinderlich,
Berliner Hochschule für Technik,
Fachbereich – *lifesciences and technology*, Labor Biochemie,
Forum Seestraße F528, Luxemburger Straße, 10, 13353, Berlin.

Online veröffentlicht auf dem
Publikationsserver der Universität Potsdam:
<https://doi.org/10.25932/publishup-61987>
<https://nbn-resolving.org/urn:nbn:de:kobv:517-opus4-619872>

Summary

Fluorescence calcium imaging is still used today used as the common method, mainly due to its cheaper costs for drug screening in pharmaceutical research encompassing both ion channels, and part of G-Protein Coupled Receptors (GPCRs) in the major share of drug targets. Eukaryotic cell-free protein translation overcomes several drawbacks that might occur for overexpression of these ion-permeable proteins in the cells such as cell toxicity, poor protein expression, and deletion due to modified protein domain and time-consuming cell line maintenance. Expressing ion channels in the cell-free protein synthesis platform for future drug screening processes is still ongoing basic research and so far, no calcium imaging technique for cell-free expressed ion channels is available. Taken together, the novel application of the fluorescence calcium imaging method in eukaryotic cell-free systems is a prerequisite for rapid pharmacological drug investigations, which are not feasible using conventional cell-based approaches. The aim of this thesis is to investigate the common calcium signaling pathways relevant to drug research via ion channels and GPCRs in cell-based systems. Thereby, the basic mechanism of the cell-based calcium imaging for chemical calcium indicators is studied and then translate its principle to the cell-free protein synthesis platforms. In order to study the cell-based calcium imaging and calcium pathways, two types of eye tumor cell-based models, namely benign pterygial tumor cells and malign uveal melanoma 92.1 cells were used. Specifically, the interplay between the natively expressed Transient Receptor Potential Channels (TRPs) like TRP-Vanilloid 1 (TRPV1) (Capsaicin receptor) and TRP-Melastatin 8 (TRPM8) (Menthol receptor) in these tumor cells was investigated by application of various drugs and hormones. The second aim of this thesis was to investigate the cell-based calcium mechanism of GPCRs. For this, overexpressed Mas, a GPCR and Angiotensin-(1-7) hormone receptor, from the Renin Angiotensin Aldosterone System (RAAS) in the Human Embryonic Kidney (HEK293) cells was used. Particularly, the activation of classical GPCR pathways like Phospholipase C and Proteinkinase C via Ang-(1-7) through Mas and the involvement of TRPs was proven in this study. The third aim of this thesis is to translate the cell-based calcium imaging principle to cell-free systems. Cell-based calcium imaging for chemical calcium indicators could be performed with all ease due to the presence of a large amount of cytosolic carboxylesterase, the crucial enzyme which handles the chemical calcium dyes. But this enzyme is absent in microsomes. Microsomes are used as a backbone membrane to integrate the synthesized ion channels in a eukaryotic cell-free system. Cell-free synthesized carboxylesterase in *Spodoptera frugiperda* (*Sf21*) microsomes is established as a viable calcium imaging tool to study both natively present ion permeable proteins and cell-free synthesized ion channels. The enzyme activity of the carboxylesterase in microsomes was confirmed by esterase assays and fluorescent calcium dye Fluo-5N Acetoxymethyl ester (Fluo-5N AM) loading assays. Fluorescent calcium imaging of natively present SERCA (Sarco Endoplasmic Reticulum Calcium ATPase) and ryanodine channels in the microsomes and cell-free expressed TRPV1 channel was demonstrated using Fluo-5N AM fluorescent dye in carboxylesterase pre-synthesized microsomes. With adequate research in future, the established method could be promisingly extended to study other cell-free expressed GPCRs or other ion channels like potassium, sodium, and chloride ion channels.

Zusammenfassung

Die Fluoreszenz-Calcium-Imaging-Methode wird auch heute noch als gängige Methode verwendet, vor allem wegen der geringeren Kosten für das Wirkstoffscreening in der pharmazeutischen Forschung, wobei Ionenkanäle sowie einige der G-Protein gekoppelte Rezeptoren (GPCRs) die Mehrzahl der Wirkstoffziele ansprechen. Die zellfreie Synthese eukaryotischer Proteine hat nicht die Nachteile, die bei der Überexpression dieser ionenpermeablen Proteine in Zellen auftreten können, wie z. B. Zelltoxizität, geringere Proteinexpression und die Beseitigung der exprimierten Proteine aufgrund veränderter Domänen sowie die zeitaufwändige Pflege von Zelllinien. Die Synthese von Ionenkanälen in zellfreien Proteinsyntheseplattformen für das künftige Wirkstoffscreening ist noch in der Grundlagenforschung. Obwohl die Fluoreszenz-Calcium-Imaging-Methode in zellbasierten Assays weit verbreitet ist, wurde diese Methode bisher noch nicht in zellfreien Proteinexpressionssystemen verwendet. Insgesamt ist die neue Anwendung der Calcium-Imaging-Methode in eukaryontischen zellfreien Systemen eine Voraussetzung für die schnelle pharmakologische Analyse von Wirkstoffen. Das erste Ziel dieser wissenschaftlichen Arbeit bestand darin, die grundlegenden Prinzipien der Calcium-Imaging-Methode zur Untersuchung von Ionenkanälen in zellbasierten Systemen zu untersuchen. Hierfür wurden zwei Tumorzelllinien des Auges verwendet, und zwar benigne Pterygiumzellen und maligne Aderhautmelanom 92.1 Zellen. In diesen Studien wurde die Interaktion zwischen den nativ überexprimierten *transient-receptor-potential-Ionenkanälen* (TRPs) wie TRP Vanilliod 1 (TRPV1) (Capsaicinrezeptor) und TRP Melastatin 8 (TRPM8) (Mentholrezeptor) in diesen Tumorzellen nach Zugabe von verschiedenen Medikamenten und Hormonen untersucht. Das zweite Ziel dieser Arbeit war es, den Calcium-Mechanismus von GPCRs in den Zellen zu untersuchen. Zu diesem Zweck wurde Mas, ein GPCR und Angiotensin (1-7)-Hormonrezeptor, aus dem *renin-angiotensin-aldosteron-system* (RAAS) in der *Human Embryonic Kidney-293* (HEK293) Zelllinie überexprimiert. In dieser Studie wurden insbesondere die Aktivierung klassischer GPCR-Signalwege wie Phospholipase C und Proteinkinase C durch Angiotensin-(1-7) über Mas und die Beteiligung von TRP-Kanälen nachgewiesen. Die zellbasierte-Calcium-Imaging-Methode für chemische Calcium-Indikatoren ließ sich aufgrund der Anwesenheit einer großen Menge cytosolischer Carboxylesterasen gut anwenden. Carboxylesterase ist das wichtigste Enzym in der Calcium Imaging Methode, das die Verarbeitung chemischen Calcium-Farbstoffe behandelt. Dieses Enzym fehlt jedoch in Mikrosomen, die als Basismembran für die Integration synthetisierter Ionenkanäle in eukaryontischen zellfreien Systemen verwendet werden. Das dritte Ziel dieser Forschungsarbeit war die Umsetzung der zellbasierten Calcium-Imaging Methode und der Calcium-Signalwege in zellfreie Systeme. Hier wurde die zellfrei synthetisierte Carboxylesterase in Mikrosomen von *Spodoptera frugiperda* (*Sf21*) als praktikables Calcium-Imaging-Werkzeug etabliert, um sowohl native ionenpermeable Proteine als auch zellfrei-synthetisierte Ionenkanäle zu untersuchen. Die Enzymaktivität der zellfrei-synthetisierten Carboxylesterase in Mikrosomen wurde durch Esterase-Assays und den Calcium-Fluoreszenzfarbstoff Fluo-5N Acetoxymethylester (Fluo-5N AM) Belastungstests nachgewiesen. Das Calcium-Imaging der nativ vorhandenen Ca^{2+} -ATPase des sarkoplasmatischen/endoplasmatischen Retikulums (SERCA) und der Ryanodin-Rezeptoren (RyR) in den Mikrosomen sowie der zell-frei exprimierten TRP-Ionenkanäle wurden mit dem Fura-5N-AM- Fluoreszenzfarbstoff in mit Carboxylesterase vorsynthetisierten Mikrosomen nachgewiesen.

Zusammenfassend lässt sich sagen, dass das Prinzip der zellbasierten Calcium-Imaging -Methode vielversprechend an das eukaryotische zellfreie *Sf21*-System angepasst werden konnte, um Ionenkanäle zu analysieren. Nach entsprechender Forschung könnte die etablierte Methode in Zukunft auch auf andere Membranproteine ausgeweitet werden. Dies umfasst die Untersuchung anderer zellfrei exprimierte GPCRs oder anderer Ionenkanäle wie Kalium-, Natrium- und Chlorid-Ionenkanäle.

Bestandteile der publikationsbasierten These

1. **Priyavathi Dhandapani**, Srujan Kumar Dondapati, Anne Zemella, Dennis Bräuer, Doreen Anja Wüstenhagen, Stefan Mergler and Stefan Kubick, Targeted Esterase induced Dye loading (TED) supports direct calcium imaging in eukaryotic Cell-Free systems, *Royal Society of Chemistry, Advances*, (2021), **11**, 16285-16296, Doi: 10.1039/d0ra08397f.
Zustand: **Veröffentlicht** durch peer-review Prozess
Beiträge: Die Experimente habe ich geplant und den überwiegenden Teil des Projekts besonders in Calcium-Imaging-Bereich selbst durchgeführt. Ich habe auch den ersten Entwurf des Manuskripts selbst geschrieben und es weiter während der ersten und zweiten Revision im Review Prozess überarbeitet. - 45% vom Dissertationsinhalt
2. **Priyavathi Sureshkumar**, Robson Augusto Souza Dos Santos, Natalia Alenina, Stefan Mergler, und Michael Bader. „Angiotensin-(1-7) Mediated Calcium Signalling by MAS“, *Peptides* 165 (Juli 2023): 171010, Doi: 10.1016/j.peptides.2023.171010.
Zustand: **Veröffentlicht** durch peer-review Prozess
Beiträge: Ich habe teilweise die Experimente geplant und alle Experimente selbst durchgeführt. Den ersten Entwurf des Manuskripts habe ich selbst skizziert und es weiter während der Revision in Review Prozess überarbeitet. - 35% von Dissertation Inhalt
3. Lia Walcher, Clara Budde, Arina Böhm, Peter S. Reinach, **Priyavathi Dhandapani**, Nina Ljubojevic, Markus W. Schweiger, Henriette von der Waydbrink, Ilka Reimers, Josef Köhrle, Stefan Mergler, TRPM8 Activation via 3-Iodothyronamine Blunts VEGF-Induced Transactivation of TRPV1 in Human Uveal Melanoma Cells. *Frontiers in Pharmacology*, (2018) 9:1234, Doi:10.3389/fphar.2018.01234.
Zustand: **Veröffentlicht** durch peer-review Prozess
Beiträge: Die Calcium-Imaging-Experimente habe ich selbst teilweise durchgeführt.– 10 % von Dissertation Inhalt
4. Fabian Garreis, Antje Schröder, Peter S. Reinach, Stefanie Zoll, Noushafarin Khajavi, **Priyavathi Dhandapani**, Alexander Lucius, Uwe Pleyer, Friedrich Paulsen, Stefan Mergler, 3-Iodothyronamine increases transient receptor potential melastatin channel 8 (TRPM8) activity in immortalized human corneal epithelial cells. *Cellular Signaling* (2016) vol. 28 (3) p. 136 -147, Doi: 10.1016/j.cellsig.2015.12.005.
Zustand: **Veröffentlicht** durch peer-review Prozess
Beiträge: Einige Calcium Experimente habe ich für dieses Projekt durchgeführt. Dieses Projekt hat mich gut vorbereitet weiter im Calcium-Imaging-Bereich zu arbeiten – 10% von Dissertation Inhalt.

Inhaltsverzeichnis

Summary	iii
Zusammenfassung	iv
Bestandteile der Publikation basierte Dissertation	vi
Inhaltsverzeichnis	vii
Abkürzungsverzeichnis.....	ix
1 Einleitung	1
1.1 Grundlagen	1
1.1.1 Zell-basiertes Calcium-Imaging	1
1.1.2 Zelfreie Proteinsynthese	4
1.2 Calcium-Imaging der <i>transient-receptor-potential</i> (TRP)-Ionenkanäle in den Augentumorzellen	6
1.3 Calcium-Imaging im zellbasierten Überexpressionssystem von Mas, ein Ang-(1-7)-Rezeptor	7
1.4 Calcium-Imaging-Methode im eukaryotischen zelfreien Proteinsynthese-System	8
1.4.1 Grund der Etablierung der Methode	8
1.4.2 Hypothese der neuen Methode	9
2 Manuskriptkompendium.....	13
2.1 Manuskript I	
Targeted Esterase induced Dye loading (TED) supports direct calcium imaging in eukaryotic Cell-Free systems	14
2.2 Maunskript II	
Ang-(1-7) mediated calcium regulation of Mas	41
2.3 Manuskript III	
TRPM8 Activation via 3-Iodothyronamine Blunts VEGF-Induced Transactivation of TRPV1 in Human Uveal Melanoma Cells	52
2.4 Manuskript IV	
Upregulation of Transient Receptor Potential Vanilloid Type-1 Channel Activity and Ca ²⁺ Influx Dysfunction in Human Pterygial Cells	71

3 Diskussion.....	86
3.1 Calcium-Imaging der transient-receptor-potential (TRP)-Ionenkanäle in den Augentumorzellen	86
3.2 Calcium-Imaging im zellbasierten Überexpressionssystem von Mas, ein Ang-(1-7) -Rezeptor	87
3.3 Etablierung der Calcium-Imaging-Methode in einem eukaryotischen zellfreien Proteinsynthese-System.	88
4 Referenzen.....	97
5 Danksagung.....	102
6 Publikationsliste.....	104
7 Eidesstattliche Erklärung	106

Abkürzungsverzeichnis

3-T1AM.....	3-iodothyronamine
AM.....	Acetoxymethylester-Gruppe
AngII.....	Angiotensin II
Ang-(1-7).....	Angiotensin 1-7 Peptid
AT1-Rezeptor.....	Angiotensin II-Rezeptor, Typ I
AT2-Rezeptor.....	Angiotensin II-Rezeptor, Typ II
ATP.....	Adenosintriphosphat
CAP.....	Capsaicin
CB1.....	Cannabinoid-Rezeptor1
CPZ.....	Capsazepin
CrpV-IRES.....	Cricket-Paralysis-Virus- interne ribosomale Eintrittsstelle
DMEM.....	<i>dulbecco's-modified-eagle's-medium</i>
DTT.....	Dithiothreitol
EGTA.....	Ethylene glycol-bis(β-aminoethyl ether)-N,N,N',N'-tetraacetic acid
ER.....	endoplasmatisches Retikulum
Fluo-5N AM.....	Fluo-5N AM Acetoxyethyl ester
fura 2/AM.....	fura 2-Acetoxyethyl-Ester
GPCR.....	G-Protein kuppelte Protein Rezeptor
HBSS.....	Hanks-balancierte Salzlösung
HEK293-Zellen.....	<i>human-embryonic-kidney 293-Zellen</i>
HEPES.....	2-[4-(2-hydroxyethyl)piperazin-1-yl]ethanesulfonic acid
IP3.....	Inositol-1,4,5-trisphosphat
CECF-Modus.....	<i>continuous-exchange-cell-free-Modus</i>
<i>m</i> CES2.....	maus-Carboxylesterase-2
MRGPR.....	Mas-verwandten G-Protein-gekoppelten Rezeptoren
NPFF.....	Neuropeptid FF
NTC	<i>no-template-control</i>
PKC.....	Proteinkinase C
PLC.....	Phospholipase C
PNPA.....	4-para-Nitrophenylacetat

RAAS.....	<i>renin-angiotensin-aldosterone-system</i>
RPMI-Medium.....	<i>rosewell-park-memorial-institute-Medium</i>
SDS-PAGE-Gel.....	<i>Sodium Dodecyl Sulfate PolyAcrylamide gel</i>
SERCA.....	Sarkoplasmatisches /Endoplasmatisches Retikulum Ca^{2+} - ATPase
<i>Sf21</i>	<i>Spodoptera frugiperda 21</i>
TAAR1.....	<i>trace-amine-associated-receptor-1</i>
TAAR2.....	<i>trace-amine-associated-receptor 2</i>
TRP-Ionenkanäle.....	<i>transient-receptor-potential-Ionenkanäle</i>
TRPA1.....	TRP-Ionenkanal, Unterfamilie-Ankyrin, Subtyp 1
TRPC3.....	TRP-Ionenkanal, Unterfamilie- kanonischer Rezeptor, Subtyp 1
TRPM8.....	TRP-Ionenkanal, Unterfamilie-Melastatin,Subtyp 8
TRPV1.....	TRP-Ionenkanal, Unterfamilie-Vanilloid, Subtyp 1
TRPV3.....	TRP-Ionenkanal, Unterfamilie-Vanilloid, Subtyp 3
VEGF.....	vasculare endotheliale Wachstumfaktor

1. Einleitung

1.1. Grundlagen

1.1.1. Zell-basiertes Calcium-Imaging

Calcium (Ca^{2+}) ist ein wichtiger Botenstoff, der viele zelluläre Aktivitäten reguliert, zum Beispiel, Befruchtung, Sekretion, Neurotransmission und Zellmigration, Zellwachstum, Hormonausschüttungen, Zelldifferenzierung, Apoptose, Genexpression, Zellmotilität, Zelladhäsion. Calcium ist allgegenwärtig und ein äußerst wichtiges intrazelluläres Signalmolekül. Die Calciumsignalwege werden durch Calciumionen gesteuert. Ca^{2+} kann aus intrazellulären Speichern freigesetzt werden oder über Ca^{2+} permeable Ionenkanäle an der Plasmamembran in die Zelle gelangen. Ca^{2+} ist historisch als sekundärer Botenstoff beschrieben, weil seine Erhöhung in dem Zytoplasma von den extrazellulären Signalen oder primären Botenstoffen abhängig ist ([Carofoli et al., 2002](#)).

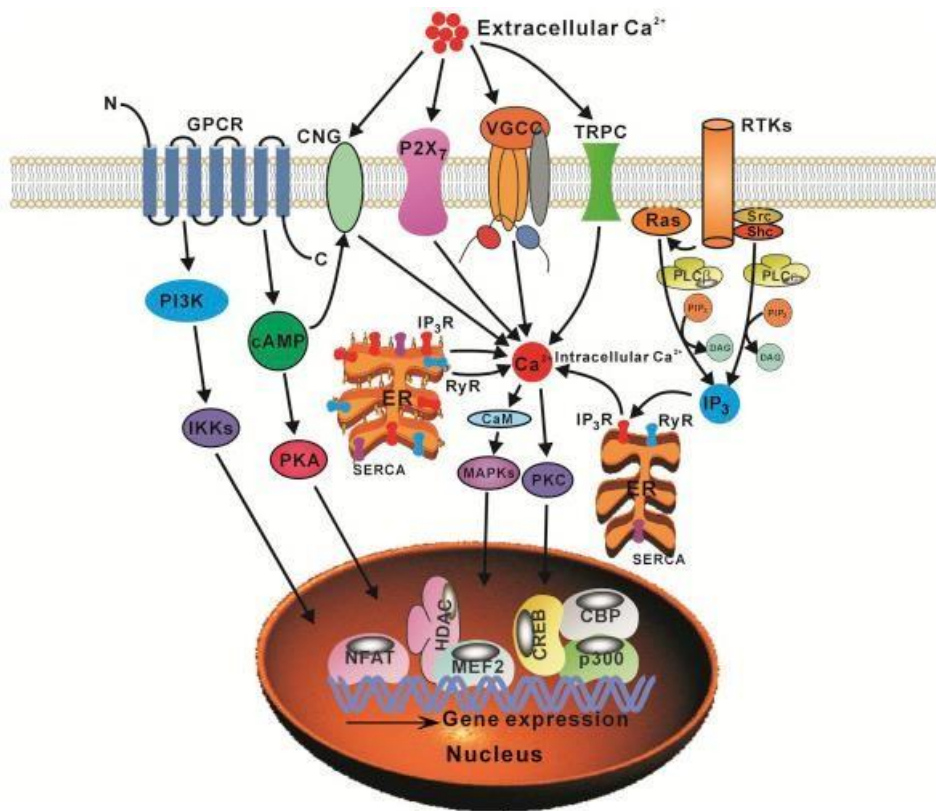


Abbildung 1: Calcium als Sekundärbotenstoff in den Zellphysiologie, [Song al., 2015](#) (mit Genehmigung von Elsevier). Extrazelluläres Ca^{2+} wird durch *transient-receptor-potential*-Ionenkanäle (als TRPC in der Abbildung bezeichnet), Spannungsgesteuerte Ionen Kanäle und zyklische Nukleotid-gesteuerte Kanäle (als CNG bezeichnet) und Purinerge Rezeptorionen Kanäle in den intrazellulären Raum gebracht. G-Protein gekoppelte Rezeptoren (GPCRs) und Rezeptortyrosinkinasen (RTKs) können auch, wenn sie durch ihre Aktivatoren gesteuert werden, das intrazelluläre Calcium durch Freisetzung aus dem Endoplasmatisches-Retikulum erhöhen.

Zu den Ca^{2+} -permeablen Proteinen gehören Ionenkanäle, Pumpen und Transporterproteine. Die Ionenkanäle von der Plasmamembran sind die am häufigsten untersuchten ionendurchlässigen Proteine ([Abbildung 1](#)). Die Ca^{2+} -permeablen Ionenkanäle werden je nach ihren Eigenschaften wie Ionenspezifität, Liganden Empfindlichkeit und Spannungsempfindlichkeit in verschiedene Untergruppen eingeteilt. Nach Ionenspezifität werden Ionenkanäle als Natrium-Ionenkanäle, Calcium-Ionenkanäle und Kalium-Ionenkanäle oder Chlorid-Ionenkanäle benannt. *Transient-receptor-potential*-Ionenkanäle sind nicht-selektive Kationenkanäle. Diese sind für Kaliumionen, Natriumionen und Calciumionen permeabel.

Auch zwischen den GPCRs und den *transient-receptor-potential* (TRP)-Ionenkanälen besteht eine Wechselwirkung, die zur Erhöhung des intrazellulären Calciumspiegels führt. Die Achse GPCR -TRP-Ionenkanäle wurde auf dem Gebiet der Schmerz- und Entzündungsforschung eingehend beschrieben. GPCRs können die direkte Aktivierung oder Sensibilisierung von TRP-Ionenkanälen über verschiedene Proteinkinasen oder Phospholipase C (PLC) steuern ([Veldhuis et al., 2015](#)).

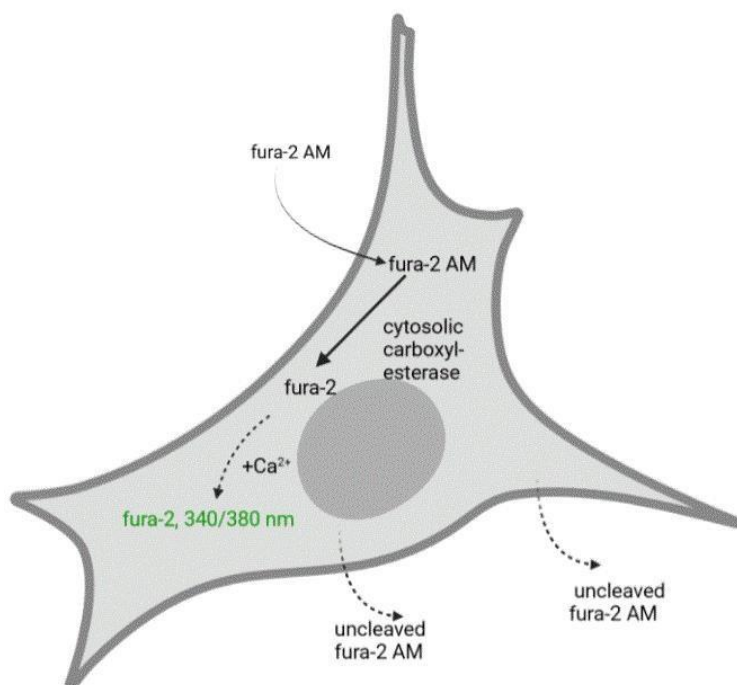


Abbildung 2: Vereinfachtes Schema einer Calciumindikator Beladung einer Zelle: Während der fura-2 AM Beladung wird die AM Gruppe von fura-2-AM durch zytologische Carboxylesterase gespalten. Nach der Spaltung bleibt der Calciumindikator in den Zellen, weil er die Zellmembran nicht durchqueren kann (mit Biorender Software gezeichnet von Autorin)

Fluoreszenzfarbstoffe für das Calcium-Imaging wurden in den 1980er Jahren entwickelt und werden seither verwendet ([Zhou et al., 2021](#)). Die Entdeckung einer neuen Reihe von Calciumindikatoren auf Fluoreszenzbasis durch das Labor des Nobelpreisträgers Roger Y. Tsien hat das Forschungsfeld der Calciumregulation und der damit verbundenen Ca^{2+} -leitenden Ionenkanäle revolutioniert. Seither ist Calcium-Imaging die am häufigsten verwendete Technik zur Messung von sehr kleiner Messung von sehr kleinen Calciumkonzentrationsänderungen in den Zellen ([Grynkiewicz et al., 1985](#)) ([Tsien et al., 1981](#)).

Für das High-throughput Screening von Arzneimitteln für Ionenkanäle und GPCRs ist die Calcium-Imaging-Methode ein äußerst kosteneffizienter Funktionstest. Insbesondere wird das Mikroplatten-basierte Calcium-Imaging für das Wirkstoffscreening im Großmaßstab eingesetzt. Elektrophysiologische Methoden wie die planare Bilayer-Methode oder das planare Patch-Clamping sind für solche Anwendungen hingegen kostspieliger ([Garcia und Kaczorowski et al., 2016](#)). Später wurde das Fluoreszenz-Imaging auch für andere Ionen wie Chlorid, Kalium und Natrium Ionen eingeführt. Zum Beispiel, Asante Natrium Grün-2 (ANG-2), ein Fluoreszenz-basierter Natriumindikator ([McManus et al., 2012](#)). Es gibt zwei Hauptklassen von Calciumindikatoren: Chemische Calciumindikatoren ([Parades et al., 2008](#)) und genetisch kodierte Calciumindikatoren ([Tang et al., 2020](#)). Aufgrund der erforderlichen Transfektion-Schritte und Proteinexpression-Schrittes von Calciumindikatoren in den Zellen sind die genetisch kodierten Calciumindikatoren zeitaufwendig. Calcium-sensitive Fluoreszenzfarbstoffe sind für die Messung der intrazellulären Calciumkonzentration wegen ihrer einfachen Anwendung gut geeignet. Die chemische Calciumindikatoren wie Fura-2-AM hat zwei spezifische Absorptionswellenlängen (340 und 380 nm).

Beladung von Zellen mit Fluoreszenzfarbstoff (AM) Estern:

Chemische Calciumindikatoren allein können aufgrund ihrer polaren Eigenschaften die Lipidmembran nicht durchqueren. Die meisten hydrophoben Calciumindikatoren tragen eine Negativladung wegen der Carboxylgruppe. Eine chemische Veränderung mit der sogenannten Acetoxymethylester-Gruppe (AM-Gruppe) ist erforderlich. Diese Negativladung in der Carboxylgruppe wird durch AM-Ester maskiert. Mit der maskierten negativen Ladung kann der Calcium-Indikator die Zellmembran ungehindert durchqueren. Daher werden anstelle des Fluoreszenzfarbstoffsalzes ausschließlich Fluoreszenzfarbstoffester (mit der AM-Gruppe) für Zellen verwendet. Kommerziell erhältliche Calciumindikatoren haben in der Regel die AM-Gruppe. (z.B. fura-2/AM, Calcein/AM).

Die zytosolische Carboxylesterase spaltet die AM-Gruppe des Calciumindikators ab, wodurch der Calciumindikator seine negative Ladung erhält. Da der gespaltene Calcium-Indikator negativ geladen ist, kann er nicht nach außen in den extrazellulären Raum gelangen und bleibt daher im Zytosol. Auf diese Weise werden die Calciumindikatoren in die Zellen eingebracht. Ein Schema dieses Prozesses ist in der [Abbildung 2](#) dargestellt.

Während der Beladung von Calcium-Indikatoren ist eine vollständige Hydrolyse der Acetoxyethyl-Estergruppe durch Carboxylesterase wichtig. Falls die Esterhydrolyse nicht vollständig abgeschlossen ist, gibt es eine Mischung aus Calcium-Indikator ohne AM-Gruppe (frei und an Calcium gebunden) und Calcium-Indikator mit AM-Gruppe (frei und calciumgebundene Formen). Das Farbmittel mit AM- Gruppe kann allein bereits fluoreszierend sein. Zum Beispiel kann der beladene Fluo-5N AM in den Mikrosomen auch fluoreszieren, weil er bereits calciumunempfindlich ist. Bei einer unvollständigen Hydrolyse des Calciumindikators kann das Calciumfluoreszenzsignal während der Messung schwächer werden. Der Grund dafür ist der Transport von den nicht hydrolysierten Calciuminduktoren durch die Membran während der Messung. Auch bei einer vollständigen Hydrolyse des Calciumindikators kann das Calciumfluoreszenzsignal während der

Messung aus anderen Gründen, wie z.B. durch die Photobleichung abnehmen.

1.1.2. Zellfreie Proteinsynthese

Die zellfreie Proteinsynthese ist eine Technik, mit der man rekombinante Proteine synthetisieren kann. Die Entdeckung und Erforschung der zellfreien Proteinsynthese begann in den 1960er Jahren. Zellfreie Proteinsynthesen sind in zwei Arten unterteilt, und zwar in prokaryotische und eukaryotische-zellfreie Proteinsynthese. Die prokaryotische zellfreie Proteinsynthese ist seit mehreren Jahrzehnten weitgehend erforscht und gut fortgeschritten. Das am häufigsten verwendete prokaryotische Lysat für die zellfreie Proteinsynthese rekombinanter Proteine stammt aus dem *Escherichia coli*-Stamm BL21 (DE3). Das *E. coli* BL21 (DE3)-Lysat wird bereits von mehreren Unternehmen als zuverlässiges Proteinsyntheseprodukt auf dem Markt angeboten. Demgegenüber ist die eukaryotische zellfreie Proteinsynthese noch in Forschung und Entwicklung. Die zellbasierte Proteinproduktion hat mehrere Nachteile. Dazu gehören die geringere Transfektionseffizienz, die geringe Durchführbarkeit von Genveränderungen und die daraus resultierende Toxizität in den Zellen mit hoher Proteinexpression. Genveränderungen in den zellfreien Systemen sind im Vergleich zu den zellbasierten Proteinexpressionsplattformen viel einfacher. Die zellbasierte Proteinsynthese unterscheidet sich in vielerlei Hinsicht von der zellfreien Proteinsynthese, wobei letztere mehrere Vorteile hat wie schnellere Proteinsynthese, Herstellbarkeit von Toxinen oder virusartigen Partikeln, Herstellung von Membranproteinen ohne Zelltoxizität und Nebenwirkungen, erleichterte Einführung von nicht-kanonischen Aminosäuren sowie orthogonale Aminosäure-Modifikation der synthetisierten Proteine und höhere Flexibilität für genetische Veränderungen. ([Khambati et al., 2019](#)).

In der eukaryotischen zellfreien Proteinsynthese gibt es zwei verschiedene Synthesemethoden. Diese sind folgende:

- Batchmodus
- Dialysemodus

Batch-Modus: Die Reaktion im Batch-Modus wird in 1,5-mL-Reaktionsgefäßchen durchgeführt. Diese Form der Synthese benötigt durchschnittlich 30 bis 180 Minuten Inkubationszeit. Bei der Proteinsynthese im Batch-Modus entstehen viele toxische Nebenprodukte. Diese Nebenprodukte können die zellfreie Proteinsynthese hemmen. Daher ist die Batch-Synthese für eine kürzere Reaktionszeit geeignet. Der Batch-Modus bei der eukaryotischen zellfreien Proteinsynthese besteht aus den folgenden Komponenten: Lysat eukaryotischer Zellen (aus lysierten Zellen ohne hochdichte Membranphase, z. B. Zellkern, Mitochondrien und plasmatische Phase der Membranen), Template-DNA für die Transkription, RNA-Nukleotide, proteinbildenden Aminosäuren, Energiekomponenten, wie., Adenosintriphosphat (ATP), Pufferkomponenten (z. B. HEPES-KOH), Mg (OAc), Spermidin und andere zusätzliche Komponenten. Diese sind z. B. Poly-G-Nukleotide (30 Aminosäuren lang) in Fällen, in denen die *cricket-paralysis-virus*-interne ribosomale Eintrittsstelle (CrPV-IRES) die Protein-Translation initiiert ([Brödel et al., 2013](#)). Um das Problem der geringen Proteinausbeute im Batch-Modus zu lösen, wird eine repetitive Batch-Synthese durchgeführt. Die repetitive Batch-Synthese besteht aus dreimal wiederholten Batch-Syntheseschritten. Die Mikrosomen aus der ersten Synthesereaktion werden in den nächsten Synthesereaktionsschritten weiterverwendet. Bei den

nächsten Synthesereaktionen wird nur der lösliche Teil des neuen Lysats zugegeben. Auf diese Weise werden die Mikrosomen mit synthetisierten Proteinen angereichert, um die Proteinausbeute zu erhöhen.

Dialyse-Modus: Der Dialyse-Modus beziehungsweise *continuous-exchange-cell-free* (CECF)-Modus enthält ein Zweikammersystem ([Abbildung 3](#)). In der kleineren Reaktionskammer wird die Synthese der Proteine durchgeführt. In diese Kammer werden alle Reaktionskomponenten, die in der Batchsynthese verwendet wurden, pipettiert. In der größeren Kammer bzw. der Feedkammer werden Energiekomponenten (ATP), Aminosäuren und Pufferkomponenten pipettiert. Die beiden Kammern sind durch eine Dialysemembran getrennt, die für Proteine und Komponenten bis zu 10 kDa durchlässig ist. Diese Dialysemembran ist für die Energiekomponenten (ATP), Aminosäuren aus der Feedkammer und die giftigen Nebenprodukte aus der Reaktionskammer permeabel. Daher sind die inhibierenden giftigen Nebenprodukte während der zellfreien Synthese durch selektive Diffusion von der Hauptreaktion entfernt.

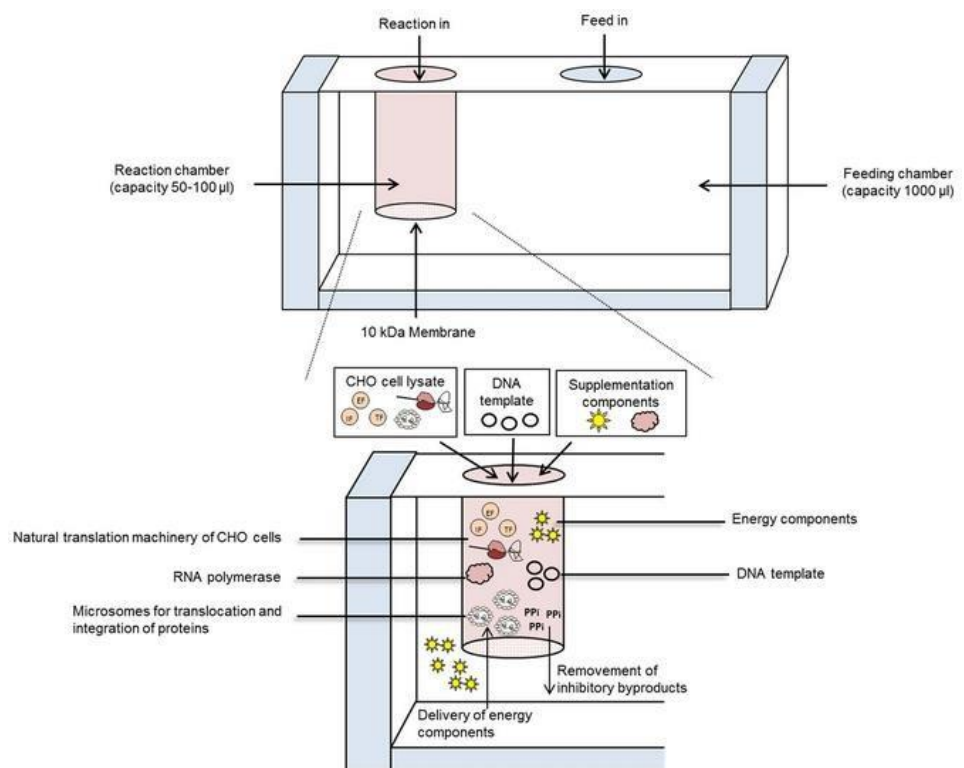


Abbildung 3: Schematische Darstellung vom Dialyse-Modus der eukaryotischen Proteinsynthese, ([Thoring et al., 2017](#)): Oben wird der Dialyse-Modus in einem Reaktionsgefäß mit zwei Kammern dargestellt. Die verschiedenen Reaktionskomponenten, die in den beiden Kammern zugegeben werden, sind unten aufgelistet.

Die zellfreie Proteinsynthese wird als 24- bis 48-stündige Inkubationsreaktion durchgeführt. Außerdem wird für jede eukaryotische zellfreie Proteinsynthese in beiden Kammern ein angepasster Caspase- Inhibitor ergänzt. Caspase-Inhibitoren können die Ausbeute der synthetisierten Proteine erhöhen, da sie vermutlich den Proteinabbau hemmen ([Stech et al., 2014](#)). Um das Bakterienwachstum während der längeren Inkubationszeiten zu hemmen, wurde Natriumazid in beiden Kammern in einer Endkonzentration von 0,02 % zugesetzt.

1.2. Calcium-Imaging der transient-receptor-potential-Ionenkanäle (TRPs) in den Augentumorzellen

Transient-receptor-potential-Ionenkanäle (TRPs) sind in eukaryotischen Zellen ubiquitär vorhanden. Tumorzellen weisen im Vergleich zu gesunden Zellen eine höhere Expression von TRPs auf. Zum Beispiel ist TRP-Ionenkanal, Unterfamilie-Melastatin, Subtyp 8 (TRPM8) in Prostatakarzinomen stark erhöht. Und TRP-Ionenkanal, Unterfamilie-Vanilloid Subtyp 1 (TRPV1) ist ein prognostischer Marker für Metastasen und Entzündungen bei verschiedenen Tumorerkrankungen. Daher ist es sinnvoll, zu untersuchen, ob die oben genannten Ionenkanäle in Augentumorzellen funktionell hochreguliert sind oder nicht.

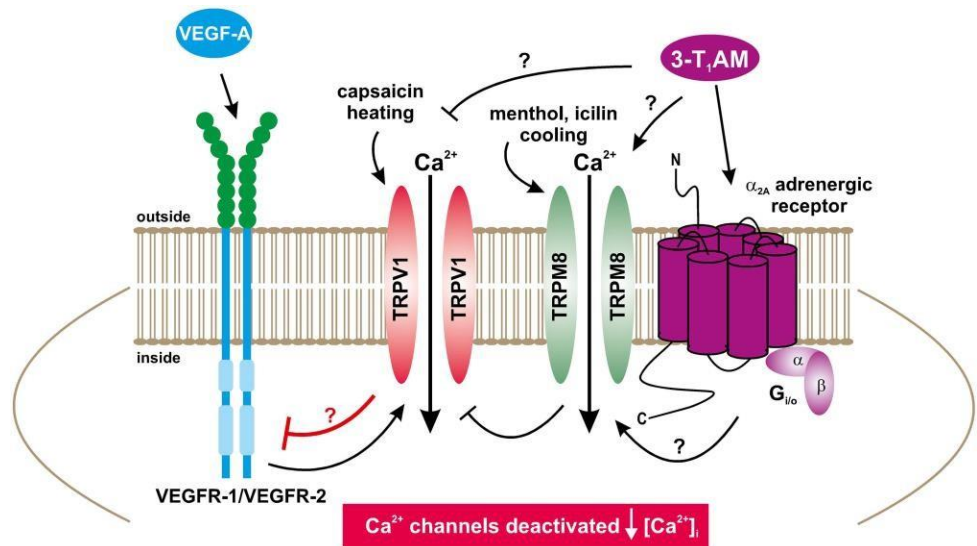


Abbildung 4: Vorgeschlagene Signaltransduktionswege zwischen VEGF und 3T₁AM ([Walcher und Budde et al., 2017](#)). VEGF-A aktiviert TRPV1 durch VEGF-Rezeptor-1/2 und 3-T1AM aktiviert TRPM8 durch Adrenozeptor. 3-T1AM hemmt die Erhöhung des intrazellulären Calciums, die durch VEGF-A verursacht wird.

Das Aderhautmelanom ist einer der häufigsten Augentumore. Ziel dieser Untersuchung ist es, Interaktionsstudien von verschiedenen Hormonen und deren Auswirkung auf das Zusammenspiel zwischen dem Thermorezeptor (TRPV1) und dem Kälterezeptor (TRPM8) durchzuführen ([Abbildung 4](#)). Die Aktivität des vaskulären endothelialen Wachstumsfaktors (VEGF) ist bei primären Hautmelanomen höher, was zu einer Angiogenese und damit zur Metastasierung führt ([Rajabi et al., 2012](#)). VEGF-A wurde in menschlichen Aderhautmelanomen durch Immunhistochemie nachgewiesen ([Kase et al., 2006](#)). 3- Iodthyronamin (3-T₁AM) ist ein decarboxyliertes Schilddrüsenhormon und hat bei Nagetieren eine physiologisch kühlende Wirkung ([Cichero et al., 2014](#)). Es moduliert den *trace-amine-associated-receptor-1*, (TAAR-1) und den β -Adrenozeptoren ([Dinter et al., 2015](#)). Sowohl TRPV1 als auch TRPM8 wurden zuvor in Aderhautmelanomzellen funktionell charakterisiert ([Mergler et al., 2014](#)). Insgesamt ist die Untersuchung des Zusammenspiels zwischen dem vaskulären endothelialen Wachstumsfaktor, VEGF und dem Schilddrüsenhormonderivat, 3-T₁AM und ihrer konsekutiven Rolle bei der Calciumregulierung durch den Thermorezeptor, TRPV1 und Kälterezeptor, TRPM8 erforderlich. Wenn das Zusammenspiel von

VEGF und 3-T₁AM gut verstanden wird, könnte 3-T₁AM als endogener Modulator für die Therapie des Aderhautmelanoms vorgeschlagen werden.

Pterygiumzellen stammen aus dem benignen Tumor der humanen Bindegewebe und werden für *in-vitro*-Studien immortalisiert. Das Pterygium ist eine häufige Zellwucherung mit hoher Inzidenz in Ländern in Äquatornähe. Pterygium ist auch mit dem Syndrom des trockenen Auges verbunden ([Hashemi et al., 2014](#); [Lee et al., 2004](#)). VEGF und sein Rezeptor sind in den Pterygiumzellen hochreguliert ([Gebhardt et al., 2005](#); [Khalfou et al., 2011](#)). Humane konjunktive Epithelzellen sind die gesunde Version des benignen Tumors der Pterygium-Zellen. Das Vorhandensein von TRPV1 und seine Funktionalität in den humanen konjunktiven Epithelzellen wurde bereits untersucht ([Mergler et al., 2012](#)). Da TRPV1 in den meisten Tumorzellen hoch exprimiert ist, ist es sinnvoll, zu untersuchen, ob TRPV1 auch in Pterygiumzellen funktionell aktiv und hoch exprimiert ist. Darüber hinaus soll auch die Interaktion zwischen VEGF und TRPV1 weiter untersucht werden.

1.3. Calcium-Imaging im zellbasierten Überexpressions-system von Mas, ein Ang-(1-7) -Rezeptor

Angiotensin-(1-7) [Ang-(1-7)] ist der bekannte endogene Ligand von Mas, einem wichtigen G-Protein-gekoppelten Rezeptor (GPCR) im *renin-angiotensin-aldosteron-system* (RAAS) ([Santos et al., 2018](#)) ([Bader et al., 2018](#)). Das RAAS ist an der Regulierung des Blutdrucks und des Flüssigkeits-/Elektrolytgleichgewichts sowie an Herz-Kreislauf-Erkrankungen beteiligt. Ang-(1-7) ist ein Heptapeptid-Hormon. Es spielt eine wichtige Rolle bei verschiedenen physiologischen Stoffwechselwegen, zum Beispiel bei der Verringerung von Entzündungen, der Verbesserung der Insulinsensitivität und der Verringerung der Angiogenese in krebserregenden Tumoren. Es ist auch für die Hemmung der Fibrose und die Verbesserung der Lern- und Gedächtnisfunktionen im Gehirn verantwortlich ([Passos Silva DG et al., 2013](#)). Aufgrund seiner zahlreichen positiven Auswirkungen auf pathophysiologische Erkrankungen ist die Charakterisierung der Mas-Signalwege bei der Entwicklung neuer Therapeutika besonders wichtig.

Das Calcium-Imaging ist ein wichtiges Werkzeug für das Arzneimittel-Screening bei GPCRs. Calcium ist ein wichtiges Botenmolekül, das auch durch die GPCR-Aktivität aktiviert wird. Mas ist ebenfalls ein GPCR. Bei Gq-aktivierten GPCRs führt die Bindung eines Agonisten über die Aktivierung der Phospholipase-C-IP3-Signalkaskade zu erhöhtem intrazellulärem Calcium. Dieser beobachtete Anstieg des intrazellulären Calciumspiegels wird durch die Freisetzung von Calcium aus dem endoplasmatischen Retikulum verursacht, was mit dem Begriff, „Speicherdepletion“ bezeichnet wird. ([Kieselyov et al., 2003](#)).

Ob Ang-(1-7) bei der Calciumregulation durch Aktivierung von Mas eine Rolle spielt, ist noch nicht geklärt. Mehrere Experimente *in-vivo* und *in-vitro* führten zu widersprüchlichen Ergebnissen, und es fehlte ein klares Bild. Tierversuche mit Ang-(1-7) haben gezeigt, dass Ang-(1-7) das zytosolische Calcium nur in pathologischen Zuständen erhöhen kann. Ang-(1-7) erhöhte den Einwärts-Calciumstrom in herzinsuffizienten Rattenherzen um 21 % ([Zhou et al. 2015](#)). In den Untersuchungen aus proximalen Tubuli von SHR (*spontan-hypertensive-Ratten*) erhöhte Ang-(1-7) die intrazellulären Calciumspiegel im nM- und μM-Bereich ([Mellow-Aires et al., 2017](#)).

Im Gegensatz dazu zeigten die meisten *in-vitro*-Studien keinen nachweisbaren Anstieg des

intrazellulären Calciumspiegels nach Anwendung von Ang-(1-7) unter gesunden Zuständen. Bei der Anwendung von peptidischen Mas-Agonisten wie Ang-(1-7) und Angioprotectin und nicht-peptidischen Mas-Agonisten wie cGEN856S und AVE0991 wurde kein Anstieg des intrazellulären Calciumspiegels beobachtet. Hingegen wirken Neuropeptid FF (NPFF), ein Peptid-Agonist, und AR234960, ein nicht-peptidisches Agonist, auf Mas und erhöhen das intrazelluläre Calcium über den klassischen Gq-Weg sowie durch Aktivierung der PLC-IP3-Signalkaskade ([Santos et al., 2003](#), [Pinheiro et al., 2004](#)). Nur eine Studie zeigte, dass Ang-(1-7) in der Lage war, intrazelluläres Calcium über Mas-Aktivierung durch Mikroperfusion in proximalen Tubuli von Ratten zu erhöhen. Weitere Signalkaskaden von Mas sind jedoch nicht untersucht worden ([Castelo-Branco, Leite-Delova, and de Mello-Aires 2013](#)).

Da es sich bei Mas um einen GPCR handelt und bekannt ist, dass ein Teil des GPCRS das intrazelluläre Calcium reguliert, ist es sehr interessant zu untersuchen, ob Ang-(1-7) das intrazelluläre Calcium über die Aktivierung von Mas regulieren könnte. Ein zellbasiertes Proteinexpressionsmodell, d.h., *Human embryonic kidney 293* (HEK293) wurden für die Mas Überexpression verwendet. Das Ziel dieser Studie ist es, herauszufinden, ob Ang-(1-7) das intrazelluläre Calcium in Mas-überexprimierten HEK293-Zellen erhöhen kann und wenn ja, ob dieser erhöhte Calciumspiegel mit einem Mas-spezifischen Inhibitor gehemmt werden kann. Die nächste Frage wäre, welche Familie von Ionenkanälen daran beteiligt ist. Weitere Signalübertragungswege, z. B. über Phospholipase C oder Proteinkinase C (PKC), sollen ebenfalls untersucht werden, um die Calciumregulation von Mas über Ang-(1-7) zu verifizieren.

1.4. Calcium-Imaging-Methode im eukaryotischen zellfreien Proteinsynthese-System

1.4.1. Grund der Etablierung der Methode

Ionendurchlässige Proteine sind Ionenkanäle, Pumpen und Ionentransporter. Etwa 30 % der für den therapeutischen Einsatz geeigneten Membranproteine sind Ionenkanäle ([Santos et al., 2017](#)). Therapeutische Membranproteine werden in mehrere Gruppen unterteilt. Die erste Hauptgruppe der therapeutischen Membranproteine gehört zu den G-Protein-gekoppelten Rezeptoren und die zweite Hauptgruppe zu den Ionenkanälen. Mutierte Ionenkanäle führen zu einer Störung der Ionenhomöostase und führen zu sogenannten Channelopathien ([Kim et al., 2014](#)). Viele Krankheiten werden durch Mutationen von Ionenkanälen verursacht. So werden zum Beispiel Tachykardie und maligne Hyperthermie durch Mutationen der Ryanodin-Rezeptoren (RyR1 und RyR2) verursacht ([Hübner und Jentsch et al., 2002](#)).

Ionenkanäle werden normalerweise in den Zellen überexprimiert und mit verschiedenen Techniken untersucht, um ihre Rolle bei verschiedenen Krankheiten zu entziffern. Die Herstellung nativer und funktionsfähiger ionendurchlässiger Proteine mit pharmakologischen Eigenschaften ist oft schwierig und hängt von verschiedenen Faktoren ab. Einige Faktoren sind die effiziente Expression, Lokalisierung und Orientierung der Ionenkanal-Untereinheiten. Darüber hinaus haben die meisten Ionenkanäle mehrere Transmembrandomänen. Wenn Ionenkanäle in Zellen überexprimiert werden, besteht daher ein enormes Potenzial für Fehlfaltungen und Fehlorientierungen. Zusätzlich zu den Problemen bei der Faltung und dem Zusammenbau der Untereinheiten sind überexprimierte Ionenkanäle häufig instabil. Zum Beispiel entsteht bei der Überexpression von calciumdurchlässigen

Ionenkanälen häufig eine funktionelle Toxizität, weil sie die Calciumhomöostase in der Wirtszelle stören und dadurch zahlreiche schädliche Auswirkungen auf die Zellen haben können. Die Überexpression von Ionenkanälen kann zu Mängeln bei der Verarbeitung essentieller Wirtszellproteine führen. Die Toxizität wird durch die Anhäufung der fehlgefalteten Ionenkanäle in den Membranen der Wirtszelle verursacht. Die Toxizität kann auch durch überexprimierte Kanalproteine verursacht werden, die die Sekretionsmaschinerie der Wirtszelle pathologisch beeinflussen ([Eertmood et al., 2004](#)). Wegen fehlgefalteter Ionenkanäle und Instabilität durch höhere Proteinexpression kommt es zudem zu proteolytischen Aktivitäten. Instabile und fehlgefaltete Ionenkanäle werden durch Proteasom in den Zellen abgebaut. Aus den oben genannten Gründen ist die zellfreie Proteinsynthese für die Expression von Ionenkanälen notwendig.

Die Planare-Lipiddoppelschicht-Methode, radioaktive Ionenfluss-Assays und Fluoreszenztechniken (ionenempfindliche Farbstoffe) sind gängige Methoden zur Untersuchung von Ionenkanälen. Die Planare-Lipiddoppelschicht-Methode der Elektrophysiologie ist bereits für zell-frei synthetisierte Ionenkanäle etabliert. Radioaktive Ionenfluss-Assays werden grundsätzlich vermieden, da nicht alle Labore für die Arbeit mit radioaktivem Material ausgerüstet sind. Die Arbeit mit radioaktivem Material erfordert außerdem eine Sondergenehmigung der Aufsichtsbehörden. Auf Fluoreszenzfarbstoffen basierende Methoden sind ein unverzichtbares Werkzeug, das eine Reihe von Vorteilen mit sich bringt: einfache Anwendung für das *high-throughput-screening* (HTS) mit einem Mikroplattenlesegerät, niedrige Kosten pro Datenpunkt, minimale Anforderungen an die Instrumentierung, hohe räumliche Auflösung und eine relativ unkomplizierte Datenanalyse. Neben der von uns in dieser Forschungsarbeit verwendeten Methode können auch andere Fluoreszenzmethoden eingesetzt werden, wie z.B. die Verwendung von membranundurchlässigen Ca^{2+} -Farbstoffen zur Messung des Calciums in der extra- mikrosomalen Lösung, wo die luminalen Calciumspiegel nicht direkt überwacht werden können ([Dusza et al., 2018](#)). Da die Mikrosomen bei dieser Methode nicht auf der Mikroplatte/Küvette fixiert sind, ist eine Live-Überwachung von Ca^{2+} während des Austauschs von Aktivator und Inhibitor Lösungen nicht möglich. In Anbetracht der Nachteile der derzeitigen Methoden wird die Notwendigkeit der Entwicklung einer direkten Calcium-Imaging-Methode in Mikrosomen für zell-frei synthetisierte Ionenkanäle deutlich.

1.4.2. Hypothese der neuen Methode

Das vorliegende Vorhaben, Calcium-Imaging in der zellfreien Proteinsynthese zu etablieren, hat Schnittstellen zu zwei verschiedenen Forschungsbereichen, der zellfreien Proteinsynthese und dem Bereich der Ionenkanäle.

Für die Entwicklung der Calcium-Imaging-Methode wurde die eukaryotische zellfreie Proteinsynthese herangezogen. Prokaryotische zellfreie Synthese-Plattformen sind für diese Verfahrensweise nicht geeignet, da in prokaryotischen Zellen keine membranreichen Organellen wie das endoplasmatische Retikulum vorhanden sind. Während der Lysat-Herstellung werden die Mikrosomen aus dem endoplasmatischen Retikulum geformt. Die zell-frei synthetisierten Ionenkanäle werden in die mikrosomalen Membranen des eukaryotischen Zell-Lysats integrieren. Daher ist es sinnvoll, die Calcium-Imaging-Methode in eukaryotischen zellfreien Proteinsynthese-Plattformen zu entwickeln.

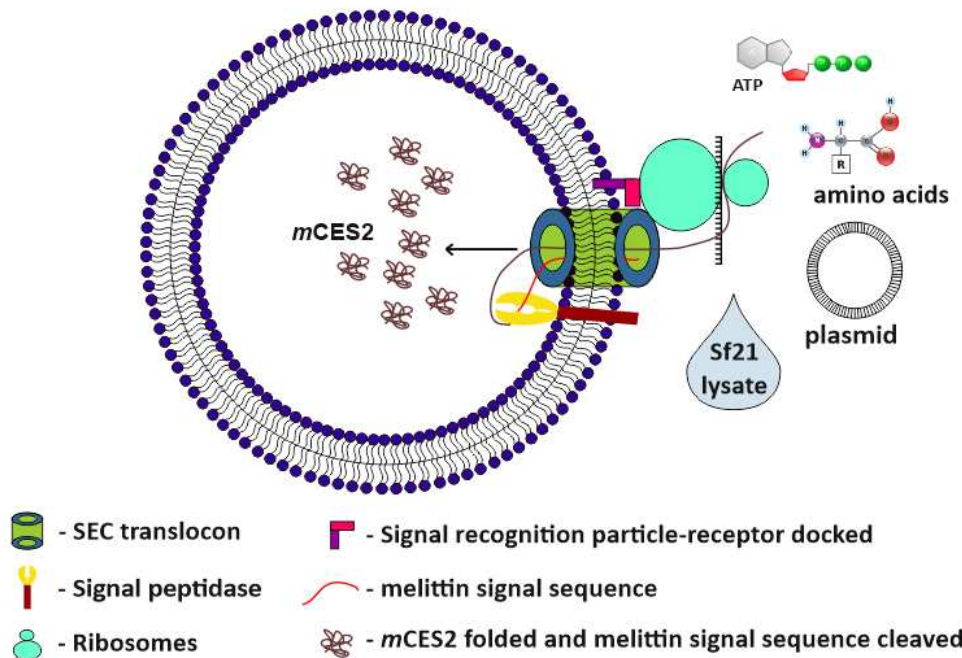


Abbildung 5: Darstellung auf zellfreie Proteinsynthese von Carboxylesterase Enzyme in Sf21 Mikrosomen: mCES2 wird in dem extra-mikrosomalen Raum durch zellfrei Reaktionskomponenten synthetisiert und in die mikrosomalen Lumen mit Hilfe der Melittin-Signalpeptid durch SEC-Translokon transportiert ([Dhandapani et al., 2021](#)).

Für die Behandlung von AM -basierten Calciumindikatoren ist eine Carboxylesterase erforderlich. Carboxylesterase ist in den meisten eukaryotischen Zellen endogen in großen Mengen im Zytoplasma vorhanden. Im endoplasmatischen Retikulum gibt es jedoch keine Carboxylesterase. Einige Studien haben gezeigt, dass Calcium im endoplasmatischen Retikulum der Zellen messbar ist. Für eine solche Anwendung werden die Zellen erst mit Carboxylesterase im endoplasmatischen Retikulum überexprimiert ([Samtleben et al., 2013; Blum et al., 2010; Rehberg et al., 2008](#))

Während der Herstellung von Lysaten könnte die endogen vorhandene zytosolische Carboxylesterase auch in die zellfreien Lysate übertragen werden. Diese aus dem Zytosol übertragene Carboxylesterase befindet sich jedoch außerhalb der Mikrosomen. Für das Calcium-Imaging des mikrosomalen Lumens sollte die Carboxylesterase im Lumen der Mikrosomen exprimiert werden. Frühere Studien mit zellfreier Proteinsynthese haben gezeigt, dass die löslichen Proteine, die zell-frei synthetisiert werden, mit Hilfe des Melittin-Signalpeptids in die Mikrosomen transportiert werden können ([Wüstenhagen et al., 2020; Thoring et al., 2019](#)). Zusammengekommen lautet die begründete Hypothese, dass die Carboxylesterase zell-frei synthetisiert und mithilfe des Melittin-Signalpeptids in das Lumen der Mikrosomen transportiert wird (dargestellt in Abbildung 5).

Die Carboxylesterase mit Melittin-Signalpeptid wird in verfügbaren eukaryotischen Systemen synthetisiert, z. B. im *Sf21*-basierten zellfreien Systemen. Als DNA-Template für die Proteinsynthese wird ein Plasmid (Plasmid: pIX3.0-CrPV IRES-Mel Carboxylesterase) verwendet, das im N-Terminus eine CRPV-IRES-Sequenz und eine Melittin-Signalpeptid-Kodierungssequenz enthält. Ohne Melittin-Signalpeptid wird die Carboxylesterase außerhalb der Mikrosomen synthetisiert und verbleibt dort, da sie ein lösliches Protein ist. Das SEC-Translokon hilft beim Transport der Polypeptide durch eine hydrophobe Phospholipid-Doppelschicht, z. B. die ER-Membran. Mit Melittin-Signalpeptid werden sie durch das SEC-Translocon in das mikrosomale Lumen transportiert. Das Signalpeptid der Carboxylesterase wird mit Hilfe der Signalpeptidase gespalten, die sich in den Mikrosomenmembranen befindet ([Zimmermann and Mollay et al., 1986](#)) ([Abbildung 5](#))

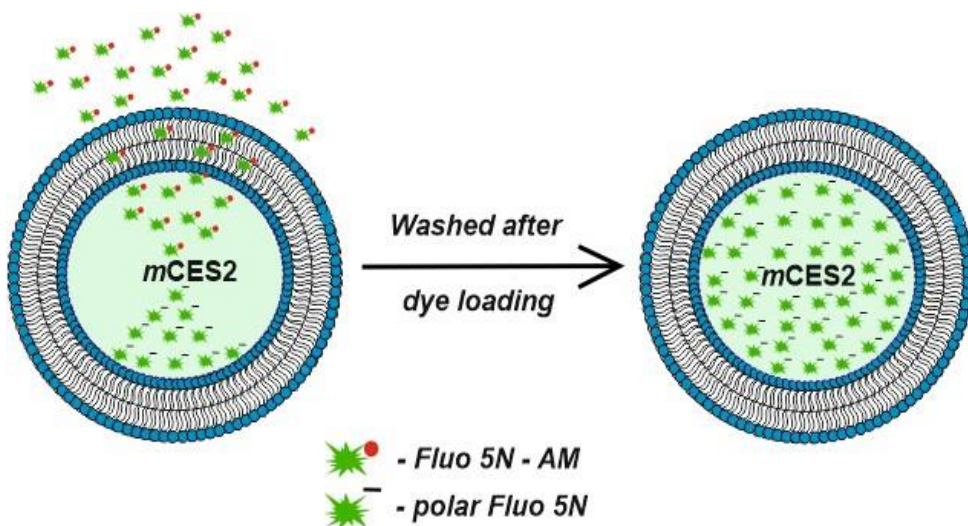


Abbildung 6: Darstellung der Aufspaltung von Farbmittel durch Carboxylesterase in Mikrosomen, [Dhandapani et al., 2021](#).

Die in den Mikrosomen vorhandenen Chaperone falten die Carboxylesterase zu einem funktionellen Enzym. Nachdem die Carboxylesterase gefaltet ist, ist sie bereit, die Calciumindikatoren mit der funktionellen Acetoxymethylester-Gruppe (AM-Gruppe) zu verarbeiten. Die AM-Gruppe ermöglicht den Calcium-Indikatoren, durch biologische Membranen zu gelangen. Nach der Abspaltung der AM-Gruppe durch die Carboxylesterase wird die negative Polarität des Calciumindikators enthüllt und kann nicht mehr durch biologische Membranen wandern. Einige Waschschritte mit Phosphatpuffer ermöglichen die Entfernung der ungespaltenen Calciumindikatoren in den Mikrosomen. Auf diese Weise können die Calciumindikatoren in hoher Konzentration in den Mikrosomen angereichert werden. Der entsprechende Vorgang ist in der [Abbildung 6](#) dargestellt.

Die Mikrosomen, die mit dem Calcium-Indikator angereichert sind, können für Calcium-Imaging verwendet werden. Durch Calcium-Imaging können nativ vorhandene ionenpermeable Proteine wie Ryanodin-Rezeptoren, die SERCA-Pumpe oder IP3-Rezeptoren untersucht werden. Neben den nativ vorhandenen ionenpermeablen Proteinen können auch zell-frei exprimierte Ionenkanäle untersucht werden, die für die Forschung nach neuen Medikamenten relevant sind. Für die Untersuchung der zell-frei synthetisierten Ionenkanäle wurden TRP-Ionenkanäle ausgewählt. Viele frühere Studien haben nachgewiesen, dass TRP-Ionenkanäle im endoplasmatischen Retikulum vorhanden sind. TRPV1 wird in Neuronen endogen im endoplasmatischen Retikulum exprimiert und steuert die

Calciumfreisetzung aus dem endoplasmatischen Retikulum, die hier also nicht durch Inositoltriphosphat (IP3) vermittelt ([Dong et al., 2010](#)). Ein ähnlicher Mechanismus wurde auch in anderen Studien beobachtet. Die Calcium-Imaging-Untersuchungen von überexprimiertem TRPV1-Ionenkanal im ER von *Sf21*- und HEK293-Zellen führten ebenfalls zur Calcium-Freisetzung aus dem endoplasmatischen Retikulum in das Zytosol, die ohne IP3-Vermittlung erfolgt ([Wisnosky et al., 2003](#)). TRPV1 wird auch endogen im ER von nicht-erregbaren Zellen wie Myozyten und Krebszellen ([Haustrate et al. 2020](#)) und in menschlichen Lungenzellen ([Thomas et al., 2007](#)) exprimiert. Diese Zelltypen zeigen auch eine ähnliche Regulierung des Calciums im ER, wenn sie mit Aktivatoren angeregt werden. Es ist daher zu erwarten, dass TRP-Ionenkanäle, wenn sie in einem zellfreien System in Mikrosomen exprimiert werden, bei Anwendung von Aktivatoren zu einer Calciumfreisetzung aus dem Mikrosomen führen können.

Basierend auf der oben beschriebenen Herangehensweise kann ein neuartiges Calcium-Imaging in einem zellfreien System etabliert werden, um sowohl die nativ vorhandenen ionenpermeablen Proteine als auch zell-frei synthetisierte TRP-Ionenkanäle in Mikrosomen zu untersuchen.

2. Manuskriptkompendium

2.1. Manuskript I


Cite this: *RSC Adv.*, 2021, **11**, 16285

Targeted esterase-induced dye (TED) loading supports direct calcium imaging in eukaryotic cell-free systems†

Priyavathi Dhandapani,^a Srujan Kumar Dondapati,^a Anne Zemella,^a Dennis Bräuer,^a Doreen Anja Wüstenhagen,^a Stefan Mergler^c and Stefan Kubick  ^{*ab}

Calcium imaging is an important functional tool for analysing ion channels, transporters and pumps for drug screening in living cells. Depicted eukaryotic cell-free systems utilize microsomes, derived from the endoplasmic reticulum to incorporate the synthesized membrane proteins-like ion channels. Carboxylesterase is required to cleave the acetoxyethyl ester moiety of the chemical calcium indicators in order to ensure its immobility across the endoplasmic reticulum membrane. Absence or an inadequate amount of carboxylesterase in the endoplasmic reticulum of different eukaryotic cells poses a hindrance to perform calcium imaging in microsomes. In this work, we try to overcome this drawback and adapt the cell-based calcium imaging principle to a cell-free protein synthesis platform. Carboxylesterase synthesized in a *Spodoptera frugiperda* Sf21 lysate translation system is established as a viable calcium imaging tool in microsomes. Cell-free synthesized carboxylesterase inside microsomes is validated with esterase and dye loading assays. Native proteins from the endoplasmic reticulum, such as ryanodine channels and calcium ATPase, are analysed. Cell-free synthesized transient receptor potential channels are used as model proteins to demonstrate the realization of this concept.

Received 1st October 2020
Accepted 25th March 2021

DOI: 10.1039/d0ra08397f
rsc.li/rsc-advances

1 Introduction

Ion permeable membrane proteins such as ion channels, transporters and pumps contribute to the majority of eukaryotic membrane proteins, serving as viable drug targets for several pathological diseases next to the large family of G-protein coupled receptors.¹ Eukaryotic cell-free protein translation overcomes several disadvantages that could be met for over-expression of these ion permeable proteins in cells, such as cell-toxicity, poor expression and deletion due to engineered protein domains, and reduction of expression in permanent cell lines.² Taken together, the development of functional assays targeting ion channels in eukaryotic cell-free systems is a pre-requisite for rapid pharmacological discoveries.

The planar bilayer, radioactive ion-flux assays and fluorescent techniques (ion-sensitive dyes) are common methods to study ion channels. Eukaryotic cell-free systems use

microsomes to integrate synthesized membrane proteins. A handful of planar bilayer investigations in eukaryotic cell-free systems have been previously reported.^{3,4} But the planar bilayer method requires the solubility of ion channels using detergents for subsequent evaluation. Notwithstanding the temporal resolution given by electrophysiological techniques like planar bilayer, fluorescent dye-based methods have been an indispensable tool encompassing a plethora of advantages: ease of applicability for High Throughput Screening (HTS) using a microplate reader, low cost per data point, minimum instrumentation requirements, high spatial resolution and relatively less sophisticated data analysis. Another method to analyse ion permeable proteins in microsomes would be by employing radioactive calcium. Intraluminal calcium is the prime regulator for endoplasmic reticulum (ER) function^{5,6} and has been analysed concomitantly in microsomes using ⁴⁵Ca²⁺ to study native ion channels and pumps.^{7–11} Apart from the undesirable radioactivity, with a major drawback being an end-point based method, it will also increase the material costs to study the kinetics. Moreover, first the microsomes should be enriched with ⁴⁵Ca²⁺ using Ca²⁺ ATPase (SERCA) for any kind of calcium efflux studies. Apart from the TED method which we utilize in this work, also other fluorescent methods can be employed, for instance, using membrane impermeable Ca²⁺ dyes to measure the calcium present in the extra-microsomal solution,¹² where luminal calcium levels cannot be monitored directly. As the microsomes are not fixed on the microplate/cuvette in this

^aFraunhofer Institute of Cell Therapy and Immunology, Branch of Bioanalytics and Bioprocesses (IZI-BB), Am Muehlenberg 13, Potsdam-Golm, Germany. E-mail: stefan.kubick@izi-bb.fraunhofer.de

^bFaculty of Health Sciences, Joint Faculty of Brandenburg University of Technology, Cottbus – Senftenberg, Theodor Fontane Medical School of Brandenburg, University of Potsdam, Germany

^cDepartment of Ophthalmology, Charité – Universitätsmedizin Berlin, Campus Virchow-Hospital, Berlin, Germany

† Electronic supplementary information (ESI) available: Supplementary data and video file. See DOI: 10.1039/d0ra08397f



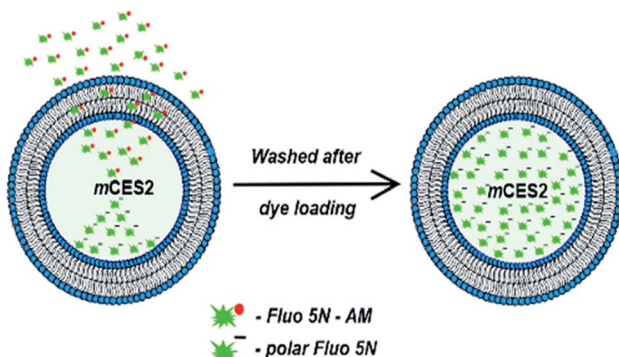


Fig. 1 Unmasking polarity of the dye by carboxylesterase *mCES2* in microsomes.

method, live monitoring of Ca^{2+} is impracticable while exchanging activator and inhibitor solutions. Considering the disadvantages of the present methods, the necessity to establish direct calcium imaging to monitor the microsomal lumen for ion channels expressed in eukaryotic cell-free platforms is substantiated. The previously reported idea of targeted esterase-induced dye (TED) loading of the endoplasmic reticulum (ER) in mammalian cells,^{13–15} augmented with the current knowledge of eukaryotic cell-free systems^{2,16} led us to develop this new method to address the aforementioned shortcomings and also to explore new topics of research.

Eukaryotic cell-free protein synthesis platforms use microsomes in order to incorporate the membrane proteins. The soluble proteins like carboxylesterases can be engineered with signal peptide sequences to be delivered inside the microsomes after synthesis. Carboxylesterase, ubiquitously present in the cytoplasm of most of the eukaryotic cells, is the crucial enzyme for cell-based calcium imaging using acetoxymethyl ester (AM) based chemical dyes. The carboxylesterase enzyme aids in cleaving the AM moiety of the chemical indicator, thereby making the dye immobile across any biological membrane. Immobility of the cleaved dye is caused due to the unmasking of the polar negative charge of the dye. Absence or an inadequate amount of carboxylesterase in the endoplasmic reticulum of different eukaryotic cells, which is necessary to cleave the acetoxymethyl ester moiety of the chemical calcium indicators effectuates the insufficiency of immobile dye formation inside the microsomes. In this work, we try to overcome this drawback and adapt the cell-based calcium imaging principle to a cell-free protein synthesis platform as depicted in Fig. 1. Carboxylesterase synthesized in the *Sf21* lysate translation system which is targeted to be delivered inside the microsomes is established as a viable calcium imaging tool to investigate both native proteins present in the ER and also cell-free synthesized ion channels.

2 Materials and methods

2.1. Continuous exchange cell-free (CECF) translation

Eukaryotic CECF translation of proteins was performed using *Sf21* lysates in a special dialysis chamber (SCIENOVA) containing two compartments separated by a 10 kDa cut off dialysis membrane in between the reaction mixture and the feeding

mixture. A 50 μL standard reaction mixture of a *Sf21* cell-free synthesis reaction in the reaction chamber was composed of 40% lysate, 30 mM HEPES-KOH (Merck), 2.5 mM $\text{Mg}(\text{OAc})_2$ (Merck), 75 mM KOAc (Merck), 0.25 mM spermidine (Roche), 100 μM each canonical amino acid (Merck), nucleoside triphosphates (1.75 mM ATP, 0.30 mM CTP, 0.30 mM GTP, and 0.30 mM UTP) (Roche), 120 ng μL^{-1} plasmid DNA (Biocat), 1 U mL^{-1} T7 RNA-polymerase (Agilent), 20 μM PolyG (Iba Life sciences), 30 μM caspase inhibitor – Z-VAD-FMK (benzyloxycarbonyl-Val-Ala-Asp(OMe)-fluoromethylketone) (Promega), and 0.02% of sodium azide (Merck). 1 mL of the feeding mixture contained all the above components except plasmid, PolyG, T7 RNA polymerase and *Sf21* lysate. Caspase inhibitor was used for improving yields and avoiding protein degradation during the incubation step for 24 h. No plasmid was used in NTC (non-template control) samples. For expression of both the proteins, human transient receptor potential channels, vanilloid receptor member 1, *hTRPV1* and mouse carboxylesterase 2 (*mCES2*) were correspondingly sequentially translated for 24 h each. As *mCES2* and *hTRPV1* contain disulphide bridges, prudently the translation is performed only under non-reducing conditions. As the microsomes obtained from the first translation were used in the second translation, it may occur that the first translated protein is not present in all the microsomes at the end of the second translation. To avoid this issue, we have used only the vesicular fraction obtained after the second translation for all our experiments that require tandem protein translation.

Simultaneous translation is not preferred as evaluation of the yields of individual proteins synthesized is not feasible with the same radiolabel. ^{14}C -Labeled leucine (100 dpm per pmol) (Perkin Elmer) was used for the detection of *de novo* synthesized proteins. For functional analysis like assays and calcium imaging, the proteins were synthesized in the absence of ^{14}C -leucine. Protein translation reactions based on *Sf21* lysates were incubated for 24 h at 30 °C, 600 rpm using a thermomixer (Eppendorf). The translation mixture (TM) of cell-free reactions was further fractionated for analysis. The fractionation was realized by centrifugation at 16 000 $\times g$ for 10 min at 4 °C in order to separate the ER-derived vesicular fraction (VF) of the cell lysate from the supernatant (SN). The microsomal fraction was suspended in PBS buffer without calcium and magnesium ions for further analysis such as quantification of protein yields. For storage, the total translation mix was snap frozen in liquid nitrogen and stored at –80 °C.

2.2. Quantification of cell-free synthesized protein yields

Based on the incorporation of ^{14}C -leucine in cell-free synthesized proteins, the respective protein yield can be estimated by scintillation measurement. Therefore, 5 μL aliquots of each translation mixture were mixed with 3 mL of a 10% (v/v) trichloroacetic acid–2% (v/v) casein hydrolysate (Carl Roth) solution in a glass tube and incubated at 80 °C for 15 min. Afterwards, the samples were chilled on ice for 30 min and retained on the surface of glass fiber filter papers using a vacuum filtration system (Hoefer). Filter papers were washed



twice with 5% TCA and then vacuum dried with acetone (Carl Roth). Dried filters were placed into a scintillation vial, 3 mL of scintillation cocktail was added and vials were agitated on an orbital shaker for at least 1 h. The scintillation signal was determined using an LS6500 multi-purpose scintillation counter (Beckman Coulter). The protein yields were identified based on the obtained scintillation counts and protein specific parameters including molecular mass and amount of leucine.

2.3. SDS-PAGE and autoradiography

The molecular size of radio-labelled, cell-free synthesized protein was analysed using SDS-PAGE followed by autoradiography. First, 5 μ L of the respective fraction of a cell-free synthesis reaction including the radio-labelled target protein was subjected to ice-cold acetone. Precipitated protein was separated by centrifugation ($16\,000 \times g$, 4 °C, 10 min) and then, the protein pellet was dried for at least 30 min at 45 °C. The dried protein pellet was dissolved in LDS sample loading buffer with 50 mM dithiothreitol (DTT, Life Technologies) and loaded on a pre-cast NuPAGE 10% Bis-Tris gel (Life Technologies). If the sample is a soluble protein, then it was also heated at 95 °C for 3 min prior to loading on the gel. The gel was run at 185 V for 35 min according to the manufacturer's protocol. Subsequently, the gel was dried at 70 °C using a gel dryer (Uniequip) and then placed on a phosphor screen for incubation for a minimum of two days. The radioactively labelled proteins were visualized using a Typhoon Trio + variable mode (GE Healthcare).

2.4. Esterase activity using 4-*para*-nitrophenol

First, mCES2 and NTC proteins were translated using *Sf21* CECF reaction as mentioned above. Prior to functional assessment, intensive washing of microsomes was performed to remove the cytosolic carboxylesterase which is carried over from cells to the lysate. This cytosolic carboxylesterase is present outside the microsomes. The esterase activity is preferably analysed for a maximum of 1 h. 50 μ L of total translation mix was first centrifuged at $16\,000 \times g$ for 10 minutes at 4 °C. The microsomal pellet was again washed with Phosphate Buffer Saline (PBS) with no Ca²⁺ and Mg²⁺ and centrifuged again to remove the remaining cytosolic carboxylesterases. The pellet was dissolved in esterase assay buffer containing 20 mM Tris-HCl (pH 8.0) (Sigma Aldrich), 150 mM NaCl (Sigma Aldrich), and 0.01% Triton X-100 (Sigma Aldrich). A fresh solution of 4-*para*-nitrophenylacetate (PNPA) (Sigma Aldrich) was used as the substrate. 250 μ L of PNPA substrate solution of varying concentration (mentioned in the figure legend of each experiment) was used to initiate the reaction and the mixture was incubated at 37 °C for 1 hour (or less than 1 hour with varying time for time dependent plot). For the substrate dependence plot, varied concentration of PNPA was used. The *para*-nitro phenol formed after esterase activity was measured using a Mithras Plate reader (Berthold Technologies) at 410 nm. No protein was added for blank reactions and the esterase activity was evaluated as the percentage of NTC samples.

2.5. Dye loading assays with Fluo-5N AM

First, mCES2 and NTC were translated using *Sf21* CECF reaction as mentioned above in the synthesis section. 50 μ L of translation mix was first centrifuged at $16\,000 \times g$ for 10 minutes at 4 °C to obtain the microsomal pellet to remove the cytosolic carboxylesterases present outside the microsomes. The microsomes were resuspended in ATP based calcium imaging buffer to initiate the SERCA activity. The calcium imaging buffer was composed of 75 mM KCl (Sigma Aldrich), 20 mM HEPES-KOH (Merck), 5 mM NaN₃ (Merck) and 200 μ M CaCl₂ (Sigma Aldrich) with pH 7.4. To enhance the SERCA activity, 10 mM adenosine 5'-triphosphate (ATP) (Roche), 1 mM MgCl₂ (Sigma Aldrich), 0.5 mM dithiothreitol (DTT) (Life Technologies), 5 mM phosphocreatine (PCr) (Sigma Aldrich), and 20 U mL⁻¹ creatine phosphokinase (CPK) (Sigma Aldrich) were used. SERCA activity induced Ca²⁺ loading was performed at 37 °C for varying time (mentioned in the figure legend of each experiment) and then stopped by centrifuging and removing the supernatant. The pellet was suspended in 100 μ L of Fluo-5N AM dye (Thermo Fischer) of varying concentration (mentioned in the figure legend of each experiment) and then incubated at 37 °C at 500 rpm. The reaction was stopped by centrifugation and removal of the dye. Microsomes were further washed with 100 μ L of PBS to purge the un-cleaved Fluo-5N AM at 37 °C for 20 minutes and centrifuged to obtain the microsomal pellet containing only the cleaved dye. Then, the pellet was washed and the fluorescence removed subsequently was measured in a plate reader (Berthold Technologies) with Ex 488 and Em 515 nm with the help of a black plate. The blank sample measurements were subtracted and the data were analysed.

2.6. SERCA activity by fluorescence spectroscopy

50 μ L of cell-free translation mix after the reaction was first centrifuged at $16\,000 \times g$ for 10 minutes at 4 °C to obtain the pellet containing the vesicular fraction. The pellet was suspended in ATP based calcium imaging buffer to initiate the SERCA activity. SERCA activity induced Ca²⁺ loading was performed at 37 °C for 60 minutes and then stopped by centrifuging and removing the supernatant. To see the effect of thapsigargin (TG) on the SERCA activity, microsomes were also additionally incubated with SERCA buffer in the presence of 100 nM TG, with and without ATP. After the SERCA activity step, the pellet was suspended in 100 μ L of Fluo-5N AM dye of 5 μ M concentration and then incubated at 37 °C at 500 rpm. The reaction was stopped by centrifugation and removal of the dye. Microsomes were further washed with 100 μ L of PBS to remove the uncleaved Fluo-5N AM from the microsomes by incubation at 37 °C for 20 minutes and centrifuged to obtain the microsomal pellet containing only the cleaved dye. Then, the suspended pellet was measured using a plate reader with Ex 488 and Em 515 nm. The blank values were subtracted and data were analysed.

2.7. Calcium imaging using confocal laser microscopy

For all calcium measurements, the microsomes were seeded for attachment on the coverslip coated with poly-D-lysine



hydrobromide preferably with a high molecular weight for microsomal membranes. The coverslips were autoclaved and coated overnight with poly-D-lysine hydrobromide (0.1 mg mL^{-1}) (Sigma Aldrich), dried and stored at room temperature. The microsomes were seeded for 1 h at 37°C and the coverslips were washed with the calcium imaging buffer for the removal of unsettled microsomes. Though $5\text{ }\mu\text{M}$ Fluo-5N AM was used for dye loading experiments performed using a microplate reader, $2\text{ }\mu\text{M}$ Fluo-5N AM was enough for qualitative and quantitative measurements of calcium with confocal microscopy without any loading enhancers like Pluronic F-127, probenecid or saponin. A flow chamber (Warner Instruments) fitted with a coverslip at the bottom with the aid of a vacuum sealing agent was used for all measurements. An argon laser with Alexa 488 with 3% intensity, maximum gain and 5–6 airy units was used for all measurements using the LSM Meta 510 software (Carl Zeiss) time series function with a frequency of one data point per 30 s. A $40\times$ oil immersion objective with a numerical aperture of 1.3 was used. All data are represented as delta F/F , where delta F represents the difference in fluorescence of microsomes and the background. Different regions of interest

were selected from each individual experiment from a frame of $512\text{ }\mu\text{M}\times 512\text{ }\mu\text{M}$ to ensure whether an identical increase or decrease in intensity is observable. The slope of bleaching was drift corrected using the 'peak and baseline correction protocol' with the help of OriginPro 2015 software. For comparison of individual experiments with activators and inhibitors, the baseline fluorescence intensity was normalized to 100 a.u. and then an increase or decrease in intensity was analysed. Plotting graphs was performed using OriginPro and Microsoft Excel software.

2.8. Statistical analysis

For all statistical analysis, GraphPad Prism Version 5.0 software was used. The data used for statistical analysis were first checked by the normality test (at least one of the tests such as KS normality test, Shapiro-Wilk normality test or D'Agostino and Pearson omnibus test should be passed to consider the data in Gaussian distribution). When the data sets fall under Gaussian distribution, student t tests are performed for paired sample data and unpaired student t tests are performed for unpaired

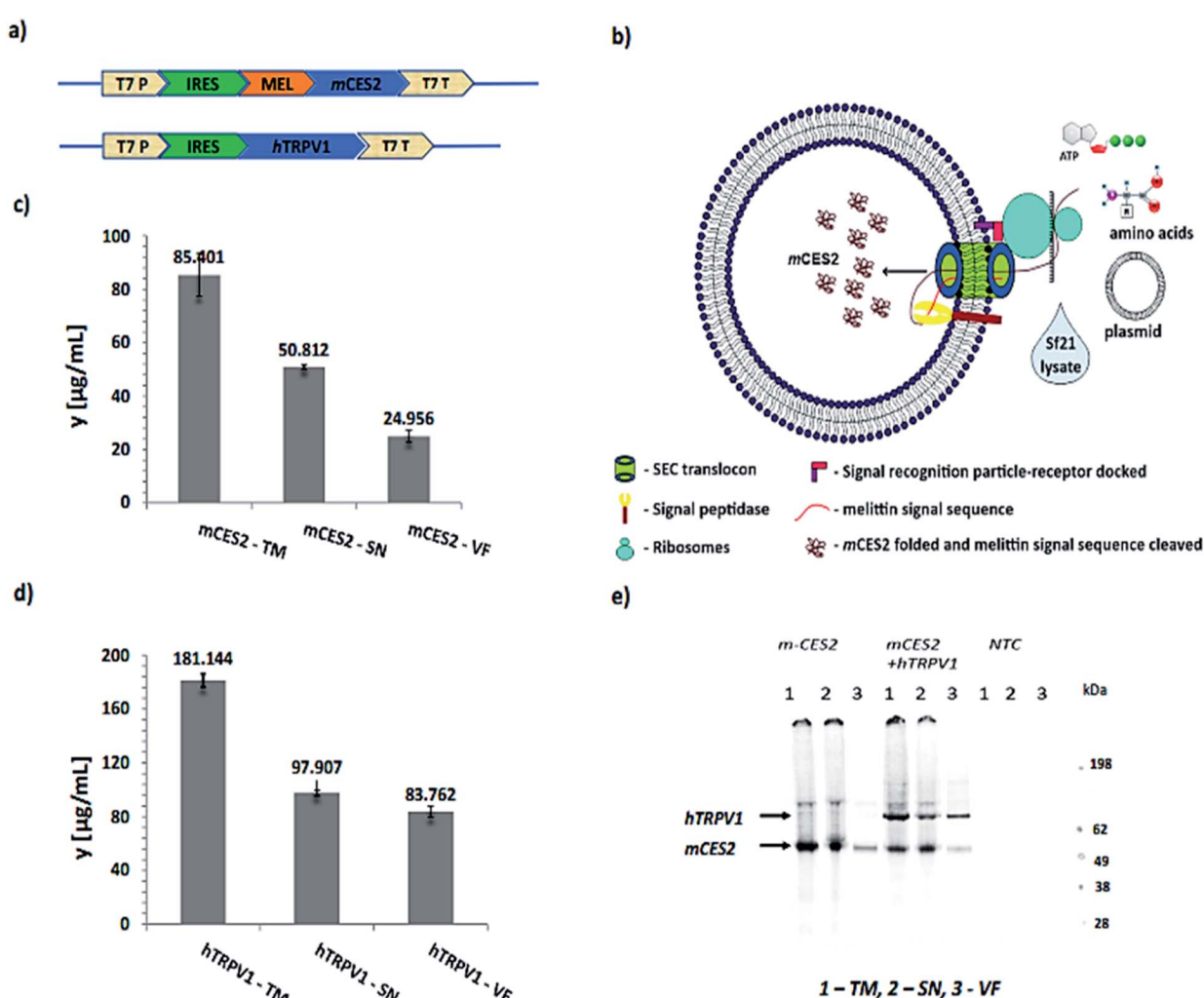


Fig. 2 Cell-free protein synthesis of *hTRPV1* and *mCES2*: (a) template design of *mCES2* and *hTRPV1*; MEL – melittin signal sequence, T7 P – T7 promoter, T7 T – T7 terminator, and IRES – cricket paralysis virus Internal Ribosome Entry Site; (b) schematic representation of cell-free synthesis of *mCES2*; (c) protein yields of *mCES2* by scintillation counting via CECF reaction for 24 h at 30°C in the Sf21 system; (d) protein yields of *hTRPV1* by scintillation counting via CECF reaction for 24 h at 30°C in the Sf21 system; (e) autoradiogram of proteins run on SDS MES gel.



sample data. For datasets that don't fall in Gaussian distribution, non-parametric tests such as the Wilcoxon matched pairs test are performed for paired sample data and the Mann-Whitney test is performed for unpaired sample data. Welch correction is applied when two data sets have non-equal variances. All the tests were performed to evaluate two-tailed *p* values with a confidence level of 95% and statistical significance is indicated by * or #.

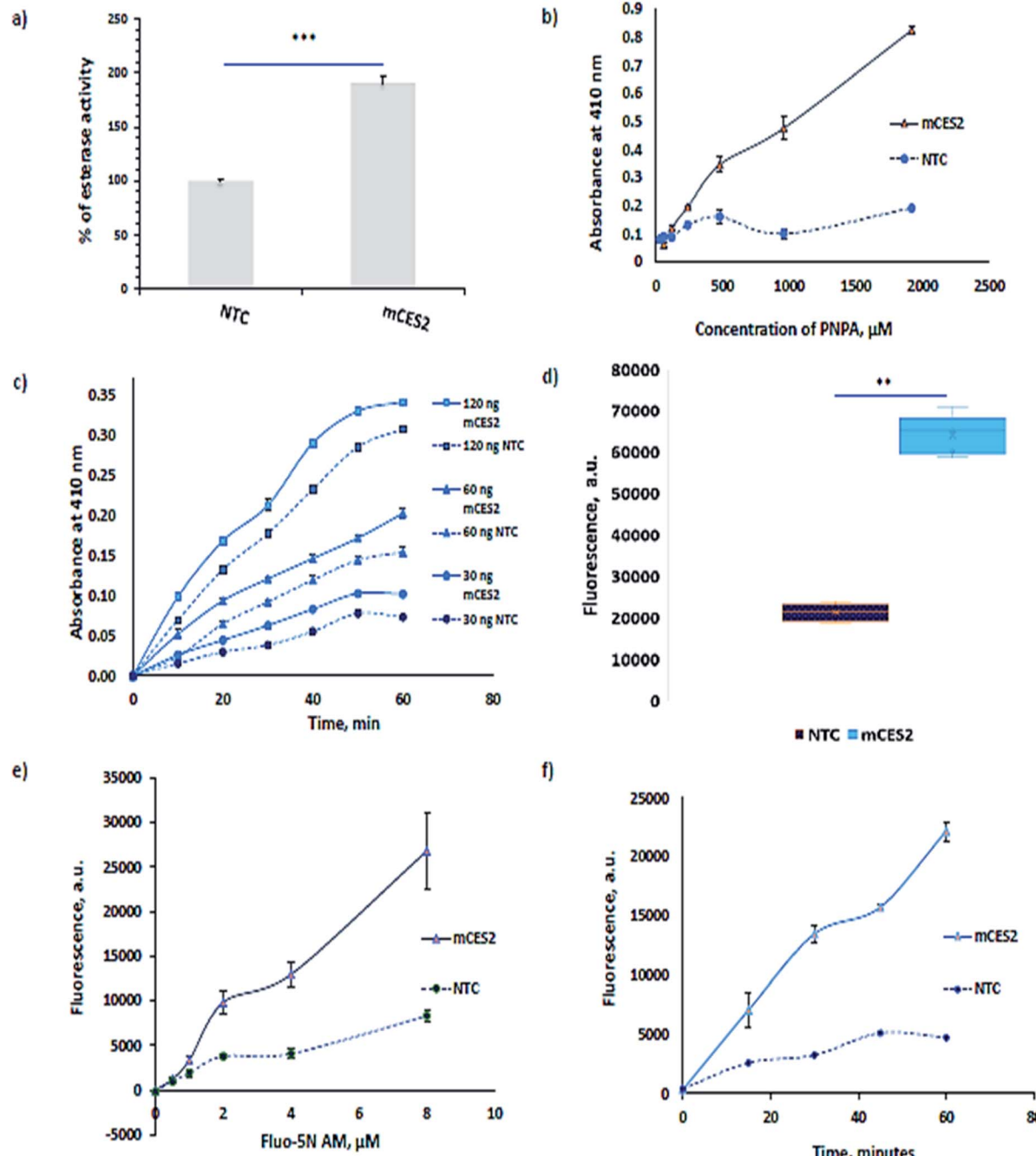


Fig. 3 Esterase activity using PNPA: (a) esterase activity of *mCES2* using PNPA in the microsomes, 37 °C, 60 min, 100 ng in 0.3 mM PNPA, $n = 6$; ***, $p = 0.0003$, unpaired *t* test, two tailed; (b) substrate concentration dependent esterase activity plot of *mCES2*, 37 °C, 60 min, 60 ng of *mCES2*, $n = 3$; (c) time and enzyme concentration dependence plot of *mCES2*, 37 °C with 0.3 mM PNPA, $n = 3$. Calcium dye loading experiments: (d) esterase activity performed with 200 ng of *mCES2* each in 100 μ L of 5 μ M Fluo 5N-AM, 37 °C, 60 min, $n = 5$; ***, $p < 0.0001$, unpaired *t* test, two tailed; (e) Fluo 5N-AM concentration dependent activity with 100 ng of *mCES2* protein each in 100 μ L reaction, 60 minutes, 37 °C, $n = 2$; (f) time dependent esterase activity with 100 ng of *mCES2* each in 100 μ L of 5 μ M Fluo 5N-AM, 37 °C, $n = 2$.

the gene was utilized in order to deliver the soluble protein inside the microsomal lumen as mentioned previously.¹⁸ The *mCES2* with a melittin signal sequence is recruited inside the lumen through the SEC translocon and the signal sequence is

cleaved by the signal peptidase present in the microsomal membrane as depicted in Fig. 2b. T7 promoter and T7 terminator were used for mRNA transcription. No signal sequence was used for the *hTRPV1* construct as *hTRPV1* is a poly-

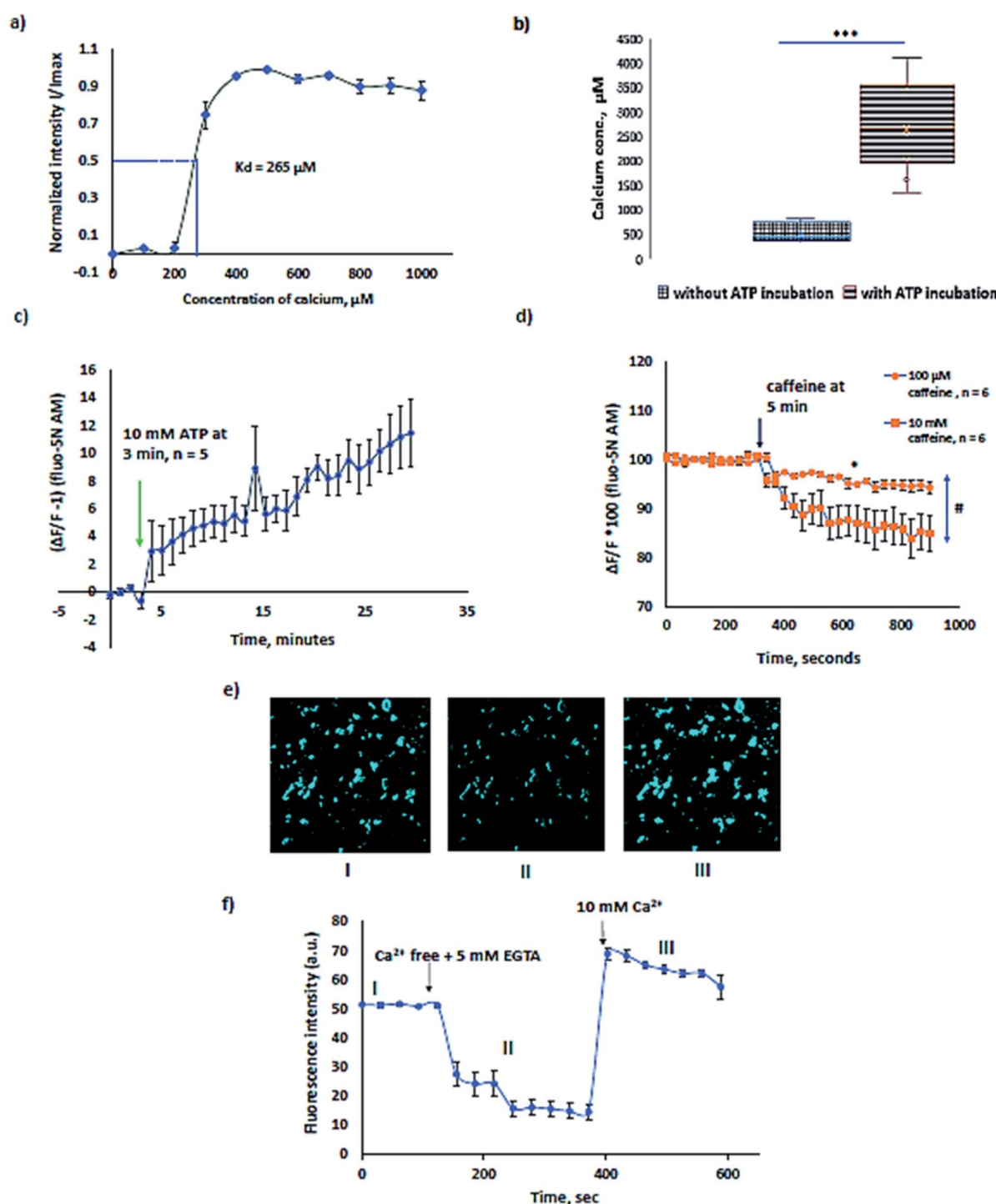


Fig. 4 Direct calcium imaging using *mCES2* microsomes: (a) K_d evaluation of Fluo 5N-AM in the *Sf21* microsomes in the presence of 10 μM ionomycin, $n = 4$; (b) calcium levels of ATP induced Ca^{2+} loaded and non-loaded microsomes at 37 °C for 1 h, $n = 5$ each; the data are represented as a box plot with max and min, and *** indicates significant difference, $p < 0.0001$, Mann-Whitney test, two tailed; (c) SERCA pump activity in microsomes with 10 mM ATP added at 3 min and measured for 30 min, RT, $n = 5$. The data before adding ATP are normalized to 0; (d) caffeine induced calcium release in *mCES2* microsomes via ryanodine receptor (RyR2) activation, $n = 6$ each for 10 mM and 100 μM caffeine; * indicates the significant difference of 100 μM caffeine sample data at 150 s and 600 s, $p = 0.0313$, Wilcoxon matched pair test, two tailed. # indicates the significant difference between 100 μM and 10 mM caffeine samples at 600 s, p value = 0.0247, Mann-Whitney test, two tailed. Calcium was loaded in the *mCES2* microsomes with ATP for 60 min at 37 °C prior to caffeine experiments; (e) representative confocal images of I, II and III from different states of graph (f); (f) representative graph of calcium concentration determination using Ca^{2+} free + 5 mM EGTA and 10 mM Ca^{2+} in the presence of 10 μM ionomycin. All data in (a), (c), (d), and (f) are presented as mean \pm S.E.M.



transmembrane protein. For the cell-free synthesis of *mCES2* and *hTRPV1*, we used the Continuous Exchange Cell-Free (CECF) mode of our *Sf21* translation system.^{19,20} This mode of synthesis has mainly the amino acids and the energy components in a larger compartment and the eukaryotic translation mix in a smaller compartment separated by a dialysis membrane of 9 kDa cut off. Caspase inhibitor was used for improved yields and avoiding protein degradation during the incubation step for 24 h. PolyG nucleotide (30 nucleotides) was used to enhance the CrPV IRES mediated translation. As *hTRPV1* and *mCES2* contain disulphide bridges, prudently the translation is performed only under non-reducing conditions. *mCES2* and *hTRPV1* synthesized in CECF reaction in Fig. 2c and d showed 181 ng μL^{-1} and 85 ng μL^{-1} correspondingly. The synthesized *mCES2* and *hTRPV1* showed a molecular weight of 58 kDa and 98 kDa monomer bands correspondingly in the SDS gel-autoradiogram run under reducing conditions. No protein band was observed in the NTC (Non-Template Control) samples as shown in the autoradiogram in Fig. 2d.

3.2. Validation of synthesized *mCES2* in the microsomal lumen

Carboxylesterases ubiquitously present in the cytosol also result in lysates but it will not aid in calcium imaging as they are present outside the microsomes. The functionality of the *mCES2* synthesized inside the microsomes is assessed using the most commonly used *para*-nitrophenyl acetate (PNPA) method^{21,22} (Fig. 3a–c). The PNPA method is an inexpensive and prompt method to assess the esterase activity. *mCES2* microsomes showed higher activity relative to the NTC microsomes for 1 h PNPA incubation (*p* value = 0.0003, *** unpaired *t* test, two tailed) as shown in Fig. 3a. *mCES2* microsomes also showed higher esterase activity relative to NTC microsomes in substrate dependence (Fig. 3b), time dependence and dose dependence (Fig. 3c, ESI Table 1†) measurements. All the above-mentioned plots showed esterase activity, which was linearly dependent on the *x*-axis parameters.

For calcium dye loading experiments, Fluo-5N AM was used due to its low binding affinity (90 μM in buffer) for Ca^{2+} . The masked negative charge of the dye by the acetoxyethyl ester moiety is unveiled with the aid of *mCES2* inside the microsomes. Dye loading experiments also reveal a similar pattern shown by PNPA assay. *mCES2* microsomes cleaved a significantly higher amount of Fluo-5N AM dye compared to the NTC microsomes when incubated at 5 μM concentration for 1 h as shown in Fig. 3d (*p* value = <0.0001, *** unpaired *t* test, two tailed). The *mCES2* overexpression inside the microsomes significantly enhances the amount of dye loaded and reduces the dye incubation time relative to NTC microsomes as observed in Fig. 3d–f. Both time dependence plot and substrate dependence plot showed a higher amount of dye loaded and cleaved for the AM moiety by *mCES2* microsomes relative to the NTC microsomes, Fig. 3e and f. The dye concentration dependence plot and the time dependence plot both show that the AM-cleaving activity shows a linear profile with the *x*-axis parameters even at 60 min, with 8 μM of the dye, which is

coherent with the expected range of activity for calcium imaging applications.

The activity observed in the NTC microsomes is probably due to the unspecific activity of hydroxylase or a mono-oxygenase class of cytochrome P450 enzymes present in the endoplasmic reticulum.^{23,24}

3.3. Establishment of TED based calcium imaging in microsomes

The K_d of Fluo-5N AM for *Sf21* lysate microsomes was calculated to be 265 μM (Fig. 4a). The experiment was performed by first chelating resting calcium levels in the microsomes by 5 mM EGTA (ethylene glycol-bis(β-aminoethyl ether)-*N,N,N',N'*-tetraacetic acid) and then sequentially increasing the concentration of Ca^{2+} from 0 to 1 mM every step by 100 μM in the presence of 10 μM ionomycin. The binding affinity, K_d of the dye for calcium in the endoplasmic reticulum is usually higher than phosphate buffer saline buffer 90 μM (ref. 25) and varies congruently with expression levels of calcium binding proteins such as calnexin and calreticulin.²⁶ For example, SR vesicles rabbit ventricular myocytes show a K_d of 400 μM (ref. 27) and mouse skeletal muscle SR has a K_d of 133 μM .¹⁴ A change in temperature alters the K_d with a change in the sensitivity range and the fluorescence life time which in turn affects the bleaching rate of the Fluo-5N AM.²⁸ K_d and temperature are inversely related. Hence, all measurements are preferably performed at room temperature.

In order to study the native proteins in microsomes, extensively investigated proteins such as sarcoplasmic reticulum ATPase (SERCA) and ryanodine receptors were choice of interest. In *Sf21* microsomes, SERCA activity was previously recorded with radiolabelled $^{45}\text{Ca}^{2+}$.^{29,30} The typical $[\text{Ca}^{2+}]$ concentration in the ER varies from few μM to mM.³¹ Calcium binding proteins like calreticulin, calnexin, Glucose Regulated Protein 78 (GRP78), glucose regulated protein 94 (GRP94), Endoplasmic Reticulum Protein (ERp72), protein disulphide isomerase, reticulocalbin, and Endoplasmic Reticulum Calcium binding protein 55 (ERC55) act as buffers, causing multiple orders of variation in the $[\text{Ca}^{2+}]$ of the ER due to different individual binding affinities.^{32,33} The free $[\text{Ca}^{2+}]$ in *Sf21* microsomes that undergo CECF translation was estimated to be in the range of 100 to 1000 μM (Fig. 4b) which is coherent with previously reported data in other eukaryotic cells. To avoid artifacts caused by temperature, we preferred to evaluate the increase in Ca^{2+} levels in microsomes at room temperature after treatment of microsomes at 37 °C with ATP. Microsomes treated with 10 mM ATP, 1 mM Mg^{2+} and 200 μM Ca^{2+} for 1 h at 37 °C showed a 4–5 times higher range of luminal Ca^{2+} . The sensitivity range of the dye varies from 0.1 to 100 $\times K_d$. Microsomes treated for SERCA activity showed a median value of 2500 μM (Fig. 4b) which is in accordance with the expected sensitivity range (10^{-7} to 10^2 M Ca^{2+} i.e., 0.1 to 100 $\times K_d$) for fluorescent dyes. Experiments with and without ATP shown in Fig. 4b alone can substantiate the pumping of calcium due to SERCA. Further experiments were performed to see the inhibitory function of thapsigargin, a SERCA inhibitor. 100 nM thapsigargin was



enough to inhibit SERCA activity. For data, refer to ESI Fig. 1.† SERCA activity at room temperature was observed for about 30 min in the presence of 10 mM ATP with a slow increase in microsomal Ca^{2+} (Fig. 4c).

Ryanodine receptors RYR1 and RyR2 perform a plethora of functions in mammalian physiology, ranging from skeletal muscle and cardiac muscle contraction to cognitive functions such as learning and memory. Ryanodine channels that deplete the calcium stores in response to ryanodine are ER resident leak channels. RyRs respond to ryanodine at low concentrations and caffeine. Ryanodine receptors have been extensively investigated in eukaryotic cells.^{34–37} The graph in Fig. 4d presents the calcium response of 100 μM and 10 mM caffeine. 10 mM

caffeine induced a higher calcium efflux relative to 100 μM caffeine. Dantrolene inhibited the calcium release induced by caffeine. For inhibitory experiments using dantrolene, refer to ESI Fig. 2.†

In order to estimate the amount of calcium present in the microsomes, we have used 10 μM ionomycin + 5 mM EGTA for F_{\min} and 10 μM ionomycin + 10 mM Ca^{2+} for F_{\max} in the formula,

$$[\text{Ca}^{2+}] = K_d \times (F - F_{\min})/(F_{\max} - F)$$

The representative graph for calcium concentration determination is shown in Fig. 4e and f. The sensitivity of the Fluo-5N

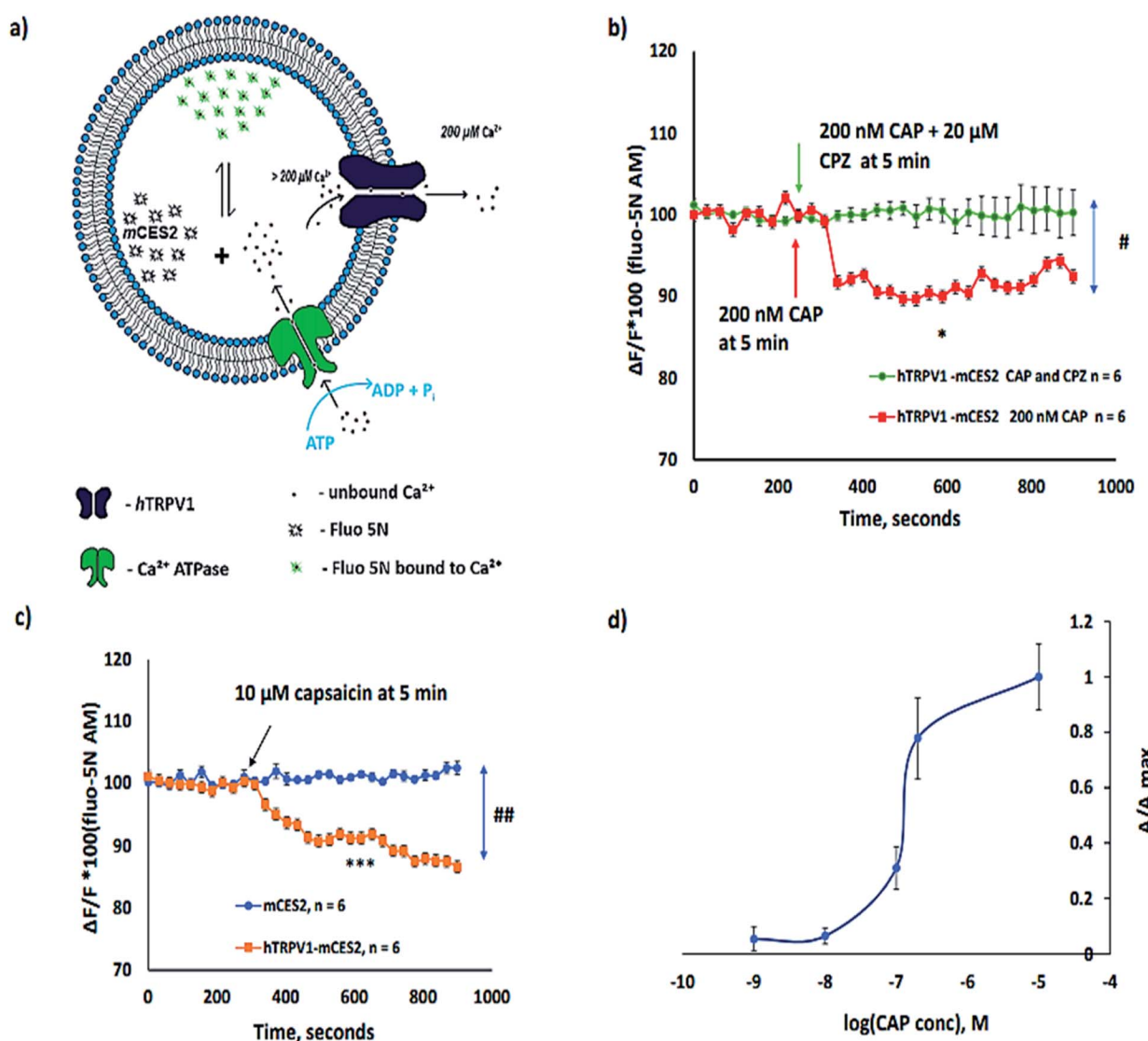


Fig. 5 Functional assessment of cell-free synthesized hTRPV1: (a) illustration of calcium dynamics in microsomes expressed with hTRPV1 and mCES2; (b) capsazepine, CPZ (20 μM), mediated inhibition of calcium release caused by capsaicin, CAP, 200 nM, in hTRPV1-mCES2 microsomes, $n = 6$ each. # indicates the significant difference between two sample groups at 600 s, $p = 0.0121$, unpaired t test, two tailed. * indicates the significant difference of data sets at 150 s and 600 s of 200 nM CAP stimulation, $p = 0.0182$, paired t test, two tailed. (c) Comparison plot of hTRPV1-mCES2 and mCES2 microsomes for 10 μM CAP induced Ca^{2+} release at 5 min from microsomes, $n = 6$ each. No Ca^{2+} release was observed in the mCES2 microsomes. ## indicates the significant difference between two sample groups at 600 s, $p = 0.0043$, Mann-Whitney test, two tailed. *** indicates the significant difference of hTRPV1-mCES2 sample data at 150 s and 600 s, i.e., before and after CAP addition, $p < 0.0001$, paired t test, two tailed; all samples in (b), (c) and (d) were calcium loaded for 60 min at 37 °C using ATP before CAP and CPZ studies. All data in (b) and (c) are presented as $\Delta F/F \times 100$ of the baseline before adding the stimulant; (d) dose dependent response of CAP in hTRPV1-mCES2 microsomes presented as a ratio of area of the curve A/A_{\max} , $n = 4$ to 7 per each data point.



AM can be visually observed and is shown in Fig. 4e, presenting I, II, and III experimental conditions of Fig. 4f. With the depletion of Ca^{2+} in microsomes, a decrease in fluorescence is noted in II and when the buffer is completely exchanged to 10 μM ionomycin + 10 mM Ca^{2+} , a increase in intensity is observed in III as recorded in the ESI video file.[†]

Studying native ER proteins using our method has a couple of advantages: (a) increased signal to noise ratio in microsomes relative to ER in intact cells. As the low affinity AM dyes have to reach the endoplasmic reticulum through the cytosol where the carboxylesterases are abundant, a significant amount of fluorescent dye is cleaved and remains in the cytosol. Despite using low affinity Ca^{2+} indicators, which diminish the sensitivity to cytosolic Ca^{2+} levels, it will still contribute to the large noise relative to signal due to the high amount of cleaved dye present in the cytosol. (b) The flexibility to alter the calcium levels outside the microsomes, to reduce the intrinsic calcium leakage due to the potentiation of Ca^{2+} between the luminal and outer face of the microsomes.³⁸ For all calcium experiments, we used 200 μM calcium in the buffer in order to reduce the spontaneous leakage from microsomes as using 300 nM Ca^{2+} in the buffer caused extensive leakage relatively (ESI Fig. 3[†]).

3.4. Analysis of the cell-free synthesized *hTRPV1* channel

In pursuance of calcium imaging with cell-free synthesized channels, we have chosen a human Transient Receptor Potential Channel, Vanilloid Receptor member 1 (*hTRPV1*), as a model protein and also bovine Transient Receptor Potential Channel, Vanilloid receptor member 3, TRPV3 (ESI Fig. 4[†]). *hTRPV1* expressed in cells in the plasma membrane has been studied for calcium entry into the cytoplasm using Fura 2-AM.^{39,40} *hTRPV1* is largely present in the plasma membrane with a large N terminal and the C terminal that stretches towards the cytosol in cells.

As expected, in cell-free synthesis, the orientation of the protein incorporated in the microsome is opposite to the native plasma membrane orientation. Hence, the cytoplasmic side is outside the microsomes and the extracellular domain is on the side of the microsomal lumen. Both the N-terminal and the C-terminal cytosolic domains of *hTRPV1* are expected to be expressed on the outside of the microsomes during cell-free protein synthesis. Although most of the activators and inhibitors for the TRP channel family are organic membrane permeable compounds, attention should be paid while working with the non-polar activators or inhibitors. It has been reported that TRPV1 expressed both endogenously and heterologously in the ER causes Ca^{2+} release. TRPV1 is expressed in neurons endogenously in the ER and mediates calcium release from the ER which is not Inositol Triphosphate (IP_3) mediated store release.⁴¹ Calcium imaging of TRPV1 overexpression in the ER of *Sf21* and HEK (Human Embryonic Kidney) 293 cells with the KDEL sequence also showed Ca^{2+} release into the cytosol without the aid of IP_3 mediation from the ER.⁴² TRPV1 is also expressed endogenously in the ER of non-excitable cells such as myocytes and cancer cells⁴³ and in human lung cells,⁴⁴ which

also show calcium regulation similar to the overexpression systems in the ER.

All experiments depicted in Fig. 5 are performed after calcium loading into the microsomes for 1 h in order to ensure uniform and higher $[\text{Ca}^{2+}]$ inside the microsomes. The calcium homeostasis in microsomes along with cell-free synthesized ion channels is depicted in Fig. 5a. Under the above-mentioned experimental conditions, we have observed that the activation of the *hTRPV1* caused Ca^{2+} release from *hTRPV1-mCES2* microsomes as shown in Fig. 5b and c. The Ca^{2+} release by 200 nM CAP was abolished completely by 20 μM capsazepine (CPZ) (Fig. 5b). No Ca^{2+} release was observed in *mCES2* samples even at 10 μM CAP (Fig. 5c). Saturation of capsaicin induced Ca^{2+} release was observed even with 200 nM CAP in the *hTRPV1-mCES2* microsomes. The CAP activation profile of cell-free synthesized *hTRPV1* (Fig. 5d) is coherent in the molar range as the cell-based expression.⁴⁵ Presence of phosphatidylinositol 4,5-bisphosphate, (4,5)PIP₂, for the activation of TRP channels has been debated by several researchers.^{46–48} In our work, we have shown that without external (4,5)PIP₂, activation of TRPV1 was feasible. On the other hand, the phenomenon we observe can be supported by the presence of (4,5)PIP₂ in the endoplasmic reticulum and in the cytosol.^{48–50}

4 Conclusion and outlook

In conclusion, our work is promising to enhance the following areas of research: (a) to probe other ions such as Cl^- , Mg^{2+} and K^+ using AM-based indicators, (b) to study native channels present in the ER membrane by direct ion-sensitive dye imaging of the lumen, (c) drug toxicity studies in microsomes – environmental toxicologists and pharmacologists investigate microsomal Ca^{2+} levels to estimate the cell toxicity. Ca^{2+} release by microsomes caused by drug or drug metabolites is the direct indicator of cell toxicity succumbing to higher cytosolic Ca^{2+} that triggers apoptosis,^{51–54} (d) potentially it could be used further to develop High Throughput Screening (HTS) for drugs in CFPS platforms for ion permeable proteins that include different families of ion channels, pumps and exchangers. When converted into an HTS assay, the characteristics of the assay will also be changed apparently. For example, it is expected that the spatial resolution of observed calcium or the sensitivity of calcium dye which we observe in confocal microscopy will be reduced in an HTS assay in the microplate. But an HTS platform comes with other advantages such as reduced imaging time and high turnover of measured samples in a short time.⁵⁵ In summary, in order to cope up with the sustenance needs of the above-mentioned areas, cell-free synthesized carboxylesterases could be a viable calcium imaging platform in microsomes, thereby overcoming the conventional disadvantages of cell-based protein synthesis.

Author contributions

PD and SK have framed the basic idea for this work. DAW was responsible for the production and quality control of the cell-



free lysates used in this manuscript. AZ, DB, SD, PD and SK have performed all experiments and analysis of the data. PD, SD and SK have contributed to the preparation of the manuscript. SM has provided his decades long expertise in calcium imaging and corrected the manuscript.

Conflicts of interest

The authors declare no conflicts of interest.

Acknowledgements

This work was supported by German Ministry of Education and Research, BMBF (BMBF, No. 031B0078A). We would like to appreciate Dr Rita Sachse for her preliminary attempts in this topic during her Ph.D. thesis in our lab. We would like to acknowledge Ms Dana Wenzel (Fraunhofer IZI, Potsdam-Golm, Germany) for technical support and Dr Lena Thoring and Dr Marlitt Stech (Fraunhofer IZI, Potsdam-Golm, Germany) for providing their insights and discussion in the cell-free synthesis platform in due course of this research work. We would also like to thank Dr Michael Kirschbaum for helping us with the imaging platforms.

References

- R. Santos, O. Ursu, A. Gaulton, A. P. Bento, R. S. Donadi, C. G. Bologa, *et al.*, A comprehensive map of molecular drug targets, *Nat. Rev. Drug Discovery*, 2017, **16**(1), 19–34.
- A. Zemella, L. Thoring, C. Hoffmeister and S. Kubick, Cell-Free Protein Synthesis: Pros and Cons of Prokaryotic and Eukaryotic Systems, *ChemBioChem*, 2015, **16**(17), 2420–2431.
- R. Sachse, S. K. Dondapati, S. F. Fenz, T. Schmidt and S. Kubick, Membrane protein synthesis in cell-free systems: from bio-mimetic systems to bio-membranes, *FEBS Lett.*, 2014, **588**(17), 2774–2781.
- S. K. Dondapati, M. Stech, A. Zemella and S. Kubick, Cell-Free Protein Synthesis: A Promising Option for Future Drug Development, *BioDrugs*, 2020, **34**(3), 327–348.
- D. Burdakov, O. H. Petersen and A. Verkhratsky, Intraluminal calcium as a primary regulator of endoplasmic reticulum function, *Cell Calcium*, 2005, **38**(3–4), 303–310.
- A. Raffaello, C. Mammucari, G. Gherardi and R. Rizzuto, Calcium at the Center of Cell Signaling: Interplay between Endoplasmic Reticulum, Mitochondria, and Lysosomes, *Trends Biochem. Sci.*, 2016, **41**(12), 1035–1049.
- C. Betzer, L. B. Lassen, A. Olsen, R. H. Kofoed, L. Reimer, E. Gregersen, J. Zheng, T. Calì, W. P. Gai, T. Chen, A. Moeller, M. Brini, Y. Fu, G. Halliday, T. Brudek, S. Aznar, B. Pakkenberg, J. P. Andersen, P. H. Jensen, *et al.*, Alpha-synuclein aggregates activate calcium pump SERCA leading to calcium dysregulation, *EMBO Rep.*, 2018, **19**(5), e44617.
- D. C. McMullen, W. S. Kean, A. Verma, J. T. Cole and W. D. Watson, A microplate technique to simultaneously assay calcium accumulation in endoplasmic reticulum and SERCA release of inorganic phosphate, *Biol. Proced. Online*, 2012, **14**(1), 4.
- L. Navazio, M. A. Bewell, A. Siddiqua, G. D. Dickinson, A. Galione and D. Sanders, Calcium release from the endoplasmic reticulum of higher plants elicited by the NADP metabolite nicotinic acid adenine dinucleotide phosphate, *Proc. Natl. Acad. Sci. U. S. A.*, 2000, **97**(15), 8693–8698.
- A. N. K. Yusufi, J. Cheng, M. A. Thompson, J. C. Burnett and J. P. Grande, Differential mechanisms of Ca(2+) release from vascular smooth muscle cell microsomes, *Exp. Biol. Med.*, 2002, **227**(1), 36–44.
- R. Giunti, A. Gamberucci, R. Fulceri, G. Bánhegyi and A. Benedetti, Both translocon and a cation channel are involved in the passive Ca²⁺ leak from the endoplasmic reticulum: a mechanistic study on rat liver microsomes, *Arch. Biochem. Biophys.*, 2007, **462**(1), 115–121.
- H. M. Dusza, P. H. Cenijn, J. H. Kamstra, R. H. S. Westerink, P. E. G. Leonards and T. Hamers, Effects of environmental pollutants on calcium release and uptake by rat cortical microsomes, *Neurotoxicology*, 2018, **69**, 266–277.
- S. Samtleben, J. Jaepel, C. Fecher, T. Andreska, M. Rehberg and R. Blum, Direct imaging of ER calcium with targeted-esterase induced dye loading (TED), *J. Visualized Exp.*, 2013, (75), e50317.
- M. Rehberg, A. Lepier, B. Solchenberger, P. Osten and R. Blum, A new non-disruptive strategy to target calcium indicator dyes to the endoplasmic reticulum, *Cell Calcium*, 2008, **44**(4), 386–399.
- R. Blum, O. H. Petersen and A. Verkhratsky, Ca²⁺ Imaging of Intracellular Organelles: Endoplasmic Reticulum, in *Calcium Measurement Methods [Internet]*, ed. A. Verkhratsky and O. H. Petersen, Humana Press, Totowa, NJ, 2010, pp. 147–67, (Neuromethods), DOI: 10.1007/978-1-60761-476-0_8.
- M. Stech, A. K. Brödel, R. B. Quast, R. Sachse and S. Kubick, Cell-free systems: functional modules for synthetic and chemical biology, *Adv. Biochem. Eng./Biotechnol.*, 2013, **137**, 67–102.
- A. Zemella, S. Grossmann, R. Sachse, A. Sonnabend, M. Schaefer and S. Kubick, Qualifying a eukaryotic cell-free system for fluorescence based GPCR analyses, *Sci. Rep.*, 2017, **7**(1), 3740.
- A. K. Brödel, A. Sonnabend, L. O. Roberts, M. Stech, D. A. Wüstenhagen and S. Kubick, IRES-mediated translation of membrane proteins and glycoproteins in eukaryotic cell-free systems, *PLoS One*, 2013, **8**(12), e82234.
- M. Stech, R. B. Quast, R. Sachse, C. Schulze, D. A. Wüstenhagen and S. Kubick, A continuous-exchange cell-free protein synthesis system based on extracts from cultured insect cells, *PLoS One*, 2014, **9**(5), e96635.
- R. B. Quast, A. Sonnabend, M. Stech, D. A. Wüstenhagen and S. Kubick, High-yield cell-free synthesis of human EGFR by IRES-mediated protein translation in a continuous exchange cell-free reaction format, *Sci. Rep.*, 2016, **6**, 30399.



- 21 D. Gilham and R. Lehner, Techniques to measure lipase and esterase activity in vitro, *Methods*, 2005, **36**(2), 139–147.
- 22 Y. Zhu, J. Li, H. Cai, H. Ni, A. Xiao and L. Hou, Characterization of a new and thermostable esterase from a metagenomic library, *Microbiol. Res.*, 2013, **168**(9), 589–597.
- 23 A. R. B. do Nascimento, P. Fresia, F. L. Cônsmoli and C. Omoto, Comparative transcriptome analysis of lufenuron-resistant and susceptible strains of *Spodoptera frugiperda* (Lepidoptera: Noctuidae), *BMC Genomics*, 2015, **16**, 985.
- 24 M. Giraudo, F. Hilliou, T. Fricaux, P. Audant, R. Feyereisen and G. Le Goff, Cytochrome P450s from the fall armyworm (*Spodoptera frugiperda*): responses to plant allelochemicals and pesticides, *Insect Mol. Biol.*, 2015, **24**(1), 115–128.
- 25 R. M. Paredes, J. C. Etzler, L. T. Watts, W. Zheng and J. D. Lechleiter, Chemical calcium indicators, *Methods*, 2008, **46**(3), 143–151.
- 26 J. J. Caramelo and A. J. Parodi, Getting in and out from calnexin/calreticulin cycles, *J. Biol. Chem.*, 2008, **283**(16), 10221–10225.
- 27 T. R. Shannon, T. Guo and D. M. Bers, Ca²⁺ scraps: local depletions of free [Ca²⁺] in cardiac sarcoplasmic reticulum during contractions leave substantial Ca²⁺ reserve, *Circ. Res.*, 2003, **93**(1), 40–45.
- 28 A. E. Oliver, G. A. Baker, R. D. Fugate, F. Tablin and J. H. Crowe, Effects of temperature on calcium-sensitive fluorescent probes, *Biophys. J.*, 2000, **78**(4), 2116–2126.
- 29 J. M. Autry and L. R. Jones, Functional Co-expression of the canine cardiac Ca²⁺ pump and phospholamban in *Spodoptera frugiperda* (Sf21) cells reveals new insights on ATPase regulation, *J. Biol. Chem.*, 1997, **272**(25), 15872–15880.
- 30 D. L. Winters, J. M. Autry, B. Svensson and D. D. Thomas, Interdomain fluorescence resonance energy transfer in SERCA probed by cyan-fluorescent protein fused to the actuator domain, *Biochemistry*, 2008, **47**(14), 4246–4256.
- 31 J. Meldolesi and T. Pozzan, The endoplasmic reticulum Ca²⁺ store: a view from the lumen, *Trends Biochem. Sci.*, 1998, **23**(1), 10–14.
- 32 D. Prins and M. Michalak, Organellar calcium buffers, *Cold Spring Harbor Perspect. Biol.*, 2011, **3**(3), a004069.
- 33 M. Michalak, J. M. Robert Parker and M. Opas, Ca²⁺ signaling and calcium binding chaperones of the endoplasmic reticulum, *Cell Calcium*, 2002, **32**(5–6), 269–278.
- 34 A. Uehara, T. Murayama, M. Yasukochi, M. Fill, M. Horie, T. Okamoto, *et al.*, Extensive Ca²⁺ leak through K4750Q cardiac ryanodine receptors caused by cytosolic and luminal Ca²⁺ hypersensitivity, *J. Gen. Physiol.*, 2017, **149**(2), 199–218.
- 35 E. Camors and H. H. Valdivia, CaMKII regulation of cardiac ryanodine receptors and inositol triphosphate receptors, *Front. Pharmacol.*, 2014, **5**, 101.
- 36 M. Fill and J. A. Copello, Ryanodine receptor calcium release channels, *Physiol. Rev.*, 2002, **82**(4), 893–922.
- 37 O. Vázquez-Martínez, R. Cañedo-Merino, M. Díaz-Muñoz and J. R. Riesgo-Escovar, Biochemical characterization, distribution and phylogenetic analysis of *Drosophila melanogaster* ryanodine and IP₃ receptors, and thapsigargin-sensitive Ca²⁺ ATPase, *J. Cell Sci.*, 2003, **116**(Pt 12), 2483–2494.
- 38 Y. Kunitomo and D. Terentyev, How to stop the fire? Control of Ca²⁺-induced Ca²⁺ release in cardiac muscle, *J. Physiol.*, 2011, **589**(Pt 24), 5899–5900.
- 39 I. Vetter, B. D. Wyse, G. R. Monteith, S. J. Roberts-Thomson and P. J. Cabot, The mu opioid agonist morphine modulates potentiation of capsaicin-evoked TRPV1 responses through a cyclic AMP-dependent protein kinase A pathway, *Mol. Pain*, 2006, **2**, 22.
- 40 E. R. Grant, A. E. Dubin, S.-P. Zhang, R. A. Zivin and Z. Zhong, Simultaneous intracellular calcium and sodium flux imaging in human vanilloid receptor 1 (VR1)-transfected human embryonic kidney cells: a method to resolve ionic dependence of VR1-mediated cell death, *J. Pharmacol. Exp. Ther.*, 2002, **300**(1), 9–17.
- 41 X.-P. Dong, X. Wang and H. Xu, TRP channels of intracellular membranes, *J. Neurochem.*, 2010, **113**(2), 313–328.
- 42 B. J. Wisnoskey, W. G. Sinkins and W. P. Schilling, Activation of vanilloid receptor type I in the endoplasmic reticulum fails to activate store-operated Ca²⁺ entry, *Biochem. J.*, 2003, **372**(Pt 2), 517–528.
- 43 A. Hastrate, N. Prevarskaya and V. Lehen'kyi, Role of the TRPV Channels in the Endoplasmic Reticulum Calcium Homeostasis, *Cells*, 2020, **9**(2), 317.
- 44 K. C. Thomas, A. S. Sabinis, M. E. Johansen, D. L. Lanza, P. J. Moos, G. S. Yost, *et al.*, Transient receptor potential vanilloid 1 agonists cause endoplasmic reticulum stress and cell death in human lung cells, *J. Pharmacol. Exp. Ther.*, 2007, **321**(3), 830–838.
- 45 E. N. Senning, M. D. Collins, A. Stratievska, C. A. Ufret-Vincenty and S. E. Gordon, Regulation of TRPV1 ion channel by phosphoinositide (4,5)-bisphosphate: the role of membrane asymmetry, *J. Biol. Chem.*, 2014, **289**(16), 10999–11006.
- 46 S. Brauchi, G. Orta, C. Mascayano, M. Salazar, N. Raddatz, H. Urbina, *et al.*, Dissection of the components for PIP₂ activation and thermosensation in TRP channels, *Proc. Natl. Acad. Sci. U. S. A.*, 2007, **104**(24), 10246–10251.
- 47 T. Rohacs, B. Thyagarajan and V. Lukacs, Phospholipase C mediated modulation of TRPV1 channels, *Mol. Neurobiol.*, 2008, **37**(2–3), 153–163.
- 48 S. Kolay, U. Basu and P. Raghu, Control of diverse subcellular processes by a single multi-functional lipid phosphatidylinositol 4,5-bisphosphate [PI(4,5)P₂], *Biochem. J.*, 2016, **473**(12), 1681–1692.
- 49 G. R. V. Hammond, G. Schiavo and R. F. Irvine, Immunocytochemical techniques reveal multiple, distinct cellular pools of PtdIns4P and PtdIns(4,5)P₂, *Biochem. J.*, 2009, **422**(1), 23–35.
- 50 M. Schramp, A. Hedman, W. Li, X. Tan and R. Anderson, PIP kinases from the cell membrane to the nucleus, *Subcell. Biochem.*, 2012, **58**, 25–59.



- 51 S. Pentyala, J. Ruggeri, A. Veerraju, Z. Yu, A. Bhatia, D. Desaiah, *et al.*, Microsomal Ca^{2+} flux modulation as an indicator of heavy metal toxicity, *Indian J. Exp. Biol.*, 2010, **48**(7), 737–743.
- 52 D. A. Stoyanovsky and A. I. Cederbaum, Metabolites of acetaminophen trigger Ca^{2+} release from liver microsomes, *Toxicol. Lett.*, 1999, **106**(1), 23–29.
- 53 C. G. Coburn, M. C. Currás-Collazo and P. R. S. Kodavanti, In vitro effects of environmentally relevant polybrominated diphenyl ether (PBDE) congeners on calcium buffering mechanisms in rat brain, *Neurochem. Res.*, 2008, **33**(2), 355–364.
- 54 P. R. S. Kodavanti and T. R. Ward, Differential effects of commercial polybrominated diphenyl ether and polychlorinated biphenyl mixtures on intracellular signaling in rat brain in vitro, *Toxicol. Sci.*, 2005, **85**(2), 952–962.
- 55 N. J. Martinez, S. A. Titus, A. K. Wagner and A. Simeonov, High throughput fluorescence imaging approaches for drug discovery using in vitro and in vivo three-dimensional models, *Expert Opin. Drug Discovery*, 2015, **10**, 1347–1361.



SUPPLEMENTARY DATA:

		mCES2 samples					
		30 ng		60 ng		120 ng	
Time (sec)	average	S.E.M	average	S.E.M	average	S.E.M	
0	0.000000	0.000000	0.000000	0.000000	0.000000	0.000000	
10	0.025467	0.000720	0.051200	0.002265	0.097800	0.003859	
20	0.043867	0.001785	0.093000	0.002868	0.167533	0.004907	
30	0.062200	0.003559	0.120333	0.001785	0.211867	0.006706	
40	0.082533	0.000720	0.145667	0.013411	0.289200	0.003266	
50	0.102000	0.001633	0.171267	0.014350	0.329000	0.005354	
60	0.101467	0.000544	0.201867	0.014631	0.340467	0.001361	
NTC samples							
		30 ng		60 ng		120 ng	
Time (sec)	average	S.E.M	average	S.E.M	average	S.E.M	
0	0.000000	0.000000	0.000000	0.000000	0.000000	0.000000	
10	0.015133	0.002880	0.023467	0.005761	0.069133	0.001515	
20	0.029200	0.001247	0.064200	0.003399	0.131867	0.004481	
30	0.037867	0.003954	0.091533	0.001785	0.176867	0.003839	
40	0.054867	0.004119	0.118867	0.004907	0.231533	0.003067	
50	0.077333	0.003839	0.143667	0.004380	0.284333	0.002373	
60	0.072800	0.000817	0.153467	0.005664	0.306467	0.003345	

Table 1: Esterase activity of mCES2 (mouse Carboxyl Esterase 2) and NTC (Non-Template Control) samples using PNPA method. Data table of Fig 3 c representing time dependent and dose-dependent curve shown above as absorbance at 410 nm, n=3.

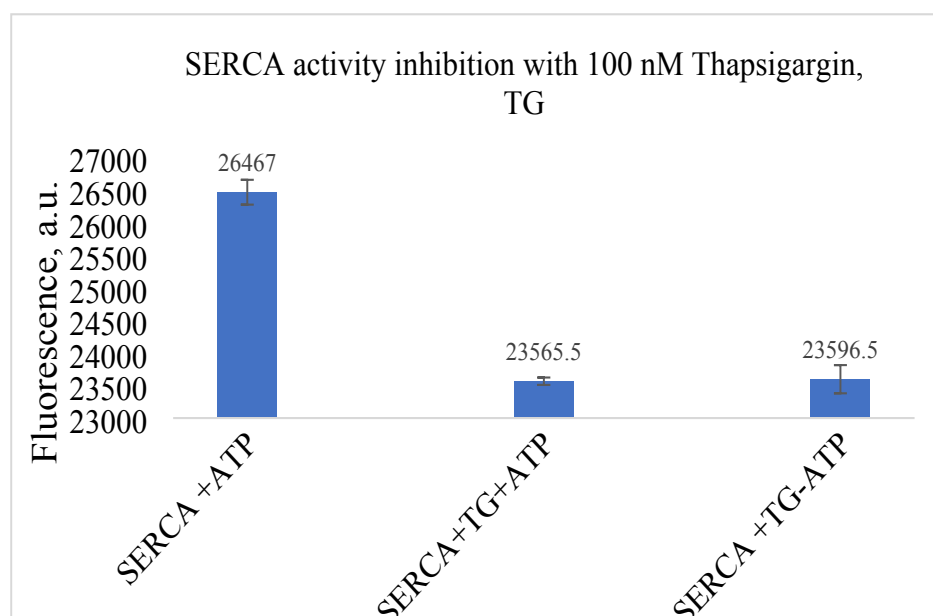


Figure1: SERCA activity measured by fluorescence spectroscopy: Fluorescence activity measured with the *mCES2* microsomes pre-loaded with Ca²⁺ under different experimental conditions. SERCA activity in the presence of ATP (SERCA + ATP), SERCA activity in the presence of TG and ATP (SERCA + TG+ATP) and SERCA activity measured in the presence of 100 nM TG without any ATP (SERCA+TG-ATP), n=2, 10 µg of *mCES2* protein each well, data represented mean +/- S.E.M. Clear inhibition of SERCA activity is observed with TG in samples with and without ATP.

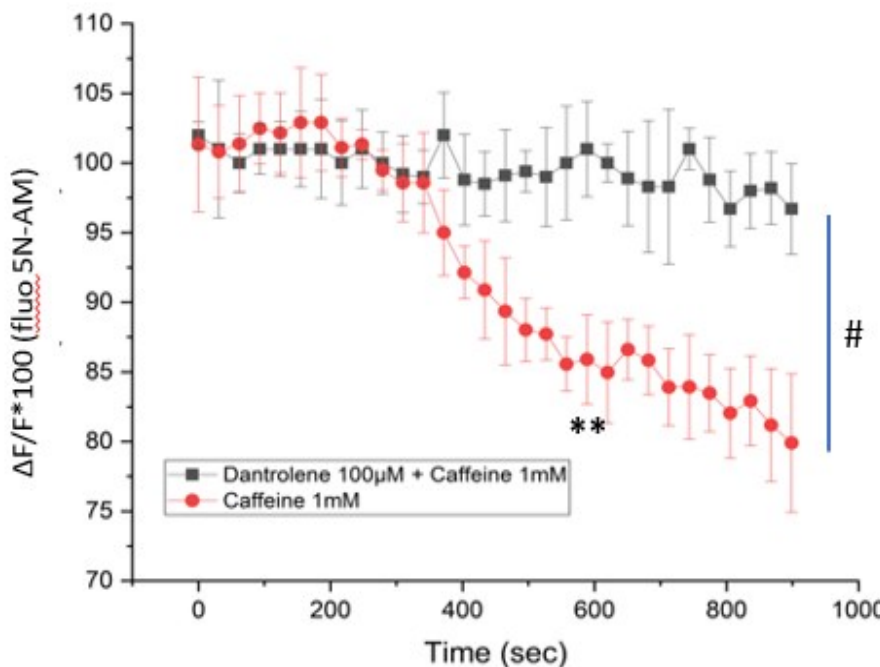


Figure 2: Inhibitory effects of dantrolene on caffeine induced calcium release via ryanodine receptor (RyR2) activation in *mCES2* microsomes, n=5 each. ** indicate significant difference of caffeine sample dataset before (150 s) and after adding caffeine (600 sec) with p value = 0.002, paired t test, two tailed. # indicate the significant difference between the two sample groups at 600 sec with p value = 0.0159, Mann Whitney test, two tailed. The fluorescence value is represented as $\Delta F/F * 100$ of Fluo 5N-AM +/- S.E.M. All the samples were calcium loaded with ATP for 60 min, 37°C prior to caffeine and dantrolene experiments. For caffeine experiments, 1 mM caffeine was used for activation of ryanodine channel at 5 min. For inhibition experiments, the samples were pre-incubated with dantrolene minimum 20 min prior to start of the experiments and also additionally maintained in the baseline buffer from time 0 to 5 min. No calcium release induced by caffeine added at 5 min was observed in samples in the presence of dantrolene.

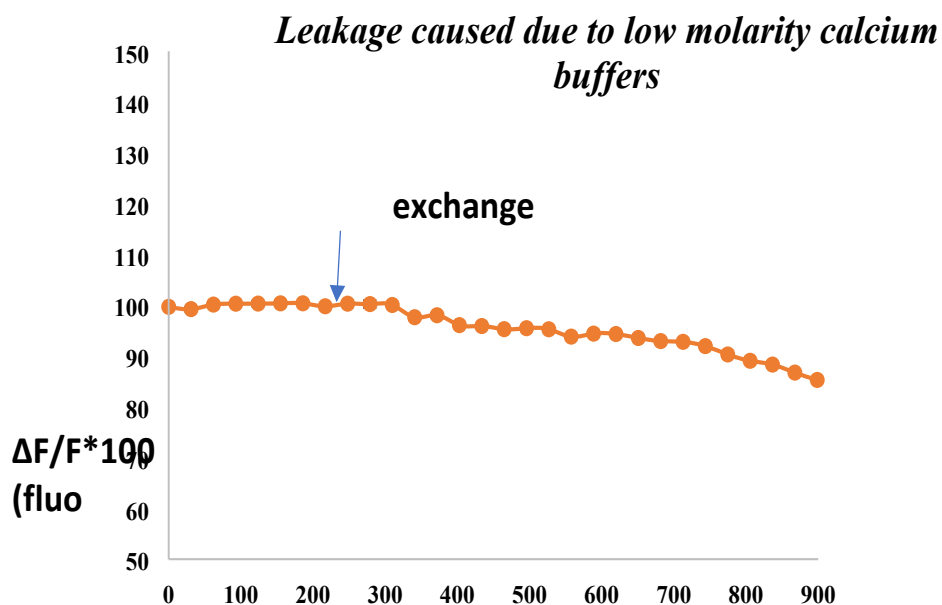


Fig3: Gradual leakage caused due to change in the buffer from 200 μM to 300 nM Ca^{2+} , n=5; data represented mean +/- S.E.M.

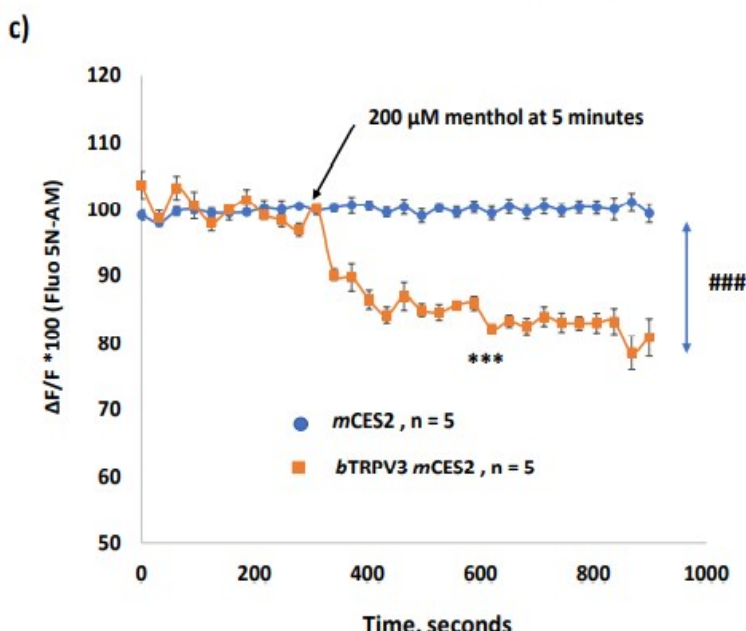
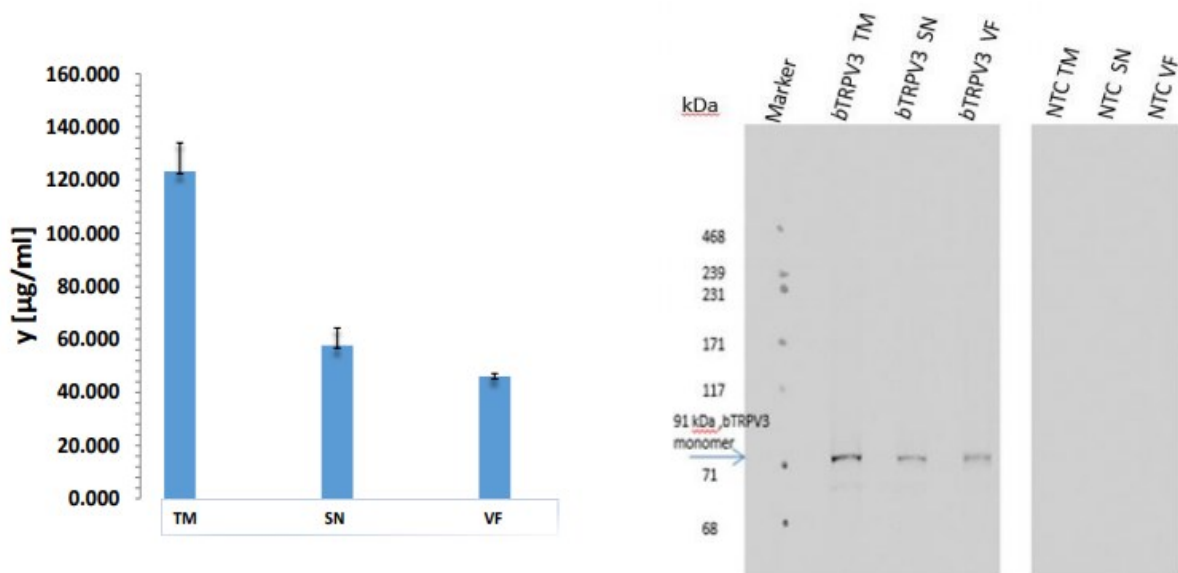
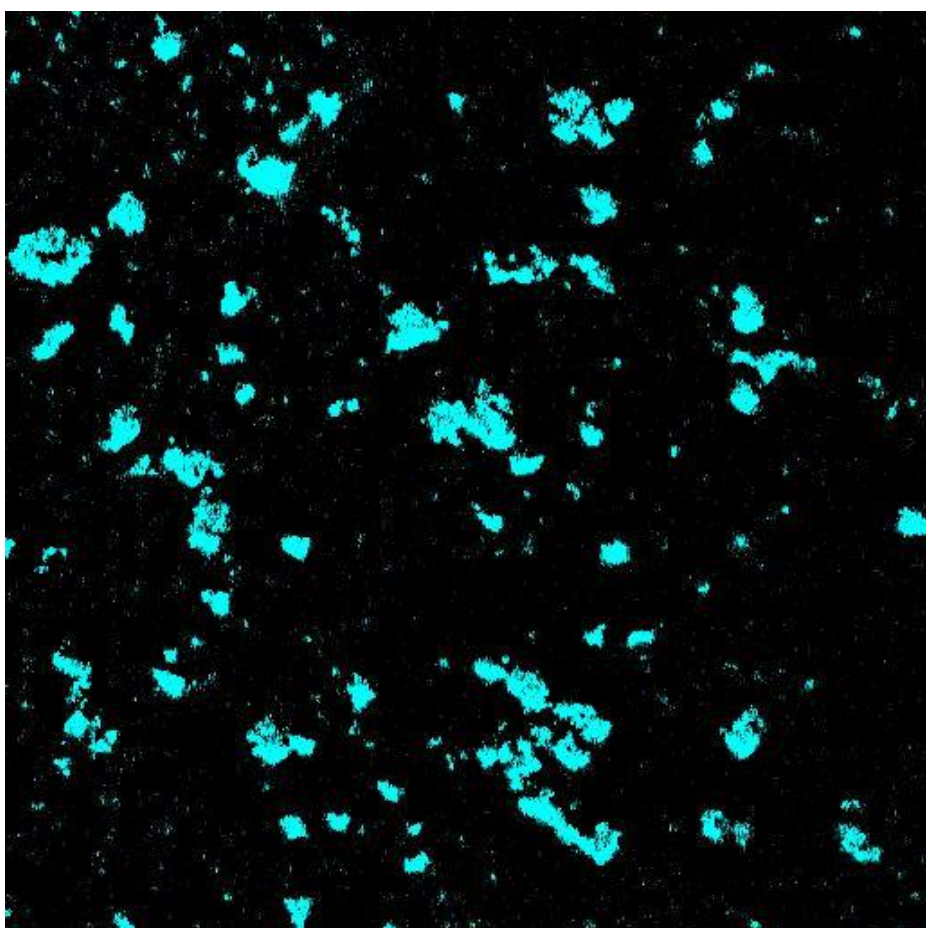


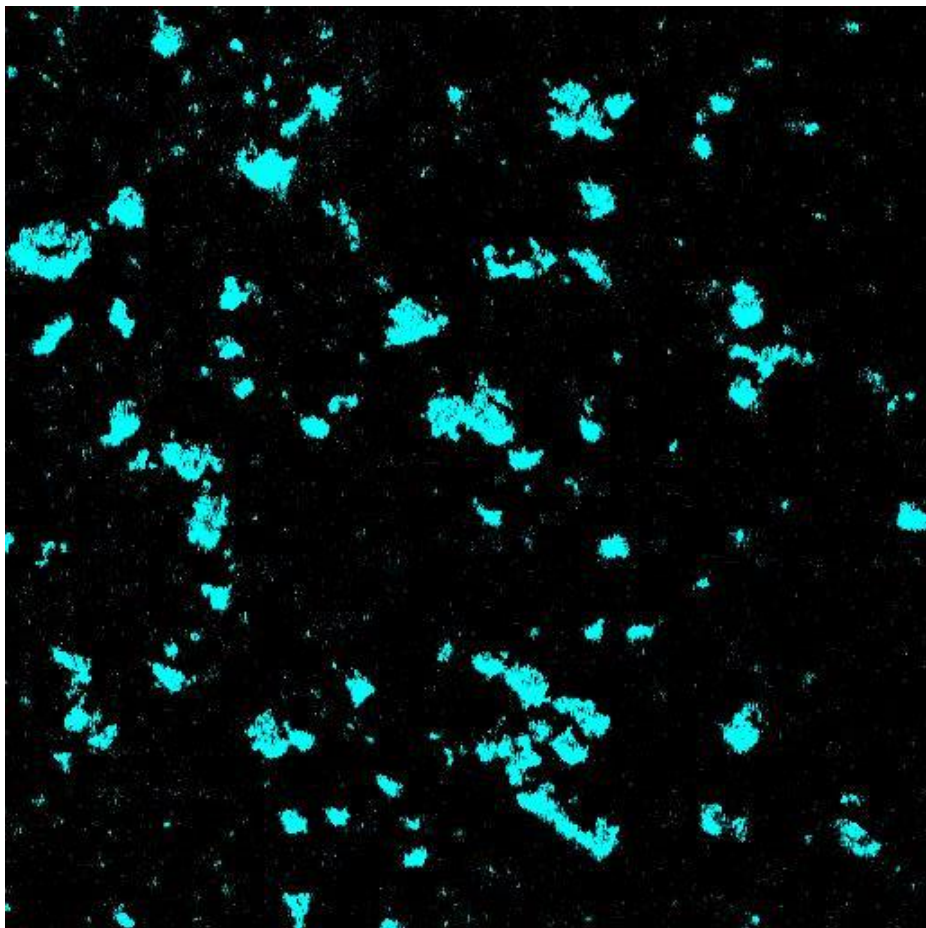
Fig 4: a) Protein yields of *bTRPV3*, bovine Transient Receptor Potential Channel Vanilloid Receptor member 3. by scintillation counting via CECF reaction for 24 h, 27 °C in *Sf21* system; suspension and pellet correspond to translation mix and vesicular fraction correspondingly. The plasmid construct was similar to *hTRPV1* construct as mentioned in this work. Data is represented as mean+/- S.E.M, n = 3, TM- Translation mix, SN- Supernatant, VF- Vesicular fraction. b) Autoradiogram of proteins run on SDS MES gel, no band was observed in Non-template Control microsomes and 91 kDa protein was observed in *bTRPV3* samples; c) Calcium imaging of *mCES2* and *bTRPV3-mCES2* cell-free synthesized microsomes with menthol, 200 µM for activation of *bTRPV3* functionality. Ca²⁺ release was observed only in *bTRPV3-mCES2* microsomes, data is represented as $\Delta F/F *100$ +/- S.E.M, of dye fluorescence, n=5 each. #### indicate the significant difference between the *mCES2* samples and *bTRPV3-mCES2* samples at 600 s, p value < 0.0001, unpaired t test, two tailed. *** indicate the significant difference of *bTRPV3-mCES2* sample data at 150 s and 600 s, before and after menthol addition, p < 0.0001, Paired t test, two tailed.

Supplementary video data

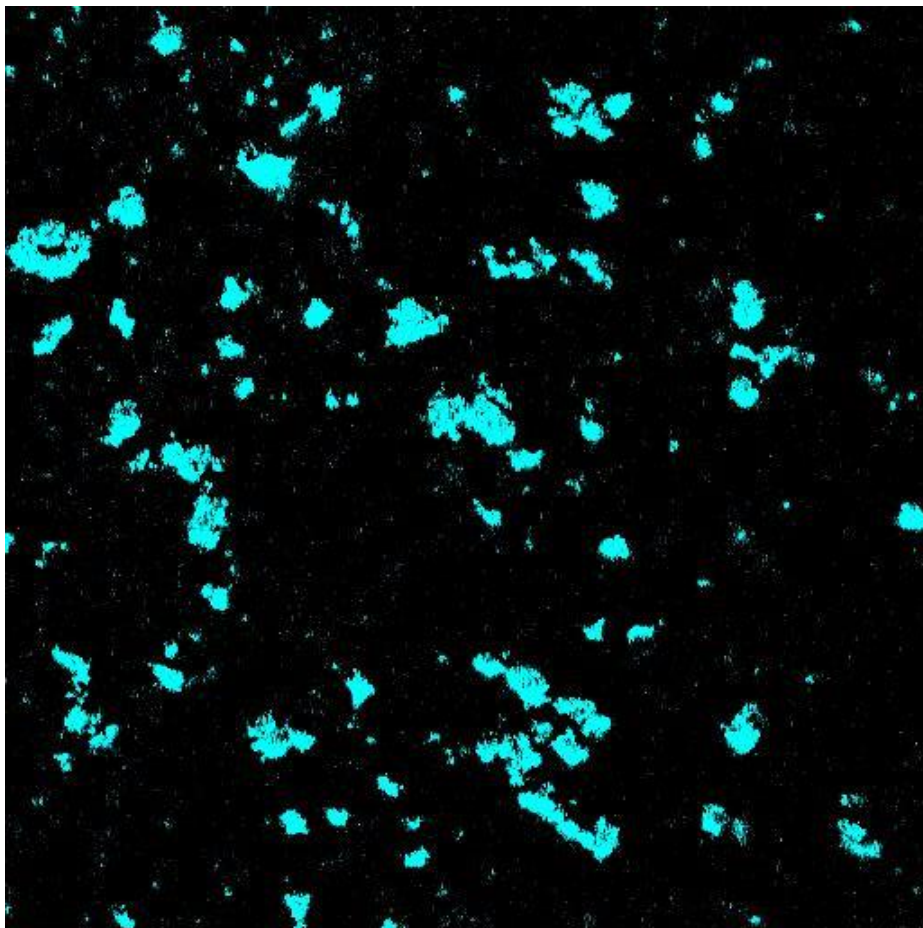
Video Series Fig 1



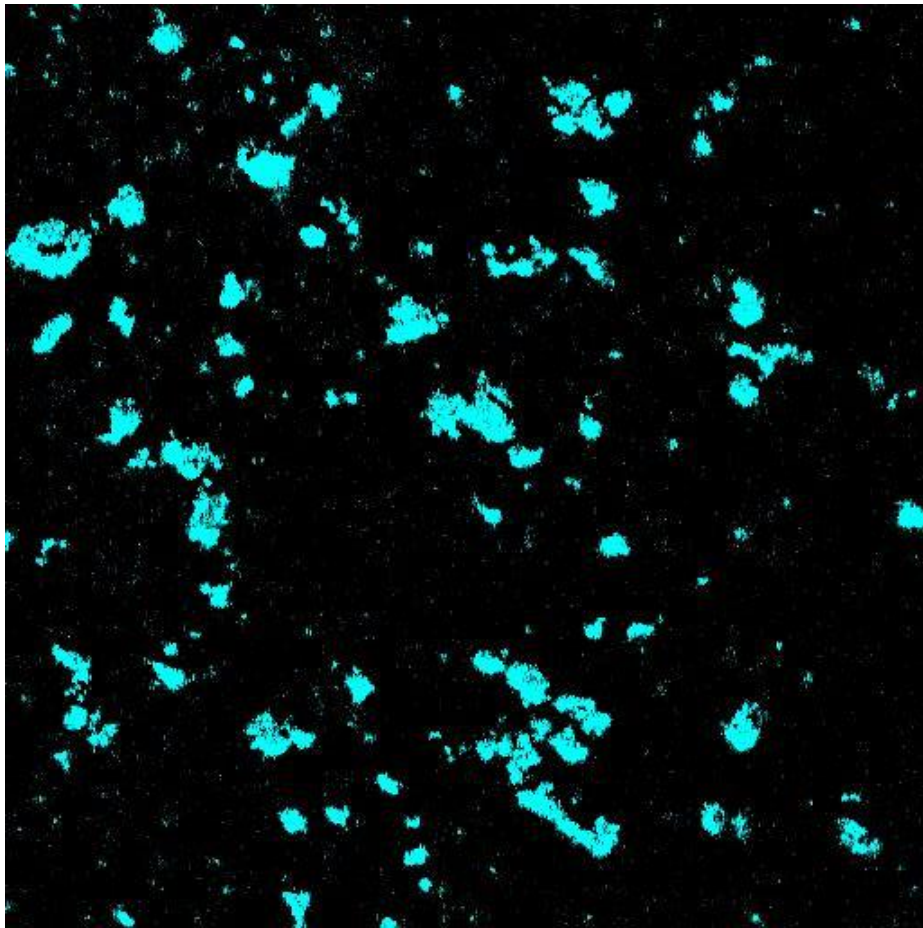
Video Series Fig 2



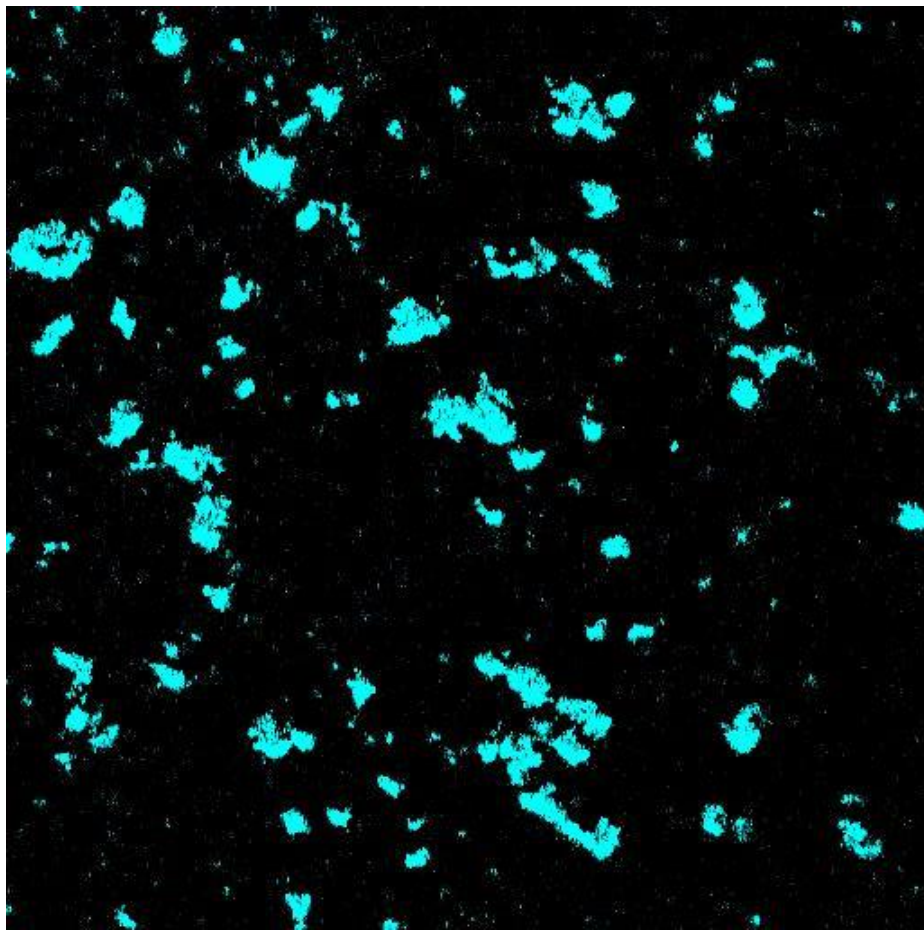
Video Series Fig 3



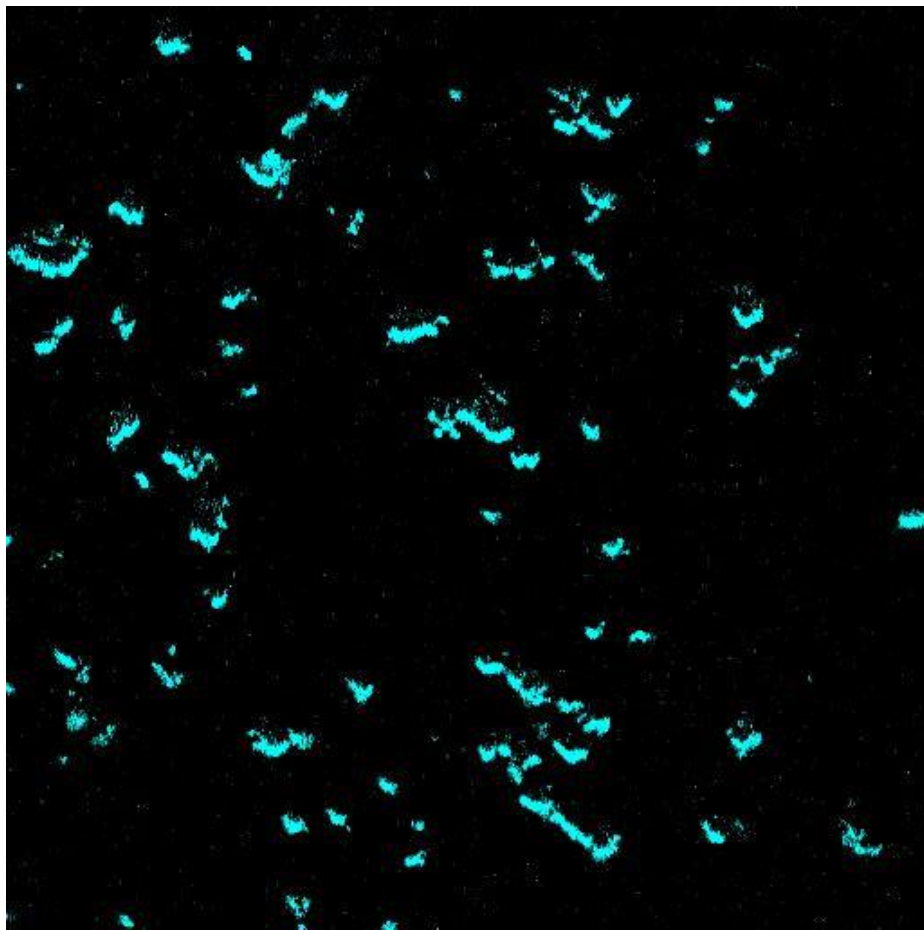
Video Series Fig 4



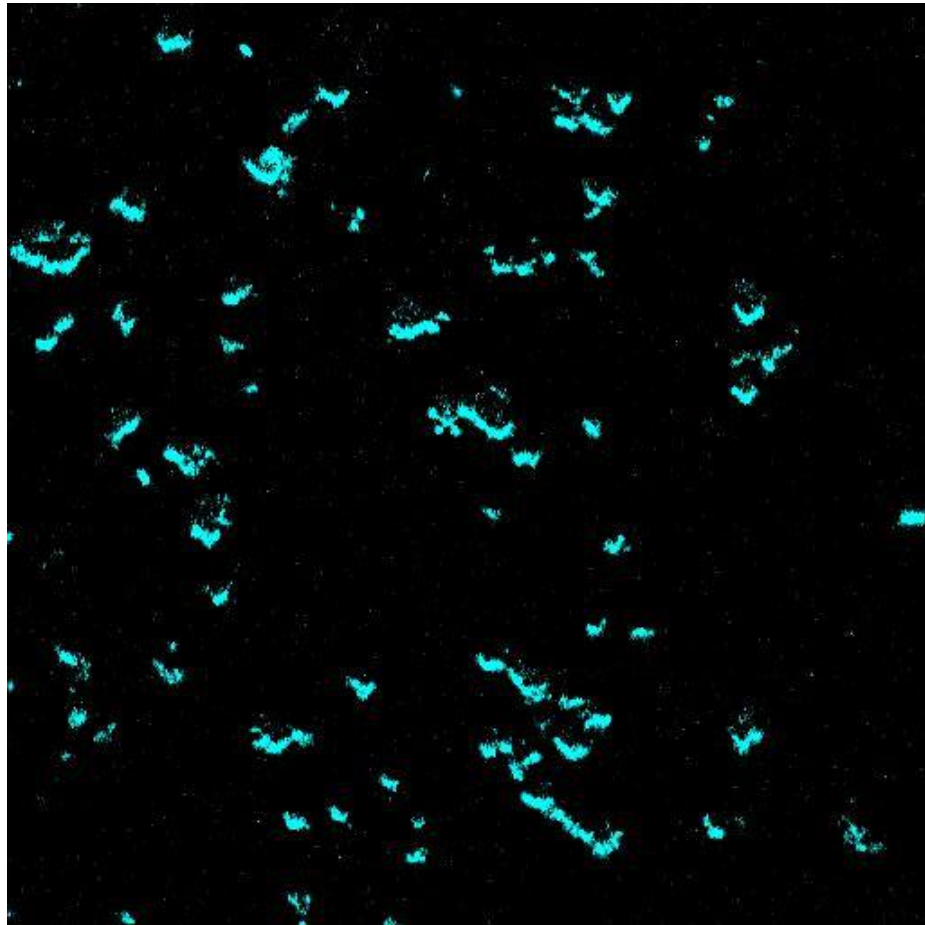
Video Series Fig 5



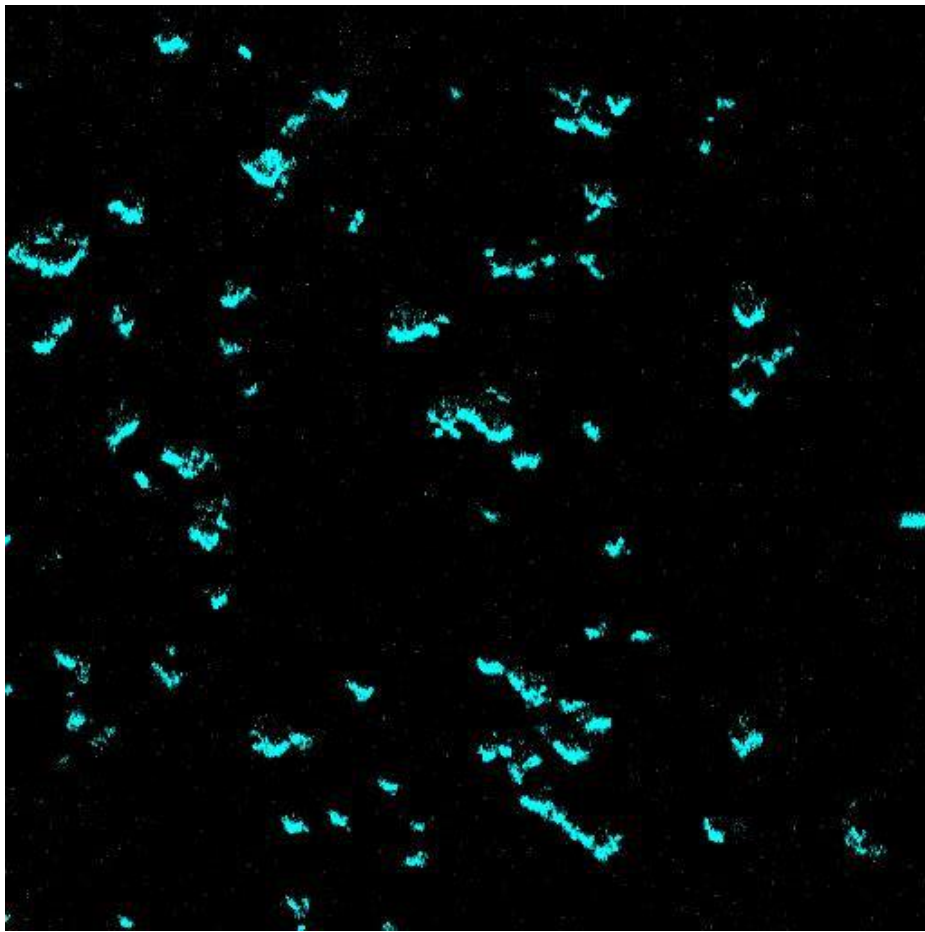
Video Series Fig 6



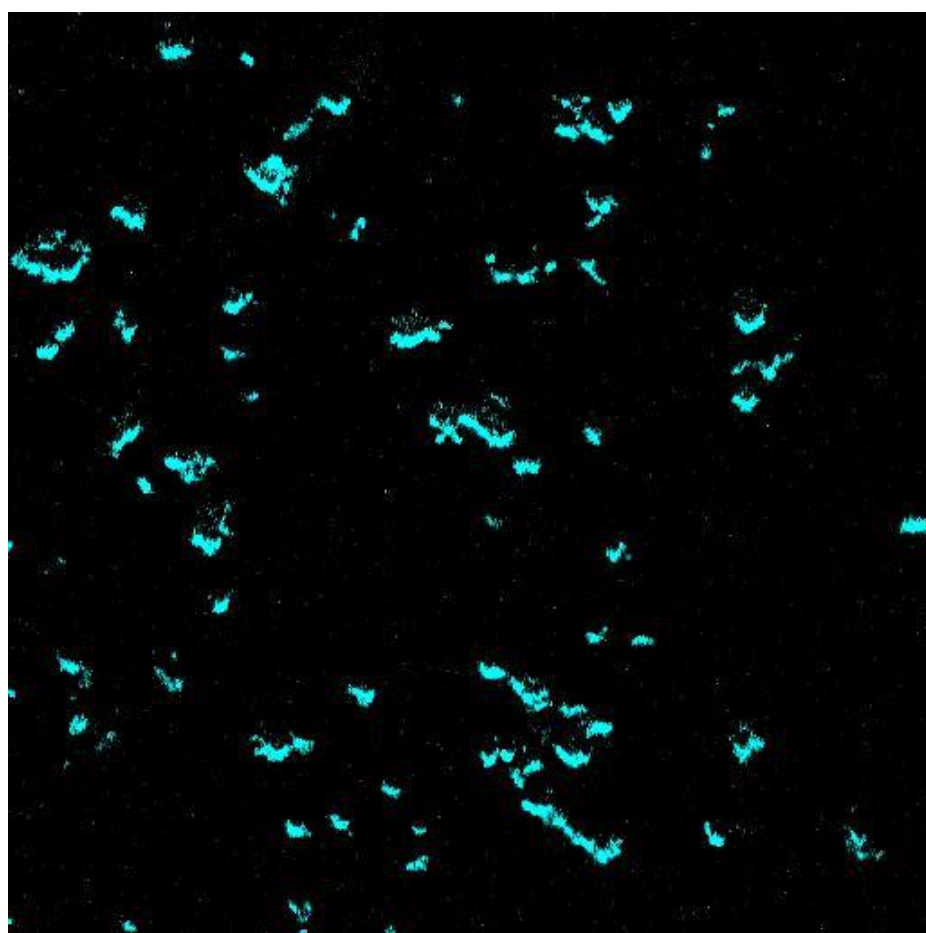
Video Series Fig 7



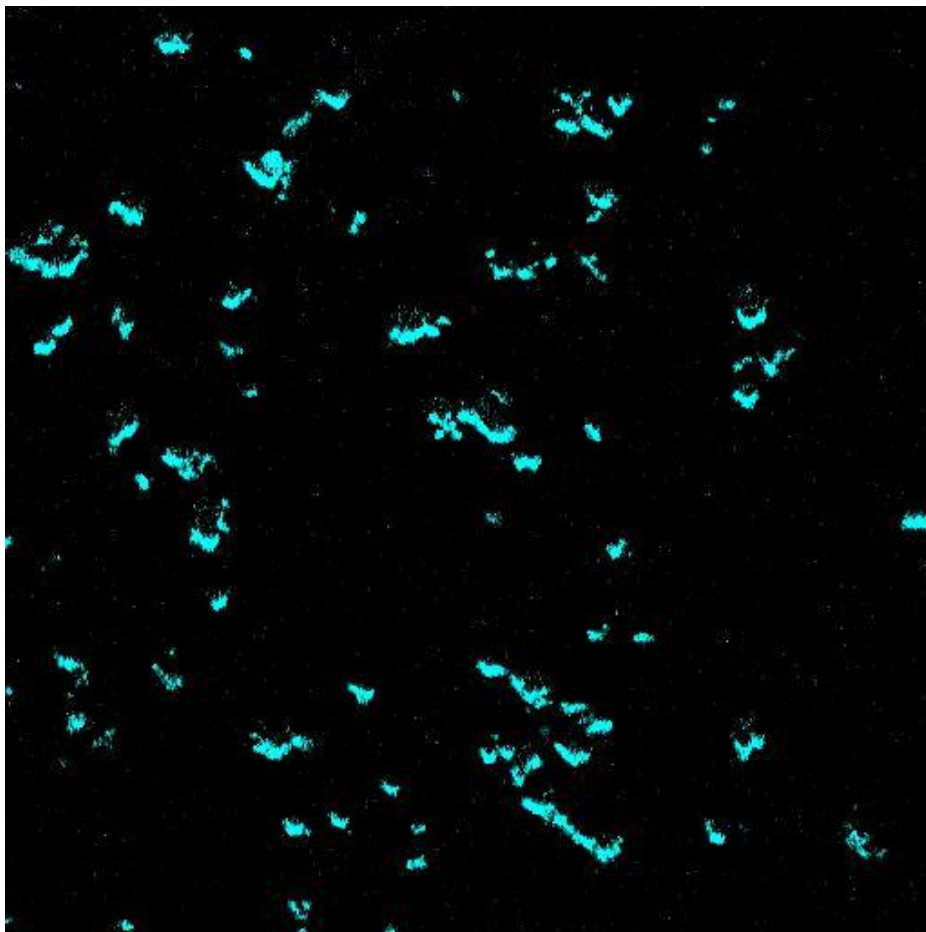
Video Series Fig 8



Video Series Fig 9

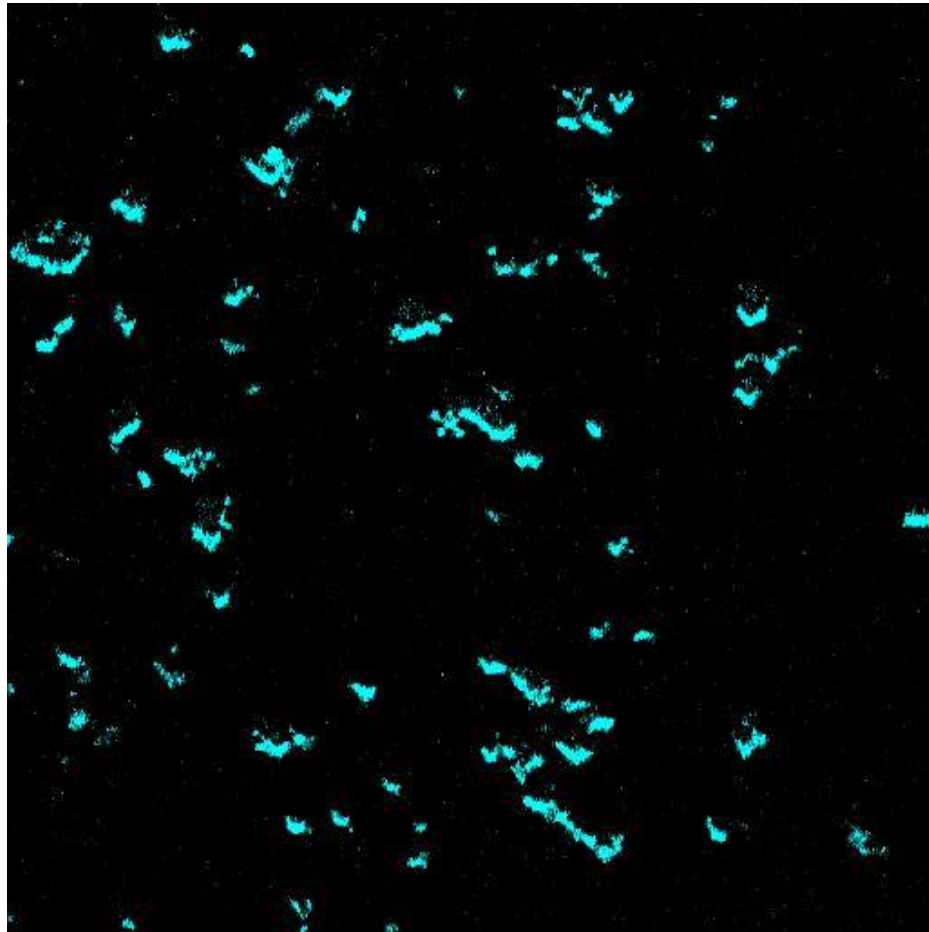
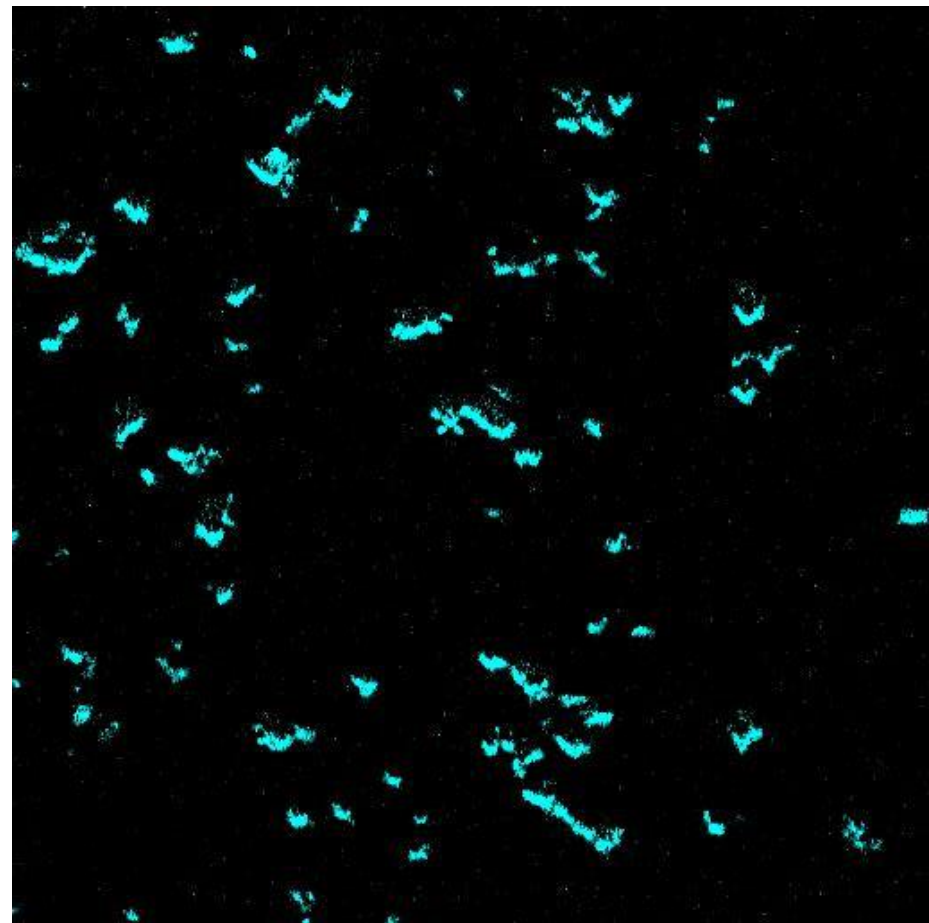


Video Series Fig 10



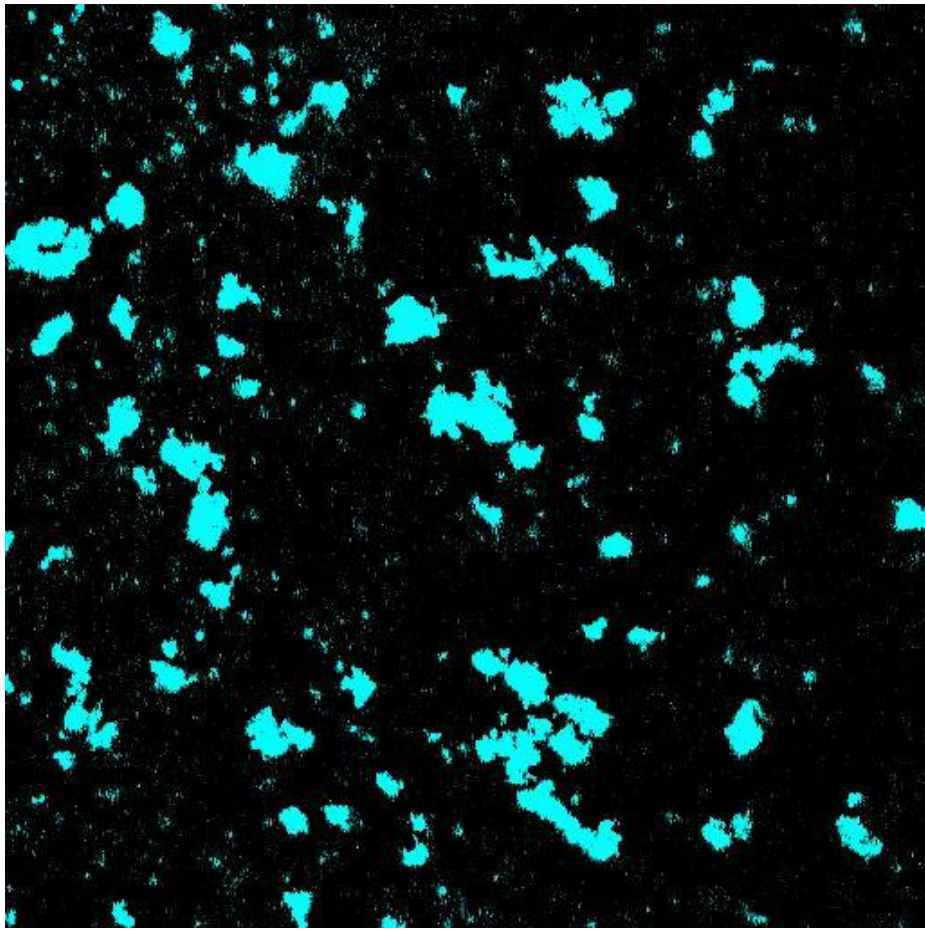
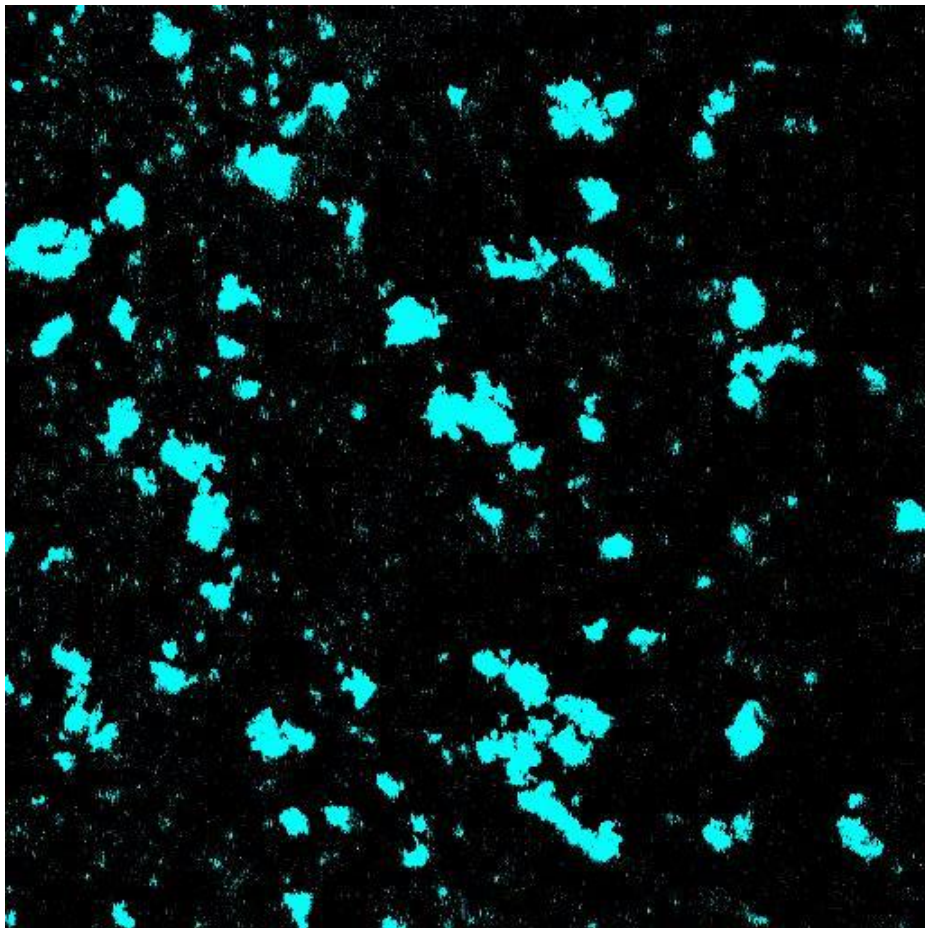
Video Series Fig 11

Video Series Fig 12

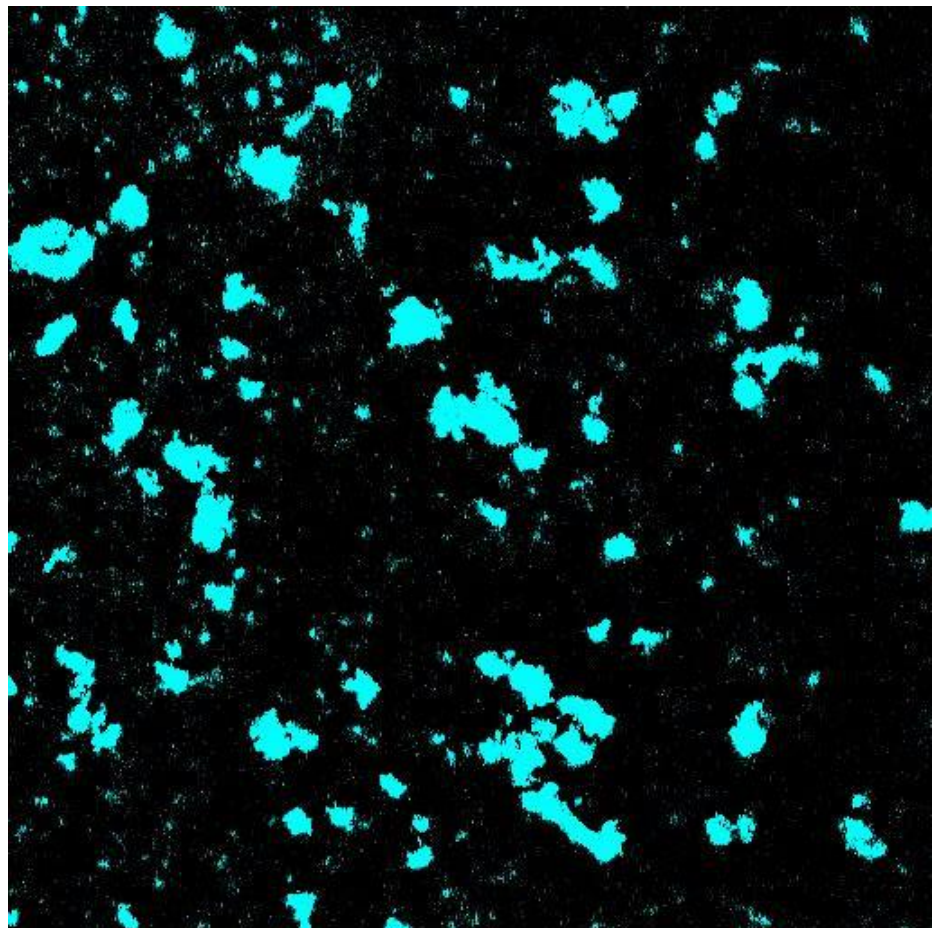


Video Series Fig 13

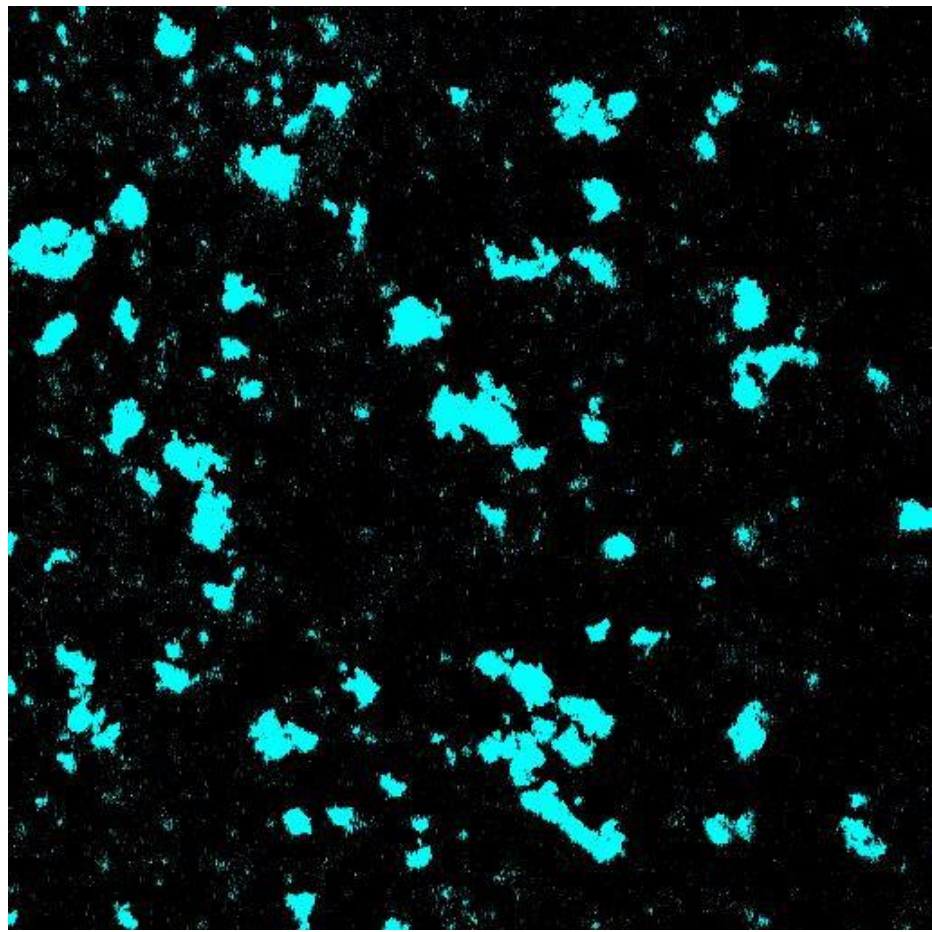
Video Series Fig 14



Video Series Fig 15

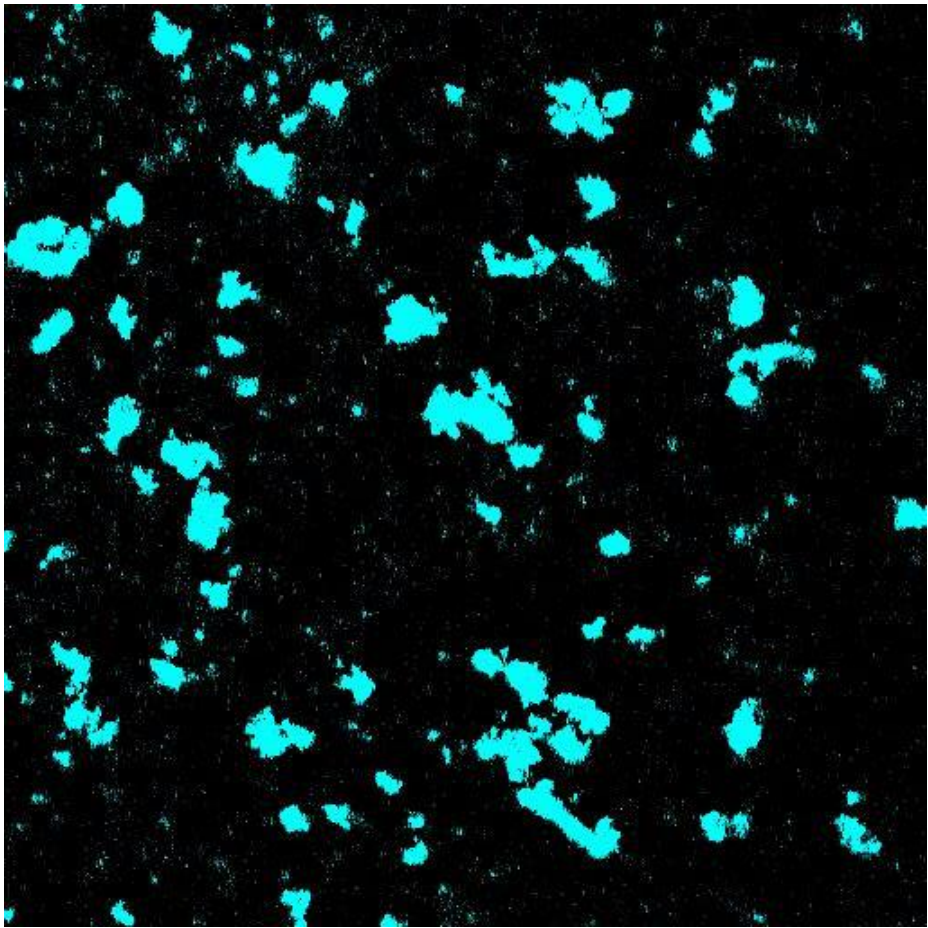
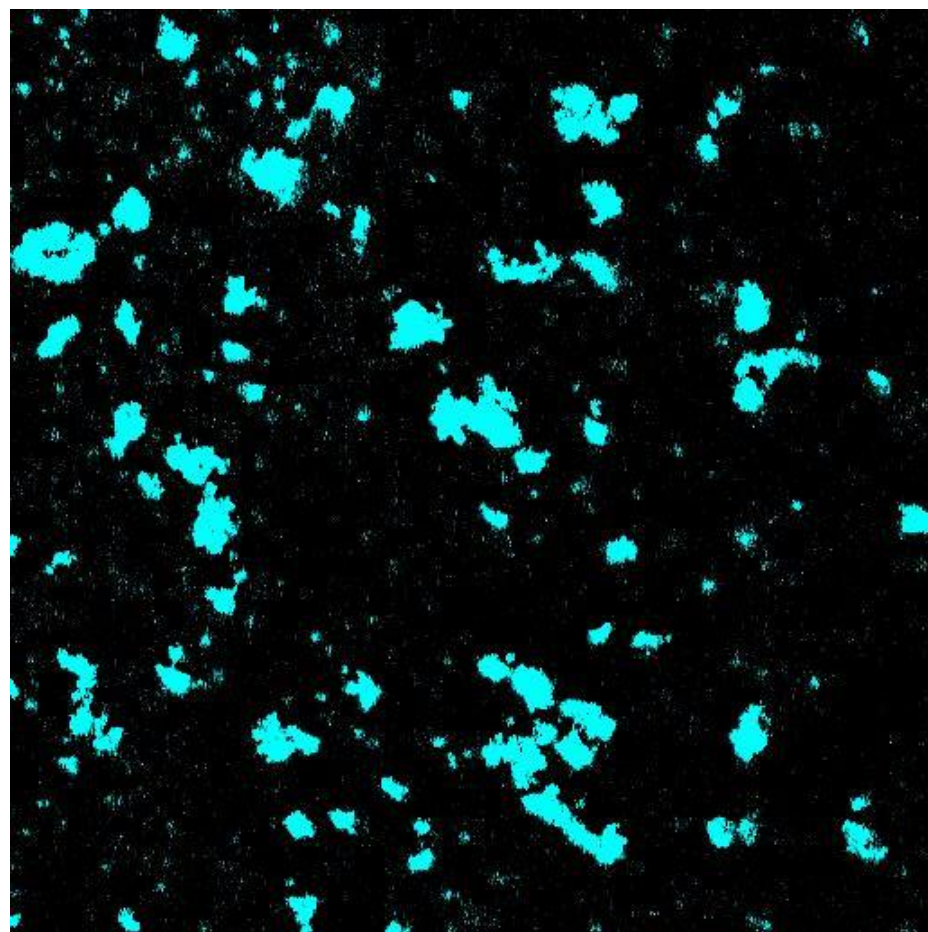


Video Series Fig 16

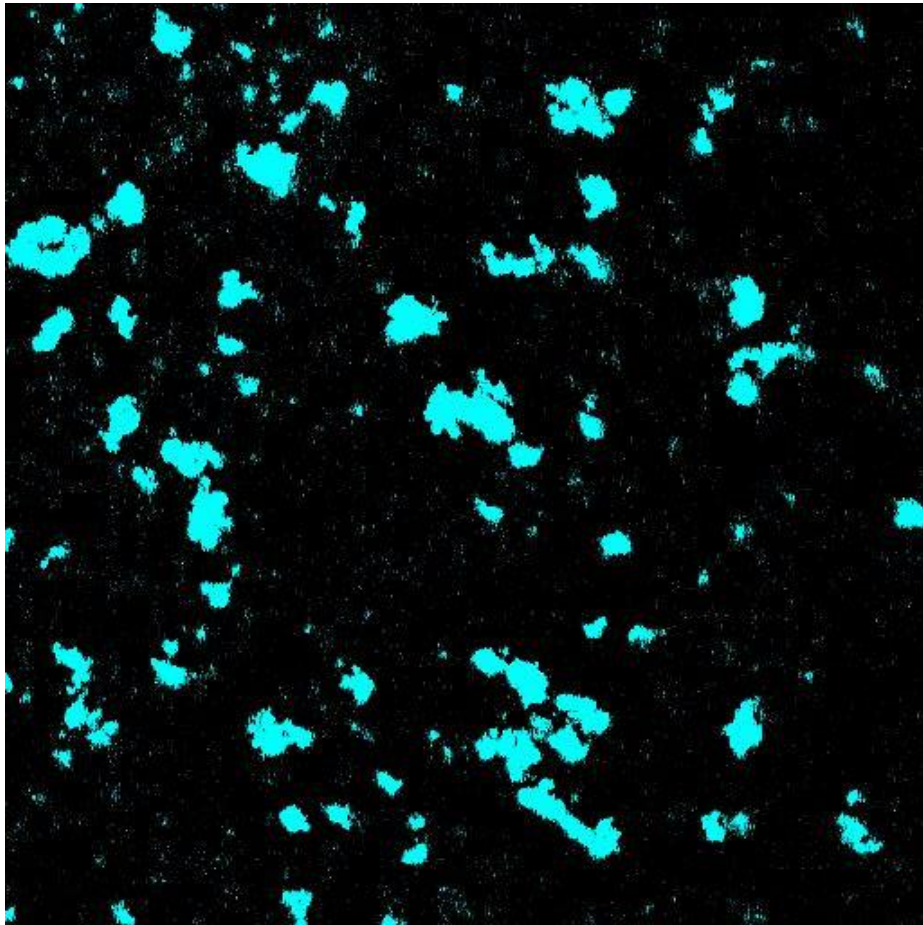


Video Series Fig 17

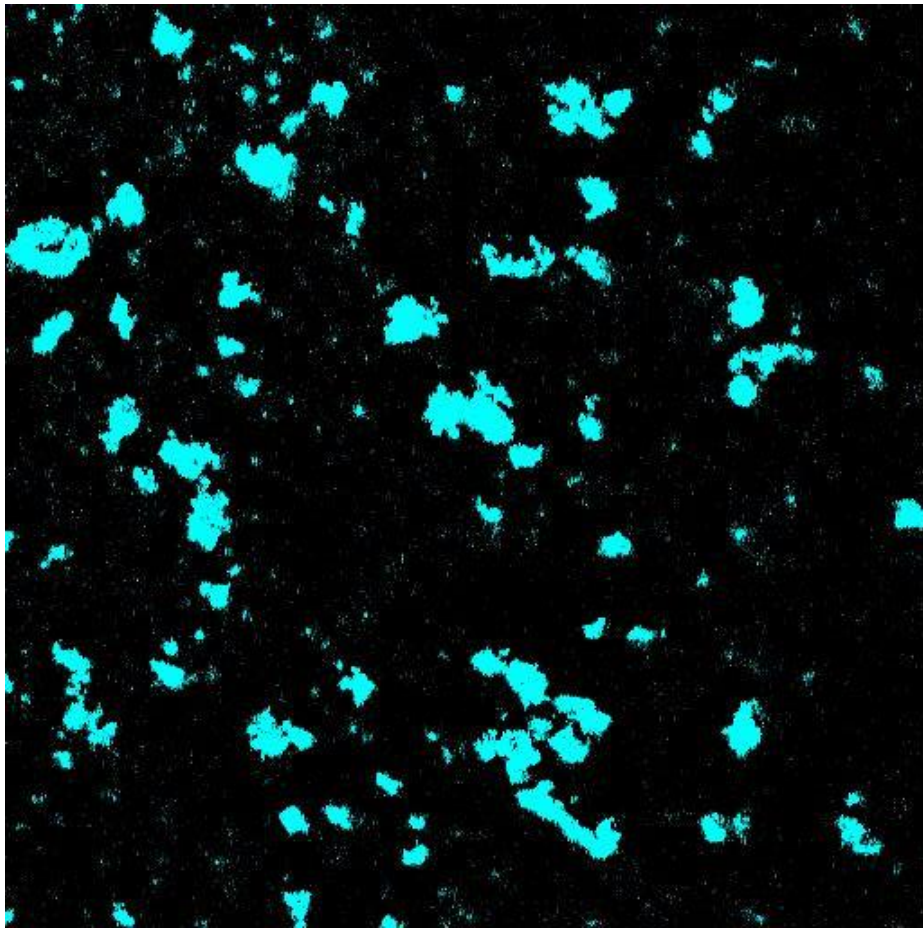
Video Series Fig 18



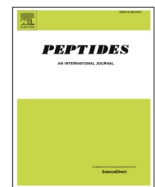
Video Series Fig 19



Video Series Fig 20



2.2. Manuskript II



Angiotensin-(1–7) mediated calcium signalling by MAS



Priyavathi Sureshkumar ^{a,b}, Robson Augusto Souza dos Santos ^c, Natalia Alenina ^{a,d}, Stefan Mergler ^{b,1}, Michael Bader ^{a,d,e,f,*1,2}

^a Max Delbrück Center for Molecular Medicine in the Helmholtz Association, Robert-Rössle-Straße 10, 13125 Berlin, Germany

^b Department of Ophthalmology, Charité Universitätsmedizin Berlin, Corporate Member of Freie Universität Berlin, Berlin Institute of Health, Humboldt-Universität zu Berlin, Berlin, Germany

^c National Institute of Science and Technology in Nanobiopharmaceutics, Department of Physiology and Biophysics, Institute of Biological Sciences, Federal University of Minas Gerais, Belo Horizonte, Brazil

^d DZHK (German Center for Cardiovascular Research), Partner Site Berlin, Berlin, Germany

^e Charité Universitätsmedizin Berlin, Corporate Member of Freie Universität Berlin, Berlin Institute of Health, Humboldt-Universität zu Berlin, Berlin, Germany

^f Institute for Biology, University of Lübeck, Germany

ARTICLE INFO

Keywords:

Angiotensin
Calcium
MAS
Trp channel

ABSTRACT

The G protein-coupled receptor, MAS, is the receptor of the endogenous ligand, Angiotensin (Ang)-(1–7). It is a promising drug target since the Ang-(1–7)/MAS axis is protective in the cardiovascular system. Therefore, a characterization of MAS signalling is important for developing novel therapeutics for cardiovascular diseases. In this paper, we show that Ang-(1–7) increases intracellular calcium in transiently *MAS*-transfected HEK293 cells. The calcium influx induced by the activation of MAS is dependent on plasma membrane Ca^{2+} channels, phospholipase C, and protein kinase C. Specifically, we could demonstrate that MAS employs non-selective, transient receptor potential channels (TRPs) for calcium entry.

1. Introduction

Angiotensin (Ang)-(1–7) is the known endogenous ligand of MAS, an important G protein-coupled receptor (GPCR) in the renin angiotensin aldosterone system (RAAS) [25,22,3]. The RAAS regulates blood pressure, fluid/electrolyte balance, and is involved in the pathogenesis of most cardiovascular diseases. In relevance to this context, the second messenger calcium has been previously studied both in vitro and in vivo in order to investigate the signalling pathways of MAS.

Chronic MAS deficiency causes impairment in calcium homeostasis. MAS-deficient cardiomyocytes show lower expression levels of the sarco/endoplasmatic reticulum calcium ATPase, SERCA, and no increase in the intracellular calcium concentration after treatment with 10 nM of Ang-(1–7) [11]. In another study, Ang-(1–7) did not induce any changes in intracellular calcium concentration in quiescent atrial myocytes [23]. The crosstalk between Ang-(1–7) and aldosterone and its

consequence on calcium regulation was also investigated in cardiomyocytes. Aldosterone increases intracellular calcium in cardiomyocytes. Ang-(1–7) mediates calcium influx in cells pretreated with aldosterone. However, Ang-(1–7) alone was unable to induce a calcium influx [1]. In another previous study, it was observed that there was no increase in calcium transients in isolated rat ventricular myocytes at normal conditions. However, in myocytes after simulated ischemic reperfusion, Ang-(1–7) significantly attenuated the increased diastolic intracellular calcium during reperfusion and restored the decreased peak calcium transients during ischemia. Ang-(1–7) also reversed the decreased amplitude of calcium transients throughout the ischemic reperfusion periods [30]. In cardiomyocytes from rats with heart failure, the current induced by L-type voltage operated calcium channels (VOCCs) was reduced compared to cells from normal rats. Ang-(1–7) significantly increased this calcium current in cardiomyocytes from rats with heart failure [35] [34]. Ang-(1–7) increased

Abbreviations: Ang-1–7, Angiotensin 1–7; AT1 Receptor, Angiotensin II Type 1 receptor; AT2 Receptor, Angiotensin II Type 2 receptor; GPCR, G-Protein coupled Receptor; RAAS, Renin Angiotensin Aldosterone System; TRP, Transient receptor potential; PLC- β , Phospholipase C, isoenzyme β ; PKC, Protein kinase C; HBSS, Hank's Balanced Salt Solution.

* Correspondence to: Max-Delbrück-Center for Molecular Medicine, Robert-Rössle-Str. 10, 13125 Berlin, Germany.

E-mail address: mbader@mdc-berlin.de (M. Bader).

¹ Equal contribution

² Max-Delbrück-Center for Molecular Medicine, Robert-Rössle-Str. 10, 13125 Berlin, Germany

<https://doi.org/10.1016/j.peptides.2023.171010>

Received 10 February 2023; Received in revised form 12 April 2023; Accepted 12 April 2023

Available online 13 April 2023

0196-9781/© 2023 Elsevier Inc. All rights reserved.

calcium levels at nM and μ M range in the proximal tubules of spontaneously hypertensive rats (SHR) [19]. Unambiguously from the above-mentioned *in vitro* studies, the role of Ang-(1–7) on calcium regulation was observed only in diseased conditions.

In contrast to what is known about calcium regulation *in vivo*, Ang-(1–7) regulates intracellular calcium *in vitro* even in healthy conditions. Ang-(1–7) increased calcium at higher concentrations from 20 to 50 μ M in Madin-Darby canine kidney (MDCK) renal tubular cells, but activated only the Ang II (AT1) receptor. Ang-(1–7) action via AT1 was mediated by store operated calcium channels (SOCCs) and the intracellular calcium increase was abolished by La³⁺ [17]. Ang-(1–7) increased intracellular calcium at moderate levels, which was partially suppressed by A779, a known MAS inhibitor, in the micro-perfused proximal tubule isolated from rats [8]. In contrast, one study showed that the peptide MAS agonist, Ang-(1–7) was not able to induce calcium influx in MAS-transfected HEK293 cells. However, the peptide agonist, NPFF, and the non-peptide agonist, AR234960, activated MAS and increased intracellular calcium via the classical Gq and PLC – IP3 (Inositol triphosphate) signalling pathways [27].

These contradictory findings sparked our study, in which we have performed fluorescence calcium imaging experiments in *Mas*-over-expressing HEK293 cells to get a clear view whether Ang-(1–7) regulates calcium influx and further calcium signalling cascades via MAS and TRPs.

2. Materials and methods

2.1. Activators and inhibitors

Ang-(1–7), Ang II, A779 and Candesartan were bought from Bachem, Bubendorf, Switzerland. Phospholipase C- β (PLC- β) inhibitor, U73122, was bought from Tocris Biosciences, Bristol, UK. Protein Kinase C (PKC) inhibitor Go697 was bought from Calbiochem, San Diego, USA. Transient Receptor Potential Channels Inhibitor Lanthanum Chloride, LaCl₃, from Sigma, Steinheim, Germany was used.

2.2. Cell culture

The human embryonic kidney cell line, HEK293, was used to express human MAS. HEK293 cells were grown in Dulbecco Modified Eagle Medium-low glucose with pyruvate (Gibco, Paisley, Scotland, UK), supplemented with 10% FBS (Gibco, Paisley, Scotland, UK) and 1% Penicillin/Streptomycin (Sigma, Steinheim, Germany) and incubated at 37 °C humidified 5% CO₂ incubator. For transfection experiments, around 1 million cells were seeded in 6 well plates with three 15 mm glass coverslips precoated with poly-L-lysine (Sigma, Steinheim, Germany) per well. After the cells reach 60–70% confluence, the medium was changed to Optimem (Gibco, Paisley, Scotland, UK) for 2–6 hrs and then the cells were transfected with a pcDNA3.1-hMAS plasmid using Lipofectamine 2000 (ThermoFisher, Waltham, MA, USA) according to the protocol of the manufacturer. 6 hrs after transfection, the medium was changed to complete growth medium supplemented with G418 (600 ng/ml) (Invitrogen, California, USA) for further 2 days to increase the number of MAS-expressing cells through selection.

2.3. Fluorescence calcium imaging

After the cells had reached 80–90% confluence on glass coverslips, they were pre-incubated with serum-free culture medium containing Fura-2/AM (2 μ M) (Promokine, Heidelberg, Germany) for 15–45 min at 37 °C for calcium dye loading. The dye loading was stopped with a Hank's Balanced Salt Solution (HBSS) (all chemicals from Sigma Aldrich, Steinheim, Germany) solution. HBSS solution with a composition of CaCl₂ (1.26 mM), KCl (5.33 mM), KH₂PO₄ (0.44 mM), MgCl₂·6 H₂O (0.50 mM), MgSO₄·7 H₂O (0.41 mM), NaCl (138 mM), NaHCO₃ (4.0 mM), Na₂HPO₄ (0.30 mM) and glucose (5.6 mM) with pH 7.4 and

300 mOsMol was used for all calcium measurements.

Cells were then washed several times further with this solution and placed in a chamber containing the aforementioned HBSS solution on the stage of an inverted microscope (Olympus BW50WI, Olympus Europa Holding GmbH, Hamburg, Germany) connected to a digital imaging system (TILL Photonics, Munich, Germany). Fura-2/AM fluorescence was alternately excited at 340 nm and 380 nm wavelength. The emission was detected from cell clusters every 500 ms at 510 nm. If stabilization had not occurred within the first 5 min, adaptation to room temperature (\approx 22 °C) was prolonged until a stable baseline was observed. Results are shown as mean traces of the F_{340 nm}/F_{380 nm} ratio \pm SEM with n-values indicating the number of experiments per data point. The measurements lasted for 10 min. Drugs were dissolved in dimethyl sulfoxide (DMSO) to obtain a stock solution and diluted to obtain a working concentration that did not exceed 0.1% DMSO. In case of inhibitor studies, the cells were also pretreated with the respective inhibitor for 20 min before the calcium measurement in serum free cell-culture medium.

2.4. Statistical analysis

Significance was determined using Student's t-test for paired data (p-values: two-tailed) provided they passed a normality test according to Kolmogorov-Smirnov. If the normality test failed, non-parametric Wilcoxon matched pairs were used. For non-paired data, Student's t-test for unpaired data were used, if a normality test was passed. If this was not the case, non-parametric Mann-Whitney-U test was performed. Welch's correction was applied if data variance of the two groups were not at the same level. p < 0.05 was considered to be significant. The number of repeats is shown in each case in brackets, near the traces or bars. All values are means \pm SEM. All plots were generated with SigmaPlot software version 12.0 (Systat Software, San Jose, California, U.S.A.). Bar charts were plotted with GraphPad Prism (version 5).

3. Results

3.1. Effect of Ang-(1–7) in *Mas*-transfected and non-transfected HEK293 cells

Application of Ang-(1–7) increased intracellular calcium levels in the MAS-expressing cells (Fig. 1a). The change in the batch solution was carried out at the 4th min (240 s). The maximum of the peak was observed around 100 s after the change of bath solution from HBSS to 1 μ M Ang-(1–7) supplemented HBSS (p = 0.0078, Wilcoxon signed rank test, two tailed, Fig. 1b). The basal calcium levels remained increased for the whole duration of the experiment. As control experiment, the bath solution was not changed from HBSS to Ang-(1–7) in HBSS solution for 10 min continuously. No change in calcium levels was observed in the control experiments (calcium base line). In non-transfected HEK293 cells, no significant calcium response was recorded after Ang-(1–7) treatment (Fig. 1c) confirming that MAS expression in the non-transfected HEK293 cells is negligible. The calcium response of transfected HEK293 cells was at clearly higher levels than of non-transfected ones (p = 0.0062, two tailed Mann-Whitney test, Fig. 1d).

Another activator of MAS, e.g., AVE0991, was also checked for its activity in the *Mas*-transfected HEK293 cells. 1 μ M of AVE0991 was able to increase the cytosolic calcium levels (Supplementary Fig. 1, a, b), in accordance with previously reported data [16]. As positive control, NPFF (Neuropeptide FF), a known peptide activator of MAS, was also tested. Consistent with previous studies ([27]; [12]), 1 μ M of NPFF also increased intracellular calcium levels in *Mas*-transfected HEK293 cells (Supplementary Fig. 2).

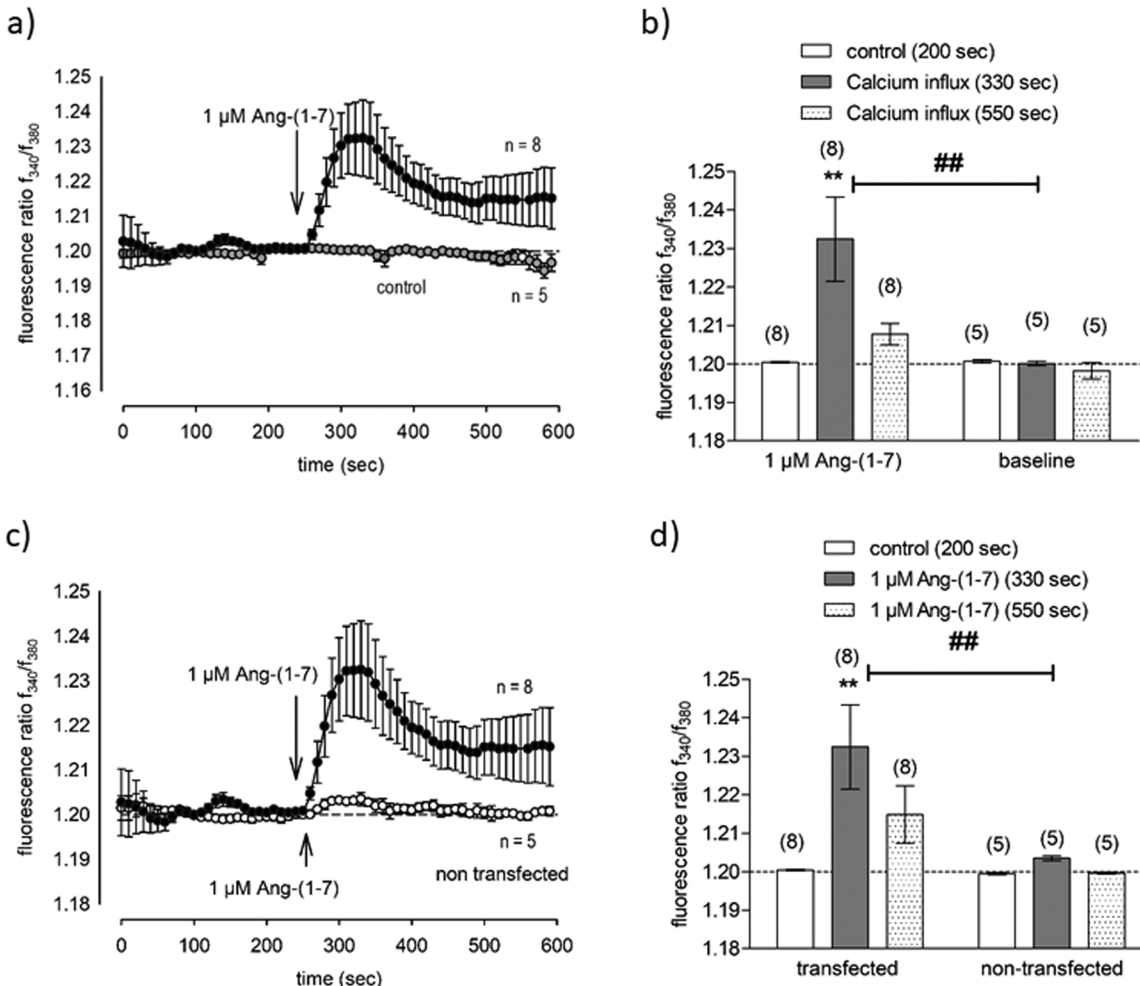


Fig. 1. a) Effect of 1 μM Ang-(1–7) on MAS-transfected HEK293 cells (filled circles) compared to the baseline/control measurement without Ang-(1–7) (open circles), b) Statistical analysis of Fig. 1a, c) Effect of Ang-(1–7) on MAS-transfected (filled circles) and non-transfected (open circles) HEK293 cells, d) Statistical analysis of Fig. 1c. * *p < 0.01 vs control (200 s) for the same condition, paired test; ##p < 0.01 Ang-(1–7) vs baseline (b) or transfected vs non-transfected (d) for the same time point, unpaired test.

3.2. Effect of inhibitors of the Renin Angiotensin Aldosterone System (RAAS) on the Ang-(1–7) induced calcium influx in MAS-transfected HEK293 cells

In the next set of experiments, we tested whether the observed calcium influx caused by Ang-(1–7) was abolished by the specific MAS antagonist, A779. For experiments with inhibitors, the cells were preincubated with the inhibitor during the dye loading and washing steps. When MAS-transfected cells were preincubated with 20 μM A779, the calcium transient of 1 μM Ang-(1–7) was abolished (Fig. 2a). A779 was added both in HBSS control solution and in the Ang-(1–7)-HBSS solution in order to ensure constant inhibition of the A779 throughout the calcium measurements and statistically significant difference was observed between A779 supplemented samples and A779 non-supplemented samples ($p = 0.0016$, two tailed, Mann-Whitney test, Fig. 2b).

Increased protein expression of AT1 in HEK293 cells overexpressing MAS was previously reported [7]. When MAS-transfected cells were pre-incubated with the AT1 antagonist, candesartan (CV-11974, 20 μM), the 1 μM Ang-(1–7)-induced calcium influx was only partially suppressed (Fig. 2c). Candesartan preincubated samples still showed the increase in calcium influx caused by Ang-(1–7) with statistical significance ($p = 0.0024$, paired t test). At 330 s and 550 s, the candesartan preincubated samples and non-treated samples did not show any

statistical difference, when activated by Ang-(1–7) (Fig. 2d). To further exclude the involvement of AT1 in the calcium influx caused by Ang-(1–7) in MAS-transfected HEK293 cells, losartan was used as a second AT1-blocker. With application of 20 μM losartan, no suppression of the calcium influx caused by Ang-(1–7) in the MAS-transfected HEK293 cells was observed (Supplementary Fig. 1 c, d).

3.3. The calcium influx induced by Ang-(1–7) is mediated through plasma membrane ion channels and probably through transient receptor potential channels

We next wanted to find out if the observed calcium influx induced by Ang-(1–7) is mediated by Ca²⁺ permeable ion channels. To test this, a calcium free HBSS was used in the experiments to ascertain whether there is an internal Ca²⁺ release or a Ca²⁺ influx through Ca²⁺ permeable ion channels. As a result, no calcium influx was observed when 1 μM Ang-(1–7) was added in calcium free HBSS supplemented with 5 mM EGTA, a calcium chelator (Fig. 3a). The reduction in calcium influx induced by Ang-(1–7) in calcium-free conditions was highly significant ($p < 0.0007$, unpaired, Mann-Whitney test, Fig. 3b).

The next question was which family of calcium channels might contribute to this calcium influx. Lanthanum(III) chloride, La³⁺, a broad TRP channel blocker, was used to test whether any of TRPs are involved in the calcium influx mediated by Ang-(1–7). 500 μM La³⁺ was

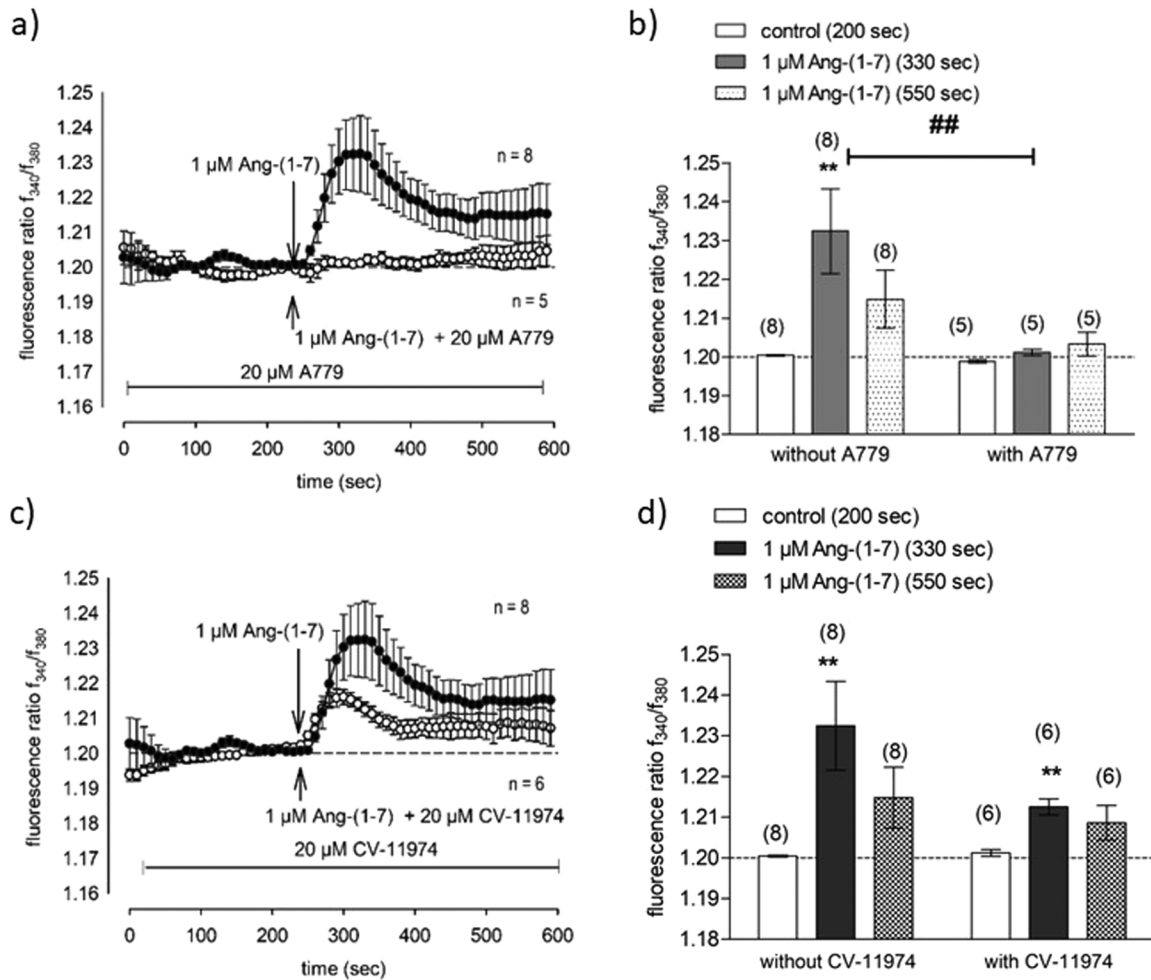


Fig. 2. a) Effect of 1 μM Ang-(1–7) on *MAS*-transfected HEK293 cells preincubated with 20 μM A779 (open circles) compared to 1 μM Ang-(1–7) without A779 preincubation (filled circles), b) Statistical analysis of Fig. 2a, c) Effect of 1 μM Ang-(1–7) on *MAS*-transfected HEK293 cells preincubated with 20 μM candesartan (CV-11974) (open circles) compared to 1 μM Ang-(1–7) without preincubation (filled circles), d) Statistical analysis of Fig. 2c. * *p < 0.01 vs control (200 s) for the same condition, paired test; ##p < 0.01 with vs without compound for the same time point, unpaired test.

preincubated for 30 min and a significant ($p = 0.0027$, non-paired, Mann-Whitney test) suppression of calcium influx was observed (Fig. 3c, d). These data show that TRPs were involved in the Ang-(1–7) mediated calcium entry via MAS activation.

3.4. Interplay of Phospholipase C and Protein Kinase C on activation of MAS by Ang-(1–7)

As Phospholipase C (PLC) and Protein kinase C (PKC) are known to be involved in the signalling cascade of GPCRs and TRPs, the next study was performed using inhibitors of these two enzymes. The effect of 1 μM Ang-(1–7) on calcium influx in *MAS*-transfected HEK293 cells was completely abolished when the cells were preincubated with the non-specific PLC- β inhibitor, 10 μM U73122 for 10–15 min, as shown in Fig. 4a ($p = 0.0006$, non-paired, two tailed, Mann Whitney test, Fig. 4b).

Next, the *MAS*-transfected HEK293 cells were preincubated with PKC inhibitor Go6976, 200 nM for 30 min, and then the effect of Ang-(1–7) on calcium influx was recorded. The PKC inhibitor preincubation resulted in a smaller calcium transient peak with 1 μM Ang-(1–7) and also showed a biphasic effect with alterations in the baseline calcium levels ($p = 0.0127$, two tailed, Mann-Whitney test, Fig. 4c, d).

4. Discussion

In summary, we have shown that Ang-(1–7) can increase

intracellular calcium in *MAS*-expressing HEK293 cells. This transient increase is mediated by an influx of calcium through Ca^{2+} permeable ion channels present in the plasma membrane, most possibly of the TRP channel family since the broad-band Trp channel blocker La^{3+} [15] inhibited this effect. Furthermore, we were able to show that PLC- β and PKC are also involved in this Ang-(1–7) induced calcium response via MAS activation.

Previous investigations have shown that Ang-(1–7) can increase intracellular calcium levels both via MAS and AT1 in the proximal tubules of spontaneously hypertensive rats and can influence the Na^+ / H^+ exchanger [9]. Another study has also seen similar effects in astroglia cells from brain sections of Wistar and spontaneously hypertensive rats [14]. Additionally, it was shown that cytosolic Ang-(1–7) was able to cause increased peak inward calcium currents and this peak inward calcium currents were abolished by A779 [10]. However, it remained unclear how the peptide could bind to MAS when approaching it from the cytosolic side of the membrane, when the binding site is on the extracellular side. In our experiments, we have expressed MAS in HEK293 cells in plasma membrane and therefore expect to see only effects of extracellularly applied Ang-(1–7).

In our experiments we have used 1 μM of AVE0991, a non-peptide agonist on *MAS*-overexpressing HEK293 cells and observed an increase in intracellular calcium, which had different kinetics compared to the peptide agonist Ang-(1–7) (Supplementary Fig. 1a, b). The phenomenon, that non-peptide agonists have different kinetics in

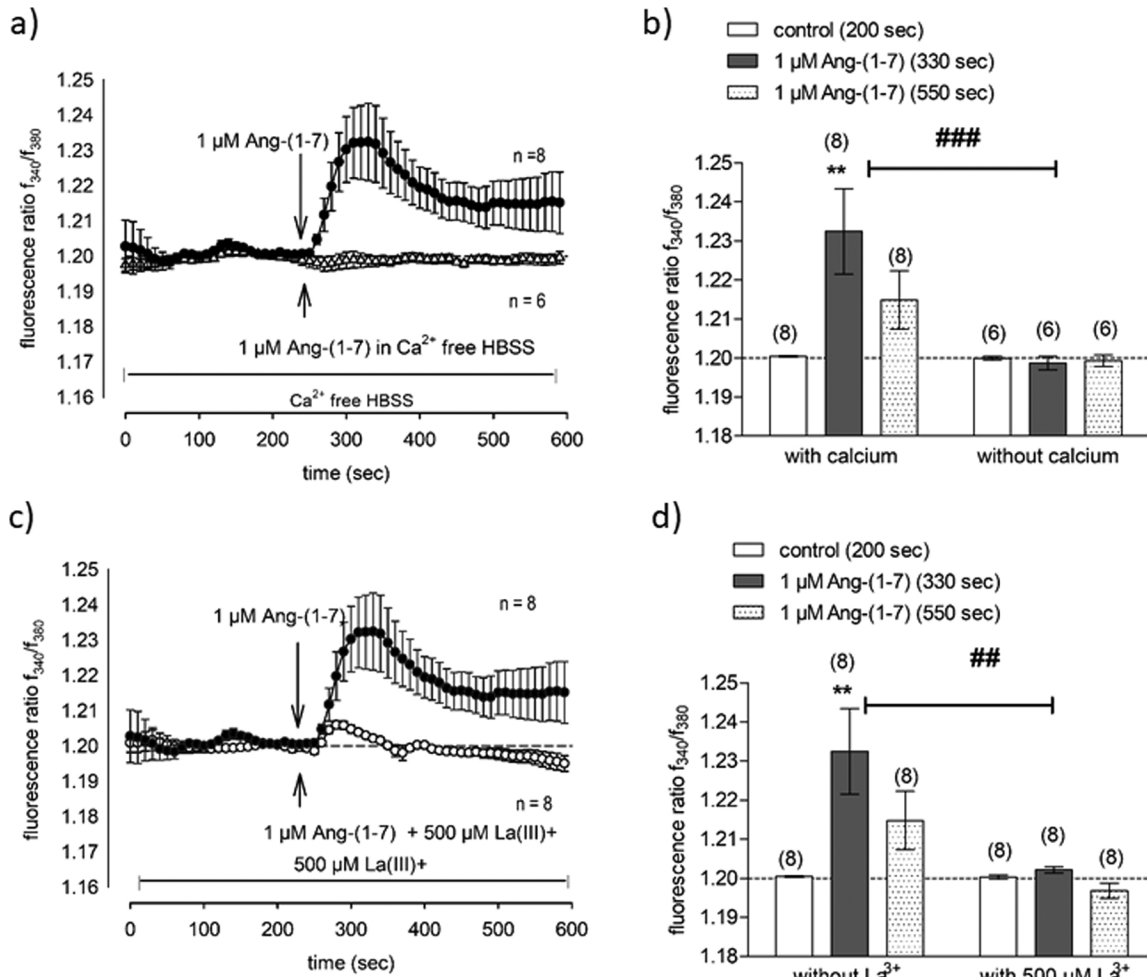


Fig. 3. a) Effect of 1 μM Ang-(1–7) on MAS-transfected HEK293 cells (filled circles) vs 1 μM Ang-(1–7) without calcium in HBSS buffer (open triangles), b) Statistical analysis of Fig. 3a, c) Effect of La³⁺ on Ang-(1–7) mediated calcium influx in MAS-transfected HEK293 cells without La³⁺ (closed circles) and with La³⁺ (open circles) d) Statistical analysis of Fig. 3c. * *p < 0.01 vs control (200 s) for the same condition, paired test; **p < 0.01, ***p < 0.001 with vs without compound for the same time point, unpaired test.

comparison to the peptide agonists of MAS was also observed by other groups [27].

The concentration of Ang-(1–7) used in our experiments was 1 μM, which is much higher compared to the amount of Ang-(1–7) expected in human serum [29]. However, earlier studies have also observed intracellular calcium influx at micromolar range [9,14]. Ang-(1–7) also binds to Ang II receptor type 1 (AT1) and Ang II receptor type (AT2) with modest affinity [5]. Interestingly, the Ang-(1–7) induced intracellular increase in calcium is negligible in the non-transfected HEK293 cells in our experiments. This indicates a low expression of endogenous AT1 receptors in this cell line (Fig. 1c). Moreover, we have used candesartan, an AT1 blocker, to check whether the Ang-(1–7) induced calcium response is mediated via MAS or through AT1 (Fig. 2c, d). The concentration of candesartan inhibiting AT1 receptors is in the nanomolar range [13] and for AT2, the inhibition starts at 1 μM [5]. In our experiments, only a slight but not statistically significant effect was observed between the candesartan pretreated and non-treated samples even at the high concentration of 20 μM candesartan (Fig. 2c, d). This provides further evidence that the observed Ang-(1–7) induced calcium influx is primarily mediated via MAS. Moreover, previous investigations have shown that Ang-(1–7) activates AT1 primarily via the β-arrestin pathway and not through the Gq mediated signalling cascade [26]. The slight effect of candesartan on Ang-(1–7) induced calcium influx may be caused by a small cross-inhibitory effect on MAS, since the specific AT1 blocker losartan had no effect (Supplementary Fig. 1c, d).

The calcium influx induced by Ang-(1–7) is completely absent in calcium free HBSS with 5 mM EGTA (Fig. 3a) showing that it is mediated by Ca²⁺ permeable ion channels present in the plasma membrane and not through endo/sarcoplasmic reticulum via store depletion or channels in mitochondria or other organelles. The partial suppression of this calcium influx by the universal TRP channel blocker lanthanum-III-chloride (La³⁺) suggests that TRPs are involved but also, that other family of channels participate in this process (Fig. 3b).

Activation of MAS by NPFF, MPF7, CGEN-856S and AR234960 stimulates PLC-β via Gq signalling thereby inducing the cleavage of PIP₂ (Phosphatidylinositol-4,5-bisphosphate) to DAG and IP₃ (Inositol triphosphate) [4] [2]. In a previous study, Ang-(1–7) did however not increase IP₃ levels [27]. Since other cell types were used in these experiments, the signalling pathways of MAS may be cell-type dependent. In our experiments, calcium influx induced by Ang-(1–7) is completely abolished by the PLC-β inhibitor, U73122 (Fig. 4a), indicating that Ang-(1–7) can also initiate Gq signalling similar to NPFF and other agonists. This result is supported by the previous evidence that Ang-(1–7) mediated MAS activation employs the Akt/PLC-β signalling pathway [32]. Activation of PLC-β can also cause store depletion through IP₃ receptor-mediated cytosolic calcium influx from the endoplasmic reticulum [20] [6]. Hence, active store depletion by Ang-(1–7) might be a secondary source for cytosolic calcium influx, which is still dependent on the calcium influx via plasma membrane channels. However, this putative signalling pathway of MAS needs experimental

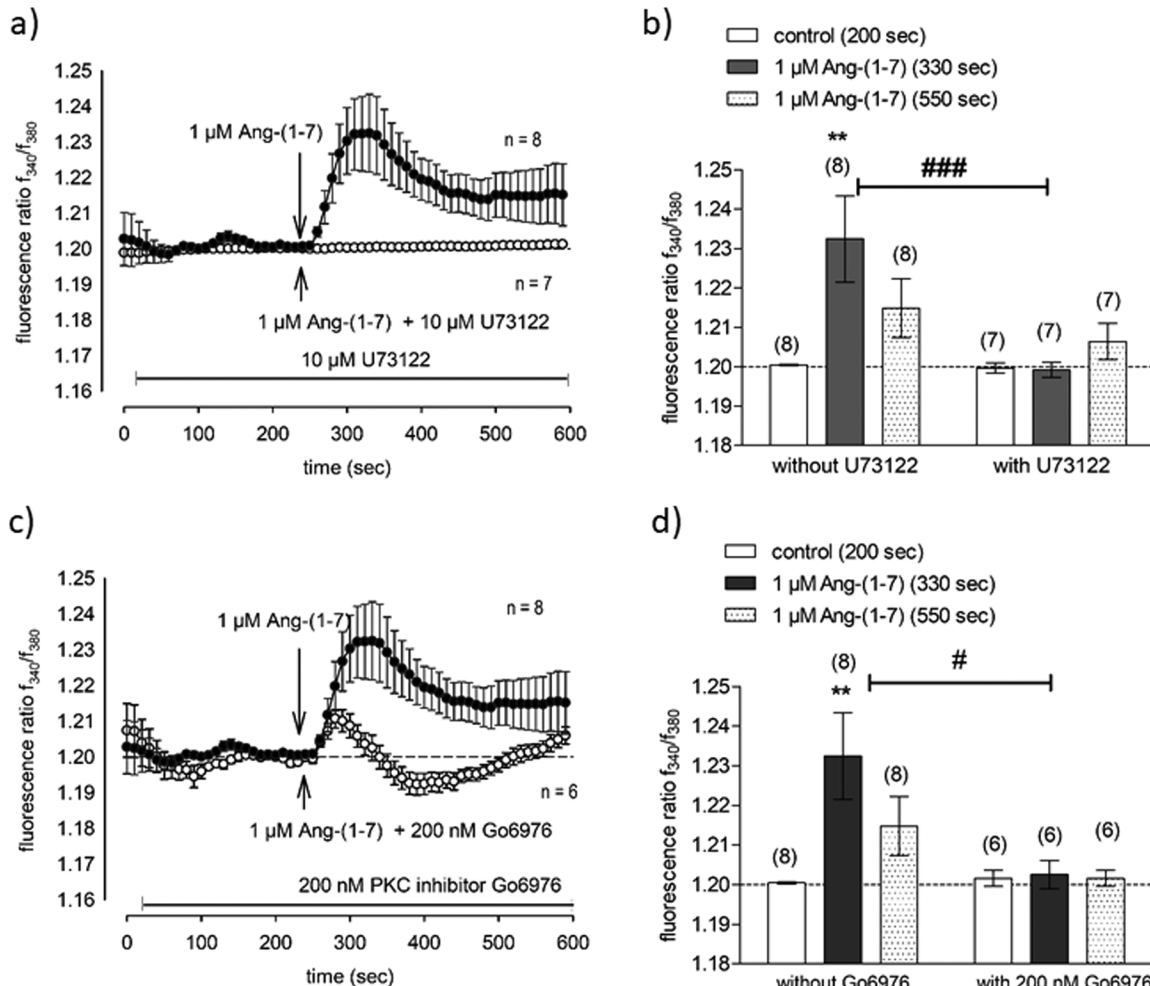


Fig. 4. a) Effect of 1 μM Ang-(1–7) on MAS-transfected HEK293 cells preincubated with 10 μM PLC-β inhibitor, U73122 (n = 7, open circles) compared to 1 μM Ang-(1–7) without PLC-β inhibitor, U73122 (n = 8, closed circles), b) Statistical analysis of Fig. 4a, c) Effect of 1 μM Ang-(1–7) on MAS-transfected HEK293 cells preincubated with PKC inhibitor, 200 nM Go6976 (n = 6, open circles) compared to 1 μM Ang-(1–7) without preincubation of PKC inhibitor, 200 nM Go6976, (n = 8, closed circles), d) Statistical analysis of Fig. 4c. * *p < 0.01 vs control (200 s) for the same condition, paired test; #p < 0.05, ###p < 0.001 with vs without compound for the same time point, unpaired test.

verification.

The PKC inhibitor Go6976 also significantly reduced the Ang-(1–7) induced Ca^{2+} influx (Fig. 4c). A number of TRPs are activated through phosphorylation via PKC which is activated downstream of PLC-β [33] and this signalling pathway may explain the known activation of TRPs by other GPCRs [28]. Our study indicates that MAS belongs to this class of GPCRs confirming the GPCR-TRP axis suggested by Veldhuis et al. [28]. Therefore, we suggest that TRPs are involved in the Ang-(1–7)-induced Ca^{2+} increase via MAS. Indeed, it could be shown that TRPs are involved in the signalling of other Mas-related G protein-coupled receptors (MRGPRs). More specifically, mMRGPR-A3 activates TRPA1 (ankyrin family, member1), TRPV1 (Vallinoid family, member1), TRPM8 (melastatin family, member 8) and TRPC3 (canonical family, member3). MRGPR-X1 exhibit TRPV1 mediated calcium entry through PLC-β and PKC activation [24] and has recently been shown to also sensitize TRPA1 [18]. Moreover, TRPA1 has been described as downstream signalling mediator of Mrgpr-D and Mrgpr-C11 [31].

Taken together, we have shown that MAS stimulation by Ang-(1–7) leads to calcium entry partially by TRPs in the plasma membrane, which are activated by PLC-β and PKC.

5. Conclusion

A better understanding of MAS signalling is required in order to find new agonists for MAS, which may be promising drugs for cardiovascular and metabolic diseases [21]. Calcium imaging of cells expressing MAS and probably specific TRPs in connection with MAS are interesting targets, which may contribute to a possible adjuvant therapy of heart failure. Further experiments using specific TRP channel modulators are therefore warranted to uncover the role of TRPs involved in MAS signaling.

Funding

This study was funded by a grant of the Deutsche Forschungsgemeinschaft to MB and NA (SFB1365 Renoprotection).

CRediT authorship contribution statement

Priyavathi Sureshkumar: Design of methodology; Performing of experiments, Paper writing; **Robson Santos:** Conceptualization, Provision of materials, Paper editing; **Natalia Alenina:** Funding, Paper editing; **Stephan Mergler:** Design of methodology, Provision of instrumentation, Supervision, Paper writing; **Michael Bader:** Conceptualization, Funding, Supervision, Paper writing.

Declaration of Competing Interest

None.

Data Availability

Data will be made available on request.

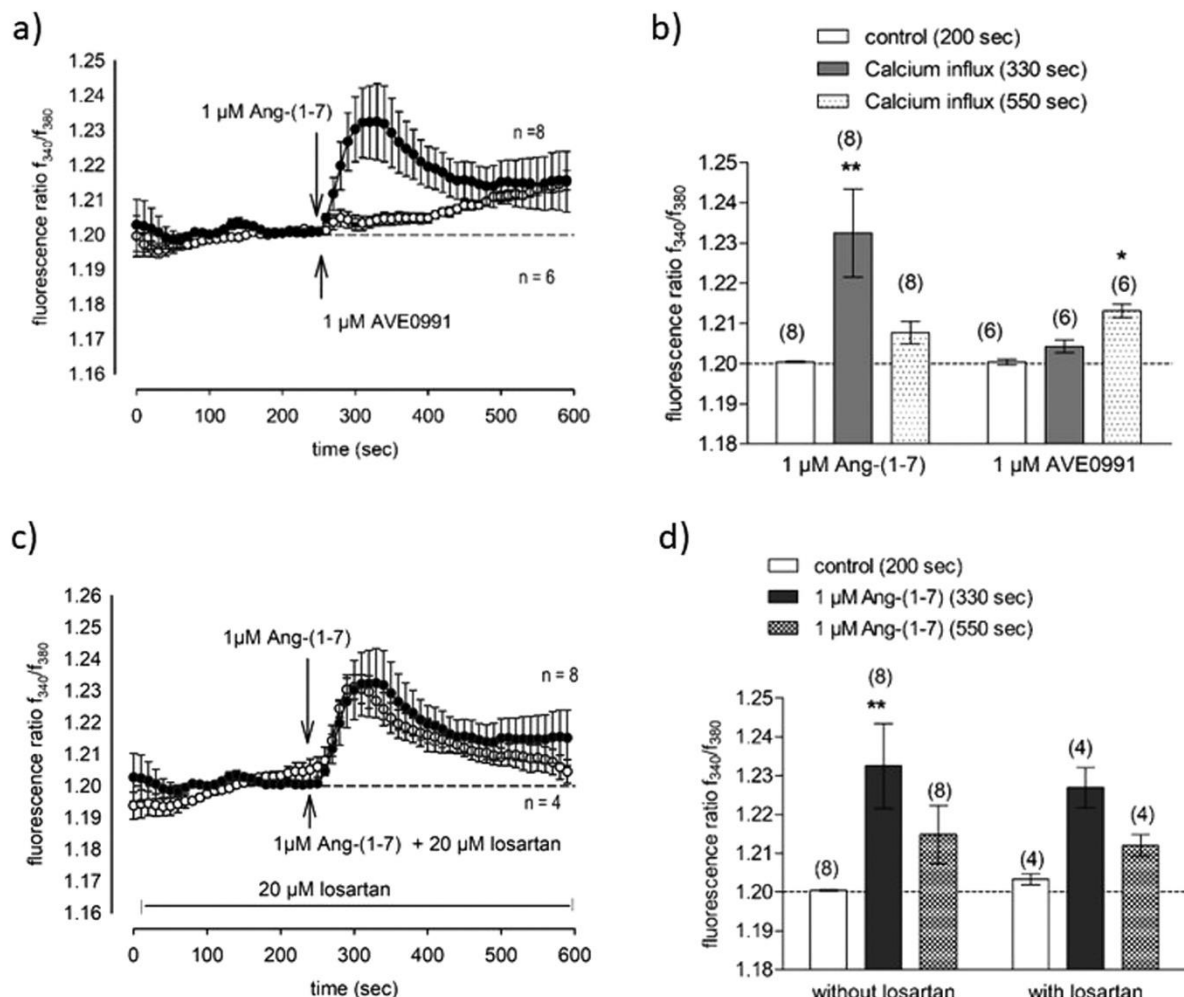
Appendix A. Supporting information

Supplementary data associated with this article can be found in the online version at [doi:10.1016/j.peptides.2023.171010](https://doi.org/10.1016/j.peptides.2023.171010).

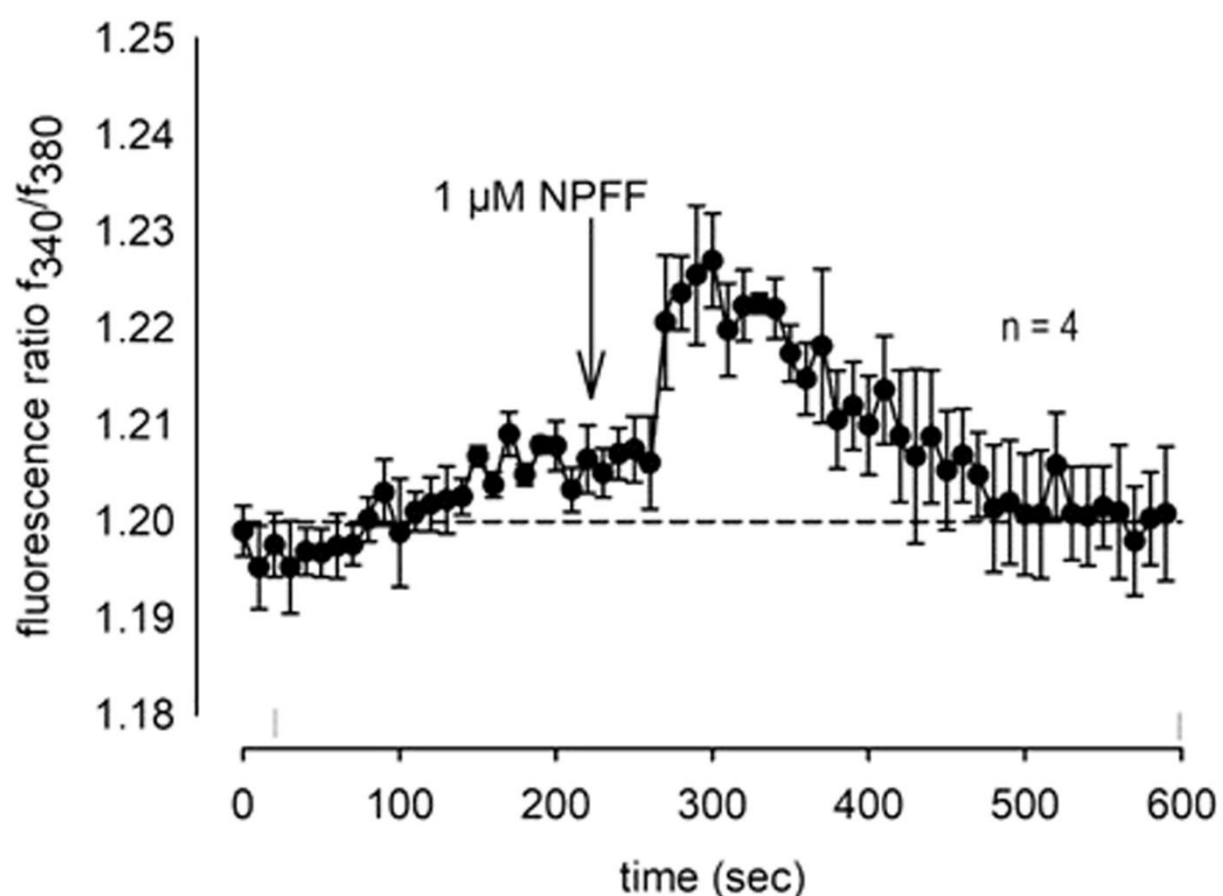
References

- [1] P.W.M. Almeida, R. de Freitas Lima, E.R. de Moraes Gomes, C. Rocha-Resende, D. Roman-Campos, A.N.S. Gondim, et al., Functional cross-talk between aldosterone and angiotensin-(1-7) in ventricular myocytes, *Hypertension* 61 (2) (2013) 425–430, <https://doi.org/10.1161/HYPERTENSIONAHA.111.199539>.
- [2] M. Bader, N. Alenina, M.A. Andrade-Navarro, R.A. Santos, MAS and its related G protein-coupled receptors, *Mrgprs, Pharm. Rev.* 66 (4) (2014) 1080–1105, <https://doi.org/10.1124/pr.113.008136>.
- [3] M. Bader, N. Alenina, D. Young, R.A.S. Santos, R.M. Touyz, The meaning of Mas, *Hypertension* 72 (5) (2018) 1072–1075, <https://doi.org/10.1161/HYPERTENSIONAHA.118.10918>.
- [4] Y. Banno, Y. Yada, Y. Nozawa, Purification and characterization of membrane-bound phospholipase C specific for phosphoinositides, *Hum. Platelets J. Biol. Chem.* 263 (23) (1998) 11459–11465.
- [5] S. Bosnyak, E.S. Jones, A. Christopoulos, M.I. Aguilar, W.G. Thomas, R.E. Widdop, Relative Affinity of Angiotensin Peptides and Novel Ligands at AT1 and AT2 receptors, *Clin. Sci.* 121 (7) (2011) 297–303, <https://doi.org/10.1042/CS20110036>.
- [6] L.M. Broad, F.J. Braun, J.-P. Lievremont, G.S.J. Bird, T. Kurosaki, J.W. Putney, Role of the phospholipase C-Inositol 1,4,5-trisphosphate pathway in calcium release-activated calcium current and capacitative calcium entry, *J. Biol. Chem.* 276 (19) (2001) 15945–15952, <https://doi.org/10.1074/jbc.M011571200>.
- [7] M. Canals, L. Jenkins, E. Kellett, G. Milligan, Up-regulation of the angiotensin II type 1 receptor by the MAS Proto-Oncogene is due to constitutive activation of Gq/G11 by MAS, *J. Biol. Chem.* 281 (24) (2006) 16757–16767, <https://doi.org/10.1074/jbc.M601121200>.
- [8] R.C. Castelo-Branco, D.C.A. Leite-Delova, M. de Mello-Aires, Dose-dependent effects of angiotensin-(1–7) on the NHE3 exchanger and [Ca²⁺]i in vivo proximal tubules, *Am. J. Physiol. -Ren. Physiol.* 304 (10) (2013) F1258–F1265, <https://doi.org/10.1152/ajprenal.00401.2012>.
- [9] R.C. Castelo-Branco, D.C.A. Leite-Delova, F.B. Fernandes, G. Malnic, M. de Mello-Aires, The effects of angiotensin-(1–7) on the exchanger NHE3 and on [Ca²⁺]i in the proximal tubules of spontaneously hypertensive rats, *Am. J. Physiol. -Ren. Physiol.* 313 (2) (2017) F450–F460, <https://doi.org/10.1152/ajprenal.00557.2016>.
- [10] W.C. De Mello, Intracellular angiotensin (1–7) increases the inward calcium current in cardiomyocytes. On the role of PKA activation, *Mol. Cell. Biochem.* 407 (1) (2015) 9–16, <https://doi.org/10.1007/s11010-015-2449-4>.
- [11] M.F. Dias-Peixoto, R.A.S. Santos, E.R.M. Gomes, M.N.M. Alves, P.W.M. Almeida, L. Greco, et al., Molecular mechanisms involved in the angiotensin-(1–7)/mas signalling pathway in cardiomyocytes, *Hypertension* 52 (3) (2008) 542–548, <https://doi.org/10.1161/HYPERTENSIONAHA.108.114280>.
- [12] X. Dong, S.-k Han, M.J. Zylka, M.I. Simon, D.J. Anderson, A diverse family of GPCRs expressed in specific subsets of nociceptive sensory neurons, *Cell* 106 (5) (2001) 619–632, [https://doi.org/10.1016/S0092-8674\(01\)00483-4](https://doi.org/10.1016/S0092-8674(01)00483-4).
- [13] A.H. Gradman, AT1-receptor blockers: differences that matter, *J. Hum. Hypertens.* 16 (3) (2002) S9–S16, <https://doi.org/10.1038/sj.jhh.1001434>.
- [14] F. Guo, B. Liu, F. Tang, S. Lane, E.S. Souslova, D.M. Chudakov, J.F.R. Paton, S. Kasparov, Astroglia are a possible cellular substrate of angiotensin(1–7) effects in the rostral ventrolateral medulla, *Cardiovasc. Res.* 87 (3) (2010) 578–584, <https://doi.org/10.1093/cvr/cvq059>.
- [15] P. Hochstrate, Lanthanum mimicks the trp photoreceptor mutant of drosophila in the blowfly calliphora, *J. Comp. Physiol. A* 166 (1989) 179–187, <https://doi.org/10.1007/BF00193462>.
- [16] Y. Kong, X. Zhao, M. Qiu, Y. Lin, P. Feng, S. Li, et al., Tubular mas receptor mediates lipid-induced kidney injury, *Cell Death Dis.* 12 (2021) 1–20, <https://doi.org/10.1038/s41419-020-03375-z>.
- [17] C.-P. Liu, C.-T. Chou, C.-C. Chi, K.-L. Lin, H.-H. Cheng, Y.-C. Lu, et al., Mechanism of [Ca²⁺]i rise induced by angiotensin 1–7 in MDCK renal tubular cells, *J. Recept. Signal Transduct. Res.* 32 (6) (2012) 335–341, <https://doi.org/10.3109/10799893.2012.738690>.
- [18] H. McMillan, F.T. Lundy, O.M. Dunne, B. Al-Natour, C. Jeanneau, I. About, T. M. Curtis, I. El Karim, Endogenous mas-related G-protein-coupled receptor XI activates and sensitizes TRPA1 in a human model of peripheral nerves, *FASEB J.* 35 (5) (2021), e21492, <https://doi.org/10.1096/fj.202001667RR>.
- [19] M. Mello-Aires, D.C.A. Leite-Delova, R.C. Castelo-Branco, G. Malnic, M. Oliveira-Souza, ANG II, ANG-(1–7), ALDO and AVP biphasic effects on Na⁺/H⁺ transport: the role of cellular calcium, *Nephrol. Ren. Dis.* 2 (1) (2017), <https://doi.org/10.15761/NRD.1000115>.
- [20] K. Mikoshiba, IP3 Receptor/Ca²⁺ channel: from discovery to new signalling concepts, *J. Neurochem.* 102 (5) (2007) 1426–1446, <https://doi.org/10.1111/j.1471-4159.2007.04825.x>.
- [21] R.A.S. Santos, G.Y. Oudit, T. Verano-Braga, G. Canta, U.M. Steckelings, M. Bader, The Renin-Angiotensin system: going beyond the classical paradigms, *Am. J. Physiol. Heart Circ. Physiol.* 316 (5) (2019) H958–H970, <https://doi.org/10.1152/ajpheart.00723.2018>.
- [22] R.A.S. Santos, W.O. Sampaio, A.C. Alzamora, D. Motta-Santos, N. Alenina, M. Bader, M.-J. Campagnole-Santos, The ACE2/Angiotensin-(1–7)/MAS axis of the renin-angiotensin system: focus on angiotensin-(1–7), *Physiol. Rev.* 98 (1) (2018) 505–553, <https://doi.org/10.1152/physrev.00023.2016>.
- [23] A. Shah, R. Gul, K. Yuan, S. Gao, Y.-B. Oh, U.-Y. Kim, S.H. Kim, Angiotensin-(1–7) stimulates high atrial pacing-induced ANP secretion via mas/PI3-kinase/Akt axis and Na⁺/H⁺ exchanger, *Am. J. Physiol. Heart Circ. Physiol.* 298 (5) (2010) H1365–H1374, <https://doi.org/10.1152/ajpheart.00608.2009>.
- [24] H.J. Solinski, T. Gudermann, B. Breit, Pharmacology and signalling of MAS-related G protein-coupled receptors, *Pharmacol. Rev.* 66 (3) (2014) 570–597, <https://doi.org/10.1124/pr.113.008425>.
- [25] C. Sumners, M. Horiuchi, R.E. Widdop, C. McCarthy, T. Unger, U.M. Steckelings, Protective arms of the renin-angiotensin-system in neurological disease, *Clin. Exp. Pharmacol. Physiol.* 40 (8) (2013) 580–588, <https://doi.org/10.1111/1440-1681.12137>.
- [26] L.B. Teixeira, L.T. Parreira-e-Silva, T. Bruder-Nascimento, D.A. Duarte, S. C. Simões, R.M. Costa, et al., Ang-(1–7) is an endogenous β-arrestin-biased agonist of the AT1 receptor with protective action in cardiac hypertrophy, *Sci. Rep.* 7 (1) (2017) 11903, <https://doi.org/10.1038/s41598-017-12074-3>.
- [27] K.C. Tirupula, R. Desnoyer, R.C. Speth, S.S. Karnik, Atypical signalling and functional desensitization response of MAS receptor to peptide ligands, *PloS One* 9 (7) (2014), e103520, <https://doi.org/10.1371/journal.pone.0103520>.
- [28] N.A. Veldhuis, D.P. Poole, M. Grace, P. McIntyre, N.W. Bunnett, The G protein-coupled receptor-transient receptor potential channel axis: molecular insights for targeting disorders of sensation and inflammation, *Pharm. Rev.* 67 (2015) 36–73, <https://doi.org/10.1124/pr.114.009555>.
- [29] E.P. Velloso, R. Vieira, A.C. Cabral, E. Kalapothakis, R.A.S. Santos, Reduced plasma levels of angiotensin-(1–7) and renin activity in preeclamptic patients are associated with the angiotensin I-converting enzyme deletion/deletion genotype, *Braz. J. Med. Biol. Res.* 40 (4) (2007) 583–590, <https://doi.org/10.1590/s0100-879x2007000400018>.
- [30] L. Wang, D. Luo, X. Liao, J. He, C. Liu, C. Yang, H. Ma, Ang-(1–7) offers cytoprotection against ischemia-reperfusion injury by restoring intracellular calcium homeostasis, *J. Cardiovasc. Pharm.* 63 (3) (2014) 259–264, <https://doi.org/10.1097/FJC.0000000000000043>.
- [31] S.R. Wilson, K.A. Gerhold, A. Bifolck-Fisher, Q. Liu, K.N. Patel, X. Dong, D. M. Bautista, TRPA1 is required for histamine-independent, mas-related G protein-coupled receptor-mediated itch, *Nat. Neurosci.* 14 (5) (2011) 595–602, <https://doi.org/10.1038/nn.2789>.
- [32] Y. Yang, J. Liang, C. Zhao, Y. Chen, S. Gu, X. Yang, et al., NHERF4 hijacks mas-mediated PLC/AKT signalling to suppress the invasive potential of clear cell renal cell carcinoma cells, *Cancer Lett.* 519 (2021) 130–140, <https://doi.org/10.1016/j.canlet.2021.06.021>.
- [33] X. Yao, H.-Y. Kwan, Y. Huang, Regulation of TRP channels by phosphorylation, *Neurosignals* 14 (6) (2005) 273–280, <https://doi.org/10.1159/000093042>.
- [34] X. Zhang, H.-J. Cheng, P. Zhou, D.W. Kitzman, C.M. Ferrario, W.-M. Li, C.P. Cheng, Cellular basis of angiotensin-(1–7)-induced augmentation of left ventricular functional performance in heart failure, *Int. J. Cardiol.* 236 (2017) 405–412, <https://doi.org/10.1016/j.ijcard.2017.01.071>.
- [35] P. Zhou, C.P. Cheng, T. Li, C.M. Ferrario, H.-J. Cheng, Modulation of cardiac L-type Ca²⁺ current by angiotensin-(1–7): normal versus heart failure, *Ther. Adv. Cardiovasc. Dis.* 9 (6) (2015) 342–353, <https://doi.org/10.1177/1753944715587424>.

Supplementary data



Supplementary Figure 1: a) Comparison plot of Mas agonists 1 μM AVE0991 vs 1 μM Ang-(1-7) on Mas transfected HEK293 cells, b) Statistical analysis of Fig 1 a, increase in calcium influx with application of 1 μM AVE0991 at 550 s was observed with statistical significance, $p=0.0313$, Wilcoxon signed rank test, two tailed, c) Effect of 1 μM Ang-(1– 7) on MAS-transfected HEK293 cells preincubated with 20 μM losartan (CV-11974) (open circles) compared to 1 μM Ang-(1– 7) without preincubation (filled circles), d) Statistical analysis of Fig. 2c, no statistical significance with and without losartan was observed for Ang-(1-7) induced calcium increase through Mas.



Supplementary Figure 2: 1 μ M of NPFF induced calcium increase in Mas transfected HEK-293 cells observed at 240 sec.

2.3. Manuskript III



TRPM8 Activation via 3-Iodothyronamine Blunts VEGF-Induced Transactivation of TRPV1 in Human Uveal Melanoma Cells

OPEN ACCESS

Edited by:

Antonio Ferrer-Montiel,
Universidad Miguel Hernández de
Elche, Spain

Reviewed by:

Asia Fernandez Carvajal,
Universidad Miguel Hernández de
Elche, Spain

Antonio R. Artalejo,
Universidad Complutense de Madrid,
Spain

***Correspondence:**
Stefan Mergler
stefan.mergler@charite.de

[†]These authors have contributed
equally to this work

Specialty section:

This article was submitted to
Pharmacology of Ion Channels and
Channelopathies,
a section of the journal
Frontiers in Pharmacology

Received: 20 June 2018

Accepted: 11 October 2018

Published: 13 November 2018

Citation:

Walcher L, Budde C, Böhm A,
Reinach PS, Dhandapani P,
Ljubojević N, Schweiger MW, von der
Waydbrink H, Reimers I, Köhrle J and
Mergler S (2018) TRPM8 Activation
via 3-Iodothyronamine Blunts
VEGF-Induced Transactivation of
TRPV1 in Human Uveal Melanoma
Cells. *Front. Pharmacol.* 9:1234.
doi: 10.3389/fphar.2018.01234

Lia Walcher[†], Clara Budde[†], Arina Böhm¹, Peter S. Reinach², Priyavathi Dhandapani³, Nina Ljubojević¹, Markus W. Schweiger¹, Henriette von der Waydbrink¹, Ilka Reimers¹, Josef Köhrle⁴ and Stefan Mergler^{1*}

¹ Klinik für Augenheilkunde, Charité – Universitätsmedizin Berlin, Corporate Member of Freie Universität Berlin, Berlin Institute of Health, Humboldt-Universität zu Berlin, Berlin, Germany, ² School of Ophthalmology and Optometry, Wenzhou Medical University, Wenzhou, China, ³ MDC Buch, Berlin, Germany, ⁴ Institut für Experimentelle Endokrinologie, Charité – Universitätsmedizin Berlin, Corporate Member of Freie Universität Berlin, Berlin Institute of Health, Humboldt-Universität zu Berlin, Berlin, Germany

In human uveal melanoma (UM), tumor enlargement is associated with increases in aqueous humor vascular endothelial growth factor-A (VEGF-A) content that induce neovascularization. 3-Iodothyronamine (3-T₁AM), an endogenous thyroid hormone metabolite, activates TRP melastatin 8 (TRPM8), which blunts TRP vanilloid 1 (TRPV1) activation by capsaicin (CAP) in human corneal, conjunctival epithelial cells, and stromal cells. We compare here the effects of TRPM8 activation on VEGF-induced transactivation of TRPV1 in an UM cell line (92.1) with those in normal primary porcine melanocytes (PM) since TRPM8 is upregulated in melanoma. Fluorescence Ca²⁺-imaging and planar patch-clamping characterized functional channel activities. CAP (20 μM) induced Ca²⁺ transients and increased whole-cell currents in both the UM cell line and PM whereas TRPM8 agonists, 100 μM menthol and 20 μM icilin, blunted such responses in the UM cells. VEGF (10 ng/ml) elicited Ca²⁺ transients and augmented whole-cell currents, which were blocked by capsazepine (CPZ; 20 μM) but not by a highly selective TRPM8 blocker, AMTB (20 μM). The VEGF-induced current increases were not augmented by CAP. Both 3-T₁AM (1 μM) and menthol (100 μM) increased the whole-cell currents, whereas 20 μM AMTB blocked them. 3-T₁AM exposure suppressed both VEGF-induced Ca²⁺ transients and increases in underlying whole-cell currents. Taken together, functional TRPM8 upregulation in UM 92.1 cells suggests that TRPM8 is a potential drug target for suppressing VEGF induced increases in neovascularization and UM tumor growth since TRPM8 activation blocked VEGF transactivation of TRPV1.

Keywords: uveal melanoma, 3-iodothyronamine, vascular endothelial growth factor, Intracellular Ca²⁺, transient receptor potential vanilloid 1 channel, transient receptor potential melastatin 8

INTRODUCTION

Among all cancers of the eye, uveal melanoma (UM) is the most frequent form in adults. Notably, UM is mostly found in the choroid (65% of all cases) and in ciliary body (15%), but it rarely occurs in the retina (1.4%; Singh et al., 2011). About 50% of the patients with primary UM will finally develop distant metastases predominantly in the liver (90%) (Spagnolo et al., 2012). To date, the etiology of UM is not fully understood and neither metastatic properties nor patient survival has significantly improved over the last decades (Tran et al., 2013). Accordingly, there is a pressing need for developing alternative approaches to treat this disease especially since there are no FDA approved drugs available for suppressing metastatic melanoma.

A preclinical approach targeting angiogenesis in combination with irradiation has been reported using bevacizumab, a monoclonal antibody binding and inhibiting vascular endothelial growth factor (VEGF; Sudaka et al., 2013). Nevertheless, the advantage of this combination therapy is unclear because this VEGF trap did not have a dramatic impact on any of the functional activities in UM cell lines (Logan et al., 2013). As a matter of fact, such treatment is reported to even promote expansion of melanoma cells *in vitro* (Dithmer et al., 2017). Furthermore, neoadjuvant intravitreous injection of this VEGF trap failed to shrink large size melanoma and is even counter indicated in these cases because it may instead even promote melanoma growth (Francis et al., 2017).

Increases in VEGF receptor activity induce rises in intracellular calcium levels [Ca^{2+}]_i in endothelial cells exposed to serum-free conditioned medium of human malignant gliomas (Criscuolo et al., 1989). The bioactive factor is an angiogenic factor named vascular permeability factor (VPF)—more recently characterized as VEGF, which promotes various diseases including eye tumor diseases (e.g., retinoblastoma) (Jia et al., 2007). It stimulates angiogenesis through activating non-voltage-gated Ca^{2+} channels such as transient-receptor-potential-channels (TRPs) namely the canonical receptor type 4 or 6 (TRPC4 or TRPC6) in human microvascular endothelial cells (Qin et al., 2016). Dysfunctional TRPs are implicated in cancer formation (reviewed in Bödding, 2007; Prevarskaia et al., 2007). Tumor and normal cells both express TRPs, but certain TRPs are either upregulated or downregulated in a cancerous

condition. For example, TRP vanilloid receptor type 1 (TRPV1; capsaicin receptor) is overexpressed in some carcinomas (Miao et al., 2008; Marincsák et al., 2009) and neuroendocrine tumors (Mergler et al., 2012b). In addition, the highly Ca^{2+} selective TRPV6 and TRP melastatin receptor type 8 (TRPM8; menthol receptor) are overexpressed in prostate tumor cells (Fixemer et al., 2003; Bidaux et al., 2005; Bai et al., 2010; Gkika et al., 2010). The functional relevance of TRPM8 upregulation in prostatic cancer cells as a target for suppressing their proliferation was documented by showing that inhibition of TRPM8 upregulation with highly specific blockers, AMTB, JNJ41876666, and RNAi suppressed increased proliferation rates in all tumor cells but not in non-tumor prostate cells (Valero et al., 2012). We found that TRPM8 is also overexpressed in highly malignant retinoblastoma and uveal melanoma along with TRPV1 compared to their levels in healthy human uvea or retina (Mergler et al., 2012a, 2014). Even in benign pterygial eye tumor cells, functional TRPV1 expression is upregulated (Garreis et al., 2016). Such increases are associated with larger mitogenic responses to VEGF that are induced by its cognate receptor, VEGFR, transactivating TRPV1 (Garreis et al., 2016).

3-iodothyronamine (3-T₁AM) is a decarboxylated thyroid hormone (T₃ and T₄) metabolite, which activates G protein-coupled receptors (GPCRs) especially the trace amine associated receptor 1 (TAAR1). It also induces a dose-dependent reversible 10°C decrease in mice body temperature (Scanlan et al., 2004; Braulke et al., 2008; Panas et al., 2010) and hypothermia in rodents (Cichero et al., 2014; Hoefig et al., 2016). Likewise, 3-T₁AM is a multi-target ligand modulating β-adrenergic receptor 2 signaling in ocular epithelial cells (Dinter et al., 2015a). In corneal epithelial and endothelial cells as well as thyroid cells, 3-T₁AM acts as a selective TRPM8 agonist (Khajavi et al., 2015, 2017; Lucius et al., 2016; Schanze et al., 2017). Since blocking increases in VEGF levels suppress both angiogenesis and expansion of tumorous pathology, it is relevant to identify novel targets to inhibit endothelial cell proliferation. We hypothesized that TRPM8 is one such target because icilin-induced TRPM8 activation suppressed TRPV1 activity in cornea and conjunctiva epithelial cells (Khajavi et al., 2015; Lucius et al., 2016). The notion that TRPM8 activation also inhibits VEGF-induced TRPV1 activation required for increasing angiogenesis was tenable because VEGF-induced activation of its cognate receptor transactivates TRPV1 (Khajavi et al., 2015; Lucius et al., 2016).

We show here that crosstalk between members of this receptor triad affects Ca^{2+} signaling responses induced by VEGFR transactivation of TRPV1 in UM 92.1 melanoma cells. Therefore, selective targeting of TRPM8 control of TRPV1 responsiveness to transactivation by VEGF may ultimately provide an alternative approach to reduce tumor growth in a clinical setting.

MATERIALS AND METHODS

Materials

BCTC, AMTB, and fura-2AM were purchased from TOCRIS Bioscience (Bristol, United Kingdom). CPZ and icilin were procured from Cayman Chemical Company (Ann Arbor,

Abbreviations: 3-T₁AM, 3-Iodothyronamine (endogenous thyroid hormone (TH)-derived metabolite) (Scanlan et al., 2004); 92.1, human uveal melanoma cell line 92.1 (De Waard-Siebinga et al., 1995); AMTB, N-(3-Aminopropyl)-2-[(3-methylphenyl)methoxy]-N-(2-thienylmethyl)benzamide hydrochloride [TRPM8 blocker (Lashinger et al., 2008)]; BCTC, N-(4-tertiarybutyl-phenyl)-4-(3-chloropyridin-2-yl) tetrahydropyrazine-1(2H)-carboxamide; CAP, Capsaicin [TRPV1 agonist (Vriens et al., 2009)]; CB1, Cannabinoid receptor 1; CZP, Capsazepine [TRPV1 antagonist (Vriens et al., 2009)]; EGFR, Epidermal growth factor receptor; FDA, Food and Drug Administration; hTAAR1, Human trace amine-associated receptor; PM, Porcine melanocytes; RPE, Retinal pigment epithelium; TRPA, Transient receptor potential ankyrin; TRPC, Transient receptor potential canonical; TRPM, Transient receptor potential melastatin; TRPs, Transient receptor potential channels; TRPV, Transient receptor potential vanilloid; UM, Uveal melanoma; VEGF, Vascular endothelial growth factor; VEGFR, Vascular endothelial growth factor receptor; VPF, Vascular permeability factor.

Michigan, U.S.A.). Medium and supplements for cell culture were ordered from Life Technologies Invitrogen (Karlsruhe, Germany) or Biochrom AG (Berlin, Germany). Melanocyte Growth Medium M2 was obtained from Promocell (Heidelberg, Germany). Dispase II was ordered from Boehringer (Ingelheim, Germany) and accutase was provided by PAA Laboratories (Pasching, Austria). Unless otherwise stated, all other reagents were procured from Sigma (Deisenhofen, Germany).

Cell Culture

Uveal melanoma cell line 92.1 (UM 92.1) was kindly provided by Martine Jager and colleagues (Leiden University; Netherlands) (De Waard-Siebinga et al., 1995). In brief, UM cells were grown in RPMI-1640 supplemented with 10% fetal bovine serum (FBS), 4 mM L-glutamine, penicillin/streptomycin at 37°C under 10% CO₂ atmosphere and 80% humidity (Mergler et al., 2014).

Melanocyte Primary Cell Cultivation

PM were isolated from porcine eyes provided by a slaughterhouse. The preparation and primary cell cultivation were performed as described (Valtink and Engelmann, 2007). In brief, eyeballs were cut into two pieces. The choroid with the connected retinal pigment epithelium (RPE) layer was separated from the sclera and incubated in collagenase IV for several hours at 37°C in order to release RPE cells from melanocytes. After a second treatment with dispase II, the choroids were put into a shaking device in order to better isolate the cells from the tissue. Finally, the cell suspension was passed through a cell strainer. After centrifugation, cells were washed in RPMI medium and seeded in tissue culture flasks. After 24 h, the medium was changed and cells were cultivated under the same conditions as those described for the UM 92.1 cells (Mergler et al., 2014). To avoid contamination with RPE cells or fibroblasts, the culture medium was supplemented with genetin for about 5–7 days prior to subcultivation. Melanocyte cell cultivation was limited to no longer than 2 weeks to avoid cell dedifferentiation.

Intracellular Calcium Fluorescence Imaging

Semi confluent cells (\approx 80%) were loaded with fura-2/AM (2 μ M) at 37°C. After about 40 min, the cells were washed with a Ringer-like (control) solution containing (mM): 150 NaCl, 6 CsCl, 1 MgCl₂, 10 glucose, 10 HEPES, and 1.5 CaCl₂ at pH 7.4 and 317 mOsM (Mergler et al., 2014). KCl was replaced with CsCl to characterize TRP channel activity (Voets et al., 2004). Following dye loading, the cells were exposed to this solution on the stage of an inverted microscope (Olympus BW50WI, Olympus Europa Holding GmbH, Hamburg, Germany), connected with a digital imaging system (TILL Photonics, Munich, Germany). Fura-2/AM fluorescence was consecutively excited at 340 and 380 nm for different times (Grynkiewicz et al., 1985). The 510 nm emission ratio (f_{340nm}/f_{380nm}) is an index of relative intracellular Ca²⁺ ([Ca²⁺]_i) levels (Grynkiewicz et al., 1985). The 340 and 380 nm response signals were continuously detectable and did not distort the ratio. The changes in ratios were overall small because of the presetting of the single fluorescence signals at 340 and 380 nm, respectively. A control where TRPM8 was heterologously expressed and activated by their agonists is

provided (Lucius et al., 2016). Before starting a measuring session, baseline stability was established for 8–20 min. All experiments were performed at a constant room temperature (\approx 23°C). In addition, the fura-2-induced fluorescence signals were alternatively evaluated in a bath chamber using a Life Science fluorescence cell imaging software in conjunction with a high-resolution digital camera (Olympus XM-10) (Figures 9–11). Cutoff filters isolated alternative fluorescence excitation at 340 and 380 nm every 5 s wavelengths provided by a LED light source (LED-Hub by Omikron, Rodgau-Dudenhovern, Germany). Fura-2 fluorescence was alternately excited at 340 and 380 nm and emission was detected at 510 nm (250 ms–3.8 s exposure time). For image acquisition and data evaluation, the Life Science imaging software cellSens was used (Olympus, Hamburg, Germany). Results are shown as mean traces of the f_{340nm}/f_{380nm} ratio \pm SEM (error bars in both directions) with n-values indicating the number of experiments per data point. The Ca²⁺ data presented from many cells in several experiments were normalized (control set to 1.2 and 0.2, respectively) and averaged (with error bars). The time delay of 1–2 min in inducing a Ca²⁺ transient stems from exposing the cells to a stationary bath rather than a flow through superfusion. When drugs were solubilized in dimethyl sulfoxide (DMSO) solution, their working concentration did not exceed 0.1%, which did not alter the Ca²⁺ base line.

Planar Patch-Clamp Recordings

Whole-cell currents were measured with a planar patch-clamp setup (Port-a-Patch[®]; Nanion, Munich, Germany) in connection with an EPC 10 patch-clamp amplifier (HEKA, Lamprecht, Germany) and the PatchMaster software (Version 2.6; HEKA, Lamprecht, Germany) (Mergler et al., 2012a, 2014; Garreis et al., 2016). A standard intracellular solution containing (mM): 50 CsCl, 10 NaCl, 60 CsF, 20 EGTA, and 10 HEPES-acid at pH \approx 7.2 and \approx 288 mOsM was applied to the microchip (both provided by Port-a-Patch[®], Nanion, Munich, Germany). The external solution contained (mM): 140 NaCl, 4 KCl, 1 MgCl₂, 2 CaCl₂, 5 D-glucose monohydrate and 10 HEPES, pH \approx 7.4, and osmolarity \approx 298 mOsM. At first, 5–10 μ l of a single cell suspension were placed onto a microchip containing the aforementioned external solution. A software-controlled pump (Nanion) provided a connection between a single cell and the electrical system (sealing). The mean membrane capacitance was 10 pF \pm 1 pF (n = 88) and mean access resistance was 25 \pm 3 M Ω (n = 88). Series resistances as well as fast and slow capacitative transients were compensated by the PatchMaster software. The liquid junction potential was calculated (\approx 3.8 mV; Barry, 1994) and offset by the software. Notably, current recordings were all leak-subtracted and cells with leak currents above 100 pA were excluded from analysis. All experiments were performed at 21–23°C room temperature. The holding potential (HP) was set to 0 mV in order to eliminate any possible contribution of voltage-dependent Ca²⁺ channel activity. Cells were kept in the whole-cell configuration for \sim 10 min for control recordings and the compensation proceedings before starting the experiments (Pusch and Neher, 1988). Whole-cell currents were recorded over a voltage range of -60 to +130 mV for 500 ms each and measured every 5 s. The current densities (pA/pF) were

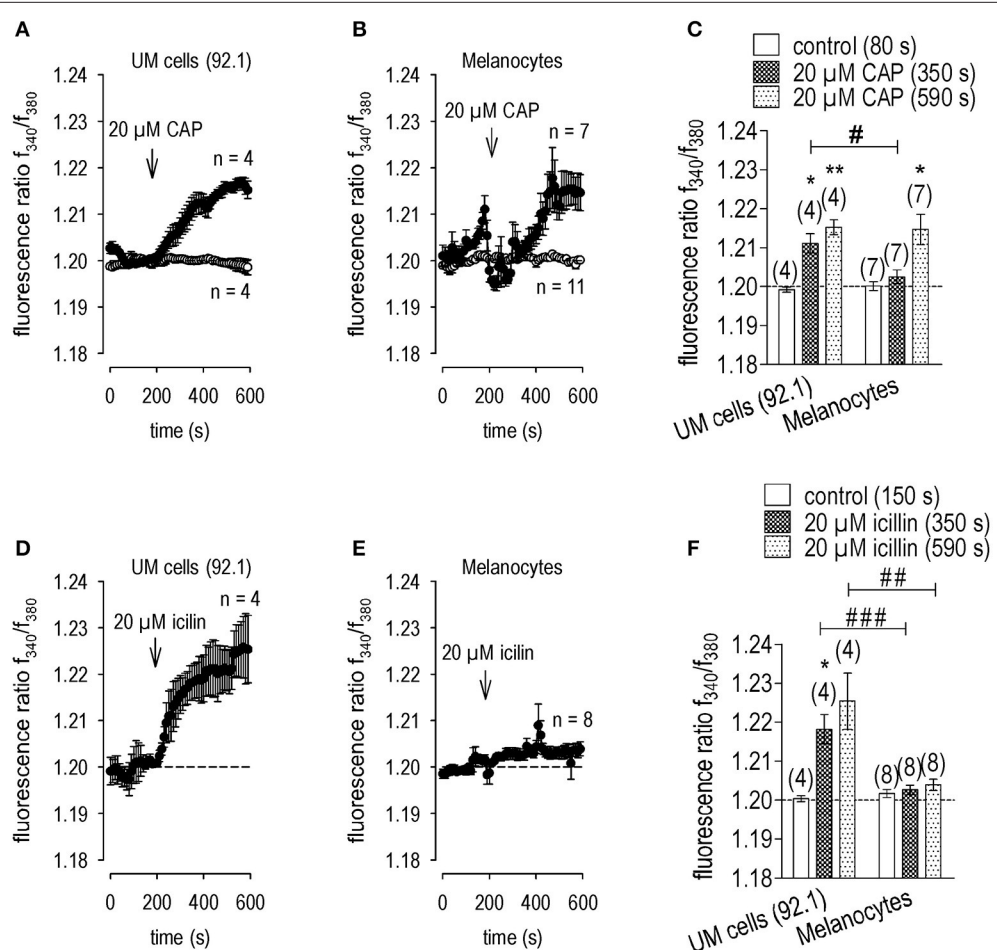


FIGURE 1 | Larger functional TRPM8 expression in UM 92.1 than PM cells. Drug additions were made at the indicated time points (arrows). Data are mean \pm SEM of 4–8 experiments. **(A)** CAP (20 μ M) induced an irreversible Ca^{2+} influx ($n = 4$) whereas non-treated control cells showed a constant Ca^{2+} baseline ($n = 4$). **(B)** The same effect could be observed in normal porcine melanocytes but with a time lag ($n = 7$; controls $n = 11$). **(C)** Summary of the experiments with CAP ($n = 4$ –7). The asterisks (*) show significant differences between control and CAP ($n = 4$; 350s; $*p < 0.05$; $n = 7$; 590s; $**p < 0.01$; paired tested). The hashtags (#) shows a significant difference of the CAP effect at 350 s between UM 92.1 cells and melanocytes ($n = 4$ –7; 590s; $#p < 0.05$; unpaired tested). **(D–F)** Same experiments as shown in **(A–C)**, but with icilin (20 μ M) ($n = 4$ –8). The icilin effect was markedly reduced in porcine melanocytes. The asterisks (*) show significant differences between control and icilin ($n = 4$; 350s; $*p < 0.05$; paired tested). The hashtags (#) shows a significant difference of the icilin effect at 350 s and 590 s between UM 92.1 cells and melanocytes ($n = 4$ –8; 350s; $##p < 0.005$; 590s; $##p < 0.01$; unpaired tested).

calculated by dividing the current (pA) by the cell membrane capacitance (pF). For purposes of comparison, the currents were normalized to control currents (set to 100%).

Statistical Analysis

The paired two-tailed Student's *t*-test was applied in conjunction with several normality tests (KS normality test, D'Agostino & Pearson omnibus normality test, and Shapiro-Wilk normality test). If these tests failed, non-parametric Wilcoxon matched pairs were used. The Student's *t*-test was also used for unpaired data, if the data also passed the aforementioned normality tests. If these tests failed, the non-parametric Mann-Whitney-*U* test was performed. Welch's correction was applied if data variance of the two groups were too different. Probabilities of $p < 0.05$ [indicated by asterisks (*) and hash tags (#)] were considered to be significant. The number of repeats is shown in each case in brackets, near the traces or bars. All values are

means \pm SEM (error bars in both directions). All plots were generated with SigmaPlot software version 12.5 for Windows (Systat Software, San Jose, California, United States) and with GraphPad Prism version 5.00 for Windows (GraphPad Software, San Diego California USA), respectively.

RESULTS

Functional TRPV1 Channel Expression in UM 92.1 and Porcine Melanocytes

TRPV1 activity in all cases was documented based on the magnitudes of the Ca^{2+} transients induced by the highly selective TRPV1 agonist, capsaicin (CAP; 20 μ M; Caterina et al., 1997; Pingle et al., 2007; Vriens et al., 2009) in PM. **Figure 1B** shows that CAP increased $f_{340\text{nm}}/f_{380\text{nm}}$ from a stable baseline value of 1.200 ± 0.001 to 1.215 ± 0.004 after 590 s ($n = 7$, $p < 0.05$). Interestingly, CAP evoked a biphasic or delayed effect on

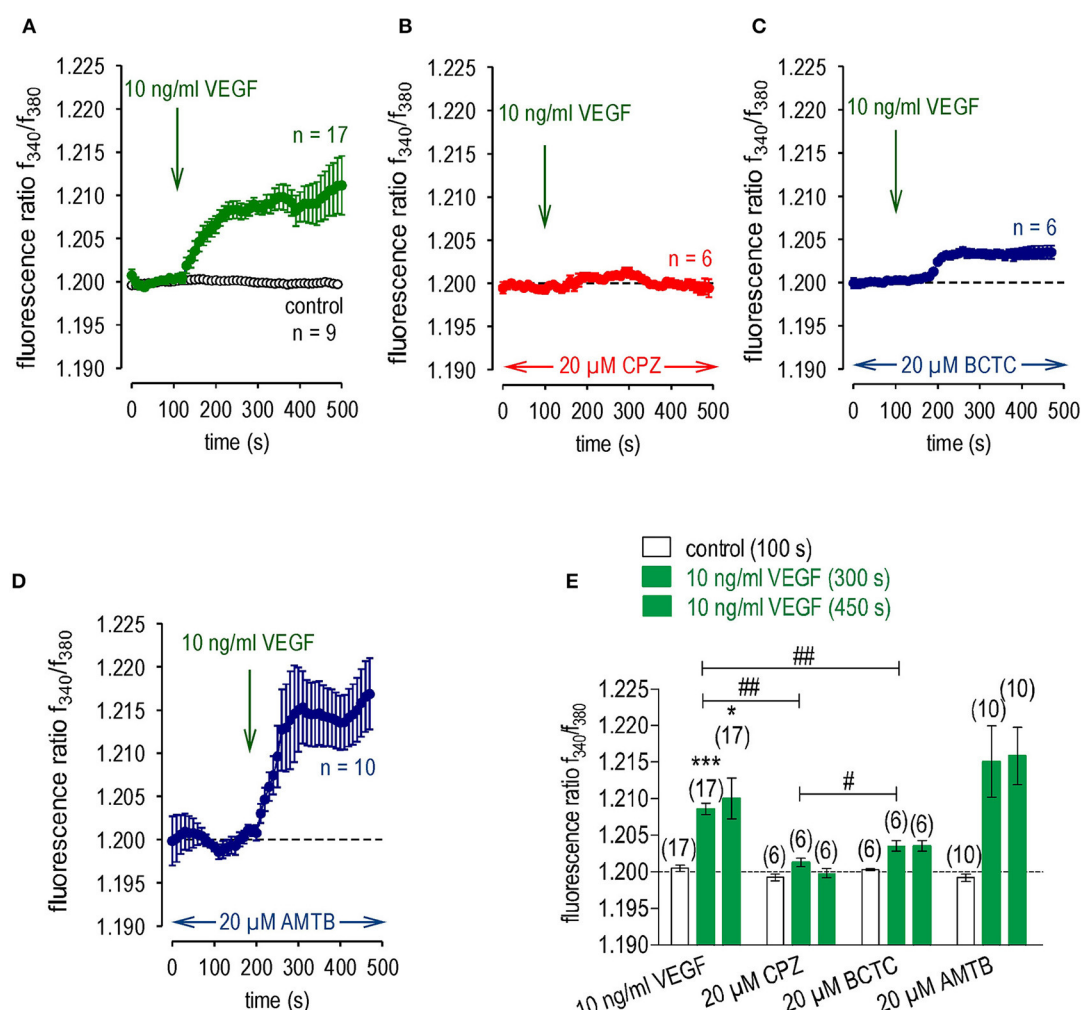


FIGURE 2 | VEGF transactivates TRPV1 channels in UM 92.1 cells. VEGF (10 ng/ml) was added at the indicated time points (arrows). Data are mean \pm SEM of 6–17 experiments. **(A)** Mean trace showing VEGF-induced Ca^{2+} increase ($n = 17$). **(B)** Same experiment as shown in **(A)**, but in the presence of CPZ (20 μM). CPZ clearly suppressed the VEGF-induced Ca^{2+} increase ($n = 6$). **(C)** Same experiment as shown in **(A)**, but in the presence of BCTC (20 μM). BCTC partially suppressed the VEGF-induced Ca^{2+} increase ($n = 6$). **(D)** Same experiment as shown in **(A)**, but in the presence of AMTB (20 μM). AMTB had no effect on the VEGF-induced Ca^{2+} increase ($n = 10$). **(E)** Summary of the experiments with VEGF and the TRP channel blockers. The asterisks (*) show significant Ca^{2+} increases with VEGF ($n = 17$; 300 s; *** $p < 0.005$; 450 s; * $p < 0.05$; paired tested). The hashtags (##) indicate statistically significant differences of fluorescence ratios between VEGF with and without the TRP channel blockers CPZ and BCTC, resp. ($n = 6-17$; 300 s; #*# $p < 0.01$; unpaired tested). One hashtag (#) indicates a statistically significant difference between CPZ and BCTC effect on VEGF-induced Ca^{2+} increase at 300 s ($n = 6$; # $p < 0.05$).

intracellular Ca^{2+} increase in PM, which was absent in UM 92.1 tumorous cells. In UM 92.1 cells, CAP instead increased the $f_{340\text{nm}}/f_{380\text{nm}}$ ratio more promptly but to the same level; namely, from 1.199 ± 0.001 (80 s) to 1.215 ± 0.002 after 590 s ($n = 4$, $p < 0.01$; **Figures 1A,C**). Overall, there is a difference in the Ca^{2+} response pattern. While in PM, there was a large data scatter and a delayed $[\text{Ca}^{2+}]_i$ transient (**Figure 1B**), this response was both more reproducible and prompt in UM 92.1 cells (**Figure 1A**).

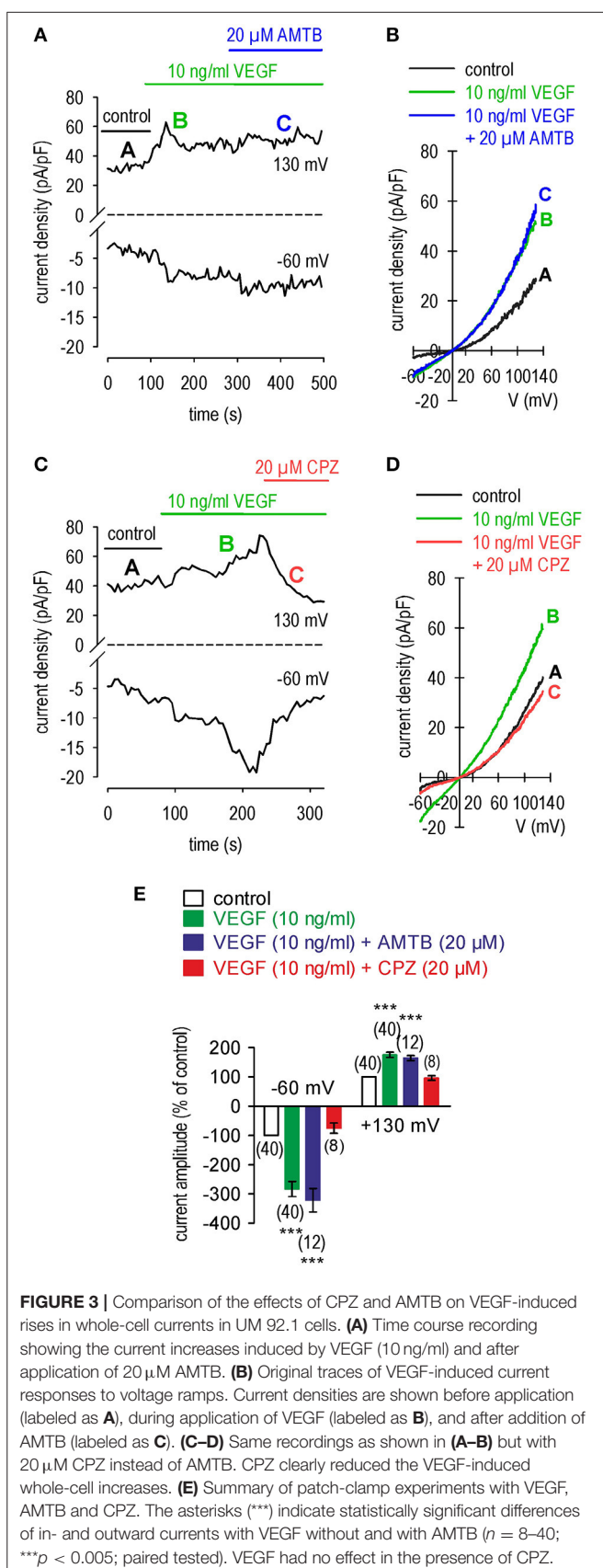
Functional TRPM8 Channel Expression in UM 92.1 Cells

Even though there was TRPM8 gene and functional expression in different UM cell lines including UM 92.1 cells, it was absent

in human uveas (Mergler et al., 2014). To confirm that lack of TRPM8 expression is indicative of normal tissue, we probed for its presence in healthy PM. Iciliin (20 μM), a mixed TRPM8/TRPA1-agonist (Andersson et al., 2004; Rawls et al., 2007) induced a Ca^{2+} transient in UM 92.1 cells ($n = 4$; $p < 0.05$; **Figures 1D,F**) whereas such an effect did not occur in PM ($n = 8$; $p > 0.05$; **Figures 1E,F**). Therefore, detectable functional TRPM8 and/or TRPA1 expression is a marker of UM cell line malignancy.

VEGF-Transactivates TRPV1

VEGF increased the $f_{340\text{nm}}/f_{380\text{nm}}$ ratio from 1.2000 ± 0.0004 to 1.209 ± 0.001 ($t = 300$ s; $n = 17$; $p < 0.01$, **Figures 2A,E**). As



VEGF induced Ca^{2+} transients through transactivating TRPV1 channels in corneal fibroblasts and conjunctival epithelial cells, we determined if such an interaction occurs in UM 92.1 cell lines. This was done by evaluating the individual effects of each of the following inhibitors at 20 μ M: (a) CPZ for TRPV1 (Vriens et al., 2009); (b) BCTC for TRPM8/TRPV1 (Behrendt et al., 2004; Weil et al., 2005; Vriens et al., 2009; Benko et al., 2012; Liu et al., 2016); and (c) AMTB for TRPM8 (Lashinger et al., 2008). With CPZ, the baseline ratio remained invariant at $f_{340\text{nm}}/f_{380\text{nm}}$ ratio = 1.2013 ± 0.0006 ($n = 6$; **Figure 2B**) whereas with AMTB this ratio rose to 1.215 ± 0.005 ; $p > 0.05$; $n = 10$; **Figure 2D**. This difference indicates that the VEGF-induced Ca^{2+} transients mediated by VEGFR solely transactivate TRPV1. With BCTC, the VEGF induced Ca^{2+} transients were only partially inhibited (**Figure 2C**). In this case, VEGF induced a transient reaching 1.2030 ± 0.0005 ($p < 0.01$; $n = 6$ **Figure 2C**), which was larger than the ratio induced by VEGF in the presence of CPZ ($p < 0.05$; $n = 6$; **Figures 2B,D**). This difference is consistent with BCTC being a mixed TRPM8/TRPV1 antagonist.

While AMTB did not influence the VEGF-induced increases in whole-cell currents (20 μ M; $n = 12$; **Figures 3A,B,E**), this increase was suppressed by CPZ (20 μ M; $n = 8$; $p < 0.005$; **Figures 3C–E**). In summary, the VEGF-induced increases in Ca^{2+} influx and whole-cell currents are mediated through transactivation of TRPV1 by VEGFR.

Equivalent Activation of TRPV1 by VEGF and CAP in UM 92.1 Cells

As VEGF induces downstream signaling through transactivating TRPV1, we determined if CAP augmented VEGF induced TRPV1 activation. The results shown in **Figures 4A,B** indicate after application of VEGF, the maximal inward— and outward currents were -30 ± 5 pA/pF and 164 ± 17 pA/pF respectively ($n = 7$). Subsequently CAP failed to significantly enhance the whole-cell currents, which stabilized at -35 ± 7 pA/pF and 154 ± 14 pA/pF respectively ($n = 4$; $p > 0.05$; **Figures 4A,C–E**).

3-T₁AM Activates TRPM8 in UM 92.1 Cells

As a positive control, the effect of 100 μ M menthol, a highly selective TRPM8 agonist, was determined on whole-cell currents since this concentration was previously used to validate functional TRPM8 expression (Knowlton et al., 2011; Hirata and Oshinsky, 2012; Robbins et al., 2012; Mergler et al., 2013). As shown in **Figures 5A,B**, menthol increased the inward currents from -15 ± 3 pA/pF (control) to -36 ± 5 pA/pF ($p < 0.01$; $n = 8$; **Figure 5C**) whereas 20 μ M AMTB suppressed this rise to -13 ± 4 pA/pF ($p < 0.05$; $n = 8$; **Figure 5C**). Similarly menthol increased the currents from 166 ± 30 pA/pF (control) to 236 ± 46 pA/pF, which AMTB suppressed to 175 ± 31 pA/pF (**Figure 5C**). The results of current normalization shown in **Figures 5D,E** (control set to 100%) affirm cell membrane delimited functional TRPM8 expression.

Irrespective of 3-T₁AM ranging from 200 nM to 10 μ M, its effects were essentially the same as those obtained with menthol (**Figures 6A,B**). The largest increases were obtained over a range between 1 and 5 μ M (Lucius et al., 2016). In

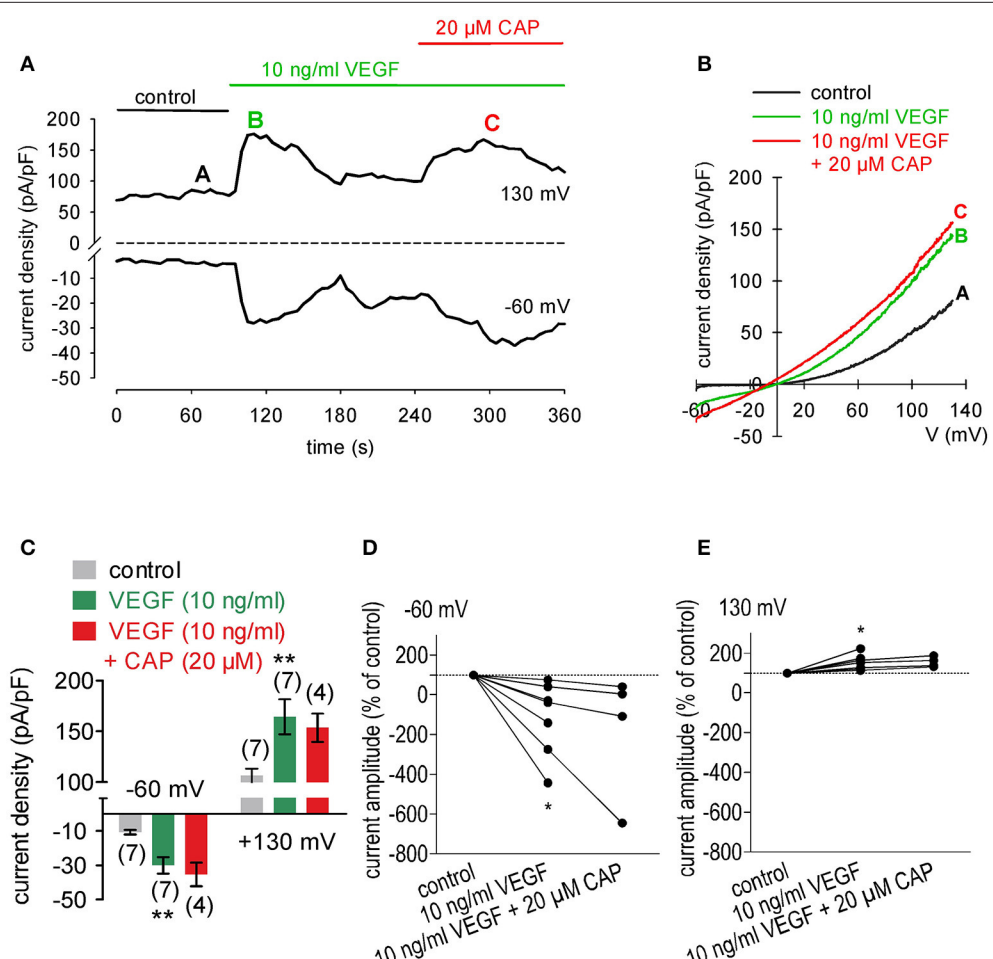


FIGURE 4 | CAP does not augment increases in whole-cell currents in VEGF treated UM 92.1 cells. **(A)** Time course recording showing the current peak induced by 10 ng/ml VEGF and current peak after application of 20 μ M CAP. **(B)** Original traces of VEGF- and CAP-induced current responses to voltage ramps. Current densities are shown before application (labeled as **A**), during application of VEGF (labeled as **B**), and after addition of CAP (labeled as **C**). **(C)** Summary of patch-clamp experiments with VEGF and CAP. The asterisks (**) indicate statistically significant increase with VEGF ($n = 7$; $p < 0.01$; paired tested) and unchanged magnitude of currents in the presence of CAP ($n = 4$; $p > 0.05$; paired tested). **(D)** Maximal negative current amplitudes induced by a voltage step from 0 to -60 mV are depicted in percent of control values before application of 10 ng/ml VEGF. VEGF-induced inward currents ($n = 7$; * $p < 0.05$) were not increased in the presence of 20 μ M CAP ($n = 4$; $p > 0.05$). **(E)** Maximal positive current amplitudes induced by a voltage step from 0 to $+130$ mV are depicted in percent of control values before application of 10 ng/ml VEGF. VEGF-induced outwardly rectifying currents ($n = 7$; * $p < 0.05$) were not increased in the presence of 10 μ M CAP ($n = 4$; $p > 0.05$).

UM 92.1 cells, 1 μ M 3-T₁AM increased the inward currents from -8 ± 2 pA/pF (control) to -25 ± 9 pA/pF ($p < 0.01$; $n = 9$; **Figure 6C**) whereas 20 μ M AMTB suppressed this rise to -18 ± 10 pA/pF ($p < 0.05$; $n = 7$; **Figure 6C**). Similarly, 3-T₁AM also increased the outward currents from 80 ± 24 pA/pF (control) to 142 ± 40 pA/pF, which AMTB suppressed to 112 ± 45 pA/pF ($n = 7-9$; $p < 0.05$) (**Figure 6C**). Similar results were obtained following current normalization shown in **Figures 6D,E**.

3-T₁AM Suppresses VEGF-Induced Rises in Whole-Cell Currents

In TRPM8 transfected cells, 3-T₁AM and BCTC increased and inhibited Ca²⁺ transients, respectively (Lucius et al., 2016). These opposing effects were used to determine if TRPM8 activation

suppresses CAP induced rises in TRPV1 activity whereas BCTC reduces the inhibitory effect of 3-T₁AM on these responses to CAP. 3-T₁AM (5 μ M) induced a [Ca²⁺]_i transient ($p < 0.01$; $n = 9$; **Figures 7A,C**) whereas 20 μ M BCTC inhibited this response ($p < 0.05$; $n = 4$; **Figures 7B,C**). Even though BCTC is reportedly as a mixed TRPM8/ TRPV1 antagonist in some cell types, it did not alter Ca²⁺ transients induced by a relatively high CAP concentration in a heterologous expression system (Lucius et al., 2016). 3-T₁AM suppressed the 10 ng/ml VEGF-induced Ca²⁺ transient (**Figures 7E,F**). Another indication of suppression by TRPM8 of VEGF transactivation by TRPV1 is that 1 μ M 3-T₁AM suppressed VEGF-induced increases in the whole-cell currents ($n = 7$; $p < 0.01$; **Figure 8**). Mimicking of this inhibitory effect by icilin validates that 3-T₁AM is a selective TRPM8 agonist (Khajavi et al., 2015, 2017; Lucius et al., 2016; Schanze et al., 2017).

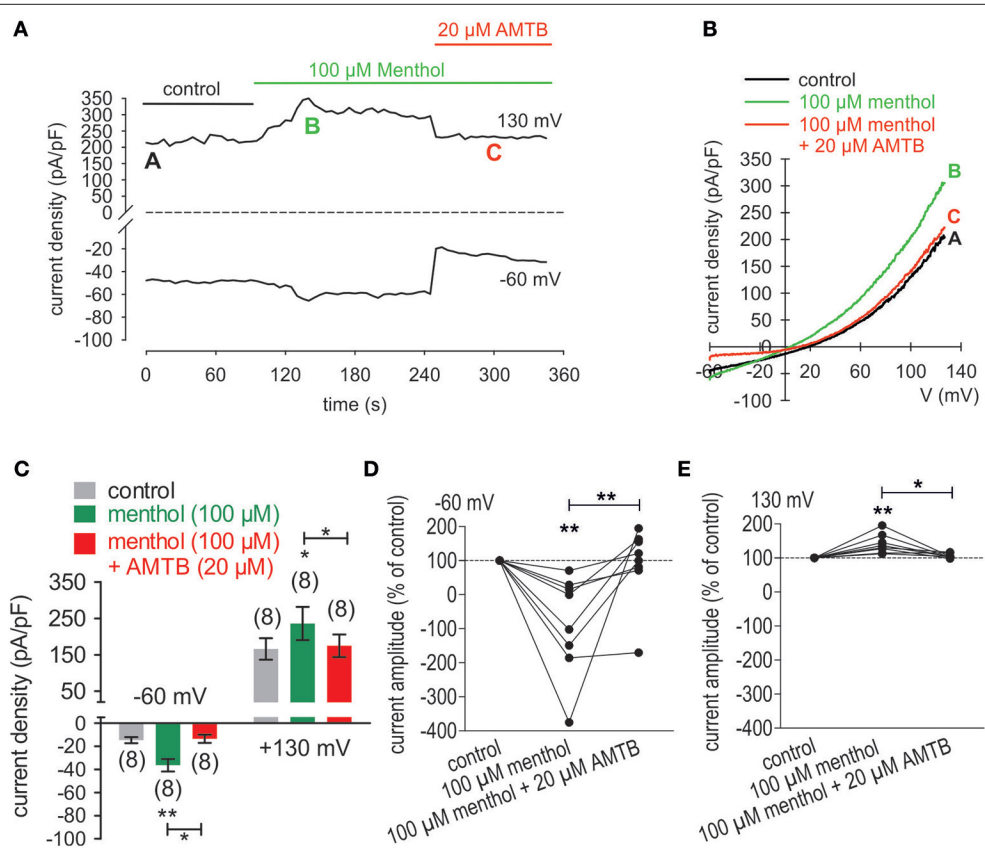


FIGURE 5 | AMTB suppresses menthol-induced rises in whole-cell currents in UM 92.1 cells. **(A)** Time course recording showing the current increases induced by menthol (100 μ M) and reduction after application of 20 μ M AMTB. **(B)** Original traces of menthol-induced current responses to voltage ramps. Current densities are shown before application (labeled as **A**), during application of menthol (labeled as **B**), and after addition of AMTB (labeled as **C**). **(C)** Summary of the patch-clamp experiments with menthol and AMTB. The asterisks (*) indicate statistically significant differences of in- and outward currents with menthol without AMTB ($n = 8$; inward currents; ** $p < 0.01$; outward currents; * $p < 0.05$; paired tested) and in the presence of AMTB ($n = 8$; in- and outward currents * $p < 0.05$; paired tested). **(D)** Maximal negative current amplitudes induced by a voltage step from 0 to -60 mV are depicted in percent of control values before application of 100 μ M menthol. Menthol-induced inward currents ($n = 8$; ** $p < 0.01$) were clearly suppressed in the presence of 20 μ M AMTB ($n = 8$; ** $p < 0.01$). **(E)** Maximal positive current amplitudes induced by a voltage step from 0 to +130 mV are depicted in percent of control values before application of 100 μ M menthol. Menthol-induced outwardly rectifying currents ($n = 8$; * $p < 0.05$) were clearly suppressed in the presence of 20 μ M AMTB ($n = 8$; * $p < 0.05$).

Icillin and Menthol Mimic Suppression by 3-T₁AM of VEGF Transactivation of TRPV1

As a positive control, the effects of CAP and VEGF were determined using an alternative fluorescence Ca^{2+} imaging data acquisition method as described in the method section. As shown in **Figure 9A**, a reduced CAP concentration (10 μ M) led to an increase of $f_{340\text{nm}}/f_{380\text{nm}}$ from 0.2021 ± 0.0004 (100 s) to 0.2094 ± 0.0013 (300 s) ($n = 19$; $p < 0.005$) whereas a washout did not reduce the Ca^{2+} level. With 10 ng/mg VEGF instead of CAP (**Figure 9B**), this ratio increased from 0.2011 ± 0.0004 (100 s) to 0.2331 ± 0.0029 (300 s) ($n = 85$; $p < 0.005$) and a washout did not augment this response Ca^{2+} transient (**Figures 9B,C**). However, preincubation of the cells with icillin suppressed the VEGF-induced increase to 0.2058 ± 0.0023 at 300 s ($p < 0.005$) and to 0.2187 ± 0.0034 at 600 s (both $n = 65$; $p < 0.01$) (**Figures 9C,D**). Menthol had the same inhibitory effect as icillin. Functional TRPM8 expression was validated based on a correspondence between the transients induced by cooling from

20 to 18°C (**Figures 10A–C**) and exposure to 200 μ M menthol (**Figures 10B,C**). Furthermore, as with icillin, preincubation of the cells with menthol suppressed the VEGF-induced Ca^{2+} transient even at a higher VEGF concentration since 20 ng/ml VEGF increased the $f_{340\text{nm}}/f_{380\text{nm}}$ ratio from 0.1991 ± 0.011 (100 s) to 0.2212 ± 0.0021 (250 s) ($n = 25$; $p < 0.005$) (**Figure 10D**). In contrast, 200 μ M menthol completely blocked this effect (e.g., $f_{340\text{nm}}/f_{380\text{nm}} = 0.2009 \pm 0.0007$ at 250 s; $n = 32$; $p < 0.005$) (**Figures 10E,F**). In summary, the near equivalence between the transients induced by either icillin, menthol, or 3-T₁AM and their inhibitory effects on VEGF-induced TRPV1 transactivation confirms that this thyroid hormone metabolite is a selective TRPM8 agonist.

Cannabinoid Receptor Type 1 Activity Modulates Inhibition of TRPV1 by 3-T₁AM

Since the G protein-coupled cannabinoid receptor 1 (CB1) is expressed in uveal melanoma cells (Mergler et al., 2014), we

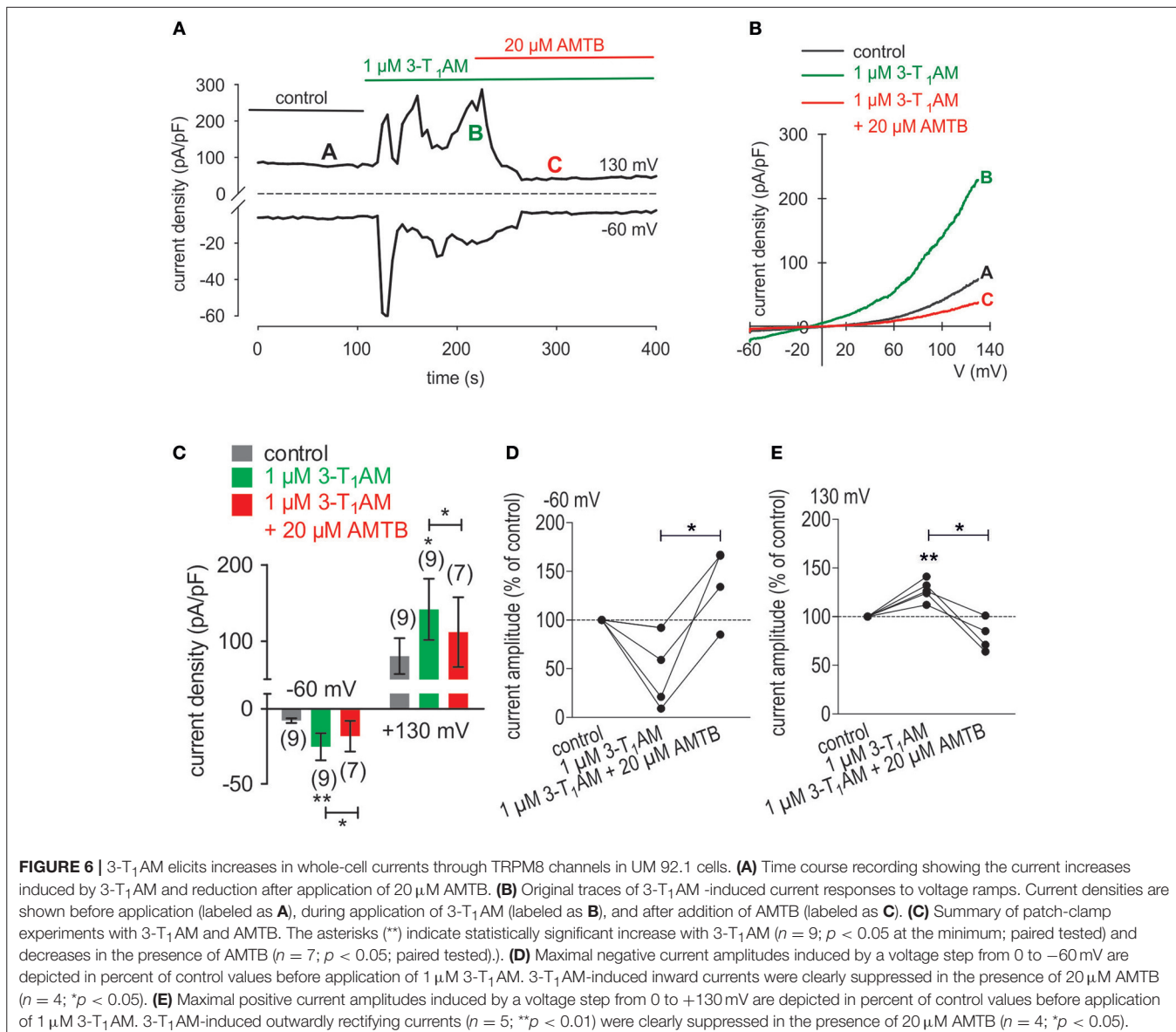


FIGURE 6 | 3-T₁AM elicits increases in whole-cell currents through TRPM8 channels in UM 92.1 cells. **(A)** Time course recording showing the current increases induced by 3-T₁AM and reduction after application of 20 μM AMTB. **(B)** Original traces of 3-T₁AM -induced current responses to voltage ramps. Current densities are shown before application (labeled as **A**), during application of 3-T₁AM (labeled as **B**), and after addition of AMTB (labeled as **C**). **(C)** Summary of patch-clamp experiments with 3-T₁AM and AMTB. The asterisks (**) indicate statistically significant increase with 3-T₁AM ($n = 9$; $p < 0.05$ at the minimum; paired tested) and decreases in the presence of AMTB ($n = 7$; $p < 0.05$; paired tested). **(D)** Maximal negative current amplitudes induced by a voltage step from 0 to -60 mV are depicted in percent of control values before application of 1 μM 3-T₁AM. 3-T₁AM-induced inward currents were clearly suppressed in the presence of 20 μM AMTB ($n = 4$; $*p < 0.05$). **(E)** Maximal positive current amplitudes induced by a voltage step from 0 to +130 mV are depicted in percent of control values before application of 1 μM 3-T₁AM. 3-T₁AM-induced outward rectifying currents ($n = 5$; $**p < 0.01$) were clearly suppressed in the presence of 20 μM AMTB ($n = 4$; $*p < 0.05$).

determined if either this receptor or its coupled G-proteins affect interactions between TRPM8 and TRPV1 in UM cells. To deal with this question, the individual effects of the selective CB1 receptor antagonist, AM251, and a corresponding agonist, WIN 55,212-2 (both 10 μM) were characterized by measuring their effects on $[Ca^{2+}]_i$ in UM 92.1 cells. WIN 55,212-2 induced a Ca^{2+} transient at a different cell passage compared to our previous studies ($n = 27$; $p < 0.005$). This validates CB1 involvement in Ca^{2+} regulation in UM 92.1 cells (Figure 11A). Interestingly, the WIN-induced Ca^{2+} increase was at significant higher levels under Ca^{2+} free conditions ($n = 53$; $p < 0.005$) (Figures 11B,C). Similarly, 1 μM 3-T₁AM also induced such a response. On the other hand, preincubation of the cells with the CB1 blocker AM251 (10 μM) augmented this rise induced by 3-T₁AM. The transient reached with 3-T₁AM by itself was 0.2155 ± 0.0014 ($n = 13$) at 400 s only whereas with AM251 (10 μM) it rose to 0.2446

± 0.0037 at the same time ($n = 46$; $p < 0.005$) (Figures 11D,E,G). In contrast, 3-T₁AM failed to induce a transient under Ca^{2+} free conditions ($n = 39$) (Figures 11F–G). In summary, changes in CB1 activity and/or coupled G-protein activity modulate interactions between TRPV1 and TRPM8.

DISCUSSION

We describe here TRPV1 and TRPM8 functional activity and their interactions in modulating VEGF-induced signaling in UM cells. Even though a short-term UM cell culture ($P < 20$) was used in this study, variations may occur in gene expression profiles between UM primary tumors and their derived cell lines. Nevertheless, there were only moderate modifications in the gene products (Mouriaux et al., 2016). Accordingly, Mouriaux et al. suggested that cell lines might represent useful tools in functional

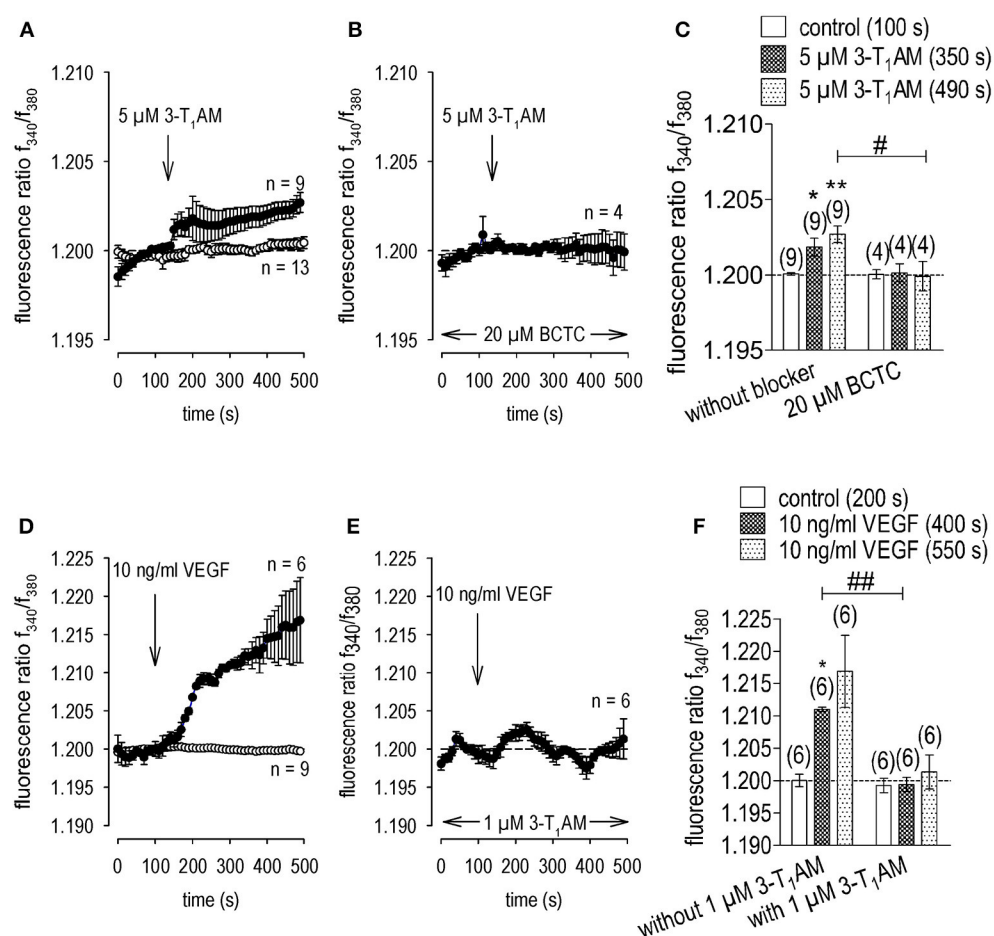


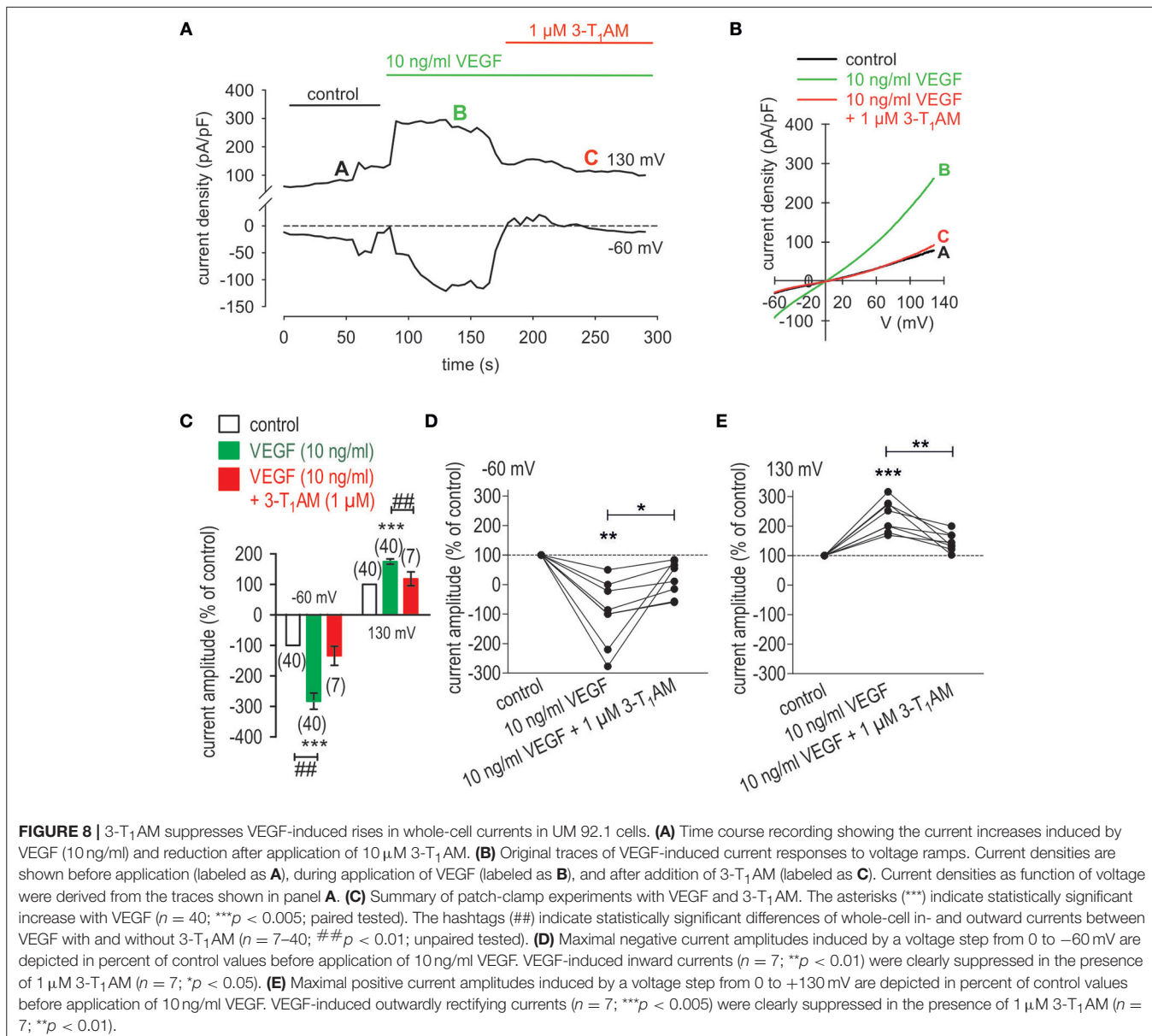
FIGURE 7 | 3-T₁AM elicits increases in Ca^{2+} entry through TRPM8 channels but instead suppresses VEGF-induced Ca^{2+} increases in UM 92.1 cells. 3-T₁AM (5 μ M) or VEGF (10 ng/ml) was added at the time points indicated by arrows. Data are mean \pm SEM of 4–9 experiments. **(A)** Mean trace showing 3-T₁AM-induced Ca^{2+} increase ($n = 9$) whereas non-treated control cells showed a constant Ca^{2+} baseline ($n = 13$). **(B)** Same experiment as shown in **(A)**, but in the presence of BCTC (20 μ M). BCTC clearly suppressed the 3-T₁AM-induced Ca^{2+} increase ($n = 4$). **(C)** Summary of the experiments with 3-T₁AM and BCTC. The asterisks (**) show significant Ca^{2+} increases with 3-T₁AM ($n = 9$; 350 s; * $p < 0.05$; 490 s; ** $p < 0.01$; paired tested). The hashtag (#) indicates a statistically significant difference of fluorescence ratios between 3-T₁AM with and without BCTC ($n = 6$; 490 s; # $p < 0.05$; unpaired tested). **(D)** Mean trace showing VEGF-induced Ca^{2+} increase ($n = 6$) whereas non-treated control cells showed a constant Ca^{2+} baseline ($n = 9$). **(E)** Same experiment as shown in **(D)**, but in the presence of 3-T₁AM (1 μ M). 3-T₁AM clearly suppressed the VEGF-induced Ca^{2+} increase ($n = 6$). **(F)** Summary of the experiments with VEGF and 3-T₁AM. The asterisk (*) shows a significant Ca^{2+} increase with VEGF ($n = 6$; 400 s; * $p < 0.05$; paired tested). The hashtags (##) indicate statistically significant differences of fluorescence ratios between VEGF with and without 3-T₁AM ($n = 6$; 400 s; ## $p < 0.01$; unpaired tested).

assays, as well as pharmacologic and genetic studies (Mouriaux et al., 2016). The TRPV1 and TRPM8 functional activity identified in these UM cells is consistent with the correspondence between the mRNA and protein expression patterns previously described in several other UM cell-line types (Mergler et al., 2014). Similarly, functional interaction between TRPM8 and TRPV1 is evident because TRPM8 activation inhibited increases in TRPV1 functional activity induced by CAP in both corneal epithelial and endothelial cells (Khajavi et al., 2015; Lucius et al., 2016). Furthermore, TRPM8 activation blunts transactivation of TRPV1 by VEGF in UM cells (Figures 7, 8). This modulation of VEGF-induced increases in Ca^{2+} influx mediated by TRPV1 activation shows that this receptor triad contributes through crosstalk to the growth promoting effects of VEGF in UM cells

derived from malignant tumors. Such crosstalk is consistent with other studies wherein TRPM8 activation dampens CAP-induced TRPV1 activation by VEGF (Millqvist, 2016; Takaishi et al., 2016). This consistency in interactions among this receptor triad in different cell types suggests that results obtained with one cell type may be applicable to various cell types.

TRPV1 Functional Expression Evidence

Even though CPZ has limited selectivity as a TRPV1 antagonist (Docherty et al., 1997; Liu and Simon, 1997; Oh et al., 2001; Ray et al., 2003; Teng et al., 2004) and limited TRPM8 selectivity (Behrendt et al., 2004; Xing et al., 2007; Mergler et al., 2013), its suppression of CAP-induced $[\text{Ca}^{2+}]_i$ transients and whole-cell currents in UM 92.1 cells are indicative of TRPV1 functional



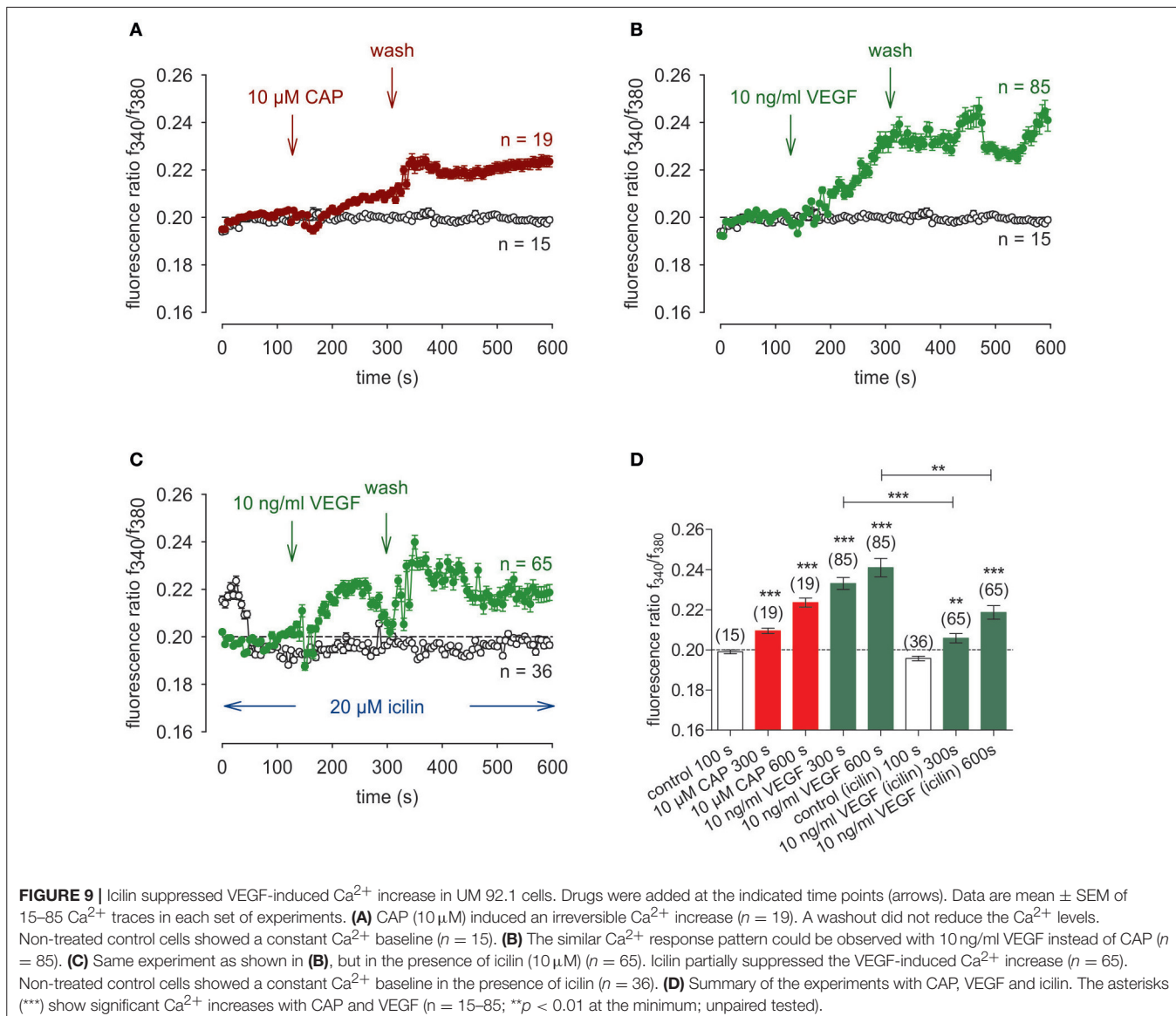
activity (Figures 2, 3). Its functional expression was also clearly detectable in both primary cultivated PM and healthy human uveas (Mergler et al., 2014). However, TRPV1 receptor density was probably at lower levels because of more extensive data scatter and a delayed response to CAP in most PM measurements (Figure 1B). Nevertheless, the maximal rises in Ca^{2+} influx in normal PM cells closely correspond to those in UM 92.1 cells.

The dynamic range of our Ca^{2+} imaging system was limited to 0.20 for detecting increases in the fluorescence ratio because the initial fluorescence responses of the two exciting wavelengths were at a relatively high level, which compressed the dynamic range of our measurements due to mathematical reasons. Therefore, even ratio changes of only 0.015 for CAP were significant and the measurements were clearly discernible and reproducible (Figure 1A). Another indication of the adequate

resolving power of our measurements is that the effects of CAP and icilin especially in UM 92.1 cells were irreversible and reached a steady state in most experiments. Similarly, this irreversibility was described in other eye tumor cells (Mergler et al., 2012a, 2014; Garreis et al., 2016) as well as healthy eye surface cells (Khajavi et al., 2015; Lucius et al., 2016).

Different TRPM8 Expression Levels in UM 92.1 Cells and PM

In healthy human uveas, TRPM8 mRNA expression was not evident whereas the TRPA1 PCR signal was present at very high levels (Mergler et al., 2014). On the other hand, icilin (Rawls et al., 2007) increased Ca^{2+} transients in UM 92.1 cells (Figure 1D) whereas this effect was not evident in PM (Figures 1E,F). Even though menthol activates TRPM8 (Eccles, 1994; Galeotti et al.,



2002; Bautista et al., 2007; Pedretti et al., 2009), the magnitudes of these transients did not correlate with the TRPM8 expression levels in certain cancer cells indicating a TRPM8-independent signaling pathway (Naziroglu et al., 2018). Irrespective of that, menthol also activated TRPM8 in the absence of extracellular Ca^{2+} , whereas responses to iciliin are Ca^{2+} dependent (McKemy et al., 2002; Chuang et al., 2004). Therefore, iciliin appears to induce Ca^{2+} transients by increasing Ca^{2+} influx from the extracellular medium (McKemy et al., 2002; Andersson et al., 2004; Behrendt et al., 2004). Nevertheless, TRPA1 involvement cannot be excluded because iciliin can also interact with TRPA1 even though iciliin was relatively ineffective at inducing Ca^{2+} transients and there is no detectable TRPA1 mRNA expression in this cell type (Mergler et al., 2014). Therefore, TRPM8 activity in PM and human uveas is relatively low compared to higher levels in malignant uveal cell types (Mergler et al., 2014). In contrast,

the CAP-induced Ca^{2+} transients were comparable suggesting no difference in TRPV1 expression levels in these two different cell types (Figure 1B).

Crosstalk Between VEGFR and TRPV1

VEGF transactivated TRPV1 through its interaction with VEGFR since the Ca^{2+} transients and their underlying currents were both fully blocked during exposure to CPZ. Furthermore, the stimulation by VEGF of TRPV1 was maximal since supplementation with CAP failed to augment the increases in whole-cell currents induced by VEGF application (Figures 4, 7, 8).

Unlike with CPZ, the TRPM8 blocker AMTB (Lashinger et al., 2008) failed to suppress these transients induced by VEGF suggesting that VEGFR solely transactivates TRPV1 (Figure 2). This agrees with what was described in a benign tumor (Garreis

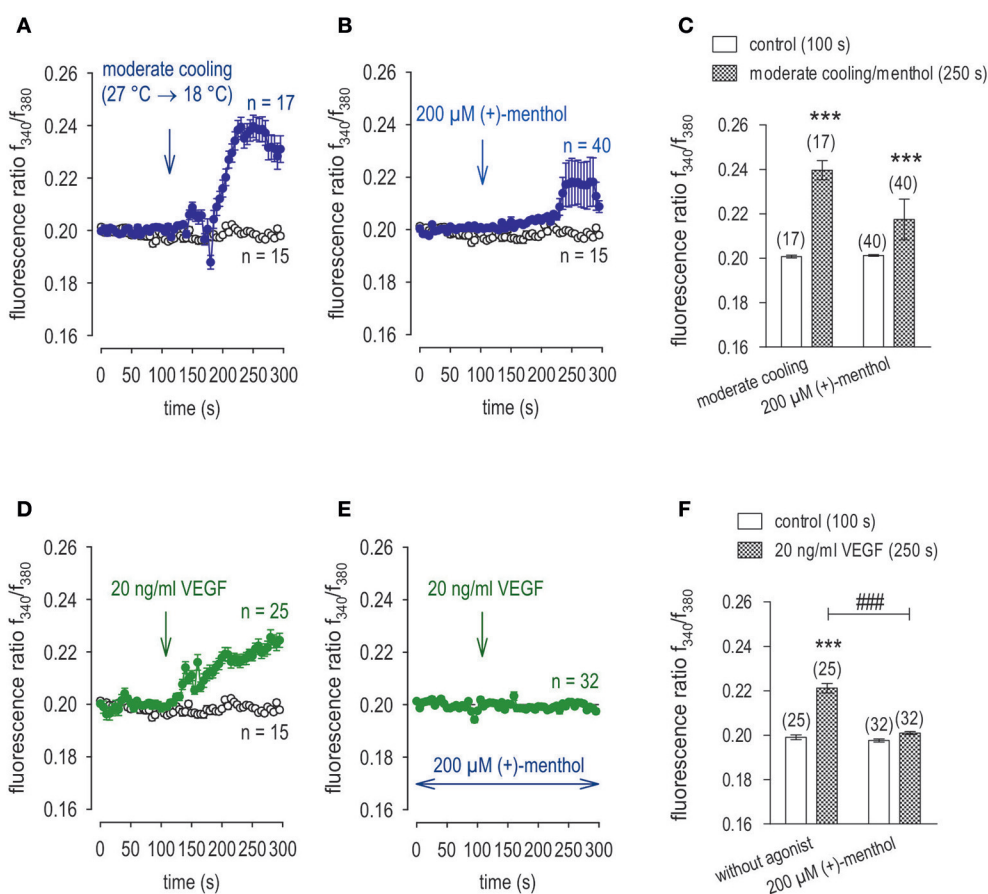


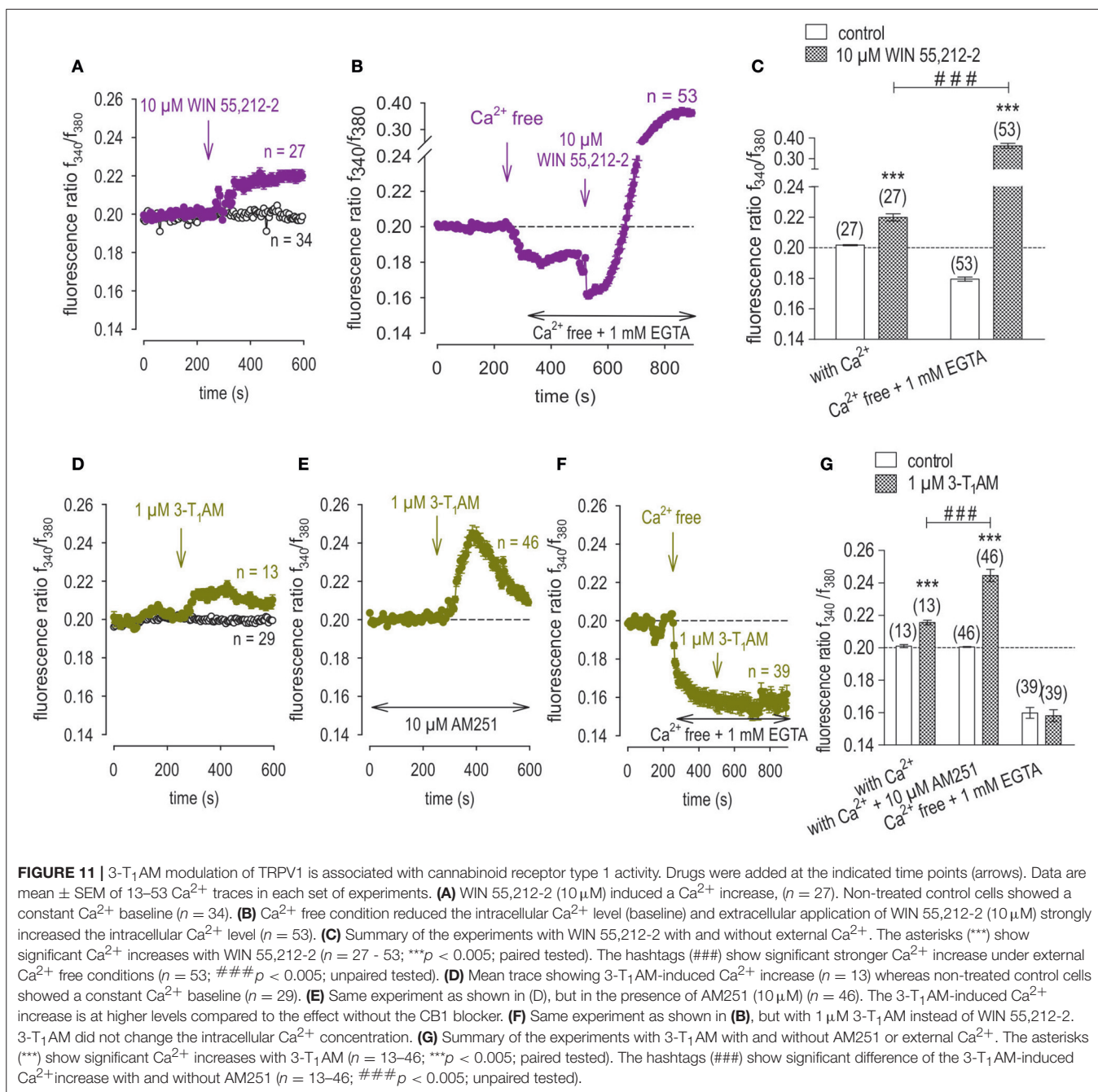
FIGURE 10 | Menthol suppressed VEGF-induced Ca^{2+} increase in UM 92.1 cells. Drugs were added at the indicated time points (arrows). Data are mean \pm SEM of 15–40 Ca^{2+} traces in each set of experiments. **(A)** Moderate cooling (≈ 27 to 18°C) induced a Ca^{2+} increase, which partially recovered ($n = 17$). Non-treated control cells showed a constant Ca^{2+} baseline ($n = 15$). **(B)** TRPM8 activation by menthol ($200 \mu\text{M}$) led to a Ca^{2+} increase, which is at lower levels compared to moderate cooling ($n = 40$). **(C)** Summary of the experiments with cooling and menthol. The asterisks (*) show significant Ca^{2+} increases with moderate cooling and menthol ($n = 17 - 40$; *** $p < 0.005$; paired tested). **(D)** The Mean trace showing VEGF-induced Ca^{2+} increase ($n = 25$). **(E)** Same experiment as shown in **(D)**, but in the presence of menthol ($200 \mu\text{M}$). Menthol clearly suppressed the VEGF-induced Ca^{2+} increase ($n = 32$). **(F)** Summary of the experiments with VEGF and menthol. The asterisks (*) show significant Ca^{2+} increases with VEGF ($n = 25$; *** $p < 0.005$; paired tested). The hashtags (####) show significant Ca^{2+} decreases in the presence of menthol ($n = 32$; #### $p < 0.005$; unpaired tested).

et al., 2016). The smaller inhibitory effects of BCTC on VEGF-induced increases in Ca^{2+} influx than those induced by CPZ are supportive of the notion that BCTC is a mixed TRPV1/TRPM8 antagonist (Behrendt et al., 2004; Weil et al., 2005; Vriens et al., 2009; Benko et al., 2012; Liu et al., 2016). In contrast, AMTB is a more selective TRPM8 antagonist (Lashinger et al., 2008) since it failed to block VEGF-induced transactivation of TRPV1 (**Figures 2D, 3A,B**). The limited specificity of BCTC as a TRPV1 blocker is supported by our finding that at a relatively high CAP concentration ($20 \mu\text{M}$), BCTC was ineffective as a blocker of TRPV1 activation in human corneal epithelial cells (Lucius et al., 2016). The marked difference between the large inhibitory effect of CPZ and the minimal effect of AMTB on increases in currents induced by VEGF confirms that VEGF solely transactivates TRPV1 (**Figure 3**). However, VEGFR is also known to regulate multiple channels including TRPs (Garnier-Raveaud et al., 2001; Hamdollah Zadeh et al., 2008; Thilo et al., 2012; Reichhart et al.,

2015; Wu et al., 2015; Qin et al., 2016). Specifically, McNaughton et al. demonstrated that nerve growth factor (NGF) receptors in HEK293 cells transfected with plasmids containing cDNAs coding for TRPV1 and for the Tropomyosin receptor kinase A (TrkA) receptor for NGF increased the expression level of TRPV1 but did not sensitize or activate the receptor (Zhang et al., 2005; Vay et al., 2012). One explanation may be that NGF is different from VEGF or that our study used non-excitable (tumor) cells.

TRPM8 Activation Suppresses VEGF-Induced Rises in Ca^{2+} Influx

3-T1AM suppressed VEGFR transactivation of TRPV1 (**Figures 7D–F, 8**) was blocked by BCTC in TRPM8-transfected cells, in corneal and conjunctival epithelial cells derived from normal cells (Khajavi et al., 2015; Lucius et al., 2016) and in UM 92.1 cells (**Figures 7, 8**) as well as in thyroid PCCL3 cells (Schanze et al., 2017). These effects were similar to those induced



by AMTB, which is consistent with significant antagonism by BCTC of TRPM8 (Figures 5, 6, 7A–C).

The 3-T₁AM mediated Ca²⁺ transients as well as increases in their underlying currents occurred at lower concentrations in UM 92.1 melanoma cells than those in healthy cells or thyroid cells (Khajavi et al., 2017; Schanze et al., 2017). Specifically, 3-T₁AM was used over a concentration range from 0.2 to 10 μM with 1–5 μM having maximal stimulatory effects on whole-cell currents, which agrees with previous studies using corneal epithelial cells (Lucius et al., 2016). 3-T₁AM had a concentration dependent inhibitory effect on Ca²⁺ transients

that may be attributable to different modes of action. With 0.5 μM 3-T₁AM, only whole-cell currents increased without any inhibitory effect on VEGF-induced rises in Ca²⁺ influx (data not shown). However, with 1 μM 3-T₁AM VEGF-induced rises in Ca²⁺ influx also declined with a time course that was similar to that obtained with CPZ (Figures 2B, 7E, 11D). It is conceivable that the effect of 0.5 μM 3-T₁AM is membrane delimited rather than causing release of Ca²⁺ from intracellular stores. Perhaps, 1 μM 3-T₁AM is at a high enough concentration for it to gain access to cytosolic intracellular TRPV1 binding sites with which CPZ also binds? If this supposition is proven to be correct,

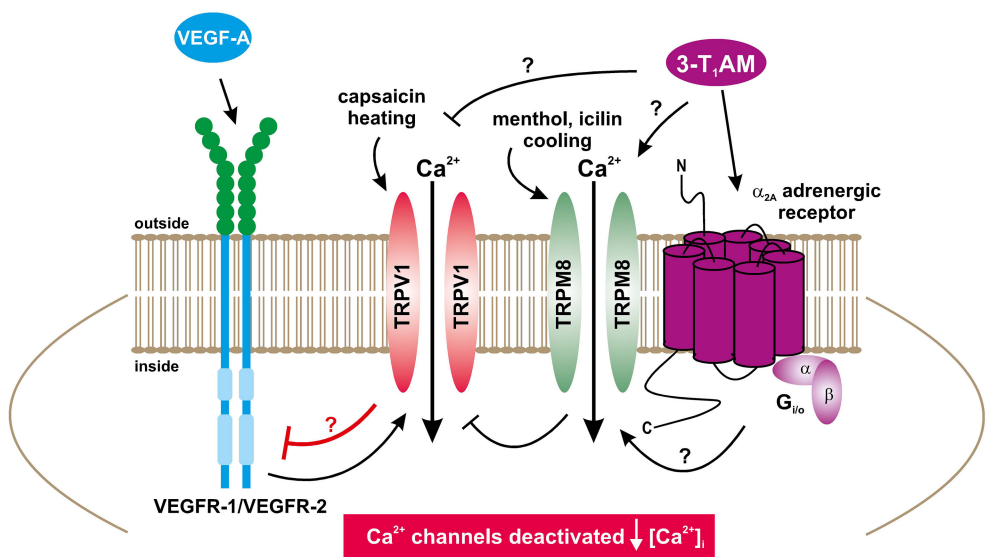


FIGURE 12 | Suggested Ca^{2+} signal transduction model accounting for how TRPM8 activation affects receptor-linked signaling pathways (Mergler et al., 2014; Khajavi et al., 2017). Ca^{2+} channels such as TRPs of the TRPV1 subtype (capsaicin receptor) can be selectively activated by heat ($>43^\circ\text{C}$) or capsaicin and blocked by CPZ (Figure 1A) (Mergler et al., 2014). VEGF-A activating VEGFR-1/VEGFR-2 can also activate TRPV1 (Figures 2, 3). The TRPM8 subtype (menthol receptor) can be selectively activated by cold ($23\text{--}28^\circ\text{C}$), menthol, icilin or 3-T₁AM and blocked by BCTC/AMTB (Figures 1D, Figures 5, 6) (Mergler et al., 2014; Khajavi et al., 2017). Notably, a G-protein coupled receptor (GPCR) coupled to $\text{G}_{i/o}$ proteins could be activated by 3-T₁AM (Dinter et al., 2015a; Khajavi et al., 2017; Schanze et al., 2017). 3-T₁AM may also directly activate TRPM8 by a GPCR-independent mechanism ($\uparrow[\text{Ca}^{2+}]_i$) (Khajavi et al., 2017). If TRPM8 is activated by 3-T₁AM, 3-T₁AM suppresses VEGF via TRPV1 (Figures 7, 8). Notably, 3-T₁AM may also directly suppress TRPV1 via VEGFR by a GPCR-independent mechanism ($\downarrow[\text{Ca}^{2+}]_i$) (Figure 8). Menthol and icilin mimic the 3-T₁AM effect and suppresses increases in TRPV1 activity by VEGF (Figures 9, 10).

3-T₁AM may have dual effects that include activating TRPM8 and at higher concentrations also suppressing TRPV1 activation induced by VEGF. As the effects of modulators of TRP channel activity on Ca^{2+} influx mirrored those on whole-cell currents (Figures 7, 8), this agreement supports the notion that 3-T₁AM has a relevant role in regulating VEGF-mediated Ca^{2+} regulation in tumor cells. In addition, we could demonstrate that TRPM8 activation by menthol or icilin mimic the 3-T₁AM effect and is able to suppress increases in TRPV1 activity by VEGF (Figures 9, 10). To the best of our knowledge, this report is the first one describing such control in both benign eye surface tumor cells (Garreis et al., 2016) and now in metastatic UM 92.1 cells. On the other hand, the possible Ca^{2+} signal transduction pathways activated by 3-T₁AM as a specific activator of TRPM8 may be more complex as suggested in Figure 12 (Khajavi et al., 2017).

There are numerous studies showing that 3-T₁AM also regulates beta-adrenergic receptors, trace amine-associated receptor 2, muscarinic receptors, and K^+ channels (Scanlan et al., 2004; Ghelardoni et al., 2009; Panas et al., 2010; Cichero et al., 2014; Dinter et al., 2015b; Hoefig et al., 2016). 3-T₁AM has also been described as an antagonist of muscarinic type 3 receptor (Laurino et al., 2016). Furthermore, beta-adrenergic receptors and muscarinic receptors are expressed in multiple melanoma cells including primary uveal melanoma (92.1, Mel202) (Janik et al., 2017). In addition, changes in K^+ channel activity have been implicated in modulating progression of melanoma (Oppitz et al., 2008; Luo et al., 2017). These studies indicate

that 3-T₁AM may not be directly or solely targeting TRPM8 (Figure 12).

G Protein-Coupled Cannabinoid Receptor-1 Modulates 3-T₁AM Suppression of TRPV1 Channels

It has been suggested that 3-T₁AM is a multitarget ligand (Zucchi et al., 2014) interacting with different TRP channel subtypes including TRPM8 (Khajavi et al., 2015, 2017; Lucius et al., 2016). Since functional CB1 expression has been described in ocular tumor cells (Mergler et al., 2012a, 2014) and in healthy ocular cells (Stumpff et al., 2005; Yang et al., 2010, 2013), we determined if 3-T₁AM interacts also with the cannabinoid receptor 1 CB1. CB1 activation by WIN 55,212-2 induced Ca^{2+} transients, which were larger in a Ca^{2+} free conditions than with 2 mM external Ca^{2+} (Figures 11A–C). On the other hand, 3-T₁AM failed to elicit a Ca^{2+} transient in a Ca^{2+} free medium (Figure 11F) whereas in the presence of AM251 and external Ca^{2+} in the medium 3-T₁AM-induced Ca^{2+} transients that were larger in the presence of the CB1 blocker than in its absence (Figures 11D,E). Since CB1 activation also suppresses TRPV1 activation (Yang et al., 2013; Mergler et al., 2014), there may be an inverse relationship between increases in TRPM8 activity and declines in CB1 activity. Overall, the mechanisms involved in 3-T₁AM modulation of TRPV1 channels may also involve contributions by other receptors such as CB1 and/or its coupled G-protein mediators.

Clinical Relevance

3-T₁AM is a potential therapeutic agent for suppressing UM expansion as already indicated in other studies demonstrating that this thyroid hormone metabolite reduces cancer cell growth and viability (Rogowski et al., 2017; Shinderman-Maman et al., 2017). In UM cells, modulation of their metastatic activity appears to include changes in TRPV1 activity induced by TRPM8 and possibly CB1. The model for such control shown in **Figure 12** proposes that VEGF secreted by UM cells stimulates intracellular Ca²⁺ influx in endothelial cells, which is a requisite for driving angiogenesis and promotes UM proliferation and metastasis. Since TRPM8 activation has an opposing effect on TRPV1 activity, targeting TRPM8 may provide an effective alternative to suppress metastatic melanoma progression without side effects. Such an approach appears to be tenable based on the fact that functional TRPM8 expression is only detectable in the UM cells rather than PM cells. There is an urgent need for further assessment of the validity of this option since there are no measures currently available to reverse melanoma metastasis.

AUTHOR CONTRIBUTIONS

LW, CB, SM, and PR designed the study, analyzed the data, wrote and edited the manuscript. LW and CB contributed equally to the work. JK contributed with his expertise on thyroid hormone metabolites, discussed data and their interpretation and helped

edit the manuscript. LW, CB, AB, PD, NL, MS, HvdW, IR, and SM performed calcium measurements and planar patch-clamp recordings as well as plot analyses. LW, CB, AB, PD, MS, HvdW, and SM created diagrams. SM created the schematic drawing.

FUNDING

This work was supported by DFG (Me 1706/14-1, Me 1706/18-1) about TRP channel related research projects. JK received grants from the DFG priority program 1629 ThyroidTransAct (Ko 922/16-1/2 and 922/17-1/2). The planar patch-clamp equipment and parts of the fluorescence calcium imaging setup were partially supported by Sonnenfeld-Stiftung (Berlin, Germany).

ACKNOWLEDGMENTS

The authors thank Martine Jager and colleagues (Leiden University; Netherlands) for providing the 92.1 cell line. Furthermore, the authors appreciate very much the collaboration with Monika Valtink (Institute of Anatomy, Medical Faculty Carl Gustav Carus, TU Dresden), who gave valuable hints regarding the preparation of the porcine melanocytes. Finally, we thank the technical assistance provided by the fellow students Philipp Leibfried, Maximilian Müller, Vivien Schmädicke, Fabian Hänsch, Alexej Zhogov, and May Ossamer Eisser Amer during their lab rotation projects.

REFERENCES

- Andersson, D. A., Chase, H. W., and Bevan, S. (2004). TRPM8 activation by menthol, icilin, and cold is differentially modulated by intracellular pH. *J. Neurosci.* 24, 5364–5369. doi: 10.1523/JNEUROSCI.0890-04.2004
- Bai, V. U., Murthy, S., Chinnakannu, K., Muhletaler, F., Tejwani, S., Barrack, E. R., et al. (2010). Androgen regulated TRPM8 expression: a potential mRNA marker for metastatic prostate cancer detection in body fluids. *Int. J. Oncol.* 36, 443–450. doi: 10.3892/ijo_00000518
- Barry, P. H. (1994). JPCalc, a software package for calculating liquid junction potential corrections in patch-clamp, intracellular, epithelial and bilayer measurements and for correcting junction potential measurements. *J. Neurosci. Methods* 51, 107–116.
- Bautista, D. M., Siemens, J., Glazer, J. M., Tsuruda, P. R., Basbaum, A. I., Stucky, C. L., et al. (2007). The menthol receptor TRPM8 is the principal detector of environmental cold. *Nature* 448, 204–208. doi: 10.1038/nature05910
- Behrendt, H. J., Germann, T., Gillen, C., Hatt, H., and Jostock, R. (2004). Characterization of the mouse cold-menthol receptor TRPM8 and vanilloid receptor type-1 VR1 using a fluorometric imaging plate reader (FLIPR) assay. *Br. J. Pharmacol.* 141, 737–745. doi: 10.1038/sj.bjp.0705652
- Benko, R., Illényi, L., Kelemen, D., Papp, R., Papp, A., and Bartho, L. (2012). Use and limitations of three TRPV-1 receptor antagonists on smooth muscles of animals and man: a vote for BCTC. *Eur. J. Pharmacol.* 674, 44–50. doi: 10.1016/j.ejphar.2011.10.021
- Bidaux, G., Roudbaraki, M., Merle, C., Crepin, A., Delcourt, P., Slomiany, C., et al. (2005). Evidence for specific TRPM8 expression in human prostate secretory epithelial cells: functional androgen receptor requirement. *Endocr. Relat. Cancer* 12, 367–382. doi: 10.1677/erc.1.00969
- Bödding, M. (2007). TRP proteins and cancer. *Cell. Signal.* 19, 617–624. doi: 10.1016/j.cellsig.2006.08.012
- Braulke, L. J., Klingenspor, M., DeBarber, A., Tobias, S. C., Grandy, D. K., Scanlan, T. S., et al. (2008). 3-iodothyronamine: a novel hormone controlling the balance between glucose and lipid utilisation. *J. Comp. Physiol. B Biochem. Syst. Environ. Physiol.* 178, 167–177. doi: 10.1007/s00360-007-0208-x
- Caterina, M. J., Schumacher, M. A., Tominaga, M., Rosen, T. A., Levine, J. D., and Julius, D. (1997). The capsaicin receptor: a heat-activated ion channel in the pain pathway. *Nature* 389, 816–824.
- Chuang, H. H., Neuhausser, W. M., and Julius, D. (2004). The super-cooling agent icilin reveals a mechanism of coincidence detection by a temperature-sensitive TRP channel. *Neuron* 43, 859–869. doi: 10.1016/j.neuron.2004.08.038
- Cichero, E., Espinoza, S., Franchini, S., Guariento, S., Brasili, L., Gainetdinov, R. R., et al. (2014). Further insights into the pharmacology of the human trace amine-associated receptors: discovery of novel ligands for TAAR1 by a virtual screening approach. *Chem. Biol. Drug Des.* 84, 712–720. doi: 10.1111/cbdd.12367
- Criscuolo, G. R., Lelkes, P. I., Rotrosen, D., and Oldfield, E. H. (1989). Cytosolic calcium changes in endothelial cells induced by a protein product of human gliomas containing vascular permeability factor activity. *J. Neurosurg.* 71, 884–891. doi: 10.3171/jns.1989.71.6.0884
- De Waard-Siebinga, I., Blom, D. J., Griffioen, M., Schrier, P. I., Hoogendoorn, E., Beverstock, G., et al. (1995). Establishment and characterization of an uveal-melanoma cell line. *Int. J. Cancer* 62, 155–161.
- Dinter, J., Khajavi, N., Mühlhaus, J., Wienchol, C. L., Cöster, M., Hermsdorf, T., et al. (2015a). The multitar target ligand 3-iodothyronamine modulates beta-adrenergic receptor 2 signaling. *Eur. Thyroid J.* 4(Suppl. 1), 21–29. doi: 10.1159/000381801
- Dinter, J., Mühlhaus, J., Wienchol, C. L., Yi, C. X., Nürnberg, D., Morin, S., et al. (2015b). Inverse agonistic action of 3-iodothyronamine at the human trace amine-associated receptor 5. *PLoS ONE* 10: e0117774. doi: 10.1371/journal.pone.0117774
- Dithmer, M., Kirsch, A. M., Gräfenstein, L., Wang, F., Schmidt, H., Coupland, S. E., et al. (2017). Uveal melanoma cell under oxidative stress – influence of VEGF and VEGF-inhibitors. *Klin. Monbl. Augenheilkd.* 234, doi: 10.1055/s-0043-103002

- Docherty, R. J., Yeats, J. C., and Piper, A. S. (1997). Capsazepine block of voltage-activated calcium channels in adult rat dorsal root ganglion neurones in culture. *Br. J. Pharmacol.* 121, 1461–1467. doi: 10.1038/sj.bjp.0701272
- Eccles, R. (1994). Menthol and related cooling compounds. *J. Pharm. Pharmacol.* 46, 618–630.
- Fixemer, T., Wissenbach, U., Flockerzi, V., and Bonkhoff, H. (2003). Expression of the Ca^{2+} -selective cation channel TRPV6 in human prostate cancer: a novel prognostic marker for tumor progression. *Oncogene* 22, 7858–7861. doi: 10.1038/sj.onc.1206895
- Francis, J. H., Kim, J., Lin, A., Folberg, R., Iyer, S., and Abramson, D. H. (2017). Growth of uveal melanoma following intravitreal bevacizumab. *Ocul. Oncol. Pathol.* 3, 117–121. doi: 10.1159/000450859
- Galeotti, N., Di Cesare Mannelli, L., Mazzanti, G., Bartolini, A., and Ghelardini, C. (2002). Menthol: a natural analgesic compound. *Neurosci. Lett.* 322, 145–148. doi: 10.1016/S0304-3940(01)02527-7
- Garnier-Raveaud, S., Usson, Y., Cand, F., Robert-Nicoud, M., Verdetti, J., and Faury, G. (2001). Identification of membrane calcium channels essential for cytoplasmic and nuclear calcium elevations induced by vascular endothelial growth factor in human endothelial cells. *Growth Factors* 19, 35–48. doi: 10.3109/08977190109001074
- Garreis, F., Schröder, A., Reinach, P. S., Zoll, S., Khajavi, N., Dhandapani, P., et al. (2016). Upregulation of transient receptor potential vanilloid Type-1 channel activity and Ca^{2+} influx dysfunction in human pterygial cells. *Invest. Ophthalmol. Vis. Sci.* 57, 2564–2577. doi: 10.1167/iovs.16-19170
- Ghelardoni, S., Suffredini, S., Frascarelli, S., Brogioni, S., Chiellini, G., Ronca-Testoni, S., et al. (2009). Modulation of cardiac ionic homeostasis by 3-iodothyronamine. *J. Cell. Mol. Med.* 13, 3082–3090. doi: 10.1111/j.1582-4934.2009.00728.x
- Gkika, D., Flourakis, M., Lemonnier, L., and Prevarskaya, N. (2010). PSA reduces prostate cancer cell motility by stimulating TRPM8 activity and plasma membrane expression. *Oncogene* 29, 4611–4616. doi: 10.1038/onc.2010.210
- Grynkiewicz, G., Poenie, M., and Tsien, R. Y. (1985). A new generation of Ca^{2+} indicators with greatly improved fluorescence properties. *J. Biol. Chem.* 260, 3440–3450.
- Hamdollah Zadeh, M. A., Glass, C. A., Magnussen, A., Hancock, J. C., and Bates, D. O. (2008). VEGF-mediated elevated intracellular calcium and angiogenesis in human microvascular endothelial cells *in vitro* are inhibited by dominant negative TRPC6. *Microcirculation* 15, 605–614. doi: 10.1080/10739680802220323
- Hirata, H., and Oshinsky, M. L. (2012). Ocular dryness excites two classes of corneal afferent neurons implicated in basal tearing in rats: involvement of transient receptor potential channels. *J. Neurophysiol.* 107, 1199–1209. doi: 10.1152/jn.00657.2011
- Hoefig, C. S., Zucchi, R., and Köhrle, J. (2016). Thyronamines and derivatives: physiological relevance, pharmacological actions, and future research directions. *Thyroid* 26, 1656–1673. doi: 10.1089/thy.2016.0178
- Janik, M. E., Szlezak, D., Surman, M., Golas, A., Litynska, A., and Przybylo, M. (2017). Diversified beta-2-adrenergic receptor expression and action in melanoma cells. *Anticancer Res.* 37, 3025–3033. doi: 10.21873/anticancres.11657
- Jia, R. B., Zhang, P., Zhou, Y. X., Song, X., Liu, H. Y., Wang, L. Z., et al. (2007). VEGF-targeted RNA interference suppresses angiogenesis and tumor growth of retinoblastoma. *Ophthalmic Res.* 39, 108–115. doi: 10.1159/000099247
- Khajavi, N., Mergler, S., and Biebermann, H. (2017). 3-Iodothyronamine, a novel endogenous modulator of transient receptor potential melastatin 8? *Front. Endocrinol.* 8:198. doi: 10.3389/fendo.2017.00198
- Khajavi, N., Reinach, P. S., Slavi, N., Skrzypski, M., Lucius, A., Strauß, O., et al. (2015). Thyronamine induces TRPM8 channel activation in human conjunctival epithelial cells. *Cell. Signal.* 27, 315–325. doi: 10.1016/j.cellsig.2014.11.015
- Knowlton, W. M., Daniels, R. L., Palkar, R., McCoy, D. D., and McKemy, D. D. (2011). Pharmacological blockade of TRPM8 ion channels alters cold and cold pain responses in mice. *PLoS ONE* 6:e25894. doi: 10.1371/journal.pone.0025894
- Lashinger, E. S., Steiginga, M. S., Hieble, J. P., Leon, L. A., Gardner, S. D., Nagilla, R., et al. (2008). AMTB, a TRPM8 channel blocker: evidence in rats for activity in overactive bladder and painful bladder syndrome. *Am. J. Physiol. Renal. Physiol.* 295, F803–F810. doi: 10.1152/ajprenal.90269.2008
- Laurino, A., Matucci, R., Vistoli, G., and Raimondi, L. (2016). 3-iodothyronamine (T1AM), a novel antagonist of muscarinic receptors. *Eur. J. Pharmacol.* 793, 35–42. doi: 10.1016/j.ejphar.2016.10.027
- Liu, L., and Simon, S. A. (1997). Capsazepine, a vanilloid receptor antagonist, inhibits nicotinic acetylcholine receptors in rat trigeminal ganglia. *Neurosci. Lett.* 228, 29–32.
- Liu, T., Fang, Z., Wang, G., Shi, M., Wang, X., Jiang, K., et al. (2016). Anti-tumor activity of the TRPM8 inhibitor BCTC in prostate cancer DU145 cells. *Oncol. Lett.* 11, 182–188. doi: 10.3892/ol.2015.3854
- Logan, P., Burnier, J., and Burnier, M. N. Jr. (2013). Vascular endothelial growth factor expression and inhibition in uveal melanoma cell lines. *Eccancermedicalscience* 7:336. doi: 10.3332/ecancer.2013.336
- Lucius, A., Khajavi, N., Reinach, P. S., Köhrle, J., Dhandapani, P., Huimann, P., et al. (2016). 3-Iodothyronamine increases transient receptor potential melastatin channel 8 (TRPM8) activity in immortalized human corneal epithelial cells. *Cell. Signal.* 28, 136–147. doi: 10.1016/j.cellsig.2015.12.005
- Luo, L., Cui, J., Feng, Z., Li, Y., Wang, M., Cai, Y., et al. (2017). Lentiviral-mediated overexpression of KCTD12 inhibits the proliferation of human uveal melanoma OCM-1 cells. *Oncol. Rep.* 37, 871–878. doi: 10.3892/or.2016.5325
- Marincsák, R., Tóth, B. I., Czifra, G., Márton, I., Rédl, P., Tar, I., et al. (2009). Increased expression of TRPV1 in squamous cell carcinoma of the human tongue. *Oral Dis.* 15, 328–335. doi: 10.1111/j.1601-0825.2009.01526.x
- McKemy, D. D., Neuhauser, W. M., and Julius, D. (2002). Identification of a cold receptor reveals a general role for TRP channels in thermosensation. *Nature* 416, 52–58. doi: 10.1038/nature719
- Mergler, S., Cheng, Y., Skosyrsky, S., Garreis, F., Pietrzak, P., Kociok, N., et al. (2012a). Altered calcium regulation by thermo-sensitive transient receptor potential channels in etoposide-resistant WERI-Rb1 retinoblastoma cells. *Exp. Eye Res.* 94, 157–173. doi: 10.1016/j.exer.2011.12.002
- Mergler, S., Derckx, R., Reinach, P. S., Garreis, F., Böhm, A., Schmelzer, L., et al. (2014). Calcium regulation by temperature-sensitive transient receptor potential channels in human uveal melanoma cells. *Cell. Signal.* 26, 56–69. doi: 10.1016/j.cellsig.2013.09.017
- Mergler, S., Mertens, C., Valtink, M., Reinach, P. S., Székely, V. C., Slavi, N., et al. (2013). Functional significance of thermosensitive transient receptor potential melastatin channel 8 (TRPM8) expression in immortalized human corneal endothelial cells. *Exp. Eye Res.* 116, 337–349. doi: 10.1016/j.exer.2013.10.003
- Mergler, S., Skrzypski, M., Sasiek, M., Pietrzak, P., Pucci, C., Wiedenmann, B., et al. (2012b). Thermo-sensitive transient receptor potential vanilloid channel-1 regulates intracellular calcium and triggers chromogranin A secretion in pancreatic neuroendocrine BON-1 tumor cells. *Cell. Signal.* 24, 233–246. doi: 10.1016/j.cellsig.2011.09.005
- Miao, X., Liu, G., Xu, X., Xie, C., Sun, F., Yang, Y., et al. (2008). High expression of vanilloid receptor-1 is associated with better prognosis of patients with hepatocellular carcinoma. *Cancer Genet. Cytogenet.* 186, 25–32. doi: 10.1016/j.cancergenryo.2008.05.011
- Millqvist, E. (2016). TRPV1 and TRPM8 in treatment of chronic cough. *Pharmaceutics* 9:E45. doi: 10.3390/ph9030045
- Mouriaux, F., Zaniolo, K., Bergeron, M. A., Weidmann, C., De La Fouchardière, A., Fournier, F., et al. (2016). Effects of long-term serial passaging on the characteristics and properties of cell lines derived from uveal melanoma primary tumors. *Invest. Ophthalmol. Vis. Sci.* 57, 5288–5301. doi: 10.1167/iovs.16-19317
- Naziroglu, M., Blum, W., Josvay, K., Cig, B., Henzi, T., Olah, Z., et al. (2018). Menthol evokes Ca^{2+} signals and induces oxidative stress independently of the presence of TRPM8 (menthol) receptor in cancer cells. *Redox Biol.* 14, 439–449. doi: 10.1016/j.redox.2017.10.009
- Oh, G. S., Pae, H. O., Seo, W. G., Kim, N. Y., Pyun, K. H., Kim, I. K., et al. (2001). Capsazepine, a vanilloid receptor antagonist, inhibits the expression of inducible nitric oxide synthase gene in lipopolysaccharide-stimulated RAW264.7 macrophages through the inactivation of nuclear transcription factor-kappa B. *Int. Immunopharmacol.* 1, 777–784.
- Oppitz, M., Busch, C., Garbe, C., and Drews, U. (2008). Distribution of muscarinic receptor subtype M3 in melanomas and their metastases. *J. Cutan. Pathol.* 35, 809–815. doi: 10.1111/j.1600-0560.2007.00905.x
- Panas, H. N., Lynch, L. J., Vallender, E. J., Xie, Z., Chen, G. L., Lynn, S. K., et al. (2010). Normal thermoregulatory responses to 3-iodothyronamine,

- trace amines and amphetamine-like psychostimulants in trace amine associated receptor 1 knockout mice. *J. Neurosci. Res.* 88, 1962–1969. doi: 10.1002/jnr.22367
- Pedretti, A., Marconi, C., Bettinelli, I., and Vistoli, G. (2009). Comparative modeling of the quaternary structure for the human TRPM8 channel and analysis of its binding features. *Biochim. Biophys. Acta* 1788, 973–982. doi: 10.1016/j.bbamem.2009.02.007
- Pingle, S. C., Matta, J. A., and Ahern, G. P. (2007). Capsaicin receptor: TRPV1 a promiscuous TRP channel. *Hand. Exp. Pharmacol.* 179, 155–171. doi: 10.1007/978-3-540-34891-7_9
- Prevarskaya, N., Zhang, L., and Barritt, G. (2007). TRP channels in cancer. *Biochim. Biophys. Acta* 1772, 937–946. doi: 10.1016/j.bbapap.2007.05.006
- Pusch, M., and Neher, E. (1988). Rates of diffusional exchange between small cells and a measuring patch pipette. *Pflugers Arch.* 411, 204–211.
- Qin, W., Xie, W., Xia, N., He, Q., and Sun, T. (2016). Silencing of transient receptor potential channel 4 alleviates oxLDL-induced angiogenesis in human coronary artery endothelial cells by inhibition of VEGF and NF- κ B. *Med. Sci. Monit.* 22, 930–936. doi: 10.12659/MSM.897634
- Rawls, S. M., Gomez, T., Ding, Z., and Raffa, R. B. (2007). Differential behavioral effect of the TRPM8/TRPA1 channel agonist icilin (AG-3-5). *Eur. J. Pharmacol.* 575, 103–104. doi: 10.1016/j.ejphar.2007.07.060
- Ray, A. M., Benham, C. D., Roberts, J. C., Gill, C. H., Lanneau, C., Gitterman, D. P., et al. (2003). Capsazepine protects against neuronal injury caused by oxygen glucose deprivation by inhibiting I(h). *J. Neurosci.* 23, 10146–10153. doi: 10.1523/JNEUROSCI.23-31-10146.2003
- Reichhart, N., Keckeis, S., Fried, F., Fels, G., and Strauss, O. (2015). Regulation of surface expression of TRPV2 channels in the retinal pigment epithelium. *Graefes Arch. Clin. Exp. Ophthalmol.* 253, 865–874. doi: 10.1007/s00417-014-2917-7
- Robbins, A., Kurose, M., Winterson, B. J., and Meng, I. D. (2012). Menthol activation of corneal cool cells induces TRPM8-mediated lacrimation but not nociceptive responses in rodents. *Invest. Ophthalmol. Vis. Sci.* 53, 7034–7042. doi: 10.1167/iovs.12-10025
- Rogowski, M., Gollahan, L., Chellini, G., and Assadi-Porter, F. M. (2017). Uptake of 3-iodothyronamine hormone analogs inhibits the growth and viability of cancer cells. *FEBS Open Biol.* 7, 587–601. doi: 10.1002/2211-5463.12205
- Scanlan, T. S., Suchland, K. L., Hart, M. E., Chiellini, G., Huang, Y., Kruzich, P. J., et al. (2004). 3-Iodothyronamine is an endogenous and rapid-acting derivative of thyroid hormone. *Nat. Med.* 10, 638–642. doi: 10.1038/nm1051
- Schanze, N., Jacobi, S. F., Rijntjes, E., Mergler, S., Del Olmo, M., Hoefig, C. S., et al. (2017). 3-Iodothyronamine decreases expression of genes involved in iodide metabolism in mouse thyroids and inhibits iodide uptake in PCCL3 thyrocytes. *Thyroid* 27, 11–22. doi: 10.1089/thy.2016.0182
- Shinderman-Maman, E., Cohen, K., Moskovich, D., Hercbergs, A., Werner, H., Davis, P. J., et al. (2017). Thyroid hormones derivatives reduce proliferation and induce cell death and DNA damage in ovarian cancer. *Sci. Rep.* 7:16475. doi: 10.1038/s41598-017-16593-x
- Singh, A. D., Turell, M. E., and Topham, A. K. (2011). Uveal melanoma: trends in incidence, treatment, and survival. *Ophthalmology* 118, 1881–1885. doi: 10.1016/j.ophtha.2011.01.040
- Spagnolo, F., Caltabiano, G., and Queirolo, P. (2012). Uveal melanoma. *Cancer Treat. Rev.* 38, 549–553. doi: 10.1016/j.ctrv.2012.01.002
- Stumpff, F., Boxberger, M., Krauss, A., Rosenthal, R., Meissner, S., Choritz, L., et al. (2005). Stimulation of cannabinoid (CB1) and prostanoid (EP2) receptors opens BKCa channels and relaxes ocular trabecular meshwork. *Exp. Eye Res.* 80, 697–708. doi: 10.1016/j.exer.2004.12.003
- Sudaka, A., Susini, A., Lo Nigro, C., Fischel, J. L., Toussan, N., Formento, P., et al. (2013). Combination of bevacizumab and irradiation on uveal melanoma: an *in vitro* and *in vivo* preclinical study. *Invest. New Drugs* 31, 59–65. doi: 10.1007/s10637-012-9834-6
- Takaishi, M., Uchida, K., Suzuki, Y., Matsui, H., Shimada, T., Fujita, F., et al. (2016). Reciprocal effects of capsaicin and menthol on thermosensation through regulated activities of TRPV1 and TRPM8. *J. Physiol. Sci.* 66, 143–155. doi: 10.1007/s12576-015-0427-y
- Teng, H. P., Huang, C. J., Yeh, J. H., Hsu, S. S., Lo, Y. K., Cheng, J. S., et al. (2004). Capsazepine elevates intracellular Ca²⁺ in human osteosarcoma cells, questioning its selectivity as a vanilloid receptor antagonist. *Life Sci.* 75, 2515–2526. doi: 10.1016/j.lfs.2004.04.037
- Thilo, F., Liu, Y., Loddenkemper, C., Schuelein, R., Schmidt, A., Yan, Z., et al. (2012). VEGF regulates TRPC6 channels in podocytes. *Nephrol. Dial. Transplant* 27, 921–929. doi: 10.1093/ndt/gfr457
- Tran, B. K., Schalenbourg, A., Bovey, E., Zografas, L., and Wolfensberger, T. J. (2013). Role of vitreoretinal surgery in maximizing treatment outcome following complications after proton therapy for uveal melanoma. *Retina* 33, 1777–1783. doi: 10.1097/IAE.0b013e318295f758
- Valero, M. L., Mello de Queiroz, F., Stühmer, W., Viana, F., and Pardo, L. A. (2012). TRPM8 ion channels differentially modulate proliferation and cell cycle distribution of normal and cancer prostate cells. *PLoS ONE* 7:e51825. doi: 10.1371/journal.pone.0051825
- Valtink, M., and Engelmann, K. (2007). Serum-free cultivation of adult normal human choroidal melanocytes. *Graefes Arch. Clin. Exp. Ophthalmol.* 245, 1487–1494. doi: 10.1007/s00417-007-0588-3
- Vay, L., Gu, C., and McNaughton, P. A. (2012). The thermo-TRP ion channel family: properties and therapeutic implications. *Br. J. Pharmacol.* 165, 787–801. doi: 10.1111/j.1476-5381.2011.01601.x
- Voets, T., Droogmans, G., Wissenbach, U., Janssens, A., Flockerzi, V., and Nilius, B. (2004). The principle of temperature-dependent gating in cold- and heat-sensitive TRP channels. *Nature* 430, 748–754. doi: 10.1038/nature02732
- Vriens, J., Appendino, G., and Nilius, B. (2009). Pharmacology of vanilloid transient receptor potential cation channels. *Mol. Pharmacol.* 75, 1262–1279. doi: 10.1124/mol.109.055624
- Weil, A., Moore, S. E., Waite, N. J., Randall, A., and Gunthorpe, M. J. (2005). Conservation of functional and pharmacological properties in the distantly related temperature sensors TRPV1 and TRPM8. *Mol. Pharmacol.* 68, 518–527. doi: 10.1124/mol.105.012146
- Wu, K. W., Yang, P., Li, S. S., Liu, C. W., and Sun, F. Y. (2015). VEGF attenuated increase of outward delayed-rectifier potassium currents in hippocampal neurons induced by focal ischemia via PI3-K pathway. *Neuroscience* 298, 94–101. doi: 10.1016/j.neuroscience.2015.04.015
- Xing, H., Chen, M., Ling, J., Tan, W., and Gu, J. G. (2007). TRPM8 mechanism of cold allodynia after chronic nerve injury. *J. Neurosci.* 27, 13680–13690. doi: 10.1523/JNEUROSCI.2203-07.2007
- Yang, H., Wang, Z., Capó-Aponte, J. E., Zhang, F., Pan, Z., and Reinach, P. S. (2010). Epidermal growth factor receptor transactivation by the cannabinoid receptor (CB1) and transient receptor potential vanilloid 1 (TRPV1) induces differential responses in corneal epithelial cells. *Exp. Eye Res.* 91, 462–471. doi: 10.1016/j.exer.2010.06.022
- Yang, Y., Yang, H., Wang, Z., Varadaraj, K., Kumari, S. S., Mergler, S., et al. (2013). Cannabinoid receptor 1 suppresses transient receptor potential vanilloid 1-induced inflammatory responses to corneal injury. *Cell. Signal.* 25, 501–511. doi: 10.1016/j.cellsig.2012.10.015
- Zhang, X., Huang, J., and McNaughton, P. A. (2005). NGF rapidly increases membrane expression of TRPV1 heat-gated ion channels. *EMBO J.* 24, 4211–4223. doi: 10.1038/sj.emboj.7600893
- Zucchi, R., Accoroni, A., and Chiellini, G. (2014). Update on 3-iodothyronamine and its neurological and metabolic actions. *Front. Physiol.* 5:402. doi: 10.3389/fphys.2014.00402
- Conflict of Interest Statement:** The authors declare that the research was conducted in the absence of any commercial or financial relationships that could be construed as a potential conflict of interest.
- Copyright © 2018 Walcher, Budde, Böhm, Reinach, Dhandapani, Ljubojevic, Schweiger, von der Waydbrink, Reimers, Köhrle and Mergler. This is an open-access article distributed under the terms of the Creative Commons Attribution License (CC BY). The use, distribution or reproduction in other forums is permitted, provided the original author(s) and the copyright owner(s) are credited and that the original publication in this journal is cited, in accordance with accepted academic practice. No use, distribution or reproduction is permitted which does not comply with these terms.

2.4. Manuskript IV

Upregulation of Transient Receptor Potential Vanilloid Type-1 Channel Activity and Ca^{2+} Influx Dysfunction in Human Pterygial Cells

Fabian Garreis,¹ Antje Schröder,¹ Peter S. Reinach,² Stefanie Zoll,³ Noushafarin Khajavi,³ Priyavathi Dhandapani,⁴ Alexander Lucius,³ Uwe Pleyer,³ Friedrich Paulsen,¹ and Stefan Mergler³

¹Department of Anatomy II, Friedrich Alexander University Erlangen-Nürnberg, Erlangen, Germany

²School of Ophthalmology and Optometry, Wenzhou Medical University, Wenzhou, People's Republic of China

³Department of Ophthalmology, Charité-Universitätsmedizin Berlin, Campus Virchow-Hospital, Berlin, Germany

⁴Department of Gastroenterology, Charité-Universitätsmedizin Berlin, Campus Virchow-Hospital, Berlin, Germany

Correspondence: Stefan Mergler, Charité-Universitätsmedizin Berlin, Campus Virchow-Clinic, Department of Ophthalmology, Augustenburger Platz 1, 13353 Berlin, Germany; stefan.mergler@charite.de.
Fabian Garreis, Friedrich Alexander University Erlangen-Nürnberg, Department of Anatomy II, Universitätsstraße 19, 91054 Erlangen; fabian.garreis@fau.de.

Submitted: January 18, 2016

Accepted: March 26, 2016

Citation: Garreis F, Schröder A, Reinach PS, et al. Upregulation of transient receptor potential vanilloid type-1 channel activity and Ca^{2+} influx dysfunction in human pterygial cells. *Invest Ophthalmol Vis Sci*. 2016;57:2564–2577. DOI:10.1167/ iovs.16-19170

PURPOSE. The heat-sensitive transient receptor potential vanilloid type-1 (TRPV1) channel (i.e., capsaicin [CAP] receptor) is upregulated in numerous cancers. This study determined if this response occurs in fresh and cultured hyperplastic human pterygial epithelial tissues.

METHODS. Reverse transcriptase PCR and quantitative real-time PCR, along with immunohistochemistry and Western blotting, characterized TRPV1 expression patterns in pterygial and healthy conjunctival tissue, primary and immortalized pterygial cells (hPtEC), and primary and immortalized conjunctival epithelial cells (HCjEC). Imaging of Ca^{2+} and planar whole-cell patch-clamping evaluated TRP channel activity. An MTS assay measured cell metabolic activity and a cell growth assay monitored proliferation.

RESULTS. Capsaicin (20 μM) and elevating bath temperature above 43°C activated Ca^{2+} transients more in hPtEC than HCjEC. Capsaicin induced corresponding changes in inward currents that were inhibited by 20 μM capsazepine (CPZ). Vascular endothelial growth factor (VEGF) also increased Ca^{2+} -influx and induced corresponding inward currents more in hPtEC than in HCjEC, whereas CPZ (20 μM), BCTC (20 μM), or La³⁺ (500 μM) reduced these responses, respectively. Whereas epidermal growth factor (EGF) increased proliferation more in hPtEC than in HCjEC, VEGF had no effect on this response. Capsazepine suppressed hPtEC proliferation induced by EGF and VEGF, whereas it was cytotoxic to HCjEC.

CONCLUSIONS. Mitogenic responses to EGF and VEGF are mediated through TRPV1 transactivation. Only in hPtEC do the increases in proliferation induced by EGF exceed those in HCjEC. Therefore, TRPV1 is a potential drug target whose clinical relevance in treating pterygium warrants further assessment.

Keywords: pterygium, human conjunctival epithelium, transient receptor potential vanilloid 1 channel, VEGF, EGF, intracellular Ca^{2+} , planar patch-clamp technique

Pterygium (conjunctivae) is a common ocular surface hyperproliferative tumorous disorder. Its risk factors include not only dust, wind, heat, dryness, and smoke, but also chronic UV-B light exposure, which is the main risk factor. In addition, viral infection and genetic factors contribute to initiating and promoting this disease.^{1,2} Specifically, pterygium incidence is greater in regions near the equator (pterygium belt),^{1,3–5} whereas in Europe it is substantially less.^{1,3–6} Surgical resection is the only option for reducing visual impairment caused by a pterygium-related disturbance. Because of its high recurrence rate (10%–70%), often repeated surgery may be needed, which heightens the likelihood of regrowth, inflammation, and scar formation.⁷ Advanced pterygium frequently leads to precorneal tear film dysfunction and dry eye disease (DES). In the long term, it often results in reduced vision due to astigmatism, tear film alterations, and movement restriction of the bulbus.⁶

Vascular endothelial growth factor (VEGF) and its cognate receptor are upregulated in pterygium tissue (PT).^{8–10} Reten-

tion of the pterygial cell phenotype appears to be location specific, as this tissue does not infiltrate into the cornea, suggesting that the corneal milieu is not supportive of this process.²

Transient receptor potential (TRP) channels constitute a superfamily of ligand-gated, nonselective cation channels subdivided into seven subfamilies according to differences in amino acid sequence homology (reviewed by Ramsey et al.¹¹). The heat-sensitive TRP vanilloid receptor 1 (TRPV1, capsaicin [CAP] receptor) channel is the most investigated TRP channel and it is the only one whose three-dimensional structure was determined.^{12,13} Besides being activated by heat (>43°C) and CAP, exposure to acidity and hyperosmolarity can also induce this response.^{14–16} Furthermore, changes of TRPV1 expression (in human skin) can be detected after UV irradiation.¹⁷ Transient receptor potential V1 mediates heat shock-induced matrix metalloproteinase-1 (MMP-1) expression in human keratinocytes.¹⁸ However, diverse TRPV1 activation mechanisms induced through various (physical) stimuli have not yet



been elucidated. High-resolution analysis of TRPV1 structure identified conformational changes in an outer pore domain and lower gate domain through ligand-binding. Allosteric coupling between both domains is responsible for a broad physiological range of stimuli activating TRPV1 and other TRP channels.^{19,20} Ogawa et al.²¹ showed that the oxidative status of Cys residues in the TRPV1 sequence modulated by reactive oxygen species triggers TRPV1 activation through changes in the redox environment. Additionally, TRP channels are mechanically activated directly or by signaling cascades that alter lipid composition, change conformation of plasma membrane and open TRPs by mechanical force (reviewed in Liu and Montell²²). In *Drosophila*, photoreceptors and mammalian photosensitive retinal ganglion cell phototransduction is mediated by G protein-activated phospholipase C (PLC), which generates a force in the lipid-bilayer opening TRP-Canonical channels.^{23,24}

Transient receptor potential V1 is expressed in human conjunctival epithelial cells (HCjEC),²⁵ human corneal endothelial cells,²⁶ corneal fibroblasts,²⁷ and corneal epithelial cells (HCEC)^{28,29} (reviewed in Ref.³⁰). Cellular constituent release caused by a severe chemical injury also induces TRPV1 activation, followed by corneal opacification and chronic dysregulated inflammation during wound healing.^{27,28,31,32} As increases in cell proliferation in cancer are associated with rises in functional TRPV1 expression and activity,^{33,34} we hypothesized that this change is associated with conjunctival hyperplasia in pterygium.

We show here that TRPV1 channel expression is upregulated in human PT. This upregulation is associated with dysfunctional Ca²⁺ influx. Furthermore, the mitogenic responses to EGF and VEGF are dependent on their respective cognate receptors transactivating TRPV1, as suppression of TRPV1 activation by capsazepine (CPZ) inhibited the increases in proliferation induced by these cytokines in human pterygial cells (hPtECs).

MATERIALS AND METHODS

Materials

Capsazepine (CPZ) and icilin were obtained from Cayman Chemical Company (Ann Arbor, MI, USA). N-(4-tert.butylphenyl)-4-(3-chloropyridin-2-yl) tetrahydro-pyrazine-1(2H)-carboxamide (BCTC) and fura-2/AM were obtained from TOCRIS Bioscience (Bristol, UK). Vascular endothelial growth factor was purchased from ThermoFisher Scientific (Waltham, MA, USA). Medium and supplements for cell culture came from Life Technologies Invitrogen (Karlsruhe, Germany) or Biochrom AG (Berlin, Germany). All other reagents were purchased from Sigma (Deisenhofen, Germany).

Tissue and Cell Preparation

Human PT was obtained after surgical removal from 21 patients with primary pterygium conjunctivae (no recurrent lesions and no bilateral pterygia were included in the study) by the Department of Ophthalmology, Charité University Medicine Berlin, according to the tenets of the Declaration of Helsinki. All patients provided written consent, which was approved by the ethics committee of Charité, University Medicine Berlin, Germany. For RT-PCR and Western blot analysis, eight different PT samples were used and eight others for immunohistochemistry analysis. For functional studies, PT from another five patients was mechanically reduced to small aggregates, incubated with 0.1 mg/mL collagenase type IV for 1 hour at 37°C, 5% CO₂, 21% O₂). After rinsing with 1× PBS,

aggregates were incubated again with 0.01 mg/mL collagenase IV for another 24 hours. Cells were rinsed again in 1× PBS and isolated by centrifugation (5 minutes, 145 g). Afterward, cells were transferred and cultivated in Dulbecco's modified Eagle's medium (DMEM)/Ham's F12 containing 10% fetal calf serum, 1 µg/mL insulin, 5 µg/mL hydrocortisone, and 100 U/mL penicillin/streptomycin mix. After two to four passages, cells were used for functional studies. In two of these cell preparations, primary hPtEC underwent spontaneous immortalization after several cell passages. Primary conjunctival epithelial cells obtained from healthy individuals were grown under the same conditions only for two to four passages and then discarded to avoid possible passage-dependent electrophysiological changes. In addition, an immortalized HCjEC line, was used and cultivated as previously reported.^{25,29} Furthermore, an SV40-immortalized human cornea epithelial cell line (HCEC)³⁵ was cultured according to our previous study.²⁵

Reverse Transcriptase PCR

Surgically removed PT was stored in RNAlater (Invitrogen, Karlsruhe, Germany) at 4°C and later lysed in 1 mL peqGOLD TriFast reagent (Peqlab, Erlangen, Germany) in an innuSPEED Lysis Tube placed in a SpeedMill plus homogenizer (both Analytik Jena AG, Jena, Germany). After centrifugation (10 minutes, 15,000 g), supernatants were used for RNA isolation. Pterygium tissue DNA contamination was eliminated by digestion with RNase-free DNase I (30 minutes, 37°C). DNase was heat inactivated for 10 minutes at 65°C. Reverse transcription of RNA samples to first-strand cDNA was performed by RevertAidTM H Minus M-MuL V Reverse Transcriptase Kit (Fermentas, St. Leon-Rot, Germany) according to manufacturer's protocol. Two micrograms total RNA and 10 pmol Oligo (dT) 18 primer (Fermentas) were used for each reaction. Each PCR reaction contained 2 µL cDNA in 2.5 µL 10× PCR buffer, 1 µL 50 mM MgCl₂, 1 µL 10 mM dNTP mix (Fermentas), 0.5 µL 10 pmol forward primer, 0.5 µL 10 pmol reverse primer, 0.2 µL (5 U/µL) Taq DNA Polymerase (Invitrogen) diluted with RNase-free diethylpyrocarbonate-treated water. Polymerase chain reaction amplification underwent an initial cycle at 95°C for 5 minutes followed by 35 cycles at 95°C for 30 seconds, primer-specific annealing temperature for 30 seconds, 72°C for 30 seconds, and a final elongation at 72°C for 5 minutes as well as a temperature hold at 4°C. Gene-specific intron-spanning primer sequences, annealing temperatures, cycle numbers, and product sizes are shown in the Table. Primers were synthesized at Metabion International AG (Steinkirchen, Germany). Polymerase chain reaction products were resolved by electrophoresis in a 1.5 % agarose gel and visualized via fluorescence. Base pair (bp) values were compared with Genbank data. Reverse transcriptase PCR product identity was confirmed by sequencing and sequence alignment (data not shown). Genomic contamination was prevented by omission of reverse transcriptase. Housekeeping β-actin gene expression assessed integrity and stability of the reverse transcribed cDNA.

Real Time RT-PCR

Each reaction was performed in a final volume of 20 µL containing 10 µL LightCycler 480 SYBR Green Mastermix (Roche, Penzberg, Germany), 0.5 µL gene-specific primer mix (10 pmol), 7.5 µL nuclease-free water, and 2 µL sample cDNA. Each plate was run at 95°C for 2 minutes, followed by 45 cycles at 95°C for 10 seconds, 60°C for 10 seconds, and 72°C for 10 seconds, and gene-specific transcript amplification was confirmed by obtaining a melting curve profile (60–95°C). The cycle threshold (C_t) parameter was defined by second

TABLE. Gene-Specific Intron-Spanning Primer Sequences, Annealing Temperatures, Cycle Numbers, and Product Sizes of Biomarkers and TRPs

Gene	Forward Primer	Reverse Primer	A _t , °C	Size, bp
RT-PCR				
β-actin	5'-GATCCTCACCGAGCGCGGCTACA-3'	5'-GCGGATGTCCACGTCAACTTCA-3'	60	298
CK-3	5'-TGTACCAGACCAAGTTGGGG-3'	5'-CGCCGTAACCTCCTCCATAG-3'	58	456
CK-13	5'-CGGGATGCTGAGGAATGGT-3'	5'-GGGAAACCAATCATCTGGCG-3'	62	392
CK-15	5'-ACTGAGGAGCTGAACAAAGAGG-3'	5'-CAAGCAGCATCTGTACTCCT-3'	58	280
Ki-67	5'-TATCAAAGGAGCGGGTCG-3'	5'-TTGAGCTTCTCATCAGGTCA-3'	58	388
MMP7	5'-GTTTAGAACCAAATCAAGG-3'	5'-CTTGACACTAATCGATCCAC-3'	64	100
MUC5AC	5'-CCAAGGAGAACCTCCCATA-3'	5'-CCAAGCGTCATTCTGAG-3'	61	282
TRPV1	5'-CTCCTACAAACAGCTGTAC-3'	5'-AAGGCCTCTCATGCACT-3'	63	285
TRPV2	5'-CTCTGGCTAGCTGTGACA-3'	5'-TGGGATCCCGAGCTTCTCTCA-3'	63	228
TRPV3	5'-GCTGAAGAACGCATTTGCA-3'	5'-TCATAGGCCCTCCTCTGTGTACT-3'	65	288
TRPV4	5'-TACCTGTGTGCCATGGTCATCT-3'	5'-TGCTATAGGTCCCCGTAGCTT-3'	60	379
TRPM8	5'-CCTGTTCTCTTGCGGTGTGGAT-3'	5'-TCCTCTGAGGTGTCGTTGGCTTT-3'	65	621
Real-time RT-PCR				
18S rRNA	5'-TGCCAGAGTCTCGTTCGTTA-3'	5'-GGTGCATGGCCGTTCTTA-3'	60	92
TRPM8	5'-ACACTCAGTGAACAGCTAACAG-3'	5'-GCCAAAGTGAAGAACGACATC-3'	60	93
TRPV1	5'-CCTGCAGGAGTCGGTTCA-3'	5'-CAGCAGCGAGACCCCTAA-3'	60	65

derivative maximum analysis with LightCycler480 software v1.5 (Roche). To standardize mRNA concentration, transcript levels of a reference gene in each sample, 18S rRNA was determined in parallel and relative transcript levels were corrected by normalization with the 18S Ct levels. All real-time RT-PCRs were performed in triplicate and changes in gene expression were calculated using the delta delta Ct method.³⁶ Real-time RT-PCR was performed using LightCycler 480 from Roche.

Immunohistochemistry

Surgically removed PT fixed in 4% formalin was embedded in paraffin, sectioned (7 µm) and deparaffinized. Immunohistochemistry was performed with anti-TRPV1 (ACC-030; Alomone Labs, Jerusalem, Israel), TRPM8 (HPA024117; Sigma Aldrich, Munich, Germany), cytokeratin (CK)-13 (sc-57003; Santa Cruz Biotechnology, Heidelberg, Germany), CK-15 (CBL1587417; Millipore, Darmstadt, Germany), and CK-19 (sc-53003; Santa Cruz Biotechnology) antibodies, as previously described in detail.^{25,37} Transient receptor potential V1 and -M8 antibody specificity was confirmed based on elimination of antibody reactivity by antibody preadsorption with 1 µg of a respective blocking peptide per µg antibody. Furthermore, control sections were incubated with nonimmune IgG to determine possible nonspecific binding of IgG. The slides were examined with a Keyence BZ 9000 microscope (Keyence Germany, Neu-Isenburg, Germany).

Western Blot Analysis

Cells were lysed with 1% Triton X-100 for 30 minutes on ice and centrifuged at 17,950 g for 5 minutes. Pterygium tissue was lysed with peqGOLD TriFast reagent (Peqlab). Total protein was isolated from phenol/chloroform phase as described in the manufacturer's protocol. Protein pellet was dissolved in 10 M urea/50 mM dithiothreitol and sonicated (HTU Soni130; G. HEINEMANN, Schwäbisch Gmünd, Germany) for 3 seconds. Supernatant protein concentration was determined with the Bradford assay. For Western blot analysis, 20 µg total protein was boiled for 5 minutes with a reducing buffer containing β-mercaptoethanol and loaded onto 12% SDS-PAGE, separated by electrophoresis and transferred to a nitrocellulose membrane by blotting. Blots were blocked in 5% nonfat milk/TBST (1 mL Tween 20/1 L Tris-buffered saline)

for 1 hour and probed with the primary antibody (1:100 dilution) overnight at 4°C. Washing with TBST was followed by incubation with horseradish peroxidase-conjugated secondary antibody (dilution 1:5000, 2 hours at room temperature). Signal readout was determined by chemiluminescence with an enhanced chemiluminescence substrate (Millipore) in Biorad Universalhood II (Munich, Germany). Furthermore, every blot was stripped with β-mercaptoethanol, 20% SDS, 1M Tris-HCl pH 6.8 containing buffer at 70°C for 30 minutes. Afterward, glyceraldehyde 3-phosphate dehydrogenase detection for normalization was performed. Blots were analyzed and quantified by Quantity One Software v4.6.9 (Biorad).

Proliferation Assay

Spontaneously immortalized hPtEC as well as HCjEC cells were seeded at 10⁵ cells/mL in 24-well cell culture plates. Cells were cultivated under aforementioned standard conditions in 10% fetal calf serum-containing DMEM/Ham's F12 medium (Control). Cells were cultivated with 10 ng/mL epidermal growth factor (EGF), 10 ng/mL VEGF in the presence and absence of 10 µM CAP and/or 10 µM capsazepine (CPZ). Medium with/without additives was replaced every 48 hours. At the indicated time points, cells were trypsinized and counted under a phase-contrast microscope (Axiovert 40 CFL; Zeiss, Oberkochen, Germany) using a Neubauer improved-hemocytometer (BRAND, Wertheim, Germany). At every time point and for each cell line, four different wells were counted.

Metabolic Cell Viability Assay

Using the CellTiter 96 AQueous MTS Assay System (Promega, Mannheim, Germany) according to manufacturer's protocol, cells were cultured in serum-free medium supplemented with either 10, 20, or 100 µM CAP as well as 10 or 20 µM CPZ, respectively. Metabolic cell viability was measured after 24 hours by photometry in a plate reader (MWG, Ebersberg, Germany) at 490 nm. Human pterygium epithelial cells and HCjEC without additives were used as controls.

Fluorescence Calcium Imaging

Cells were seeded on sterile glass cover slips and loaded with fura-2/AM (2 µM) for 20 to 50 minutes at 37°C. Loading was

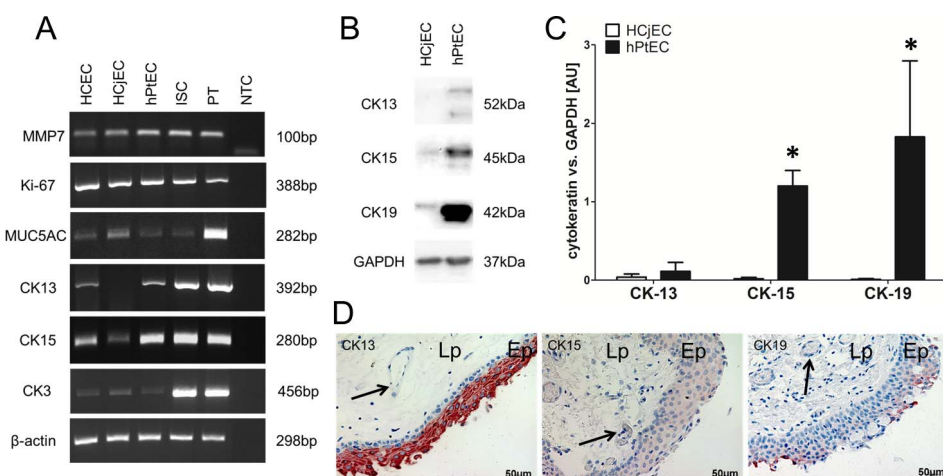


FIGURE 1. Characterization of spontaneously immortalized hPtECs. (A) Reverse transcriptase PCR analysis revealed gene expression of MMP7, Ki-67, Muc5AC, and CK-13, -15, and -19 in cultivated hPtEC as well as PT. Limbal stem cells (LSCs) as well as HCECs and HCjECs were used as controls and show a similar expression profile. (B) Detection of CK-13, -15, and -19 proteins in cultivated HCjEC and hPtEC by Western blot analysis. (C) Statistical analysis of Western blots shows increased CK-15 and -19 protein levels in cultivated hPtEC compared with HCjEC. Results presented as mean \pm SEM of three independent experiments ($n=3$). * $P < 0.05$ (2-tailed Student's *t*-test). (D) Localization (red staining) of CK-13, -15, and -19 in formalin-embedded paraffin section of pterygia by immunohistochemistry. Pterygium epithelial cells (Ep), lamina propria (Lp), and blood vessels (arrow) are marked. Nuclei (blue) counterstained with hemalum.

stopped by replacing the dye containing culture medium with a Ringer-like (control) solution optimized for TRP detection³⁸ whose composition was in mM: 150 NaCl, 6 CsCl, 1 MgCl₂, 10 glucose, 10 HEPES, and 1.5 CaCl₂ at pH 7.4. Washed cover slips were put into a bath chamber containing the aforementioned Ringer-like solution on the stage of a microscope (Olympus BW50WI; Olympus Europa Holding GmbH, Hamburg, Germany) in conjunction with a digital imaging system having UV excitation capability (TILL Photonics, Munich, Germany). Cells were alternately excited at 340 and 380 nm and fluorescence emission was detected from cell clusters every 500 ms at 510 nm. The ratio ($f_{340\text{nm}}/f_{380\text{nm}}$) is a relative index of intracellular Ca²⁺ ($[Ca^{2+}]_i$) levels.³⁹ The 340- and 380-nm signals were always detectable and did not distort the ratio. The measuring field was adapted to the number of cells (TILL Photonics view-finding system). Before the experiments, stable control baseline levels were obtained for 8 to 10 minutes. The control traces are designated with open circles in the figures. All experiments were performed at a constant room temperature ($\approx 20^{\circ}\text{--}23^{\circ}\text{C}$) because experiments performed at higher temperatures led to increased Ca²⁺ levels due to increased open probability of thermosensitive-TRPs in ocular surface cells.^{25,29} Stock solutions of drugs were prepared in dimethyl sulfoxide (DMSO). Dimethyl sulfoxide concentrations below 0.1% had no detectable effect on intracellular Ca²⁺ regulation (data not shown).^{37,40}

Planar Patch-Clamping

The whole-cell mode ("Port-a-Patch"; Nanion, Munich, Germany) was used in combination with an EPC 10 patch-clamp amplifier (HEKA, Lamprecht, Germany) and PatchMaster software (Version 2.4; HEKA).^{25,40} In brief, the standard intracellular solution contained in mM: 50 CsCl, 10 NaCl, 60 CsF, 20 EGTA, and 10 HEPES-acid at pH of approximately 7.2 and approximately 288 mOsM, which was applied to the inner side of the microchip. The external solution contained in mM: 140 NaCl, 4 KCl, 1 MgCl₂, 2 CaCl₂, 5 D-glucose monohydrate, and 10 HEPES (pH ≈ 7.4 and osmolarity ≈ 298 mOsM) was present on the external side of the microchip (resistance of 2.5–3.0 M Ω). A single cell was held in place in the aperture by

applying negative pressure (software-controlled pump). The mean membrane capacitance of HCjEC was $13 \text{ pF} \pm 1 \text{ pF}$. Mean access resistance was $11 \pm 1 \text{ M}\Omega$ (both $n = 26$). For hPtEC, the corresponding values were $9 \text{ pF} \pm 1 \text{ pF}$ and $37 \pm 4 \text{ M}\Omega$ (both $n = 26$), respectively. Series resistances, and fast and slow capacitance transients were compensated by the patch-clamp amplifier. Current recordings were all leak-subtracted and cells with leak currents above 100 pA were excluded from analysis. The I-V response patterns were generated by imposing voltages in 10 mV steps from -60 mV to $+130 \text{ mV}$.⁴¹ The holding potential was set to 0 mV to eliminate any possible contribution of voltage-dependent Ca²⁺ channels.

Statistical Analysis

Student's *t*-test for paired data (P values: 2-tailed) was used if the data passed a normality test. If this failed, the nonparametric Wilcoxon matched pairs were used. For nonpaired data, Student's *t*-test for unpaired data was used, after passing a normality test. Alternatively, the nonparametric Mann-Whitney *U* test was performed. Welch's correction was applied if data variance of the two groups was not at the same level. Probabilities of $P < 0.05$ (indicated by asterisks [*] and hashtags [#]) were considered to be significant. The number of repeats is shown in each case in brackets, near the traces or bars. All values are means \pm SEM. All plots were generated with SigmaPlot software version 12.5 (Systat Software, San Jose, CA, USA). Bar charts were plotted with GraphPad Prism (version 5) (La Jolla, CA, USA).

RESULTS

Validation of hPtEC Phenotype

Reverse transcriptase PCR documented biomarker gene expression of pterygium (MMP7 and Ki-67) and conjunctiva (MUC5AC, CK-13 and -15)⁴² in spontaneously immortalized hPtECs and in PT (Fig. 1A). Western blot analysis shows increased protein levels of CK-13, -15, and -19 in hPtEC compared with HCjECs. In hPtECs, there was a 2.9-fold increase in CK-13, 11.4-fold increase in CK-15 and 96.9-fold

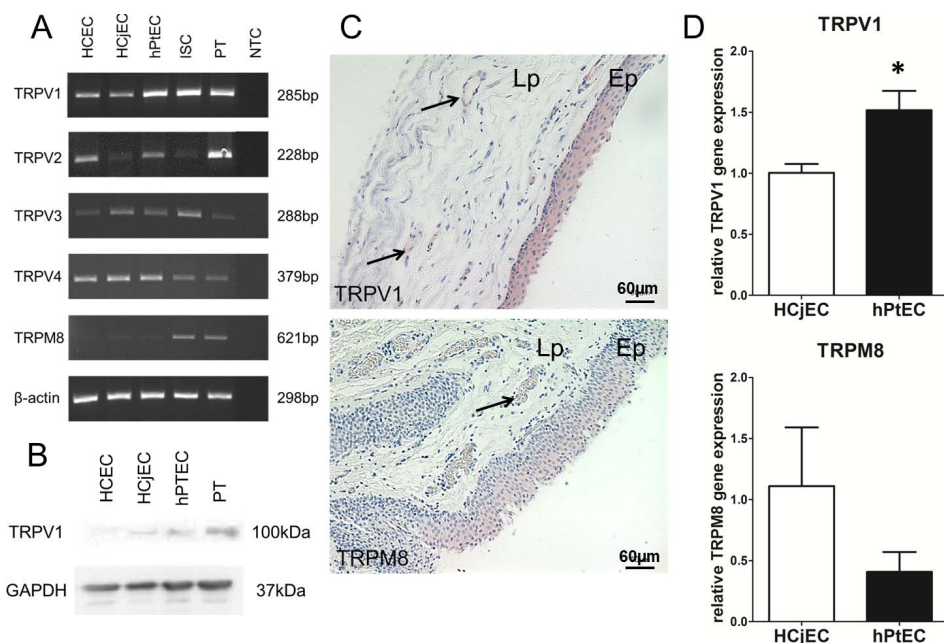


FIGURE 2. Gene and protein expression of temperature-sensitive TRP channels in pterygia. **(A)** Reverse transcriptase PCR analysis revealed gene expression of TRPV1, 2, 3, and 4 and TRPM8 in hPtECs and PT. Limbal stem cells, HCECs, and HCjECs show a similar thermo-TRP gene expression. **(B)** Western blot analysis revealed increased TRPV1 protein expression in cultivated hPtEC (2-fold) as well as PT (4.8-fold) compared with HCjEC. **(C)** Intracytoplasmic immunoreactivity (red staining) of TRPV1 and TRPM8 antibody in formalin-embedded paraffin section of pterygia. Pterygium Ep, Lp, and blood vessels (arrow) are marked. Nuclei (blue) counterstained with hemalum. **(D)** Real-time RT-PCR revealed upregulation of TRPV1 gene expression in cultivated hPtEC compared with HCjEC. Results presented as mean \pm SEM of three independent experiments ($n = 3$). * $P < 0.05$ (2-tailed Student's *t*-test).

increase in CK-19 protein expression compared with HCjEC (Figs. 1B, 1C). In formalin-fixed paraffin-embedded (FFPE) sections of PT obtained from eight different patients, CK-13, -15, and -19 expression were identified in hPtEC (Fig. 1D). There was pronounced intracytoplasmic CK-13 reactivity in intermediary and superficial pterygial epithelial cell layers, but no reactivity in the basal cell layer. Weak CK-15 expression was evident in all the pterygial epithelial layers along with CK-19 immunoreactivity in the intermediate cell layer. In the superficial epithelial cells, CK-19 expression was more intense. There were no significant differences in CK expression in these different pterygial samples irrespective of age or sex. Control sections with nonimmune IgGs were negative (not shown).

Temperature-Sensitive TRP Channel Expression

In hPtEC, PT, immortalized HCEC, HCjEC, and limbal epithelial cells, there was TRPV1, 2, 3, and 4 and TRPM8 gene expression (Fig. 2A). The TRP gene expression profiles were similar to one another and the β -actin control PCR (298 bp) products were invariant in all samples. Real-time RT-PCR analysis revealed significant TRPV1 gene expression upregulation ($P = 0.042$) in hPtEC compared with HCjEC. In the no template controls (NTC), contaminating genomic DNA was absent. Transient receptor potential V1 protein expression levels were approximately 2-fold and 4.8-fold higher in hPtEC and PT, respectively, than those in HCEC and HCjEC (Fig. 2B). In addition, there was TRPV1 and TRPM8 localized expression in FFPE sections of pterygia (Fig. 2C). Transient receptor potential V1 and weaker TRPM8 intracytoplasmic reactivity was evident in pterygial epithelial cells in all epithelial layers. Transient receptor potential V1 immunoreactivity was also present in vascular endothelial cells of the lamina propria. There was less intense intracellular TRPM8 immunoreactivity in PT sections, but none

was detected in the lamina propria. In all cases, no reactivity was detected with each preadsorbed primary antibody.

Functional Heat-Sensitive TRPV1 Expression

In hPtEC expanded from five patients, the $f_{340\text{nm}}/f_{380\text{nm}}$ ratio irreversibly increased after heating ($>43^\circ\text{C}$) from 1.197 ± 0.004 to 1.556 ± 0.045 (at 320 seconds; $n = 22$; *** $P < 0.005$, paired tested; Fig. 3A, left), but this response was partially suppressed by the TRP channel blocker lanthanum-III-chloride (La^{3+} ; 100 μM) (1.377 ± 0.035 ; $n = 18$; ** $P < 0.01$; Fig. 3A, right). Similar results were obtained in HCjEC (Fig. 3B; 1.628 ± 0.049 ; $n = 5$; ** $P < 0.01$, paired tested) and HCEC (Fig. 3C; 1.440 ± 0.065 ; $n = 10$; ** $P < 0.01$, paired tested), which could also be suppressed by La^{3+} (Figs. 3B, 3C). However, there was a sustained increase in intracellular Ca^{2+} after heat stimulation only in hPtEC. This was not obvious in HCjEC and HCEC and the Ca^{2+} transients were not significantly different shortly after heat stimulation. Specifically, after heat stimulation for 4 minutes, the duration of the TRPV1 response was longer in hPtEC than in HCjEC and HCEC (Fig. 3D). Moreover, the transient decline was more gradual in hPtEC than HCEC (Fig. 3A versus Fig. 3C). With hPtEC at 320 seconds, the $f_{340\text{nm}}/f_{380\text{nm}}$ ratio rose to 1.556 ± 0.045 ; $n = 22$ and fell slightly to 1.478 ± 0.059 ; $n = 22$ at 480 seconds. On the other hand, with HCjEC, the $f_{340\text{nm}}/f_{380\text{nm}}$ ratio rose less, from 1.200 ± 0.001 to 1.370 ± 0.022 ($n = 11$; *** $P < 0.005$, paired tested; Figs. 4A, 4B). Subsequent to reaching a peak, it partially declined to 1.315 ± 0.012 in HCjEC ($n = 11$; * $P < 0.05$, paired tested). Although the Ca^{2+} transient peaks were not different from one another in HCjEC and hPtEC (Fig. 3), at 480 seconds intracellular Ca^{2+} level remained at a higher level in hPtEC (480 seconds; Fig. 3D). Using instead primary freshly isolated hPtEC and comparing

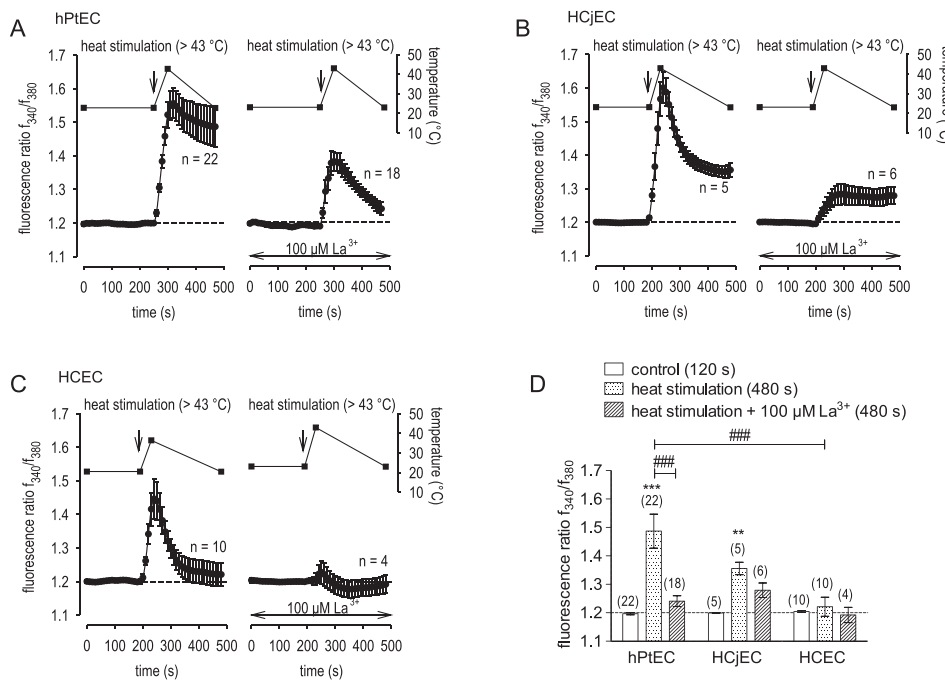


FIGURE 3. Increase in Ca^{2+} entry through heat-sensitive TRPs caused by heat exposure in hPtEC, HCjEC, and HCEC. The thermal changes were inflicted at the time points indicated by arrows. Data are mean \pm SEM of 4 to 22 experiments. (A) Rise of bath solution temperature from room temperature ($\approx 22^\circ\text{C}$) to over 43°C resulted in an irreversible Ca^{2+} elevation in hPtEC ($n = 22$; left). In the presence of La^{3+} (100 μM), the heat-induced Ca^{2+} increase was clearly suppressed ($n = 18$; right). (B–C) Same set of experiments as shown in (A), but with HCjEC (B) and HCEC (C), respectively. The heating effect was at lower levels between HCEC and hPtEC at 480 seconds. (D) Summary of the experiments with heat stimulation and La^{3+} in hPtEC, HCjEC, as well as HCEC. The asterisks (*) indicate significant differences between controls (Ca^{2+} base levels before heating) and heat-induced Ca^{2+} increase on $[\text{Ca}^{2+}]_i$ ($n = 18\text{--}22$) (paired Student's *t*-test). The hash marks (#) between the filled bars indicate significant differences between Ca^{2+} influx with and without La^{3+} (unpaired Student's *t*-test) and heat-induced Ca^{2+} influx between hPtEC and HCEC ($n = 10\text{--}22$).

its heat-induced $[\text{Ca}^{2+}]_i$ transient with that measured in healthy HCjEC, the difference was larger than obtained with immortalized hPtEC (Fig. 4). Taken together, the larger and less reversible heat-induced Ca^{2+} influx in primary passaged hPtEC indicates a longer and greater TRPV1 open probability than in the normal healthy HCjECs.

TRPV1-Induced Currents in Immortalized hPtEC

To validate that the heat-induced Ca^{2+} transients are attributable to TRPV1 activation, they were compared with the underlying currents induced by 20 μM CAP. It increased outwardly rectifying currents ($+130$ mV) from 81 ± 13 pA/pF up to 199 ± 44 pA/pF (* $P < 0.05$; $n = 16$, paired tested) (Figs. 5C, 5D). This change was

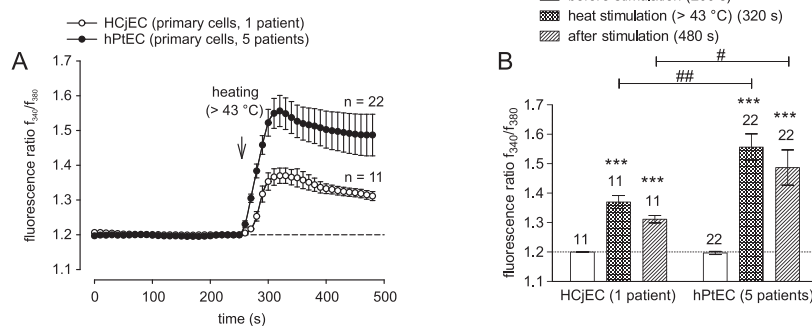


FIGURE 4. Increased heat-induced Ca^{2+} influx in primary cultivated hPtEC. The thermal change was carried out at the time point indicated by an arrow. Data from five patients with pterygium are mean \pm SEM of 22 experiments. Data from one healthy individual are mean \pm SEM of 11 experiments. (A) Rise of bath solution temperature from room temperature (22°C) to over 43°C resulted in Ca^{2+} elevation in healthy primary cultivated HCECs from one healthy individual and hPtECs from patients with pterygium. Traces show intracellular Ca^{2+} measured of several neighboring healthy HCjECs (open circles) ($n = 11$) and primary cultivated hPtECs from patients with pterygium (filled circles) ($n = 22$) (control base line; $f_{340\text{nm}}/f_{380\text{nm}} = 1.2$). In hPtEC from patients with pterygium, the heat-induced Ca^{2+} influx was clearly increased ($##P < 0.01$; $n = 11\text{--}22$). (B) Summary of the experiments with healthy HCjEC from a healthy patient and hPtEC from five patients with pterygium. The asterisks (*) indicate significant differences between controls (Ca^{2+} base levels; $n = 11\text{--}22$) and heat-induced Ca^{2+} increase on $[\text{Ca}^{2+}]_i$ ($n = 11\text{--}22$) (paired Student's *t*-test). The hash marks (#) between the filled bars indicate significant differences between healthy HCjEC and hPtEC from patients with pterygium (unpaired Student's *t*-test).

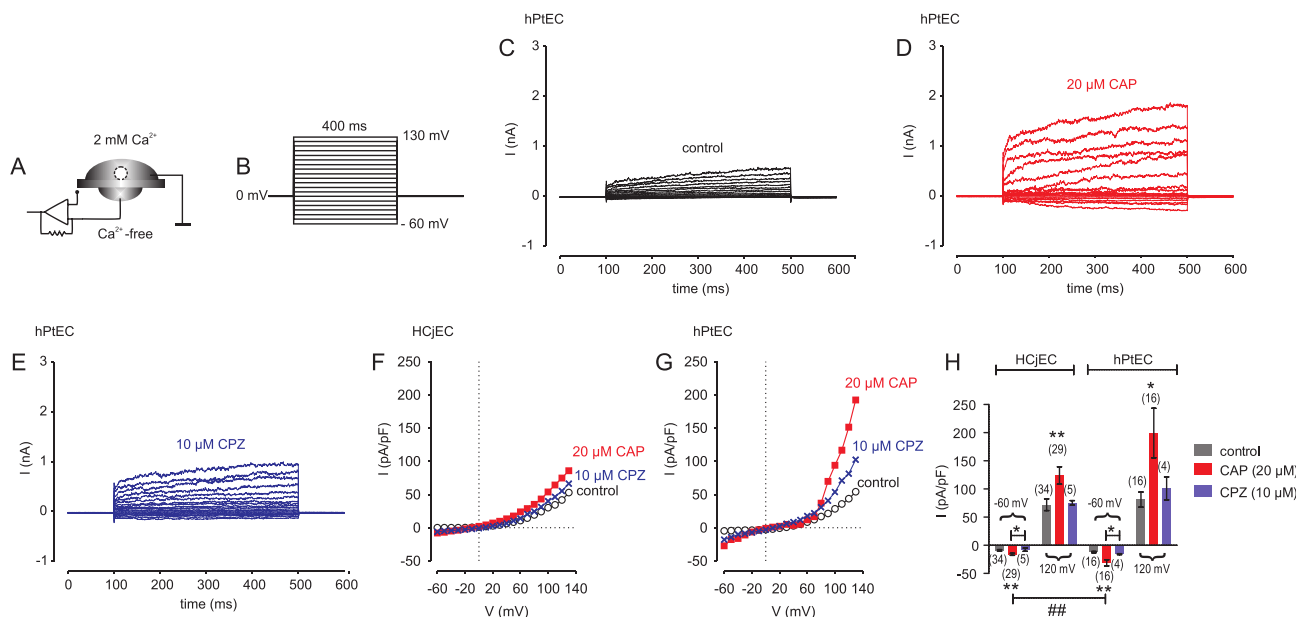


FIGURE 5. Capsaicin-induced increases of whole-cell currents in immortalized HCjEC and in hPtEC. **(A)** Simplified scheme of whole-cell configuration of the planar-patch clamp technique. **(B)** Voltage stimulation protocol. Holding potential was set to 0 mV to avoid any voltage-dependent ion channel currents. **(C)** Whole-cell channel currents induced by depolarization from -60 mV to +130 mV after establishing the whole-cell configuration (with leak current subtraction) under control conditions. **(D)** Whole-cell channel currents in the presence of 20 μ M CAP. **(E)** Whole-cell channel currents in the presence of 10 μ M CPZ. **(F)** Effect of CAP and CPZ in HCjEC is shown in a current/voltage plot (I-V plot). For the I-V plot, maximal peak current amplitudes were plotted against the voltage (mV) and normalized to cell membrane capacity (current density; pA/pF). The upper trace (*filled quadrangles*) was obtained in the presence of 20 μ M CAP and the trace below (*dash marks*) in the presence of 10 μ M CPZ. The third (*lower*) trace (*open circles*) was obtained under control conditions. **(G)** Same plot as shown in (F) but data are from hPtEC and taken from (C), (D) and (E). **(H)** Comparison of whole-cell current densities of HCjEC and hPtEC from a patient with pterygium. The inward currents of hPtEC were at higher levels compared with those of HCjEC. The asterisks (*) indicate significant differences between controls (Ca²⁺ base levels; $n = 11\text{--}22$) and CAP-induced whole-cell currents ($n = 11\text{--}22$) (paired Student's *t*-test). The hash marks (#) between the *filled bars* indicate significant differences between HCjEC and hPtEC from a patient with pterygium (unpaired Student's *t*-test).

not significantly different from that in immortalized HCjECs (Fig. 5H). On the other hand, CAP increased inward currents in hPtEC (~60 mV) from -12 ± 1 pA/pF up to -31 ± 6 pA/pF (** $P < 0.01$; $n = 16$) (Figs. 5C, 5D), which was slightly larger than that occurring in healthy HCjECs (-16 ± 2 pA/pF; Figs. 5F-H). The TRPV1 channel blocker CPZ caused these currents in hPtEC to fall by -15 ± 1 pA/pF more than in HCjEC. This difference more definitively reflects larger functional TRPV1 activity in immortalized hPtEC than immortalized HCjEC.

Heightened Functional TRPV1 Behavior in hPtEC

To validate that the difference in inward currents is accountable for larger Ca²⁺ influx in immortalized hPtEC than HCjEC, we compared the magnitudes of the Ca²⁺ transients induced by CAP. Results shown in Figures 6D-F indicate that the CAP-induced Ca²⁺ transients were at higher levels in immortalized hPtEC than in HCjEC. Specifically, the f_{340nm}/f_{380nm} ratio increased from 1.201 ± 0.002 to 1.231 ± 0.045 after CAP application (20 μ M) in immortalized hPtEC ($n = 31$; *** $P < 0.005$, paired tested; Fig. 6D), whereas in HCjEC, this ratio increased less from 1.200 ± 0.003 to 1.209 ± 0.003 ($n = 12$; ## $P < 0.01$, unpaired tested; Figs. 6D, 6F). These increases were smaller than those induced by heating to 43°C, as heating is less specifically activating TRPV1 than CAP. A difference in selectivity also is apparent between exposure to CAP and a hypertonic stress because the latter condition induced larger CPZ inhabitable intracellular Ca²⁺ transients (Figs. 6A-C). This difference among the effects of CAP, hypertonicity, and heating are not attributable to baseline variations, because in the absence of CAP, the baseline levels remained constant and

were identical to one another in HCjEC and hPtEC (Figs. 6D-F; $n = 13\text{--}19$; open circles). Taken together, these results suggest that functional TRPV1 expression in hPtEC is at higher levels in immortalized hPtEC than in HCjEC.

Dependence of VEGF-Induced Ca²⁺ Influx on TRPV1 Transactivation in hPtEC

As shown in Figure 7B, VEGF increased the f_{340nm}/f_{380nm} ratio from 1.202 ± 0.002 to 1.225 ± 0.006 ($t = 480$ seconds) in hPtEC ($n = 6$; * $P < 0.05$, paired tested), whereas the VEGF effect was smaller in HCjEC (Fig. 7A). On the other hand, in hPtEC, 20 μ M CPZ as well as a mixed TRPV1/TRPM8 antagonist, 20 μ M BCTC,⁴³ both caused the Ca²⁺ transients to even fall below their baseline (Figs. 7C, 7D). Corresponding effects of 10 ng/mL VEGF on inward currents indicate that they increased from -18 ± 2 pA/pF to -54 ± 11 pA/pF ($n = 6\text{--}12$; ** $P < 0.005$; unpaired tested in hPtEC; Fig. 8H), whereas rises in outward currents were smaller (Figs. 8D, 8H). Notably, 20 μ M CPZ inhibited the inward currents (-20 ± 4 pA/pF; $n = 8$; ** $P < 0.01$; unpaired tested), whereas 500 μ M La³⁺ only partially decreased these currents (Figs. 8A-D). This agreement between the suppressive effects of CPZ on VEGF-induced rises in inward currents and Ca²⁺ transients supports the notion that the Ca²⁺ transients induced by VEGF are mediated through TRPV1 transactivation.

Human Pterygium Epithelial Cells and HCjEC Proliferation Behavior

As functional TRPV1 activity is larger in immortalized hPtEC than in HCjEC, we hypothesized that hyperplastic hPtEC activity is dependent on enhanced TRPV1 channel activity

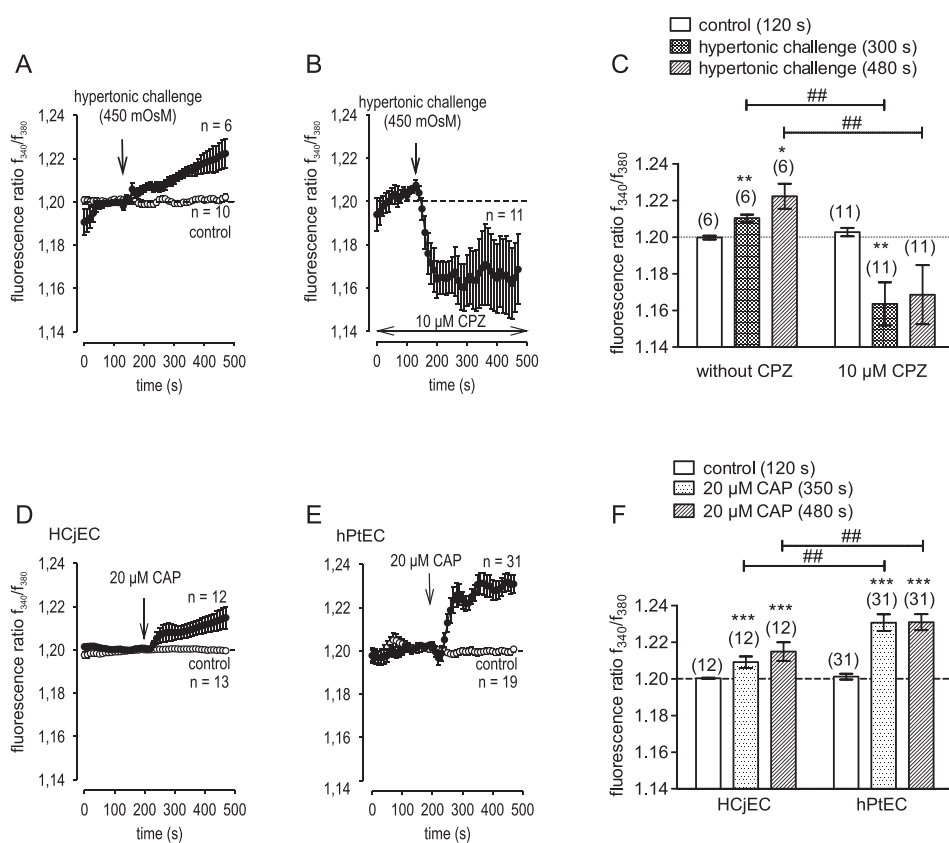


FIGURE 6. Capsaicin and hypertonic challenge induce Ca^{2+} entry in hPtEC. Data are mean \pm SEM of 6 to 31 experiments. (A) Hypertonic challenge (450 mOsm) resulted in Ca^{2+} elevation in hPtEC. Traces show intracellular Ca^{2+} measurements with hypertonic challenge ($n = 6$) and without hypertonic challenge ($n = 10$) (control Ca^{2+} baseline). (B) Similar experiments as shown in (A). The trace shows intracellular $[\text{Ca}^{2+}]_i$ measurements with hypertonic challenge in the presence of CPZ ($n = 11$). (C) Summary of the experiments with hypertonic challenge and CPZ. The hypertonic-induced Ca^{2+} increase could be clearly suppressed by CPZ. The asterisks (*) indicate significant differences between controls (Ca^{2+} base levels; $n = 6$) and hypertonic stress-induced Ca^{2+} increases on $[\text{Ca}^{2+}]_i$ ($n = 11$) (paired Student's *t*-test). The hash marks (#) between the filled bars indicate significant differences of hypertonic stress-induced Ca^{2+} response with and without CPZ (unpaired Student's *t*-test). (D) Application of 20 μM CAP resulted in Ca^{2+} elevation in HCjEC. Traces show intracellular Ca^{2+} measurements with CAP ($n = 12$) and without CAP ($n = 13$) (control Ca^{2+} base line). (E) Similar experiments as shown in (A). Traces show intracellular $[\text{Ca}^{2+}]_i$ measurements with CAP ($n = 31$) and without CAP ($n = 19$) (control Ca^{2+} baseline). (F) Comparison of Ca^{2+} entries in HCjEC and immortalized hPtEC. The Ca^{2+} entry in hPtEC was at higher levels compared with those of HCjEC. The asterisks (*) indicate significant differences between controls (Ca^{2+} base levels; $n = 12-31$) and CAP-induced Ca^{2+} increases on $[\text{Ca}^{2+}]_i$ ($n = 12-31$) (paired Student's *t*-test). The hash marks (#) between the filled bars indicate significant differences between HCjEC and immortalized hPtEC (unpaired Student's *t*-test).

mediating larger Ca^{2+} influx. To test this hypothesis, time-dependent increases in cell proliferation were compared between spontaneously immortalized hPtEC and HCjEC. The results shown in Figure 9A indicate that the number of cultivated hPtECs was significantly greater at all time points examined (${}^*P_{24} < 0.05$, ${}^{**}P_{48} < 0.01$, ${}^{***}P_{72-240} < 0.001$). During the long exponential growth phase extending from 24 to 168 hours, the population-doubling time of immortalized hPtEC was 39.09 hours compared with 54.27 hours for HCjEC, which showed no exponential growth phase.

Furthermore, we determined if this increase in immortalized hPtEC proliferation was associated with rises in metabolic activity. In HCjEC 5 μM (${}^*P < 0.05$) and 100 μM (${}^{***}P < 0.001$) CAP significantly decreased metabolic cell activity after 24 hours of cultivation (Fig. 9B). On the other hand, in immortalized hPtEC, both 5 and 20 μM CAP (${}^{***}P < 0.001$) increased metabolic activity. Cultivation with CPZ (10 μM) maximally increased immortalized hPtEC metabolic cell activity (${}^{**}P < 0.01$), because at 20 μM its effect was indistinguishable from that at the lower concentration. On the other hand, it had no effect after 24 hours in HCjEC.

Capsazepine Suppresses EGF-Induced Cell Proliferation in hPtEC

The mitogenic responses by hPtEC and HCjEC to 10 ng/mL EGF were compared to determine if they corresponded with differences in TRPV1 channel activity between these cell types. Epithelial growth factor-induced mitogenic responses were larger in hPtEC than in HCjEC (Figs. 10A, 10C). After 96 hours, cocultivation of hPtEC with EGF/CPZ cell amount was higher compared with that with CPZ alone (${}^{**}P < 0.01$). This partial inhibitory effect of CPZ suggests that other pathways besides TRPV1 contribute to mediating a rise in Ca^{2+} influx needed to induce an increase in proliferation. Capsaicin (10 μM) did not affect proliferation in HCjEC until 96 hours when it began to instead inhibit this response (Fig. 10A). Similarly, CPZ inhibited HCjEC cell proliferation and became cytotoxic (Figs. 10B, 10D; ${}^{***}P_{72/96} < 0.001$). After another 48 hours of exposure to CPZ, there were no remaining viable HCjECs. Taken together, these results suggest that larger functional TRPV1 activity in hPtEC than HCjEC is sufficient to induce hyperplastic pterygial epithelial cell behavior. Nevertheless, TRPV1 activation con-

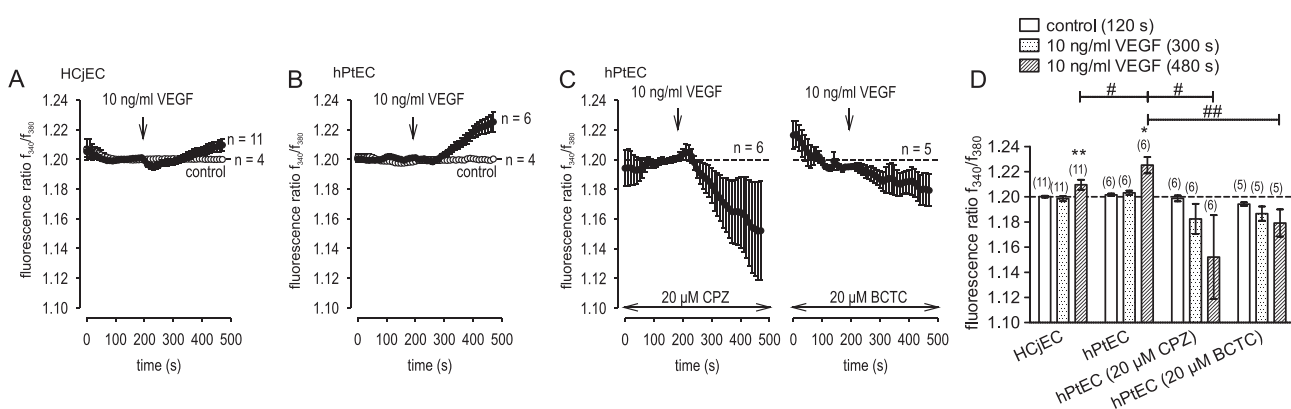


FIGURE 7. Vascular endothelial growth factor–induced increases of intracellular Ca^{2+} in immortalized HCjEC and in hPtEC. Data are mean \pm SEM of 4 to 11 experiments. (A) Application of 10 ng/ml VEGF resulted in Ca^{2+} elevation in HCjEC. Traces show intracellular Ca^{2+} measurements with VEGF (filled circles, $n = 11$) and without VEGF ($n = 4$) (control Ca^{2+} baseline). (B) Similar experiments as shown in (A) but with hPtEC. Traces show intracellular $[\text{Ca}^{2+}]_i$ measurements with VEGF (filled circles, $n = 6$) and without VEGF ($n = 4$) (control Ca^{2+} baseline). (C) Similar experiments as shown in (B) but in the presence of 20 μM CPZ (left) or 20 μM BCTC (right). The VEGF-induced Ca^{2+} entry was completely abolished in the presence of CPZ or BCTC. (D) Comparison of Ca^{2+} entries in HCjEC and immortalized hPtEC. The Ca^{2+} entry in hPtEC was at higher levels compared with those of HCjEC (480 seconds). The asterisks (*) indicate significant differences between controls (Ca^{2+} base levels; $n = 12$) and VEGF-induced Ca^{2+} increases on $[\text{Ca}^{2+}]_i$ ($n = 31$) (paired Student's *t*-test). The hash marks (#) between the filled bars indicate significant differences between HCjEC and immortalized hPtEC and VEGF effect with and without CPZ/BCTC (unpaired Student's *t*-tests).

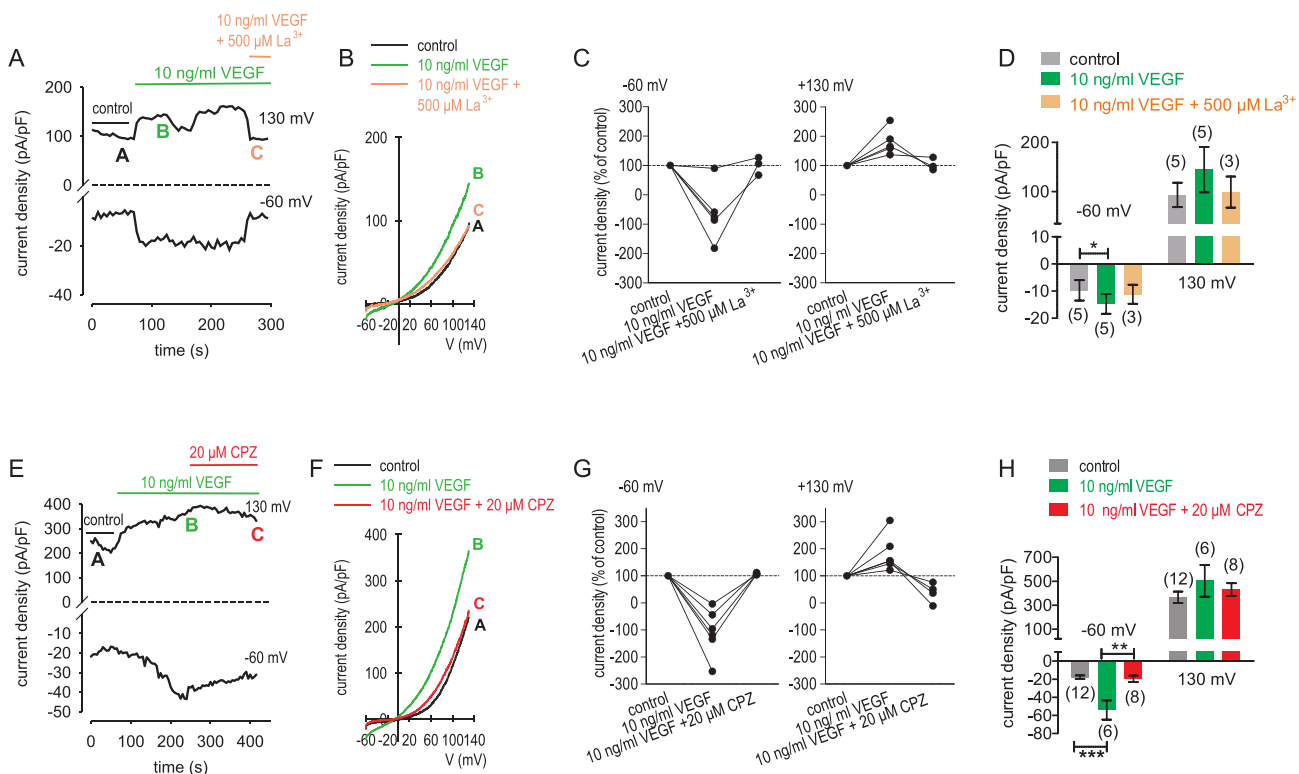


FIGURE 8. Vascular endothelial growth factor–induced increases of whole-cell currents in hPtEC. (A) Time course recording showing the current increases by 10 ng/ml VEGF and current density levels after adding La^{3+} (500 μM). (B) Original traces of VEGF-induced current responses to voltage ramps. Current densities are shown before application (labeled as [A]), during application of VEGF (labeled as [B]) and after addition of La^{3+} (labeled as [C]). Data were obtained from the data shown in (A). Notable, there was a partial decrease of VEGF-induced in- and outward currents in the presence of La^{3+} . (C) Maximal negative current density induced by a voltage step from 0 mV to -60 mV are depicted in percent of control values before application of VEGF and La^{3+} respectively (left). Vascular endothelial growth factor–induced inward currents could be partially suppressed in the presence of La^{3+} (500 μM). Same analyses are shown on the right, but of steps from 0 mV to 130 mV. (D) Summary of the experiments with VEGF and La^{3+} . The asterisk (*) indicates a statistically significant difference of whole-cell inward currents with and without VEGF ($n = 5$; * $P < 0.05$; paired tested). (E) Similar recordings as shown in (A), but with CPZ (20 μM) from approximately 250 seconds. (F) Similar traces as shown in (B) but with CPZ instead of La^{3+} . Notable, there was a clear decrease of VEGF-induced inward currents in the presence of CPZ (lower trace). (G) Similar diagrams as shown in (C) but with CPZ instead of La^{3+} . (H) Summary of the experiments with VEGF and CPZ. The asterisks (*) indicate statistically significant differences of VEGF-induced increases of inward currents with and without CPZ ($n = 6-8$; ** $P < 0.01$ at the minimum; unpaired tested).

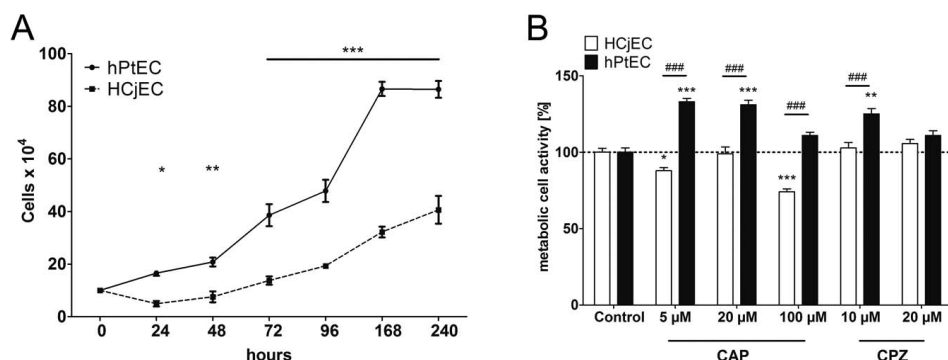


FIGURE 9. Cell proliferation and metabolic cell activity in HCjEC and hPtEC. (A) Human pterygial cells showed an increased cell proliferation compared with HCjEC. Total numbers of cells were counted at the indicated time points. Human conjunctival epithelial cells, as well as hPtECs, were cultivated under standard conditions. All data presented as mean \pm SEM of four independent experiments ($n = 4$). For statistical evaluation of cell counts, 2-way ANOVA and Bonferroni posttests were performed. (B) Metabolic cell activity is affected by TRPV1 agonist CAP in both cell lines, whereas TRPV1 antagonist CPZ affected only hPtEC. Human conjunctival epithelial cells and hPtECs were incubated with 5, 20, and 100 μ M CAP, as well as 10 and 20 μ M CPZ for 24 hours. Metabolic cell activity was colorimetric analyzed by MTS assay. Cells cultivated in standard medium containing DMSO were used as controls and set to 100%. Values represent mean \pm SEM of eight independent experiments ($n = 8$). Statistical significance was calculated by 1-way ANOVA and Dunnett's posttests and indicated by asterisks (* $P < 0.05$; ** $P < 0.01$; *** $P < 0.001$) and hashtags (## $P < 0.001$).

tributes to these mitogenic responses because CPZ always had an inhibitory effect on cell proliferation in hPtEC.

DISCUSSION

By comparing TRPV1 characteristics in clinical pterygial samples and a spontaneously immortalized pterygial epithelial cell line (hPtEC) with those in freshly isolated conjunctival tissue and an immortalized HCjEC counterpart, our results indicate that hyperplastic pterygial cell activity is associated with heightened TRPV1 channel expression levels and functional activity. This association suggests that larger TRPV1 activation may support an increased cell proliferation as a consequence of increased Ca^{2+} influx. Such an effect may more fully activate the mitogen-activated protein kinase (MAPK) signaling pathways mediating growth factor receptor control of proliferation.^{28,44}

Functional TRPV1 activity was characterized in these different tissue preparations by contrasting the effects of raising the bath temperature above 43°C (specific for TRPV1^{14,15}) with those induced by CAP on Ca^{2+} transients and underlying ionic currents. The involvement of TRPV1 in inducing these changes was validated by showing that these responses were suppressed during exposure to either La³⁺ or CPZ. These TRPV1-mediated Ca^{2+} transients and current response patterns correspond to those described in many studies using different cell types, including tumor cells.^{26,27,38,40,45-48} Because TRPV1 expression and activity are elevated in cancerous tissue, it is conceivable that TRPV1 and possible endogenous modulators may be a potential drug target to suppress proliferation not only in malignant tumors but also in benign hyperplastic tumors, such as pterygium (reviewed by Santoni et al.⁴⁹).

TRPV1 Expression and Functional Relevance

An association between increases in functional TRPV1 activity and proliferation in immortalized hPtEC relative to that in HCjEC is similar to what was described in retinoblastoma cells and in various other tumorous tissues.⁴⁶ Increased functional TRPV1 expression in immortalized hPtEC (Figs. 4-6) suggests that reducing its activity may resolve tumor progression if increases in its activity precede or occur as a consequence of

pterygial development. Dysregulated TRP channel activation contributes to also triggering, aberrant differentiation, and resistance to apoptotic cell death leading to uncontrolled tumor invasion (spread) (reviewed by Santoni et al.⁴⁹).

Transient Receptor Potential V1 (also classically known as a pain receptor⁵⁰⁻⁵²) is a nociceptor that is a potential drug target for inhibiting cancer pain in bone metastases, pancreatic cancer, and most likely in other cancers (reviewed in Refs.^{34,53}). Additionally, TRPV1 is also expressed at a multitude of nonneuronal sites, which is prompting many studies probing for their possible involvement in disease progression. Besides TRPV1, our RT-PCR results indicate that there is also TRPV2 and TRPM8 gene expression in PT. It is noteworthy that TRPV2 mRNA level in PT appears to be higher than in HCjEC (Fig. 2). Similar to TRPV1, TRPV2 is also elevated in cancerous cells compared with their healthy counterparts.⁵⁴ Furthermore, TRPV2 expression may be relevant for supporting the pterygial phenotype, because activation of TRPV2 is associated with release of VEGF in RPE cells.⁴⁵ Similarly, TRPM8 expression may contribute to the pterygial transition, as this channel plays a role in cancer diseases concerning by modulating proliferation and cell cycle progression.⁵⁵ Notably, TRPM8 is functionally expressed at higher levels in hPtEC (data not shown) compared with human corneal epithelial cells and conjunctival epithelial cells,^{41,56} whereas TRPM8 mRNA expression was not significantly different (Fig. 2). These disconnects show that there is not always an association between changes in TRP mRNA expression and their functional expression.

TRPV1 Characteristics

Inducing TRPV1 activation by a thermal stress led to continuous larger sustained intracellular Ca^{2+} increases after initiating heating in primary hPtEC (Fig. 3A) than in immortalized HCjEC or HCEC (Figs. 3B, 3C). This difference in the Ca^{2+} response patterns suggests a possible Ca^{2+} signal remodeling in tumorigenic from that in nontumorigenic cells.⁵⁷ More specifically, the time-dependent Ca^{2+} transient recovery subsequent to reducing the bath temperature back to 22°C was different between hPtEC and HCjEC. In primary hPtEC, there was no reversal, whereas in HCjEC, temperature restoration to 22°C caused a partial recovery toward its baseline level (Fig. 3B). This limited baseline restoration in

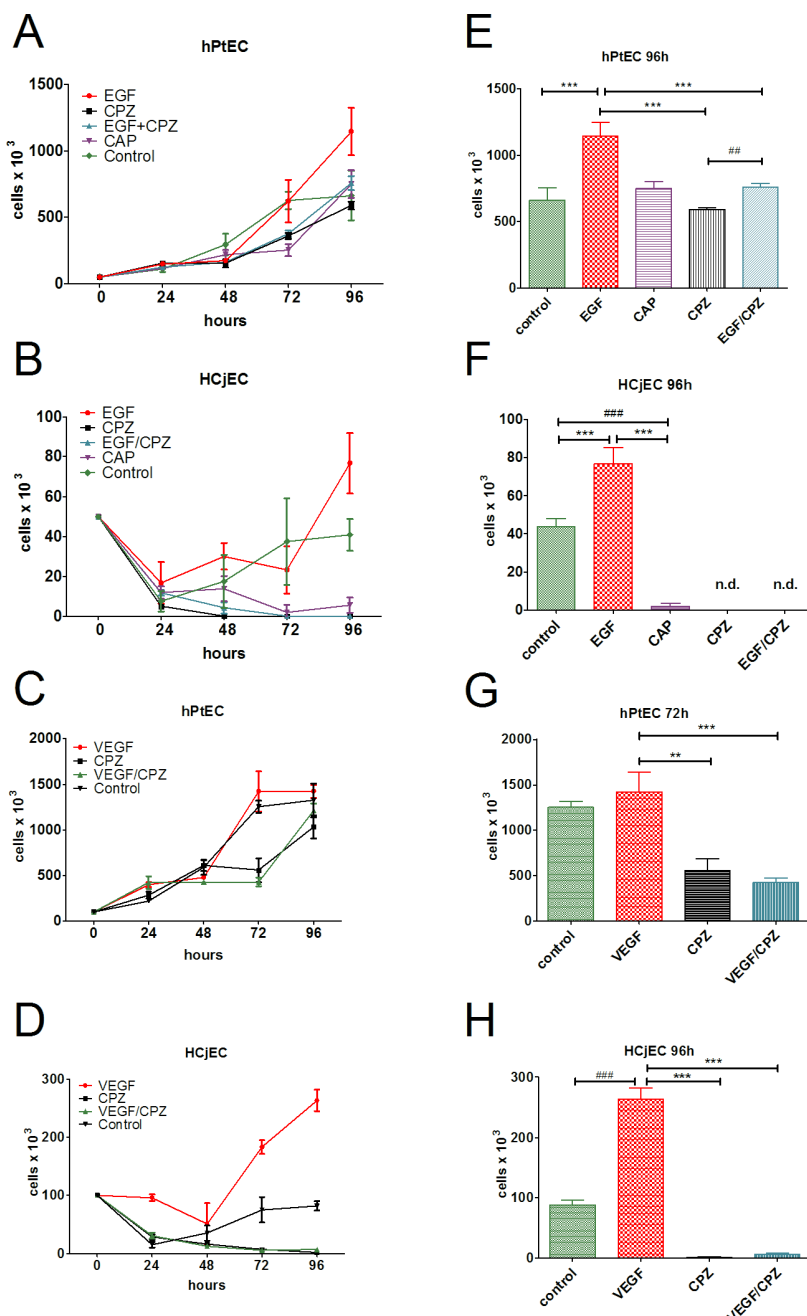


FIGURE 10. Cell proliferation in hPtEC and HCjEC with and without TRPV1 modulators as well as pterygium-associated growth factors. Capsazepine (10 μ M) suppressed EGF- but not VEGF-induced cell proliferation in hPtEC at long-term cultivation. Capsaicin (10 μ M) did not affect cell proliferation of hPtEC. Both TRPV1 modulators had a cytotoxic effect in HCjEC. (A–D) Cell proliferation assays. Human pterygial cells (A, C), as well as HCjEC (B, D), were cocultivated with CAP (10 μ M), CPZ (10 μ M), EGF and VEGF (each 10 ng/mL), and CPZ together (EGF/CPZ and VEGF/CPZ) as well as without additives (control) up to 96 hours. Total numbers of cells were counted every 24 hours. (E–H) Detailed statistical analysis of cell proliferation in hPtEC (E, G) and HCjEC (F and H). All data are presented as mean \pm SEM of four independent experiments ($n = 4$). For statistical evaluation of cell counts, 1-way ANOVA and Bonferroni posttests were performed. Statistical significance is indicated by asterisks (* $P < 0.05$; ** $P < 0.01$; *** $P < 0.001$) and hashtags (** $P < 0.01$; *** $P < 0.001$). n.d., no detectable cells.

HCjEC is somewhat similar to the complete recovery that occurred in immortalized HCEC²⁹ (Fig. 3C). Even though these are immortalized cell lines, their similar recovery patterns indicate that Ca^{2+} extrusion mechanism activation is sufficient to offset Ca^{2+} influx. In primary HCjEC, the recovery pattern was similar to that in immortalized HCjEC (Fig. 4A, open circles). Another suggestion of Ca^{2+} regulation remodeling in hPtEC is that the intracellular Ca^{2+} level was always higher in

primary hPtEC than in normal tissues (Fig. 4A, filled circles). Such remodeling may involve TRPV1 upregulation along with overexpression. This suggestion of Ca^{2+} signal remodeling is based on similar differences in Ca^{2+} transients between other hyperproliferative cancerous and normal tissues.^{57,58} For example, Stewart et al.⁵⁷ suggested, in their hypothetical remodeling of Ca^{2+} signaling, that lack of recovery is linked with a sustained increase in intracellular Ca^{2+} tumorigenic

cells. Notably, this indication of Ca^{2+} remodeling may account for the lack of recovery in both immortalized pterygial cells and in uveal melanoma cells.⁴⁷ The more prolonged Ca^{2+} transient in tumor cells suggests that TRPV1 open probability time is longer than in healthy controls. Another possibility for the lack of recovery is that calcium extrusion mechanism functional behavior (i.e., $\text{Na}^+/\text{Ca}^{2+}$ exchanger and/or plasma membrane calcium ATPase) may be reduced in pterygial cells.

The correspondence between the heat-induced Ca^{2+} transients and underlying ionic currents was validated by showing that CAP and CPZ had similar modulatory effects on TRPV1 activity. Another result reflective of TRPV1 involvement is that the reversal potential was always near 0 mV, which is consistent with behavior of a nonselective cation channel. On the other hand, any possible contributions by Cl^- channel currents are unlikely because isosmotic substitution of NaCl with Na-gluconate Ringers did not change whole-cell currents.²⁹ The CAP-induced inward current densities were larger in hPtEC than in HCjEC, whereas the outward current densities were not significantly different from one another (Fig. 5). This larger inward current indicates that Ca^{2+} influx is greater in hPtEC due to TRPV1 activation eliciting larger Ca^{2+} influx along a favorable bath to cell electrochemical Ca^{2+} gradient. However, the outward currents involve other ions than Ca^{2+} , which do not permeate against an unfavorable electrochemical gradient from cell to bath. Such a difference between the effects of CAP on the inward and outward currents supports the notion that the larger inward currents in cultivated hPtEC are attributable to greater functional TRPV1 activity in hyperplastic immortalized pterygial cells than in HCjEC.

Differential Responses by Cell Types to TRPV1 Channel Modulators

Capsaicin induced larger Ca^{2+} transients and whole-cell currents in immortalized hPtEC than in HCjEC, which were blocked by CPZ and BCTC (Figs. 7A-D, 8E-H). As this difference may be associated with hyperplastic activity in immortalized PT, we determined if mitogenic responses to EGF were dependent on Ca^{2+} influxes induced by TRPV1 activation. As CPZ had corresponding inhibitory effects on increases in Ca^{2+} influx and immortalized hPtEC proliferation, EGF receptor activation transactivates TRPV1. Another indication that larger TRPV1 activity provides the needed Ca^{2+} influx to support immortalized hPtEC hyperplastic behavior is that transient recovery in HCEC and HCjEC recovery was evident, whereas in immortalized hPtEC it was delayed. The correspondence between enhanced cell proliferation in fresh clinical pterygial samples and hPtEC shows that results obtained with immortalized hPtEC are relevant for gaining insight into the pathogenesis of this disease.² Another indication of the suitability of hPtEC as a model is that CAP increased metabolic activity in this cell type, but it was cytotoxic in HCjEC (Fig. 10). This difference may be attributable to differences in multidrug efflux resistance (i.e., MDR) behavior between hyperplastic pterygial cells and healthy cells. If there is functional MDR activity in immortalized hPtEC, extrusion by this MDR transporter of CAP may prevent it from accumulating to cytotoxic levels, whereas in HCjEC, such a protective effect may be diminished. On the other hand, CPZ increased metabolic activity in immortalized hPtEC, suggesting that suppressing TRPV1 activity improved cell viability. The lack of an inhibitory effect by CPZ on proliferation in HCjEC may indicate that functional TRPV1 activity is at a much lower level than in immortalized hPtEC (Fig. 9B). Heparin-bound EGF as well as EGF levels rise in pterygium during UV-B exposure² and contribute to mediating increases in cell proliferation. Transient receptor potential V1 transactivation seems to be

involved in inducing this response, as EGF-induced increases in cell proliferation were suppressed in hPtEC after a 48-hour exposure to 10 μM CPZ. In contrast, CAP (10 μM) had no effect on hPtEC cell proliferation, suggesting that transient increases in Ca^{2+} are inadequate to induce an increase in cell proliferation (Fig. 10).

Limitations of Current Therapeutic Options

In clinical studies, VEGF inhibitors have not consistently had a therapeutic effect.⁵⁹⁻⁶¹ Although VEGF receptor activation induces responses through TRPV1 transactivation, there are many studies indicating that antineovascularizing agents, such as bevacizumab, are ineffective in preventing recurrence of pterygial outgrowths after surgery.⁶²⁻⁶⁵ In many cases, if it is at all effective, it only delays recurrence.^{62,66} This limitation may be due to the short half-life of anti-VEGF agents at the ocular surface and to the difficulty in determining the ideal dose and treatment regimen to prevent pterygia over an extended period. Moreover, Peng et al.⁶⁷ showed that VEGF gene polymorphism contributes to the variable effectiveness of anti-VEGF agents, as their antibody complexation with VEGF targets specific isoforms that are not expressed in all patient populations. Transient receptor potential V1 inhibitors instead may be an alternative approach to suppress VEGF-induced Ca^{2+} increases, which are at higher levels in pterygium cells (Fig. 7). However, the efficacy and safety of TRPV1 inhibitors as possible drugs for adjuvant pterygium therapy awaits clarification. Another possibility for future studies may be to determine if TRPV1 inhibition can be induced by targeting another receptor besides VEGF, whose control of neovascularization elicits TRPV1 activation through transactivation. Such a strategy is tenable, as TRPM8 activation by a thyroid hormone analogue (3-T₁AM) inhibited through crosstalk CAP- and hypertonic-induced increases in TRPV1 channel activity in both HCjEC and HCEC.^{41,56}

CONCLUSIONS

Both TRPV1 gene and protein expression and its functional activity are at higher levels in hyperplastic immortalized hPtEC than in normal HCjEC. This difference is associated with larger mitogenic responses to EGF in the transdifferentiated hPtEC than in the nontumorous parental control tissue. Such differences in TRPV1 characteristics may contribute to the hyperplastic behavior of hPtEC. This is tenable because growth factor receptor control of proliferation is dependent on TRPV1 transactivation leading to increases in Ca^{2+} influx and in turn MAPK signaling activation.^{31,44} Furthermore, VEGF induced larger Ca^{2+} increases in hPtEC than in HCjEC, which is indicative of larger functional TRPV1 activity in hPtEC than in HCjEC. On the other hand, the cause-and-effect relationship between increases in functional TRPV1 activity and pterygium pathogenesis is unclear. Finally, the feasibility of noninvasively inhibiting pterygial cell proliferation in a clinical setting by drug-targeting TRPV1 with eye drops awaits the outcome of further studies.

Acknowledgments

The authors thank Ersal Türker and Gabriele Fels for the technical assistance, as well as Olaf Strauß, PhD (all Charité, Department of Ophthalmology), for helpful discussions. Furthermore, we appreciate very much the technical assistance provided by the fellow students Anna Santaella, Sahana Srinivasan, Lilly Brankova, Katherina Riffel, Nina Ljubojevic, Anja Lude, Martin Straßenburg, and Leticia Barcelos Picado during their laboratory internships, as well as Sylvia Dyczek in the translation and proof reading of the

manuscript. We acknowledge support by Deutsche Forschungsgemeinschaft and Friedrich-Alexander-Universität Erlangen-Nürnberg (FAU) within the funding programme Open Access Publishing. Friedrich Paulsen, Fabian Garreis, and Antje Schröder received grants from the DFG (Pa 738/9-2) and Uwe Pleyer received grants from an EU project. Stefan Mergler is supported by DFG (Me 1706/14-1; Me 1706/18-1) about TRP channel related research projects and received a grant from the DFG priority program 1629 ThyroidTransAct (Me 1706/13-1). Noushafarin Khajavi was supported by the DFG project of Stefan Mergler (1629 ThyroidTransAct). The planar patch-clamp equipment was partially supported by Sonnenfeld-Stiftung (Berlin, Germany).

Disclosure: **F. Garreis**, None; **A. Schröder**, None; **P.S. Reinach**, None; **S. Zoll**, None; **N. Khajavi**, None; **P. Dhandapani**, None; **A. Lucius**, None; **U. Pleyer**, None; **F. Paulsen**, None; **S. Mergler**, None

References

1. Saw SM, Tan D. Pterygium: prevalence, demography and risk factors. *Ophthalmic Epidemiol.* 1999;6:219–228.
2. Bradley JC, Yang W, Bradley RH, Reid TW, Schwab IR. The science of pterygia. *Br J Ophthalmol.* 2010;94:815–820.
3. Wong TY, Foster PJ, Johnson GJ, Seah SK, Tan DT. The prevalence and risk factors for pterygium in an adult Chinese population in Singapore: the Tanjong Pagar survey. *Am J Ophthalmol.* 2001;131:176–183.
4. Gazzard G, Saw SM, Farook M, et al. Pterygium in Indonesia: prevalence, severity and risk factors. *Br J Ophthalmol.* 2002;86:1341–1346.
5. Ang M, Li X, Wong W, et al. Prevalence of and racial differences in pterygium: a multiethnic population study in Asians. *Ophthalmology.* 2012;119:1509–1515.
6. Heindl LM, Cursiefen C. Pterygium. Etiology, clinical aspects and novel adjuvant therapies [in German]. *Ophthalmologe.* 2010;107:517–514.
7. Hirst IW. The treatment of pterygium. *Surv Ophthalmol.* 2003;48:145–180.
8. Aspiotis M, Tsanou E, Gorezis S, et al. Angiogenesis in pterygium: study of microvessel density, vascular endothelial growth factor, and thrombospondin-1. *Eye (Lond).* 2007;21:1095–1101.
9. Khalfaoui T, Mkannez G, Colin D, et al. Immunohistochemical analysis of vascular endothelial growth factor (VEGF) and p53 expression in pterygium from Tunisian patients. *Pathol Biol (Paris).* 2011;59:137–141.
10. Gebhardt M, Mentlein R, Schaudig U, et al. Differential expression of vascular endothelial growth factor implies the limbal origin of pterygia. *Ophthalmology.* 2005;112:1023–1030.
11. Ramsey IS, Delling M, Clapham DE. An introduction to TRP channels. *Ann Rev Physiol.* 2006;68:619–647.
12. Pingle SC, Matta JA, Ahern GP. Capsaicin receptor: TRPV1 a promiscuous TRP channel. *Handb Exp Pharmacol.* 2007; (179):155–171.
13. Liao M, Cao E, Julius D, Cheng Y. Single particle electron cryo-microscopy of a mammalian ion channel. *Curr Opin Struct Biol.* 2014;27:1–7.
14. Tominaga M, Tominaga T. Structure and function of TRPV1. *Pflugers Arch.* 2005;451:143–150.
15. Tominaga M, Caterina MJ. Thermosensation and pain. *J Neurobiol.* 2004;61:3–12.
16. Vriens J, Appendino G, Nilius B. Pharmacology of vanilloid transient receptor potential cation channels. *Mol Pharmacol.* 2009;75:1262–1279.
17. Lee YM, Kim YK, Chung JH. Increased expression of TRPV1 channel in intrinsically aged and photoaged human skin in vivo. *Exp Dermatol.* 2009;18:431–436.
18. Li WH, Lee YM, Kim JY, et al. Transient receptor potential vanilloid-1 mediates heat-shock-induced matrix metalloproteinase-1 expression in human epidermal keratinocytes. *J Invest Dermatol.* 2007;127:2328–2335.
19. Cao E, Liao M, Cheng Y, Julius D. TRPV1 structures in distinct conformations reveal activation mechanisms. *Nature.* 2013;504:113–118.
20. Liao M, Cao E, Julius D, Cheng Y. Structure of the TRPV1 ion channel determined by electron cryo-microscopy. *Nature.* 2013;504:107–112.
21. Ogawa N, Kurokawa T, Fujiwara K, et al. Functional and structural divergence in human TRPV1 channel subunits by oxidative cysteine modification. *J Biol Chem.* 2015;291:4197–4210.
22. Liu C, Montell C. Forcing open TRP channels: mechanical gating as a unifying activation mechanism. *Biochem Biophys Res Commun.* 2015;460:22–25.
23. Hardie RC, Franze K. Photomechanical responses in *Drosophila* photoreceptors. *Science.* 2012;338:260–263.
24. Xue T, Do MT, Riccio A, et al. Melanopsin signalling in mammalian iris and retina. *Nature.* 2011;479:67–73.
25. Mergler S, Garreis F, Sahlmüller M, et al. Calcium regulation by thermo- and osmosensing transient receptor potential vanilloid channels (TRPVs) in human conjunctival epithelial cells. *Histochem Cell Biol.* 2012;137:743–761.
26. Mergler S, Valtink M, Coulson-Thomas VJ, et al. TRPV channels mediate temperature-sensing in human corneal endothelial cells. *Exp Eye Res.* 2010;90:758–770.
27. Yang Y, Yang H, Wang Z, Mergler S, Wolosin JM, Reinach PS. Functional TRPV1 expression in human corneal fibroblasts. *Exp Eye Res.* 2013;107:121–129.
28. Zhang F, Yang H, Wang Z, et al. Transient receptor potential vanilloid 1 activation induces inflammatory cytokine release in corneal epithelium through MAPK signaling. *J Cell Physiol.* 2007;213:730–739.
29. Mergler S, Garreis F, Sahlmüller M, Reinach PS, Paulsen F, Pleyer U. Thermosensitive transient receptor potential channels in human corneal epithelial cells. *J Cell Physiol.* 2011;226:1828–1842.
30. Reinach PS, Chen W, Mergler S. Polymodal roles of transient receptor potential channels in the control of ocular function. *Eye Vis (Lond).* 2015;2:5.
31. Pan Z, Wang Z, Yang H, Zhang F, Reinach PS. TRPV1 activation is required for hypertonicity-stimulated inflammatory cytokine release in human corneal epithelial cells. *Invest Ophthalmol Vis Sci.* 2011;52:485–493.
32. Okada Y, Reinach PS, Shirai K, et al. TRPV1 involvement in inflammatory tissue fibrosis in mice. *Am J Pathol.* 2011;178:2654–2664.
33. Doucette CD, Hilchie AL, Liwski R, Hoskin DW. Piperine, a dietary phytochemical, inhibits angiogenesis. *J Nutr Biochem.* 2013;24:231–239.
34. Prevarskaya N, Zhang L, Barratt G. TRP channels in cancer. *Biochim Biophys Acta.* 2007;1772:937–946.
35. Araki-Sasaki K, Ohashi Y, Sasabe T, et al. An SV40-immortalized human corneal epithelial cell line and its characterization. *Invest Ophthalmol Vis Sci.* 1995;36:614–621.
36. Pfaffl MW. A new mathematical model for relative quantification in real-time RT-PCR. *Nucleic Acids Res.* 2001;29:e45.
37. Mergler S, Skrzypski M, Sassek M, et al. Thermo-sensitive transient receptor potential vanilloid channel-1 regulates intracellular calcium and triggers chromogranin A secretion

- in pancreatic neuroendocrine BON-1 tumor cells. *Cell Signal.* 2012;24:233–246.
38. Voets T, Droogmans G, Wissenbach U, Janssens A, Flockerzi V, Nilius B. The principle of temperature-dependent gating in cold- and heat-sensitive TRP channels. *Nature.* 2004;430:748–754.
 39. Grynkiewicz G, Poenie M, Tsien RY. A new generation of Ca²⁺ indicators with greatly improved fluorescence properties. *J Biol Chem.* 1985;260:3440–3450.
 40. Khajavi N, Reinach PS, Skrzypski M, Lude A, Mergler S. L-carnitine reduces in human conjunctival epithelial cells hypertonic-induced shrinkage through interacting with TRPV1 channels. *Cell Physiol Biochem.* 2014;34:790–803.
 41. Khajavi N, Reinach PS, Slavi N, et al. Thyronamine induces TRPM8 channel activation in human conjunctival epithelial cells. *Cell Signal.* 2015;27:315–325.
 42. Ricardo JR, Cristovam PC, Filho PA, et al. Transplantation of conjunctival epithelial cells cultivated ex vivo in patients with total limbal stem cell deficiency. *Cornea.* 2013;32:221–228.
 43. Tekus V, Bolcskei K, Kis-Varga A, et al. Effect of transient receptor potential vanilloid 1 (TRPV1) receptor antagonist compounds SB705498, BCTC and AMG9810 in rat models of thermal hyperalgesia measured with an increasing-temperature water bath. *Eur J Pharmacol.* 2010;641:135–141.
 44. Yang H, Wang Z, Capo-Aponte JE, Zhang F, Pan Z, Reinach PS. Epidermal growth factor receptor transactivation by the cannabinoid receptor (CB1) and transient receptor potential vanilloid 1 (TRPV1) induces differential responses in corneal epithelial cells. *Exp Eye Res.* 2010;91:462–471.
 45. Cordeiro S, Seyler S, Stindl J, Milenkovic VM, Strauss O. Heat-sensitive TRPV channels in retinal pigment epithelial cells: regulation of VEGF-A secretion. *Invest Ophthalmol Vis Sci.* 2010;51:6001–6008.
 46. Mergler S, Cheng Y, Skosyrski S, et al. Altered calcium regulation by thermosensitive transient receptor potential channels in etoposide-resistant WERI-Rb1 retinoblastoma cells. *Exp Eye Res.* 2012;94:157–173.
 47. Mergler S, Derckx R, Reinach PS, et al. Calcium regulation by temperature-sensitive transient receptor potential channels in human uveal melanoma cells. *Cell Signal.* 2014;26:56–69.
 48. Weil A, Moore SE, Waite NJ, Randall A, Gunthorpe MJ. Conservation of functional and pharmacological properties in the distantly related temperature sensors TRPV1 and TRPM8. *Mol Pharmacol.* 2005;68:518–527.
 49. Santoni G, Farfariello V, Amantini C. TRPV channels in tumor growth and progression. *Adv Exp Med Biol.* 2011;704:947–967.
 50. Brederson JD, Kym PR, Szallasi A. Targeting TRP channels for pain relief. *Eur J Pharmacol.* 2013;716:61–76.
 51. Fernandes ES, Fernandes MA, Keeble JE. The functions of TRPA1 and TRPV1: moving away from sensory nerves. *Br J Pharmacol.* 2012;166:510–521.
 52. Levine JD, Alessandri-Haber N. TRP channels: targets for the relief of pain. *Biochim Biophys Acta.* 2007;1772:989–1003.
 53. Lehen'kyi V, Prevarskaya N. Oncogenic TRP channels. *Adv Exp Med Biol.* 2011;704:929–945.
 54. Liberati S, Morelli MB, Amantini C, et al. Advances in transient receptor potential vanilloid-2 channel expression and function in tumor growth and progression. *Curr Protein Pept Sci.* 2014;15:732–737.
 55. Valero ML, Mello de Queiroz F, Stuhmer W, Viana F, Pardo LA. TRPM8 ion channels differentially modulate proliferation and cell cycle distribution of normal and cancer prostate cells. *PLoS One.* 2012;7:e51825.
 56. Lucius A, Khajavi N, Reinach PS, et al. 3-Iodothyronamine increases transient receptor potential melastatin channel 8 (TRPM8) activity in immortalized human corneal epithelial cells. *Cell Signal.* 2015;28:136–147.
 57. Stewart TA, Yapa KT, Monteith GR. Altered calcium signaling in cancer cells. *Biochim Biophys Acta.* 2015;1848:2502–2511.
 58. Prevarskaya N, Ouadid-Ahidouch H, Skryma R, Shuba Y. Remodelling of Ca²⁺ transport in cancer: how it contributes to cancer hallmarks? *Philos Trans R Soc Lond B Biol Sci.* 2014;369:20130097.
 59. Bahar I, Kaiserman I, McAllum P, Rootman D, Slomovic A. Subconjunctival bevacizumab injection for corneal neovascularization in recurrent pterygium. *Curr Eye Res.* 2008;33:23–28.
 60. Leippi S, Grehn F, Geerling G. Antiangiogenic therapy for pterygium recurrence [in German]. *Ophthalmologe.* 2009;106:413–419.
 61. Perez-Santonja JJ, Campos-Mollo E, Lledo-Riquelme M, Javaloy J, Alio JL. Inhibition of corneal neovascularization by topical bevacizumab (anti-VEGF) and sunitinib (anti-VEGF and anti-PDGF) in an animal model. *Am J Ophthalmol.* 2010;150:519–528.e511.
 62. Hwang S, Choi SA. Comparative study of topical mitomycin C, cyclosporine, and bevacizumab after primary pterygium surgery. *Korean J Ophthalmol.* 2015;29:375–381.
 63. Karalezli A, Kucukerdonmez C, Akova YA, Koktekin BE. Does topical bevacizumab prevent postoperative recurrence after pterygium surgery with conjunctival autografting? *Int J Ophthalmol.* 2014;7:512–516.
 64. Lekhanont K, Patarakittam T, Thongphiew P, Suwan-Apichon O, Hanutsaha P. Randomized controlled trial of subconjunctival bevacizumab injection in impending recurrent pterygium: a pilot study. *Cornea.* 2012;31:155–161.
 65. Razeghinejad MR, Banifatemi M. Subconjunctival bevacizumab for primary pterygium excision; a randomized clinical trial. *J Ophthalmic Vis Res.* 2014;9:22–30.
 66. Hu Q, Qiao Y, Nie X, Cheng X, Ma Y. Bevacizumab in the treatment of pterygium: a meta-analysis. *Cornea.* 2014;33:154–160.
 67. Peng ML, Tsai YY, Tung JN, et al. Vascular endothelial growth factor gene polymorphism and protein expression in the pathogenesis of pterygium. *Br J Ophthalmol.* 2014;98:556–561.

3. Diskussion

3.1. Calcium-Imaging der *transient-receptor-potential*- (TRP) - Ionenkanäle in den Augentumorzellen

Für die Untersuchungen der *transient-receptor-potential*-Ionenkanäle wurden kultivierte menschliche Aderhautmelanomzellen verwendet. Insbesondere wurden der Thermorezeptor, TRPV1 (Capsaicinrezeptor) und der Kälterezeptor, TRPM8 (Mentholrezeptor) charakterisiert. Das verwendete Zellmodell, die Zelllinie 92.1 wurde im Jahr 1995 etabliert ([De Waard – Sieblinga et al., 1995](#)). Zur Zellkultur wurden die 92.1-Zellen in RPM1 1640-Medium kultiviert, supplementiert mit 10% fetalem Kälberserum, 4 mM L-Glutamin und Penicillin/Streptomycin. Für die Calciummessungen wurden die Zellen über Nacht auf Deckgläsern ausgesät und Fura-2 AM, ein weithin bekannter calciumempfindlicher Fluoreszenzfarbstoff, wurde verwendet. In den Untersuchungen an Aderhautmelanomzellen erhöhte der vaskuläre endotheliale Wachstumsfaktor VEGF (10 ng/mL) den zytosolischen Calciumspiegel in mit Fura-2/AM beladenen UV 92.1-Zellen. Es wurde außerdem gezeigt, dass der durch VEGF induzierte intrazelluläre Calciumanstieg in Gegenwart des Schilddrüsenhormon-Derivats 3-T1AM (1 µM) gehemmt wurde ([Figur 7 Manuskript III](#)). Es ist jedoch unklar, über welchen Rezeptor 3-T1AM die Interaktionssignalkaskade aktivieren könnte. Obwohl 3-T1AM der Ligand vom *trace-amine-associated-receptor-1* (TAAR1) ist, wird es auch von mehreren anderen Rezeptoren wie *beta*-adrenergen Rezeptoren, Cannabinoid-Rezeptoren (CB1) und *trace-amine-associated-receptor-2* (TAAR2) sowie von Muscarin-Rezeptoren gesteuert ([Scanlan et al., 2004](#); [Dinter et al., 2015](#); [Hoefig et al., 2016](#), [Ghelardoni et al., 2009](#)). Die endogene Expression von Muscarinrezeptoren und *beta*-adrenergen Rezeptoren in der multiplen Melanomzelllinie Mel202 und dem Aderhautmelanom 92.1 wurde bereits nachgewiesen ([Janik et al., 2017](#)). Es müssen daher weitere Experimente durchgeführt werden, um zu beweisen, welcher Rezeptor an dieser 3-T1AM-Aktivierung in Aderhautmelanomzellen beteiligt ist.

In einer weiteren Studie an benignen Augentumorzellen der Konjunktiva (Pterygium) wurde anschließend geprüft, ob VEGF (10 ng/mL) den intrazellulären Calciumspiegel beeinflussen könnte. Zur Kultivierung der benignen Tumorzellen, die durch spontane Immortalisierung aus Patientenproben gewonnen wurden, wurde das Medium DMEM/Hams F12 supplementiert mit 10 % fetalem Kälberserum, 4 mM L-Glutamin und Penicillin/Streptomycin verwendet. Die funktionelle TRPV1-Expression wurde durch extrazelluläre Anwendung von Capsaicin (CAP) (10 µM) nachgewiesen ([Figur 7 Manuskript IV](#)). VEGF (10 ng/mL) erhöhte das intrazelluläre Calcium. Um zu testen, ob es eine Interaktion zwischen VEGF und TRPV1 gibt, wurde auch der TRPV1-Blocker Capsazepin (CPZ) (20 µM) verwendet ([Vriens et al., 2009](#)). Capsazepin hemmte den durch 10 ng/mL VEGF verursachten Anstieg des intrazellulären Calciums in den Pterygium Zellen ([Figur 7 Manuskript IV](#)). Bei den meisten bösartigen Tumoren gilt TRPV1 als potenzieller Wirkstoff-Target für die Therapie, da TRPV1 mit der Proliferation von Tumorzellen assoziiert ist ([Santoni et al., 2007](#)). Daher wird vorgeschlagen, dass TRPV1 ein potenzielles krebstherapeutisches Target sein könnte, um Entzündungen bei Pterygium-Konjunktivitis zu reduzieren ([Manuskript IV](#)).

3.2. Calcium-Imaging im zellbasierten Überexpressions-system von Mas, ein Ang-(1-7) Rezeptor

Für die Untersuchung der Calciumregulation von Ang-(1-7) über Mas wurde ein zellbasiertes Protein-Überexpressionsmodell verwendet. *Human embryonic kidney 293 (HEK293)* -Zellen wurden mit dem pcDNA 3.1(+) Mas Plasmid transfiziert und 48 Stunden lang weiter kultiviert. Nachdem die Zellen eine Oberflächenkonfluenz von 80 % erreicht hatten, wurden Calcium-Imaging-Experimente durchgeführt.

Der Ligand Ang-(1-7) (1 μ M) aktivierte Mas und führte zu einem erhöhten intrazellulären Calciumspiegel im Zytoplasma ([Figur 1, Manuscript II](#)). Im Hinblick auf die Spezifität der Mas-Aktivierung wurden verschiedene Wirkstoffe wie A779 (20 μ M) und Candesartan (CV-11974) (20 μ M) getestet. A779, der spezifische Mas-Inhibitor, blockierte den Anstieg des zytoplasmatischen Calciumspiegels durch Ang-(1-7) vollständig ([Figur 2, Manuscript II](#)). Frühere Studien haben gezeigt, dass Ang-(1-7) den intrazellulären Calciumspiegel sowohl über Mas als auch über den Angiotensin II -rezeptor Typ-I (AT1R) in den proximalen Tubuli von spontan hypertensiven Ratten erhöht ([Castelo-Branco, Leite-Delova, and de Mello-Aires 2013](#)) und auch den Na+/H+-Austauscher beeinflusst ([Castelo-Branco et al., 2017](#)). In einer anderen Studie wurde ein ähnlicher Effekt des Ang-(1-7) induzierten zytosolischen Calciumanstiegs in Astrogliazellen aus Gehirnschnitten von Wistar- und spontan hypertensiven Ratten beobachtet ([Guo et al., 2010](#)). Darüber hinaus wurde nachgewiesen, dass zytosolisches Ang-(1-7) in der Lage ist, erhöhte Calciumeinwärtsströme zu verursachen, und diese Spitzen-Calciumeinwärtsströme wurden durch A779 gehemmt (De Mello et al., 2015). Die oben genannten Studien stimmen mit den Ergebnissen dieser Forschungsarbeit überein, dass Ang-(1-7) das zytosolische Calcium durch Mas-Aktivierung erhöht.

Ang-(1-7) bindet auch an Ang-II-Rezeptor Typ 1 (AT1-Rezeptor) und Ang-II-Rezeptor Typ (AT2R) mit mäßiger Affinität ([Bosnyak et al., 2011](#)). Die extrazelluläre Verwendung von CV-(11974), einem Inhibitor des Angiotensinrezeptors Typ-I (AT1-Rezeptor) und Angiotensin II-Rezeptors Typ-II (AT2-Rezeptor), hatte keinen Einfluss auf den beobachteten Anstieg des zytoplasmatischen Calciumspiegels durch Ang-(1-7). Deshalb ist der beobachtete Anstieg des zytoplasmatischen Calciumspiegels nur auf die Aktivierung von Mas zurückzuführen ([Figur 2, Manuscript II](#)). Candesartan hemmt den AT1-Rezeptor bei 1 nM ([Gradman et al., 2002](#)). Bei dem AT2-Rezeptor beginnt die Hemmung bei 1 μ M ([Bosnyak et al., 2011](#)). Selbst bei der hohen Konzentration von 20 μ M Candesartan wurde in dieser Forschungsarbeit nur ein geringer, aber unsignifikanter Effekt zwischen den mit und ohne Candesartan vorbehandelten Proben beobachtet. Dies deutet darauf hin, dass der Ang-(1-7)-induzierte zytosolische Calciumeinfluss hauptsächlich durch Mas vermittelt wird.

Außerdem wurden die Auswirkungen von calciumfreier Lösung und Lanthan (III)-chlorid (La^{3+}) untersucht. In Gegenwart der Calcium-freien Lösung (mit 5 mM EGTA (Ethylenglycol-bis(aminoethylether)-N, N, N', N'-tetraessigsäure)) konnte keine Erhöhung der zytoplasmatischen Calciumkonzentration durch Ang-(1-7) beobachtet werden. Dies bedeutet, dass die durch Ang-(1-7) induzierte Erhöhung des zytosolischen Calciumspiegels durch die Aktivierung von Mas über in der Plasmamembran lokalisierte Ionenkanäle verursacht wird. Wäre ein Anstieg des zytoplasmatischen Calciumspiegels durch Ang-(1-7) in Gegenwart einer calciumfreien Lösung noch feststellbar, wäre ein Ionenkanal beteiligt, der in den intrazellulären Speichern wie dem ER lokalisiert ist. Durch die

Verwendung von Lanthan (III)-chlorid (500 µM), einem bekannten unspezifischen TRP-Ionenkanal-Inhibitor, wurde der durch Ang-(1-7) induzierte Anstieg des zytoplasmatischen Calciumspiegels deutlich reduziert. ([Figur 3, Manuskript II](#)).

Da Mas ein GPCR ist und bei der Aktivierung von Mas durch Ang-(1-7) die TRP-Ionenkanäle involviert sind, wurde untersucht, ob andere Komponenten der klassischen GPCR-TRPs-Signalkaskade beteiligt sind. Die Beteiligung des Enzyms Phospholipase C-β (PLC-β) und des Enzyms Proteinkinase C an der Calciumregulation wurde in der Gegenwart von extrazellularem Calcium (1,26 mM) in HBSS untersucht. Der Phospholipase-C-β-Inhibitor U73122 (10 µM) blockierte den durch die Mas-Aktivierung induzierten Calciumanstieg von Ang-(1-7) ([Figur 4, Manuskript II](#)). Dies weist darauf hin, dass Ang-(1-7) auch die Gq-Signalisierung ähnlich wie NPFF und andere Agonisten aktiviert. Die beobachtete Tendenz wurde durch frühere Untersuchungen bestätigt, dass die durch Ang-(1-7) vermittelte Mas-Aktivierung dem Akt/PLC-β-Signalweg folgt ([Yang et al., 2021](#)). Im Gegensatz zum PLC-β-Inhibitor verursachte der Proteinkinase-C-Inhibitor Go6976 (200 nM) in Gegenwart von Ang-(1-7) eine biphasische Kurve ([Figur 4, Manuskript II](#)). Zunächst unterdrückt der PKC-Inhibitor in Gegenwart von Ang-(1-7) den zytoplasmatischen Calciumspiegel unter den Basislinienwert und steigt dann später über den Basislinienwert an. Der beobachtete Mechanismus kann durch frühere Entdeckungen gestützt werden, wonach eine Reihe von TRP-Kanälen durch Phosphorylierung über PKC aktiviert werden, die stromabwärts von PLC-β aktiviert wird ([Yao, Kwan und Huang et al., 2005](#)).

Aus den oben genannten Experimenten wird vorgeschlagen, dass die Calciumregulation von Ang-(1-7) /Mas der klassischen GPCR-TRP-Signalachse folgt. Dieser Vorschlag wird durch mehrere früheren Untersuchungen gestützt. Mehrere Rezeptoren aus der Familie der Mas-verwandten G-Protein-gekoppelten Rezeptoren (MRGPR) können TRP-Ionenkanäle aktivieren. Zum Beispiel aktiviert mMRGPR-A3 die TRP-Ionenkanäle, Unterfamilie-Ankyrin, Typ1 (TRPA1), TRPV1, TRPM8 und Unterfamilie-kanonischer-Rezeptor, Typ 3 (TRPC3). MRGPR-X1 weist einen TRPV1-vermittelten zytosolischen Calciumeintritt durch PLC-β- und PKC-Aktivierung auf ([Solinski, Gudermann und Breit et al., 2014](#)). MRGPR-X1 aktivierte auch TRP-Ionenkanal, Unterfamilie-Ankyrin, Typ 1 (TRPA1) ([McMillan et al., 2021](#)). TRPA1 wurde als ein *downstream*-Signalvermittler von Mrgpr-D und Mrgpr-C11 identifiziert ([Wang et al., 2019](#)) ([Wilson et al., 2014](#)).

Ein besseres Verständnis der Mas-Signalübertragung ist erforderlich, um neue Agonisten für Mas zu finden, die vielversprechende Medikamente für kardiovaskuläre und metabolische Erkrankungen sein könnten ([Santos et al., 2018](#)). Es sind daher weitere Experimente erforderlich, um den oder die TRP-Ionenkanäle aufzudecken, die an der Mas-Signalgebung beteiligt sind.

3.3. Etablierung der Calcium-Imaging-Methode in einem zellfreien Proteinsynthese-System

Um die Idee zu verwirklichen, das Calcium-Imaging in einer zellfreien Proteinsyntheseplattform zu etablieren, wurde das zellfreie System der Insektenzelllinie *Spodoptera frugiperda* Sf21 verwendet ([Kubick et al., 2003](#)). Der CECF-Modus der zellfreien Synthese wurde verwendet, um eine bessere Proteinausbeute zu erzielen. Wie in der Einleitung ([Kapitel 1.4.2](#)) vorgeschlagen, wurde die

Carboxylesterase unter Verwendung des Melittin-Transport-Signalpeptids zellfrei synthetisiert und in das Lumen der Mikrosomen transportiert. Alle Synthesen wurden für maximal 24 Stunden durchgeführt, um einen Abbau der synthetisierten Proteine aufgrund der verlängerten Synthesezeit zu vermeiden. Bei der zellfreien Synthese wurde Dithiothreitol (DTT) vermieden, da die synthetisierten Proteine die Disulfid-bindungen in ihrer Struktur aufweisen. Die zellfrei synthetisierte Maus-Carboxylesterase wurde mit einem Szintillationszähler ausgewertet und das radioaktive Protein wurde ebenfalls in SDS-Gel mittels Autoradiogramm nachgewiesen. Eine 24-stündige Synthese bei 30 °C unter Verwendung von Sf21-Lysat ergab 85 ng/µL Protein im gesamten Lysat. Die mikrosomale Proteinausbeute, die für die Calcium-Imaging-Experimente entscheidend ist, betrug 25 ng/µL (50 µL = 1250 ng Protein insgesamt pro Synthese-Ansatz). Die *mCES2*-Proteinbande von 58 kDa war im Autoradiogramm nachweisbar. Die Negativkontrollen ohne Template zeigten keine Ausbeute bei der Szintillationszählung und auch keine Banden im SDS-Gel-Autoradiogramm ([Abb. 2. Manuskript I](#)).

Die in den Mikrosomen exprimierte Maus-Carboxylesterase (*mCES2*) wurde mit einem kolorimetrischen Para-Nitrophenolacetat (PNPA)-Test auf ihre Esterase-Aktivität untersucht ([Gilham und Lehner et al., 2005](#)). Die Esteraseaktivität in den *mCES2*-Mikrosomen war im Vergleich zur Negativkontrolle in einer substratkonzentrationsabhängigen und einer zeitabhängigen Kurve höher. In einem dosisabhängigen Diagramm zeigten Mikrosomen mit *mCES2* im Bereich von 30 ng/µL bis 120 ng/µL eine höhere Esteraseaktivität im Vergleich zu den Proben der Negativkontrolle. ([Figur. 3 Manuskript I](#)). Für Farbstoffbeladungstests wurde Fluo-5N AM für die Esterhydrolyse getestet. Die Proben wurden mit einer Anregungswellenlänge von 488 nM und einer Emissionswellenlänge von 515 nM gemessen. Mit steigender Konzentration von bis zu 10 µM Fluo-5N AM waren die *mCES2*-Mikrosomen in der Lage, den AM-Teil des Fluo-5N AM mit höherer Esteraseaktivität im Vergleich zu den Proben der Negativkontrolle zu spalten. Eine zeitabhängige Kurve zeigte auch eine ähnliche Wirkungsweise bis zu einer Inkubationszeit von 60 Minuten ([Figur 3 Manuskript I](#)).

Es wurden mehrere Experimente durchgeführt, um die Calcium-Imaging-Methode in den *mCES2*-Mikrosomen zu etablieren. Zunächst wurde die Farbstoffdissoziationskonstante Kd für die Sf21-Mikrosomen im zellfreien Lysat abgeschätzt, da die Menge der in den Mikrosomen vorhandenen Calcium-bindenden Proteine je nach Zelltyp variiert. Calciumbindende Proteine wie Calreticulin und Calnexin sind im endoplasmatischen Retikulum vorhanden ([Caramello und Parodi et al., 2018](#)). Diese Calcium-bindenden Proteine werden auch in die Mikrosomen im zellfreien Lysat übertragen. Die Calcium-bindenden Proteine kompetieren mit dem Calciumindikator und erhöhen dadurch den Kd-Wert. Der Kd-Wert für Fluo-5N für zellfreie Sf21-Lysat-Mikrosomen beträgt 265 µM. Die Empfindlichkeit des Calciumindikators auf Calcium in Mikrosomen wurde mit hohem und niedrigem Calcium in Gegenwart des Ionophors (Ionomycin) getestet. 10 µM Ionomycin wurde verwendet, um die Mikrosomen durchlässig für Calciumionen zu machen. Die *mCES2*-Mikrosomen haben entsprechend auf die Zugabe von hohem Calcium (10 mM) und calciumfreiem Calcium (0 µM Calcium + 5mM EGTA) reagiert. Ubiquitäre native Proteine wie die sarkoplasmatische/endoplasmatische Retikulum-Ca²⁺-ATPase (SERCA) und Ryanodin-Kanäle wurden auf ihre Aktivität getestet. Die *mCES2*-Mikrosomen, die 1 Stunde lang bei 37 °C mit 10 mM ATP inkubiert wurden, wiesen im Vergleich zu den *mCES2*-Mikrosomen 4- bis 5-fach höhere luminale Calciumspiegel auf ([Figur 4 Manuskript I](#)). Die SERCA-Aktivität war bei der Inkubation von 10 mM ATP in den *mCES2*-Mikrosomen gut nachweisbar.

([Figur 4 Manuskript I](#)). Fluoreszenzspektroskopische Messungen zeigten, dass 100 nM Thapsigargin in der Lage war, die 10 μ M ATP-induzierte Calciumbeladung zu hemmen, wenn es für 1 Stunde bei 37 °C inkubiert wurde ([Supplementäres-Manuskript I](#)). Intrazelluläre Ryanodinrezeptor-Ionenkanäle wurden mit Koffein in verschiedenen Konzentrationen wie 100 μ M und 10 mM getestet ([Figur 4 Manuskript I](#)). 100 μ M Dantrolen war in der Lage, die durch 1 mM Koffein induzierte Calciumfreisetzung in mCES2-Mikrosomen zu hemmen ([Supplementäres, Manuskript I](#)).

Es wurden einige TRP-Ionenkanäle getestet, um herauszufinden, ob ein Calcium-Imaging von zell-frei synthetisierten Ionenkanälen möglich ist oder nicht. Getestet wurden der humane TRP-Ionenkanal, Unterfamilie-Vanilloid, Subtyp 1 (TRPV1), und der Bovine TRP-Ionenkanal, Unterfamilie 3 (*b*TRPV3). Durch Calcium-Imaging mit zell-frei synthetisierten *h*TRPV1-*m*CES2-Mikrosomen konnte die Calciumfreisetzung bei Verwendung von 10 μ M Capsaicin nachgewiesen werden. *m*CES2-Mikrosomen (Kontrollproben) konnten die Capsaicin-induzierte Calciumfreisetzung nicht ermitteln. Die durch Capsaicin 200 nM induzierte Calciumfreisetzung wurde auch durch eine Vorbehandlung von TRPV1-*m*CES2-Mikrosomen mit 20 μ M Capsazepin (CPZ), ein TRPV1 Inhibitor, gehemmt. Die dosisabhängige Kurve von CAP wurde auch gegen die Fläche/maximale Fläche mit einer zunehmenden Capsaicin-Konzentration vom nM- zum mM-Bereich aufgezeichnet. ([Figur 5, Manuskript I](#)). *b*TRPV3-*m*CES2-Mikrosomen waren in der Lage, in Gegenwart von 200 μ M Menthol eine Calciumfreisetzung zu zeigen. *m*CES2-Mikrosomen wiesen keine Wirkung auf 200 μ M Menthol auf ([Supplementäres, Manuskript I](#)). Insgesamt führen zell-frei synthetisierte TRP-Ionenkanäle in den Mikrosomen bei Aktivierung zu einer Calciumfreisetzung. Dies stimmt mit der Hypothese überein ([erläutert in Kapitel 1.4.2](#)), weil TRP-Ionenkanäle, die im endoplasmatischen Retikulum exprimiert werden, bei Aktivierung eine Calciumfreisetzung verursachen ([Dong et al., 2010](#)), ([Wisnosky et al., 2003](#)).

Zusammenfassend lässt sich sagen, dass das auf chemischen Indikatoren basierende Calcium-Imaging für TRP-Kanäle in eukaryontischen zellfreien Proteinen unter Verwendung von Carboxylesterase in Mikrosomen entwickelt wurde. Nicht nur neu synthetisierte Ionenkanäle, sondern auch die vorhandenen Calcium-permeablen Kanalproteine könnten mit dieser Methode untersucht werden.

Die etablierte Calcium-Imaging-Methode hat viele Vorteile gegenüber den vorhandenen Methoden zur Analyse der Ionenkanäle in den Mikrosomen. Derzeit gibt es drei verschiedene Ansätze, um die ionenpermeablen Proteine in den Mikrosomen zu analysieren. Diese sind wie folgt:

- I. Ionenflussmethoden mit radioaktiven Materialien
- II. Elektrophysiologische Technik wie die Planare-Lipiddoppelschicht-Methode
- III. Fluoreszenzmethoden mit ionenspezifischem Farbstoff – auf dem Prinzip der etablierten Methode basierend.

Die Ionenflussmethode besteht aus radioaktivem Calcium: In mehreren früheren Studien wurde radioaktives Calcium für die Untersuchung von Ionenkanälen und Ionenpumpen verwendet. So wurde zum Beispiel eine Mikroplattenmethode zur Messung der Sarkoplasmatischen/Endoplasmatischen Retikulum Ca^{2+} ATPase (SERCA) unter Verwendung von radioaktivem $^{45}\text{Ca}^{2+}$ in Rattenhirn-Mikrosomen entwickelt ([Mc Mullen et al., 2012](#)). In einer anderen Studie wurden die IP3-Rezeptoren mit $^{45}\text{Ca}^{2+}$ in Cos7-Zellmikrosomen untersucht ([Boehning et al., 2000](#)). Mikrosomen aus glatten Muskelzellen der

Rattenaorta wurden mit radioaktivem $^{45}\text{Ca}^{2+}$ untersucht, um die Calciumfreisetzung im Auftrag von zyklischer ADP-Ribose (cADPR), Nikotinsäure-Adenin-Dinucleotid-Phosphat (NAADP) und IP3-Rezeptoren zu untersuchen ([Yusufi et al., 2002](#)). Rattenmikrosomen wurden auf die Beteiligung von Translokon und anderen mutmaßlichen Freisetzungskanälen an der passiven Calciumfreisetzung unter Verwendung von radioaktivem $^{45}\text{Ca}^{2+}$ untersucht ([Giunti et al., 2007](#)). Zum Beispiel wurden Mikrosomen von roten Rüben und Blumenkohlpflanzenzellen mit $^{45}\text{Ca}^{2+}$ auf die Calciumfreisetzung in Gegenwart von Nikotinsäure-Adenin-Dinucleotid-Phosphat (NADP) untersucht ([Navazio et al., 2000](#)).

Unabhängig von der Untersuchung zellfrei-synthetisierter Ionenkanäle oder nativ vorhandener Ionenkanäle oder zellbasierter überexprimierter Ionenkanäle in ERs, die zur Calciummessung in Mikrosomen weiterverarbeitet werden, weisen $^{45}\text{Ca}^{2+}$ -Ionenfluss-Assays viele Nachteile auf.

- Diese Methode funktioniert als endpunktbaserte Methode. Endpunktbaserte Methoden erlauben es uns, nur einen Datenpunkt pro Probe zu einem bestimmten Zeitpunkt während des Experiments aufzuzeichnen. Ionenfluss-Assays mit $^{45}\text{Ca}^{2+}$ sind eine endpunktbaserte Methode. Ein typisches Experiment mit $^{45}\text{Ca}^{2+}$ im Mikrosomen umfasst die folgenden Schritte während der Datenmessung: Nachdem das mit $^{45}\text{Ca}^{2+}$ beladene Mikrosomen mit einem Aktivator oder Inhibitor behandelt wurde, werden die Mikrosomen durch Filtration auf der Nitrocellulosemembran zurückgehalten. Die Nitrocellulosemembran, die die Mikrosomen mit $^{45}\text{Ca}^{2+}$ enthält, wird in der Szintillationsflüssigkeit aufgelöst und die Radioaktivität von $^{45}\text{Ca}^{2+}$ in den Mikrosomen wird mit einem Szintillationszähler gemessen. Bei dieser Methode wird für jede Probe nur ein Datenpunkt gemessen. Daher ist die Durchführung kinetischer Studien mit einer endpunktbasierter Methode nicht praktikabel. Im Gegensatz dazu können mit einer Live-Imaging-Methode wie der Calcium-Imaging mehrere Datenpunkte zu unterschiedlichen Zeitpunkten pro Probe während des Experiments aufgenommen werden.
- Nicht alle Labore sind für Experimente mit radioaktivem Material ausgerüstet, da sie eine Sondergenehmigung für die Arbeit mit radioaktivem Material benötigen. Aufgrund der Radioaktivität müssen bei den Arbeiten hohe Sicherheitsstandards eingehalten werden.
- Da sich die zugegebenen radioaktiven Ionen, z.B. $^{45}\text{Ca}^{2+}$, außerhalb der Mikrosomen befinden, fällt auf, dass sich diese Methoden für Ionenmessungen in den Lumen des Mikrosomen nicht eignen. Nur wenn die Mikrosomen durch die Sarkoplasmatische/Endoplasmatische Retikulum Ca $^{2+}$ ATPase (SERCA) stark mit $^{45}\text{Ca}^{2+}$ angereichert sind, kann man diese Technik für Calciummessungen in den Lumen des Mikrosomen verwenden. Obwohl der Zufluss ohne radioaktiv markierte Ca $^{2+}$ -Beladung messbar ist, ist der Abfluss nicht messbar.
- Weil die Mikrosomen nicht immobilisiert sind und aufgrund der mehrfachen Reinigung kann es zu einer hohen Standardabweichung zwischen den Proben kommen.

Alle oben genannten Nachteile der Calciummessungen mit radioaktivem $^{45}\text{Ca}^{2+}$ werden vermieden, wenn das Calcium-Imaging in Mikrosomen unter Verwendung der AM-basierten Calcium-spezifischen Farbstoffe angewendet wird. Die in dieser Forschungsarbeit entwickelte Calcium-Imaging-Methode kann zur kontinuierlichen Messung von Calcium in Mikrosomen verwendet werden. Außerdem ist das Calcium-Imaging kosteneffektiv, da es sich nicht um eine Endpunktmethode handelt. Im Gegensatz zu der Methode mit radioaktivem $^{45}\text{Ca}^{2+}$ ist sie gut für kinetische Studien geeignet. Außerdem ist es für direkte Messungen von Calcium in den Mikrosomen nicht notwendig, die Mikrosomen vor den

Messungen mit Calcium zu beladen. Dies setzt jedoch voraus, dass ausreichend Calcium in den Mikrosomen vorhanden ist.

Die zweite Klasse von Methoden besteht aus elektrophysiologischen Messungen: Untersuchungen von zellfrei synthetisierten Ionenkanalproteinen und Pumpen wurden schon durch elektrophysiologische Methoden wie die planare Lipiddoppelschicht-Methode nachgewiesen ([Sachse et al., 2014](#)), ([Dondapati et al., 2019](#)). Bei der planaren Lipiddoppelschicht-Methode wird die Stromintensität aufgrund der kontinuierlichen Ionenmobilität durch die Membran gemessen. Auch die zeitliche Auflösung, d.h. die Anzahl der Ionen, die die Membran pro Sekunde durchdringen, kann gemessen werden. Obwohl diese Methode hoch entwickelt ist, hat sie einige Nachteile. Diese sind die folgenden:

- I. Bei dieser Methode werden die Proteine mit ionischen oder nichtionischen Detergenzien solubilisiert. Die Detergenzien könnten die Proteine schädigen.
- II. Außerdem ist für die Durchführung dieser Technik eine komplexe Ausrüstung erforderlich. Des Weiteren erfordert es besondere Fachkenntnisse und Fähigkeiten.
- III. Die räumliche Auflösung der Calciumionen, z.B. die Anzahl der Calciumionen auf jeder Seite der Membran, kann nicht gemessen werden.

Die oben genannten Nachteile werden durch die etablierte Calcium-Imaging-Methode überwunden. Bei der etablierten Calcium-Imaging-Methode ist es nicht nötig,

otwendig das synthetisierte Protein mit Detergenzien zu solubilisieren. Daher wird die Intaktheit der mikrosomalen Membranen nicht gestört. Die zell-frei synthetisierten Ionenkanäle haben in den Mikrosomen die folgende Orientierung. Die zytoplasmatische Domäne des Ionenkanals befindet sich an der Außenseite der Mikrosomen und die extrazelluläre Domäne des Ionenkanals befindet sich im Lumen der Mikrosomen. Für das Calcium- Imaging von Mikrosomen sind nur ein Fluoreszenzmikroskop und eine Durchflusskammer erforderlich.

Die dritte Klasse besteht aus Fluoreszenzmethoden mit einem Fluoreszenzfarbstoff für bestimmte Ionen: Das AM-Farbstoff-basierte Calcium-Imaging hat gegenüber oben genannter Methode Vorteile. So beispielsweise,

- I. Bei der Calcium-Imaging-Methode können Ionen räumlich aufgelöst werden.
- II. Calcium-Imaging ist eine kontinuierlich messbare Methode und keine endpunktbasierte Methode wie ein radioaktiv markierter Assay.

TECHNISCHER VORTEILE DER ETABLIERTEN ZELL-FREIEN CALCIUM-IMAGING-METHODE GEGENÜBER DER ZELLBASIERTEN CALCIUM-IMAGING-METHODE:

Im Zytoplasma ist die endogene Carboxylesterase stark exprimiert. Im endoplasmatischen Retikulum gibt es keine endogen exprimierte Carboxylesterase. Einige Studien in Zellen haben gezeigt, dass Calcium-Ionen in Organellen wie dem endoplasmatischen Retikulum messbar sind. Die zielgerichtete Expression von Carboxylesterase im endoplasmatischen Retikulum hat es ermöglicht, Calcium in dieser Organelle zu untersuchen ([Samtleben et al., 2013](#); [Blum et al., 2010](#); [Rehberg et al., 2008](#)). Auch in intakten Zellen, in denen die Carboxylesterase im endoplasmatischen Retikulum überexprimiert wird, kann es bei der Verwendung für Calcium-Imaging-Experimente einige Nachteile mit sich bringen. Um in das endoplasmatische Retikulum zu gelangen, muss der Calciumindikator das

Zytoplasma durchqueren. Während dieses Vorgangs wird eine beträchtliche Menge des Calciumindikators von der AM-Gruppe abgespalten. Die Menge der endogenen Carboxylesterase im Zytoplasma ist im Durchschnitt höher als die Menge der im endoplasmatischen Retikulum überexprimierten Carboxylesterase. Dies führt zu einer hohen Menge an Calciumindikatoren mit abgespaltener AM-Gruppe im Zytoplasma und kann schließlich zu einem geringen Signal-Rausch-Verhältnis bei Calciummessungen im ER führen.

Die Expression von in der Plasmamembran lokalisierten Ionenkanälen in den Zellen hat schwere Folgen. In zellbasierten Überexpressionssystemen werden die neu synthetisierten Ionenkanäle in die Plasmamembran integriert. Die Plasmamembran beherbergt auch mehrere endogen exprimierte Ionenkanäle. Eine Überexpression von Ionenkanälen in den Zellen führt zu Toxizität und einer zerstörten Ionenhomöostase. Dies hat zur Folge, dass unsere gewünschten Ionenkanäle nur in geringem Maße exprimiert werden. Eine arme Expression von gewünschten Ionenkanälen und ein großer Hintergrund von endogen exprimierten Ionenkanälen kann bei Calciummessungen zu einem geringen Signal-Rausch-Verhältnis führen. Im Gegensatz dazu werden die zell-frei synthetisierten Ionenkanalproteine in mikrosomale Membranen integriert. Diese stammen aus dem endoplasmatischen Retikulum, wo keine endogenen Plasmamembran-Ionenkanäle vorhanden sind. Außerdem werden die Plasmamembranen bei der Lysat-Herstellung entfernt. Daher entstehen bei den zellfreien Proteinsyntheseplattformen während der Calciummessungen keine störenden Interferenz durch endogen exprimierte Plasmamembran-Ionenkanäle.

TECHNISCHE LIMITATIONEN DER ETABLIERTEN ZELL-FREIEN CALCIUM-IMAGING-METHODE:

Die Calcium-Imaging-Methode für zellfreie Systeme in dieser Dissertation hat ihre technischen Grenzen. Diese sind wie folgt:

1. In der etablierten Calcium-Imaging-Methode wurde ein *single-wavelength*-Calciumindikator, d.h. Fluo 5N-AM, verwendet. Fluoreszierende Calciumindikatoren können in zwei Kategorien unterteilt werden: Indikatoren mit einer Wellenlänge oder ratiometrische Indikatoren. *Single-wavelength*-Indikatoren werden für die qualitative Analyse empfohlen. Die *single-wavelength*-Calciumindikatoren haben einen großen dynamischen Bereich, wodurch sie selbst die kleinsten vorübergehenden Veränderungen des Calciums messen können. Sie haben jedoch erhebliche Nachteile, wie z.B. eine variierende Farbstoffbeladung und einen höheren aktiven Farbstoff-Ausstoß. Die ratiometrischen Calciumindikatoren sind für quantitative Messungen am besten geeignet. Obwohl mehrere ratiometrische Calciumfarbstoffe für zytoplasmatische Calciummessungen gut entwickelt und im Markt verfügbar sind, gibt es nicht viele Optionen für die Messung des Calciumspiegels im endoplasmatischen Retikulum ([Parades et al., 2008](#)). Fluo-FF und Fluo 6F sind andere ratiometrische Calciumindikatoren für das endoplasmatische Retikulum, aber mit niedrigeren Kd-Werten. Verbesserte ratiometrische Calciumindikatoren für das endoplasmatische Retikulum müssen noch entwickelt werden.
2. Das etablierte zellfreie Calcium-Imaging wurde für *transient-receptor-potential*-Ionenkanäle getestet. TRP-Ionenkanäle wurden in verschiedenen intrazellulären Membranen wie in den Endosomen, Lysosomen und dem endoplasmatischen Retikulum nachgewiesen. Es wurde bereits von mehreren Forschern nachgewiesen, dass TRPM8 und TRPV1 im endoplasmatischen Retikulum

endogen exprimiert werden ([Dong et al., 2010](#)). Ob die etablierte Calcium-Imaging-Methode auch für weitere Ionenkanalfamilien geeignet ist, sollte in weiteren Untersuchungen geklärt werden.

ERWEITERUNG DER ETABLIERTEN ZELL-FREIEN CALCIUM-IMAGING-METHODE:

Es gibt mehrere Möglichkeiten, wie die etablierte Calcium-Imaging-Methode weiter fortentwickelt werden könnte.

i. [*Entwicklung einer High-Throughput-Screening-Plattform für die etablierte zellfreie Calcium-Imaging-Methode für TRP-Ionenkanäle:*](#)

Die Medikamentenentwicklung ist ein komplizierter und zeitaufwendiger Vorgang. Die Wirkstoffidentifizierung ist der erste und entscheidende Schritt für fast alle Wirkstofftargets. Die Verfahren zum Wirkstoffscreening für Ionenkanäle sind in drei Stufen aufgeteilt: ein fluoreszenzbasiertes Calcium-Imaging oder ein Ligandenbindungsassay für das primäre Screening, eine automatisierte Patch-Clamp-Validierung für das sekundäre Screening und eine manuelle Patch-Charakterisierung der Interaktion zwischen Ionenkanal und Wirkstoff für das tertiäre Screening ([Yu et al., 2015](#)).

Zu den Parametern, die beim High-Throughput-Screening üblicherweise berücksichtigt werden, gehören Empfindlichkeit, Spezifität, Durchsatz, zeitliche Auflösung, Robustheit, Flexibilität, Kosten und physiologische Relevanz ([Murray et al., 2016](#)). In der Forschung und auch beim pharmazeutischen Screening von Ionenkanälen werden häufig Assays zur Messung intrazellulärer Ionenkonzentrationen verwendet. Die Calcium-/andere Ionen-spezifische-Imaging-Methode spielt eine wichtige Rolle in der frühen Phase der Arzneimittelentwicklung. Es ist zu erwarten, dass je höher der Durchsatz der Assay-Screening-Plattformen ist, desto geringer ist die Auflösung der Imaging-Technik ([Martinez et al., 2005](#)). Unter allen Testformaten für Ionenkanäle könnte die automatisierte elektrophysiologische Technik die beste Wahl sein, da sie ein

e gute Datenqualität liefert und einen höheren Durchsatz ermöglicht. Allerdings ist der automatisierte elektrophysiologische Test wie die planare Lipiddoppelschicht-Methode aufgrund der erforderlichen Zusatzmodule und Ausrüstungen derzeit sehr kostspielig. Als Kompromiss kann die mikroplattenbasierte Calcium-Imaging-Methode für Arzneimittelscreening einfach umgesetzt werden. Deshalb ist die Calcium-Imaging-Methode die am meisten bevorzugte Methode für das funktionsbasierte Wirkstoffscreening auf ionenkanalbasierten Krankheiten.

TRP-Ionenkanäle sind Wirkstofftargets für Krankheiten wie kardiometabolische Erkrankungen, Entzündungen, Krebs und Neuroerkrankungen ([Fallah et al., 2022](#)). Insgesamt besteht ein hohes Potenzial mit wirtschaftlicher Bedeutung, wenn dieses etablierte Calcium-Imaging für zellfrei synthetisierte TRP-Ionenkanäle als High-Throughput-Screening-Plattform erweitert wird.

i. [*Erweiterung des Calcium-Imaging in zellfreier Proteinsynthese für andere physiologisch relevante Ionen:*](#)

Die Calcium-Imaging-Methode in der zellfreien Proteinsynthese-Plattform kann auch auf die Untersuchung anderer Klassen von ionenpermeablen Proteinen wie Pumpen und Transportern erweitert werden. Darüber hinaus kann das Prinzip zur Untersuchung anderer Ionen wie

für Magnesium-, Kalium-, Natrium- und Chlorid-Kanäle mit einem geeigneten Indikator für die genannten Ionen verwendet werden. Es wurden mehrere ionenspezifische Indikatoren entwickelt, z. B. Calcium-Indikatoren (Fura-2, Fluo-3, Fluo-421,22), Kalium-Indikatoren (FluxOR23,24 und PBFI25) und Natrium-Indikatoren (SBFI26).

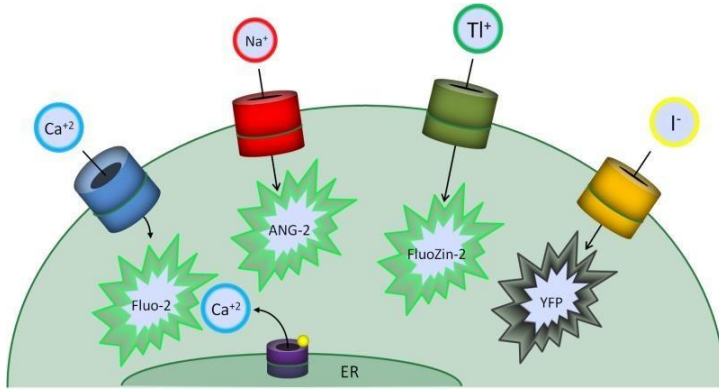


Abbildung 7: Prinzip der Ionen-Imaging für verschiedene Ionen in Zellen, [McManus et al., 2012](#)

Für die Untersuchung eines Kaliumkanals ist der Thallium-Flux-Assay das am häufigsten verwendete Assay-Format in den Zellen ([Yu et al., 2015](#)). Die Zellen werden zuvor mit dem Thallium-spezifischen Fluoreszenzindikator beladen. Um die Öffnung des Kanals auszulösen, wird in der Regel eine Lösung mit einer hohen K⁺-Konzentration verwendet, um das Membranpotenzial zu depolarisieren. Das Thallium im Puffer dringt dann durch die geöffneten Kaliumkanäle in die Zellen ein. Nach der Bindung des zytosolischen Thalliums an den Farbstoff wird das Fluoreszenzsignal kinetisch erhöht. Dieser Funktionsmechanismus ist in der [Abbildung 7](#) dargestellt. Auf diese Weise werden Kaliumkanäle untersucht. Dieser Ansatz kann auch auf zellfrei synthetisierte Kaliumkanäle in den Mikrosomen erweitert werden.

ii. Erweiterung dieser Methode für GPCRs/Tyrosine-verwandte Rezeptoren in Verbindung mit zellfreier Proteinsynthese:

Guanosintriphosphat-bindende-Protein(G-Protein) -gekoppelte Rezeptoren (GPCRs) sind die größte Familie von Membranproteinen, die für eine Vielzahl von Erkrankungen therapeutisch relevant sind. Über 30 % der vermarkteten Arzneimittel vermitteln ihre Wirkung durch GPCRs ([Santos et al., 2017](#)). Molekulare Modulatoren von GPCRs haben breite therapeutische Anwendungen zu bieten, die Agonisten, Antagonisten, inverse Agonisten und allosterische Modulatoren einschließen. Die Aktivierung von GPCRs durch Liganden führt zu verschiedenen Downstream-Signalwegen wie der Gs, Gq, Gi oder G₁₂-Signalkaskade. Bei den Gq-aktivierten GPCRs führt die Bindung eines Agonisten zu einem Anstieg des intrazellulären Calciums. GPCR-Rezeptoren, die Phospholipase-C-Enzyme (PLC-Enzyme) aktivieren können, setzen Ca²⁺ aus dem endoplasmatischen Retikulum frei ([Kieselyov et al., 2003](#)). Zusammengenommen ist es überzeugend, die etablierte Calcium-Imaging-Methode auch auf die zellfrei synthetisierten GPCRs zu erweitern.

iii. Erweiterung dieser Methode für mikrosomale Calcium-Untersuchungen in der Toxikologie:

Umwelttoxikologen und Pharmakologen untersuchen den mikrosomalen Calciumspiegel, um die Zelltoxizität zu analysieren. Die Anwendung bestimmter Arzneimittel oder Arzneimittelmetaboliten kann eine Freisetzung von Calcium durch Mikrosomen bewirken. Dies ist ein indirekter Indikator für die Zelltoxizität, da die übermäßige Menge an intrazellulärem Calcium die Apoptose auslösen kann. ([Pentyala et al., 2010](#)) ([Stoyanovsky und Cederbaum, 1999](#)) ([Coburn et al., 2008](#)), ([Kodavanti und Ward, 2005](#)). Für alle diese Untersuchungen an Mikrosomen verwenden die Wissenschaftler radioaktives Calcium. Radioaktives Calcium-basierte Untersuchungen sind normalerweise nicht erwünscht. Mikrosomen, die mit der zellfrei synthetisierten Carboxylesterase angereichert sind, könnten eine optimale Calcium-Imaging-Plattform für die Analyse der Zelltoxizität verschiedener Umwelt- und Lebensmittelwirkstoffe sein.

4. Referenzen

- Bader, Michael, Natalia Alenina, Dallan Young, Robson A.S. Santos, und Rhian M. Touyz. „The Meaning of Mas“. *Hypertension* 72, Nr. 5 (November 2018): 1072–75. <https://doi.org/10.1161/HYPERTENSIONAHA.118.10918>.
- Blum, Robert, Ole H. Petersen, und Alexei Verkhratsky. „Ca₂₊ Imaging of Intracellular Organelles: Endoplasmic Reticulum“. In *Calcium Measurement Methods*, herausgegeben von Alexei Verkhratsky und Ole H. Petersen, 147–67. Neuromethods. Totowa, NJ: Humana Press, 2010. https://doi.org/10.1007/978-1-60761-476-0_8.
- Boehning, Darren, und Suresh K. Joseph. „Functional Properties of Recombinant Type I and Type III Inositol 1,4,5-Trisphosphate Receptor Isoforms Expressed in COS-7 Cells*“. *Journal of Biological Chemistry* 275, Nr. 28 (14. Juli 2000): 21492–99. <https://doi.org/10.1074/jbc.M001724200>.
- Bosnyak, Sanja, Emma S. Jones, Arthur Christopoulos, Marie-Isabel Aguilar, Walter G. Thomas, und Robert E. Widdop. „Relative Affinity of Angiotensin Peptides and Novel Ligands at AT1 and AT2 Receptors“. *Clinical Science (London, England: 1979)* 121, Nr. 7 (Oktober 2011): 297–303. <https://doi.org/10.1042/CS20110036>.
- Brödel, Andreas K., Andrei Sonnabend, Lisa O. Roberts, Marlitt Stech, Doreen A. Wüstenhagen, und Stefan Kubick. „IRES-Mediated Translation of Membrane Proteins and Glycoproteins in Eukaryotic Cell-Free Systems“. *PLoS One* 8, Nr. 12 (2013): e82234. <https://doi.org/10.1371/journal.pone.0082234>.
- Carafoli, Ernesto. „Calcium Signaling: A Tale for All Seasons“. *Proceedings of the National Academy of Sciences* 99, Nr. 3 (5. Februar 2002): 1115–22. <https://doi.org/10.1073/pnas.032427999>.
- Caramelo, Julio J., und Armando J. Parodi. „Getting in and out from Calnexin/Calreticulin Cycles“. *The Journal of Biological Chemistry* 283, Nr. 16 (18. April 2008): 10221–25. <https://doi.org/10.1074/jbc.R700048200>.
- Castelo-Branco, Regiane C., Deise C. A. Leite-Delova, und Margarida de Mello-Aires. 2013. “Dose-Dependent Effects of Angiotensin-(1–7) on the NHE3 Exchanger and [Ca₂₊]i in vivo Proximal Tubules.” *American Journal of Physiology-Renal Physiology* 304 (10): F1258–65. <https://doi.org/10.1152/ajprenal.00401.2012>.
- Castelo-Branco, Regiane Cardoso, Deise C. A. Leite-Delova, Fernanda Barrinha Fernandes, Gerhard Malnic, und Margarida de Mello-Aires. „The Effects of Angiotensin-(1-7) on the Exchanger NHE3 and on [Ca₂₊]i in the Proximal Tubules of Spontaneously Hypertensive Rats“. *American Journal of Physiology. Renal Physiology* 313, Nr. 2 (1. August 2017): F450–60. <https://doi.org/10.1152/ajprenal.00557.2016>.
- Cichero, Elena, Stefano Espinoza, Silvia Franchini, Sara Guariento, Livio Brasili, Raul R. Gainetdinov, und Paola Fossa. „Further Insights Into the Pharmacology of the Human Trace Amine-Associated Receptors: Discovery of Novel Ligands for TAAR1 by a Virtual Screening Approach“. *Chemical Biology & Drug Design* 84, Nr. 6 (2014): 712–20. <https://doi.org/10.1111/cbdd.12367>.
- Coburn, Cary G., Margarita C. Currás-Collazo, und Prasada Rao S. Kodavanti. „In Vitro Effects of Environmentally Relevant Polybrominated Diphenyl Ether (PBDE) Congeners on Calcium Buffering Mechanisms in Rat Brain“. *Neurochemical Research* 33, Nr. 2 (Februar 2008): 355–64. <https://doi.org/10.1007/s11064-007-9430-x>.
- De Mello, Walmor C. „Intracellular Angiotensin (1-7) Increases the Inward Calcium Current in Cardiomyocytes. On the Role of PKA Activation“. *Molecular and Cellular Biochemistry* 407, Nr. 1–2 (September 2015): 9–16. <https://doi.org/10.1007/s11010-015-2449-4>.
- De Waard-Siebinga, I., D. J. Blom, M. Griffioen, P. I. Schrier, E. Hoogendoorn, G. Beverstock, E. H. Danen, und M. J. Jager. „Establishment and Characterization of an Uveal-Melanoma Cell Line“. *International Journal of Cancer* 62, Nr. 2 (17. Juli 1995): 155–61. <https://doi.org/10.1002/ijc.2910620208>.
- Dhandapani, Priyavathi, Srujan Kumar Dondapati, Anne Zemella, Dennis Bräuer, Doreen Anja Wüstenhagen, Stefan Mergler, und Stefan Kubick. „Targeted Esterase-Induced Dye (TED) Loading Supports Direct Calcium Imaging in Eukaryotic Cell-Free Systems“. *RSC Advances* 11, Nr. 27 (30. April 2021): 16285–96. <https://doi.org/10.1039/DORA08397F>.
- Dinter, Juliane, Noushafarin Khajavi, Jessica Mühlhaus, Carolin Leonie Wienholz, Maxi Cöster, Thomas Hermsdorf, Claudia Stäubert, u. a. „The Multitarget Ligand 3-Iodothyronamine Modulates β-Adrenergic Receptor 2 Signaling“. *European Thyroid Journal* 4, Nr. Suppl 1 (September 2015): 21–29. <https://doi.org/10.1159/000381801>.
- Dondapati, Srujan Kumar, Henning Lübbingding, Anne Zemella, Lena Thoring, Doreen A. Wüstenhagen, und Stefan Kubick. „Functional Reconstitution of Membrane Proteins Derived From Eukaryotic Cell-Free Systems“. *Frontiers in Pharmacology* 10 (2019). <https://www.frontiersin.org/articles/10.3389/fphar.2019.00917>.
- Dong, Xian-ping, Xiang Wang, und Haoxing Xu. „TRP Channels of Intracellular Membranes“. *Journal of neurochemistry* 113, Nr. 2 (April 2010): 313–28. <https://doi.org/10.1111/j.1471-4159.2010.06626.x>.

- Dusza, Hanna M., Peter H. Cenijn, Jorke H. Kamstra, Remco H. S. Westerink, Pim E. G. Leonards, und Timo Hamers. „Effects of Environmental Pollutants on Calcium Release and Uptake by Rat Cortical Microsomes“. *Neurotoxicology* 69 (Dezember 2018): 266–77. <https://doi.org/10.1016/j.neuro.2018.07.015>.
- Eertmoed, Alison L., Yolanda F. Vallejo, und William N. Green. „[31] Transient Expression of Heteromeric Ion Channels“. In *Methods in Enzymology*, 293:564–85. Ion Channels Part B. Academic Press, 1998. [https://doi.org/10.1016/S0076-6879\(98\)93034-8](https://doi.org/10.1016/S0076-6879(98)93034-8).
- Fallah, Hamideh P., Ekta Ahuja, Haoquan Lin, Jinlong Qi, Qian He, Shan Gao, Hailong An, Jian Zhang, Yongzhen Xie, und Dong Liang. „A Review on the Role of TRP Channels and Their Potential as Drug Targets – An Insight Into the TRP Channel Drug Discovery Methodologies“. *Frontiers in Pharmacology* 13 (24. Mai 2022): 914499. <https://doi.org/10.3389/fphar.2022.914499>.
- Garcia, Maria L., und Gregory J. Kaczorowski. „Ion channels find a pathway for therapeutic success“. *Proceedings of the National Academy of Sciences* 113, Nr. 20 (17. Mai 2016): 5472–74. <https://doi.org/10.1073/pnas.1605669113>.
- Gebhardt, Matthias, Rolf Mentlein, Ulrich Schaudig, Thomas Pufe, Kristin Recker, Bernhard Nölle, Kais Al-Samir, Gerd Geerling, und Friedrich P. Paulsen. „Differential Expression of Vascular Endothelial Growth Factor Implies the Limbal Origin of Pterygia“. *Ophthalmology* 112, Nr. 6 (Juni 2005): 1023–30. <https://doi.org/10.1016/j.ophtha.2005.01.023>.
- Ghelardoni, Sandra, Silvia Suffredini, Sabina Frascarelli, Simona Brogioni, Grazia Chiellini, Simonetta Ronca-Testoni, David K. Grandy, Thomas S. Scanlan, Elisabetta Cerbai, und Riccardo Zucchi. „Modulation of Cardiac Ionic Homeostasis by 3-Iodothyronamine“. *Journal of Cellular and Molecular Medicine* 13, Nr. 9B (September 2009): 3082–90. <https://doi.org/10.1111/j.1528-4934.2009.00728.x>.
- Gilham, Dean, und Richard Lehner. „Techniques to Measure Lipase and Esterase Activity in Vitro“. *Methods (San Diego, Calif.)* 36, Nr. 2 (Juni 2005): 139–47. <https://doi.org/10.1016/jymeth.2004.11.003>.
- Giunti, Roberta, Alessandra Gamberucci, Rosella Fulceri, Gábor Bánhegyi, und Angelo Benedetti. „Both Translocon and a Cation Channel Are Involved in the Passive Ca²⁺ Leak from the Endoplasmic Reticulum: A Mechanistic Study on Rat Liver Microsomes“. *Archives of Biochemistry and Biophysics* 462, Nr. 1 (1. Juni 2007): 115–21. <https://doi.org/10.1016/j.abb.2007.03.039>.
- Gradman, A. H. „AT1-Receptor Blockers: Differences That Matter“. *Journal of Human Hypertension* 16, Nr. 3 (August 2002): S9–16. <https://doi.org/10.1038/sj.jhh.1001434>.
- Grynkiewicz, G., M. Poenie, und R. Y. Tsien. „A New Generation of Ca²⁺ Indicators with Greatly Improved Fluorescence Properties“. *The Journal of Biological Chemistry* 260, Nr. 6 (25. März 1985): 3440–50.
- Guo, Fang, Beihui Liu, Feige Tang, Samantha Lane, Ekaterina A. Souslova, Dmitriy M. Chudakov, Julian F.R. Paton, und Sergey Kasparov. „Astroglia are a possible cellular substrate of angiotensin(1-7) effects in the rostral ventrolateral medulla“. *Cardiovascular Research* 87, Nr. 3 (1. August 2010): 578–84. <https://doi.org/10.1093/cvr/cvq059>.
- Hashemi, Hassan, Mehdi Khabazkhoob, Ahmad Kheirkhah, Mohammad Hassan Emamian, Shiva Mehravar, Mohammad Shariati, und Akbar Fotouhi. „Prevalence of Dry Eye Syndrome in an Adult Population“. *Clinical & Experimental Ophthalmology* 42, Nr. 3 (April 2014): 242–48. <https://doi.org/10.1111/ceo.12183>.
- Haustrate, Aurélien, Natalia Prevarskaya, und V'yacheslav Lehen'kyi. „Role of the TRPV Channels in the Endoplasmic Reticulum Calcium Homeostasis“. *Cells* 9, Nr. 2 (28. Januar 2020): 317. <https://doi.org/10.3390/cells9020317>.
- Hoefig, Carolin Stephanie, Riccardo Zucchi, und Josef Köhrle. „Thyronamines and Derivatives: Physiological Relevance, Pharmacological Actions, and Future Research Directions“. *Thyroid: Official Journal of the American Thyroid Association* 26, Nr. 12 (Dezember 2016): 1656–73. <https://doi.org/10.1089/thy.2016.0178>.
- Hübner, Christian A., und Thomas J. Jentsch. „Ion channel diseases“. *Human Molecular Genetics* 11, Nr. 20 (1. Oktober 2002): 2435–45. <https://doi.org/10.1093/hmg/11.20.2435>.
- Janik, Marcelina Elżbieta, Dominika Szlęzak, Magdalena Surman, Aniela Gołas, Anna Lityńska, und Małgorzata Przybyło. „Diversified β-2-Adrenergic Receptor Expression and Action in Melanoma Cells“. *Anticancer Research* 37, Nr. 6 (Juni 2017): 3025–33. <https://doi.org/10.21873/anticanres.11657>.
- Kase, Satoru, Iku Kikuchi, und Susumu Ishida. „Expression of VEGF in Human Conjunctival Melanoma Analyzed with Immunohistochemistry“. *Clinical Ophthalmology* 12 (19. November 2018): 2363–67. <https://doi.org/10.2147/OPTH.S184193>.
- Khalfaoui, T., G. Mkannez, D. Colin, A. Imen, W. Zbiba, K. Errais, R. Anane, u. a. „Immunohistochemical Analysis of Vascular Endothelial Growth Factor (VEGF) and P53 Expression in Pterygium from Tunisian Patients“. *Pathologie-Biologie* 59, Nr. 3 (Juni 2011): 137–41. <https://doi.org/10.1016/j.patbio.2009.04.006>.
- Khambhati, Khushal, Gargi Bhattacharjee, Nisarg Gohil, Darren Braddick, Vishwesh Kulkarni, und Vijai Singh. „Exploring the

- Potential of Cell-Free Protein Synthesis for Extending the Abilities of Biological Systems". *Frontiers in Bioengineering and Biotechnology* 7 (2019). <https://www.frontiersin.org/articles/10.3389/fbioe.2019.00248>.
- Kim, June-Bum. „Channelopathies“. *Korean Journal of Pediatrics* 57, Nr. 1 (Januar 2014): 1–18. <https://doi.org/10.3345/kjp.2014.57.1.1>.
- Kiselyov, Kirill, Dong Min Shin, und Shmuel Muallem. „Signalling Specificity in GPCR-Dependent Ca²⁺ Signalling“. *Cellular Signalling* 15, Nr. 3 (März 2003): 243–53. [https://doi.org/10.1016/s0898-6568\(02\)00074-8](https://doi.org/10.1016/s0898-6568(02)00074-8).
- Kodavanti, Prasada Rao S., und Thomas R. Ward. „Differential Effects of Commercial Polybrominated Diphenyl Ether and Polychlorinated Biphenyl Mixtures on Intracellular Signaling in Rat Brain in Vitro“. *Toxicological Sciences: An Official Journal of the Society of Toxicology* 85, Nr. 2 (Juni 2005): 952–62. <https://doi.org/10.1093/toxsci/kfi147>.
- Kubick, Stefan, J. Schacherl, H. Fleischer-Notter, E. Royall, L. O. Roberts, und W. Stiege. „In Vitro Translation in an Insect-Based Cell-Free System“. In *Cell-Free Protein Expression*, herausgegeben von James R. Swartz, 209–17. Berlin, Heidelberg: Springer, 2003. https://doi.org/10.1007/978-3-642-59337-6_25.
- Lee, A. J., J. Lee, S.-M. Saw, G. Gazzard, D. Koh, D. Widjaja, und D. T. H. Tan. „Prevalence and Risk Factors Associated with Dry Eye Symptoms: A Population Based Study in Indonesia“. *The British Journal of Ophthalmology* 86, Nr. 12 (Dezember 2002): 1347–51. <https://doi.org/10.1136/bjo.86.12.1347>.
- Martinez, Natalia J., Steven A. Titus, Amanda K. Wagner, und Anton Simeonov. „High-Throughput Fluorescence Imaging Approaches for Drug Discovery Using in Vitro and in Vivo Three-Dimensional Models“. *Expert Opinion on Drug Discovery* 10, Nr. 12 (Dezember 2015): 1347–61. <https://doi.org/10.1517/17460441.2015.1091814>.
- McManus, Owen B., Maria L. Garcia, David Weaver, Melanie Bryant, Steven Titus, und James B. Herrington. „Ion Channel Screening“. In *Assay Guidance Manual*, herausgegeben von Sarine Markossian, Abigail Grossman, Kyle Brimacombe, Michelle Arkin, Douglas Auld, Chris Austin, Jonathan Baell, u. a. Bethesda (MD): Eli Lilly & Company and the National Center for Advancing Translational Sciences, 2004. <http://www.ncbi.nlm.nih.gov/books/NBK100915/>.
- McMillan, Hayley, Fionnuala T. Lundy, Orla M. Dunne, Banan Al-Natour, Charlotte Jeanneau, Imad About, Tim M. Curtis, und Ikhlas El Karim. „Endogenous Mas-Related G-Protein-Coupled Receptor X1 Activates and Sensitizes TRPA1 in a Human Model of Peripheral Nerves“. *FASEB Journal: Official Publication of the Federation of American Societies for Experimental Biology* 35, Nr. 5 (Mai 2021): e21492. <https://doi.org/10.1096/fj.202001667RR>.
- McMullen, David C., William S. Kean, Ajay Verma, Jeffrey T. Cole, und William D. Watson. „A Microplate Technique to Simultaneously Assay Calcium Accumulation in Endoplasmic Reticulum and SERCA Release of Inorganic Phosphate“. *Biological Procedures Online* 14, Nr. 1 (2. April 2012): 4. <https://doi.org/10.1186/1480-9222-14-4>.
- Mello-Aires, Margarida de, Deise CA Leite-Dellova, Regiane C Castelo-Branco, Gerhard Malnic, und Maria Oliveira-Souza. „ANG II, ANG-(1-7), ALDO and AVP biphasic effects on Na⁺/H⁺ transport: the role of cellular calcium“. *Nephrology and Renal Diseases* 2, Nr. 1 (2017). <https://doi.org/10.15761/NRD.1000115>.
- Mergler, Stefan, Raissa Derckx, Peter S. Reinach, Fabian Garreis, Arina Böhm, Lisa Schmelzer, Sergej Skosyrski, u. a. „Calcium Regulation by Temperature-Sensitive Transient Receptor Potential Channels in Human Uveal Melanoma Cells“. *Cellular Signalling* 26, Nr. 1 (Januar 2014): 56–69. <https://doi.org/10.1016/j.cellsig.2013.09.017>.
- Mergler, Stefan, Fabian Garreis, Monika Sahlmüller, Ekaterini-Maria Lyras, Peter S. Reinach, Abhilash Dwarakanath, Friedrich Paulsen, und Uwe Pleyer. „Calcium Regulation by Thermo- and Osmosensing Transient Receptor Potential Vanilloid Channels (TRPVs) in Human Conjunctival Epithelial Cells“. *Histochemistry and Cell Biology* 137, Nr. 6 (1. Juni 2012): 743–61. <https://doi.org/10.1007/s00418-012-0924-5>.
- Murray, David, und Mark Wigglesworth. „Chapter 1 HTS Methods: Assay Design and Optimisation“, 2016, 1–15. <https://doi.org/10.1039/9781782626770-00001>.
- Navazio, L., M. A. Bewell, A. Siddiqua, G. D. Dickinson, A. Galione, und D. Sanders. „Calcium Release from the Endoplasmic Reticulum of Higher Plants Elicited by the NADP Metabolite Nicotinic Acid Adenine Dinucleotide Phosphate“. *Proceedings of the National Academy of Sciences of the United States of America* 97, Nr. 15 (18. Juli 2000): 8693–98. <https://doi.org/10.1073/pnas.140217897>.
- Paredes, R. Madelaine, Julie C. Etzler, Lora Talley Watts, und James D. Lechleiter. „Chemical Calcium Indicators“. *Methods (San Diego, Calif.)* 46, Nr. 3 (November 2008): 143–51. <https://doi.org/10.1016/j.ymeth.2008.09.025>.
- Passos-Silva, Danielle G., Thiago Verano-Braga, und Robson A. S. Santos. „Angiotensin-(1-7): Beyond the Cardio-Renal Actions“. *Clinical Science (London, England: 1979)* 124, Nr. 7 (April 2013): 443–56. <https://doi.org/10.1042/CS20120461>.
- Pentyala, Srinivas, Jeanine Ruggeri, Amulya Veerraju, Zhangzhang Yu, Anjori Bhatia, Durisala Desaiah, und Parminder Vig.

„Microsomal Ca²⁺ Flux Modulation as an Indicator of Heavy Metal Toxicity“. *Indian Journal of Experimental Biology* 48, Nr. 7 (Juli 2010): 737–43.

- Pinheiro, Sérgio Veloso Brant, Ana Cristina Simões e Silva, Walkyria Oliveira Sampaio, Renata Dutra de Paula, Elizabeth Pereira Mendes, Elizabete Dias Bontempo, João Bosco Pesquero, u. a. „Nonpeptide AVE 0991 Is an Angiotensin-(1–7) Receptor Mas Agonist in the Mouse Kidney“. *Hypertension* 44, Nr. 4 (Oktober 2004): 490–96. <https://doi.org/10.1161/01.HYP.0000141438.64887.42>.
- Quast, Robert B., Andrei Sonnabend, Marlitt Stech, Doreen A. Wüstenhagen, und Stefan Kubick. „High-Yield Cell-Free Synthesis of Human EGFR by IRES-Mediated Protein Translation in a Continuous Exchange Cell-Free Reaction Format“. *Scientific Reports* 6 (26. Juli 2016): 30399. <https://doi.org/10.1038/srep30399>.
- Rajabi, Parvin, Ali Neshat, Mozhgan Mokhtari, Mohammad A. Rajabi, Mehdi Eftekhari, und Payam Tavakoli. „The role of VEGF in melanoma progression“. *Journal of Research in Medical Sciences : The Official Journal of Isfahan University of Medical Sciences* 17, Nr. 6 (Juni 2012): 534–39.
- Rehberg, Markus, Alexandra Lepier, Barbara Solchenberger, Pavel Osten, und Robert Blum. „A New Non-Disruptive Strategy to Target Calcium Indicator Dyes to the Endoplasmic Reticulum“. *Cell Calcium* 44, Nr. 4 (Oktober 2008): 386–99. <https://doi.org/10.1016/j.ceca.2008.02.002>.
- Sachse, Rita, Srujan Dondapati, Susanne Fenz, Thomas Schmidt, und Stefan Kubick. „Membrane protein synthesis in cell-free systems: From bio-mimetic systems to bio-membranes“. *FEBS letters* 588 (12. Juni 2014). <https://doi.org/10.1016/j.febslet.2014.06.007>.
- Samtleben, Samira, Julianne Jaepel, Caroline Fecher, Thomas Andreska, Markus Rehberg, und Robert Blum. „Direct Imaging of ER Calcium with Targeted-Esterase Induced Dye Loading (TED)“. *Journal of Visualized Experiments: JoVE*, Nr. 75 (7. Mai 2013): e50317. <https://doi.org/10.3791/50317>.
- Santoni, Giorgio, Valerio Farfariello, und Consuelo Amantini. „TRPV Channels in Tumor Growth and Progression“. *Advances in Experimental Medicine and Biology* 704 (1. Januar 2011): 947–67. https://doi.org/10.1007/978-94-007-0265-3_49.
- Santos, Rita, Oleg Ursu, Anna Gaulton, A. Patrícia Bento, Ramesh S. Donadi, Cristian G. Bologa, Anneli Karlsson, u. a. „A Comprehensive Map of Molecular Drug Targets“. *Nature Reviews Drug Discovery* 16, Nr. 1 (Januar 2017): 19–34. <https://doi.org/10.1038/nrd.2016.230>.
- Santos, Robson A. S., Ana C. Simoes e Silva, Christine Maric, Denise M. R. Silva, Raquel Pillar Machado, Insa de Buhr, Silvia Heringer-Walther, u. a. „Angiotensin-(1–7) is an endogenous ligand for the G protein-coupled receptor Mas“. *Proceedings of the National Academy of Sciences* 100, Nr. 14 (8. Juli 2003): 8258–63. <https://doi.org/10.1073/pnas.1432869100>.
- Santos, Robson Augusto Souza, Walkyria Oliveira Sampaio, Andreia C. Alzamora, Daisy Motta-Santos, Natalia Alenina, Michael Bader, und Maria Jose Campagnole-Santos. „The ACE2/Angiotensin-(1–7)/MAS Axis of the Renin-Angiotensin System: Focus on Angiotensin-(1–7)“. *Physiological Reviews* 98, Nr. 1 (Januar 2018): 505–53. <https://doi.org/10.1152/physrev.00023.2016>.
- Scanlan, Thomas S., Katherine L. Suchland, Matthew E. Hart, Grazia Chiellini, Yong Huang, Paul J. Kruzich, Sabina Frascarelli, u. a. „3-Iodothyronamine is an endogenous and rapid-acting derivative of thyroid hormone“. *Nature Medicine* 10, Nr. 6 (Juni 2004): 638–42. <https://doi.org/10.1038/nm1051>.
- Solinski, Hans Jürgen, Thomas Gudermann, und Andreas Breit. „Pharmacology and Signaling of MAS-Related G Protein-Coupled Receptors“. *Pharmacological Reviews* 66, Nr. 3 (Juli 2014): 570–97. <https://doi.org/10.1124/pr.113.008425>.
- Song, Lele, Ruina Cui, Yourong Yang, und Xueqiong Wu. „Role of Calcium Channels in Cellular Antituberculosis Effects: Potential of Voltage-Gated Calcium-Channel Blockers in Tuberculosis Therapy“. *Journal of Microbiology, Immunology, and Infection = Wei Mian Yu Gan Ran Za Zhi* 48, Nr. 5 (Oktober 2015): 471–76. <https://doi.org/10.1016/j.jmii.2014.08.026>.
- Stech, Marlitt, Robert B. Quast, Rita Sachse, Corina Schulze, Doreen A. Wüstenhagen, und Stefan Kubick. „A Continuous-Exchange Cell-Free Protein Synthesis System Based on Extracts from Cultured Insect Cells“. *PloS One* 9, Nr. 5 (2014): e96635. <https://doi.org/10.1371/journal.pone.0096635>.
- Stoyanovsky, D. A., und A. I. Cederbaum. „Metabolites of Acetaminophen Trigger Ca²⁺ Release from Liver Microsomes“. *Toxicology Letters* 106, Nr. 1 (20. Mai 1999): 23–29. [https://doi.org/10.1016/s0378-4274\(99\)00009-0](https://doi.org/10.1016/s0378-4274(99)00009-0).
- Tang, Shen, Xiaonan Deng, Jie Jiang, Michael Kirberger, und Jenny J. Yang. „Design of Calcium-Binding Proteins to Sense Calcium“. *Molecules* 25, Nr. 9 (4. Mai 2020): 2148. <https://doi.org/10.3390/molecules25092148>.

- Thomas, Karen C., Ashwini S. Sabnis, Mark E. Johansen, Diane L. Lanza, Philip J. Moos, Garold S. Yost, und Christopher A. Reilly. „Transient Receptor Potential Vanilloid 1 Agonists Cause Endoplasmic Reticulum Stress and Cell Death in Human Lung Cells“. *The Journal of Pharmacology and Experimental Therapeutics* 321, Nr. 3 (Juni 2007): 830–38. <https://doi.org/10.1124/jpet.107.119412>.
- Thoring, Lena, Srujan K. Dondapati, Marlitt Stech, Doreen A. Wüstenhagen, und Stefan Kubick. „High-Yield Production of “Difficult-to-Express” Proteins in a Continuous Exchange Cell-Free System Based on CHO Cell Lysates“. *Scientific Reports* 7, Nr. 1 (15. September 2017): 11710. <https://doi.org/10.1038/s41598-017-12188-8>.
- Tsien, R. Y. „A Non-Disruptive Technique for Loading Calcium Buffers and Indicators into Cells“. *Nature* 290, Nr. 5806 (9. April 1981): 527–28. <https://doi.org/10.1038/290527a0>.
- Veldhuis, Nicholas A., Daniel P. Poole, Megan Grace, Peter McIntyre, und Nigel W. Bunnett. „The G Protein-Coupled Receptor–Transient Receptor Potential Channel Axis: Molecular Insights for Targeting Disorders of Sensation and Inflammation“. Herausgegeben von Arthur Christopoulos. *Pharmacological Reviews* 67, Nr. 1 (1. Januar 2015): 36–73. <https://doi.org/10.1124/pr.114.009555>.
- Vriens, Joris, Giovanni Appendino, und Bernd Nilius. „Pharmacology of Vanilloid Transient Receptor Potential Cation Channels“. *Molecular Pharmacology* 75, Nr. 6 (Juni 2009): 1262–79. <https://doi.org/10.1124/mol.109.055624>.
- Walcher, Lia, Clara Budde, Arina Böhm, Peter S. Reinach, Priyavathi Dhandapani, Nina Ljubojevic, Markus W. Schweiger, u. a. „TRPM8 Activation via 3-Iodothyronamine Blunts VEGF-Induced Transactivation of TRPV1 in Human Uveal Melanoma Cells“. *Frontiers in Pharmacology* 9 (13. November 2018): 1234. <https://doi.org/10.3389/fphar.2018.01234>.
- Wang, Lichun, Duan Luo, Xinxue Liao, Jiangui He, Chen Liu, Chuntao Yang, und Hong Ma. „Ang-(1-7) Offers Cytoprotection against Ischemia-Reperfusion Injury by Restoring Intracellular Calcium Homeostasis“. *Journal of Cardiovascular Pharmacology* 63, Nr. 3 (März 2014): 259–64. <https://doi.org/10.1097/FJC.0000000000000043>.
- Wilson, Sarah R., Kristin A. Gerhold, Amber Bifolck-Fisher, Qin Liu, Kush N. Patel, Xinzhong Dong, und Diana M. Bautista. „TRPA1 Is Required for Histamine-Independent, Mas-Related G Protein-Coupled Receptor-Mediated Itch“. *Nature Neuroscience* 14, Nr. 5 (Mai 2011): 595–602. <https://doi.org/10.1038/nn.2789>.
- Wisnoskey, Brian J., William G. Sinkins, und William P. Schilling. „Activation of Vanilloid Receptor Type I in the Endoplasmic Reticulum Fails to Activate Store-Operated Ca²⁺ Entry“. *The Biochemical Journal* 372, Nr. Pt 2 (1. Juni 2003): 517–28. <https://doi.org/10.1042/BJ20021574>.
- Wüstenhagen, Doreen A., Phil Lukas, Christian Müller, Simone A. Aubele, Jan-Peter Hildebrandt, und Stefan Kubick. „Cell-Free Synthesis of the Hirudin Variant 1 of the Blood-Sucking Leech Hirudo Medicinalis“. *Scientific Reports* 10, Nr. 1 (Dezember 2020): 19818. <https://doi.org/10.1038/s41598-020-76715-w>.
- Yang, Ying, Jihuan Liang, Chunjuan Zhao, Yibin Chen, Siyu Gu, Xiaomei Yang, Hua Liu, u. a. „NHERF4 Hijacks Mas-Mediated PLC/AKT Signaling to Suppress the Invasive Potential of Clear Cell Renal Cell Carcinoma Cells“. *Cancer Letters* 519 (28. Oktober 2021): 130–40. <https://doi.org/10.1016/j.canlet.2021.06.021>.
- Yao, Xiaoqiang, Hiu-Yee Kwan, und Yu Huang. „Regulation of TRP Channels by Phosphorylation“. *Neuro-Signals* 14, Nr. 6 (2005): 273–80. <https://doi.org/10.1159/000093042>.
- Yu, Hai-bo, Min Li, Wei-ping Wang, und Xiao-liang Wang. „High Throughput Screening Technologies for Ion Channels“. *Acta Pharmacologica Sinica* 37, Nr. 1 (Januar 2016): 34–43. <https://doi.org/10.1038/aps.2015.108>.
- Yusufi, Ahad N. K., Jingfei Cheng, Michael A. Thompson, John C. Burnett, und Joseph P. Grande. „Differential Mechanisms of Ca(2+) Release from Vascular Smooth Muscle Cell Microsomes“. *Experimental Biology and Medicine (Maywood, N.J.)* 227, Nr. 1 (Januar 2002): 36–44. <https://doi.org/10.1177/153537020222700107>.
- Zhou, Peng, Che Ping Cheng, Tiankai Li, Carlos M. Ferrario, und Heng-Jie Cheng. „Modulation of Cardiac L-Type Ca²⁺ Current by Angiotensin-(1-7): Normal versus Heart Failure“. *Therapeutic Advances in Cardiovascular Disease* 9, Nr. 6 (Dezember 2015): 342–53. <https://doi.org/10.1177/1753944715587424>.
- Zhou, Xinqi, Kayla J. Belavek, und Evan W. Miller. „Origins of Ca²⁺ Imaging with Fluorescent Indicators“. *Biochemistry* 60, Nr. 46 (23. November 2021): 3547–54. <https://doi.org/10.1021/acs.biochem.1c00350>.
- Zimmermann, R, und C Molloy. „Import of Honeybee Prepromelittin into the Endoplasmic Reticulum. Requirements for Membrane Insertion, Processing, and Sequestration.“ *Journal of Biological Chemistry* 261, Nr. 27 (September 1986): 12889–95. [https://doi.org/10.1016/S0021-9258\(18\)67176-5](https://doi.org/10.1016/S0021-9258(18)67176-5).

5. Danksagung

Zuallererst möchte ich Prof. Dr. Frank Bier, meinem Hauptbetreuer an der Universität Potsdam, dafür danken, dass er mich seit 2017 in meinem Promotionsstudium unterstützt und mich von der Anmeldung bis zur Einreichung der Dissertation begleitet hat. Als verständnisvoller Mensch hat er immer eine nette und studentenfreundliche Atmosphäre für alle Doktoranden aufrechterhalten.

Auch an PD. Dr. Stefan Mergler möchte ich mich dafür bedanken, dass er mich in seinem Labor in die Methode der Calcium Imaging eingebracht hat. Ohne seine Einführung in dieses Thema während meines Masterstudiums an der Charité Universitätsmedizin wäre es fast unmöglich gewesen, die Idee zu entwickeln, dieselbe Methode in einem zellfreien Proteinsynthese-System anzuwenden. Seine Einführung in die gängigen Methoden zur Untersuchung von Ionenkanälen gab mir die Möglichkeit, in verschiedenen Labors in Berlin und Potsdam an Projekten zum selben Thema zu arbeiten.

Ich möchte auch Prof. Dr. Michael Bader dafür danken, dass er mich in mehreren Phasen meiner wissenschaftlichen Tätigkeit als Mentor mir beraten hat. Ich danke ihm dafür, dass er mich entscheidend dabei unterstützt hat, diese Arbeit als kumulative Dissertation abzuschließen. Sein erster Rat an mich Deutsch zu lernen hatte ich es fest im Hinterkopf, und als sich mir die Gelegenheit bot, tat ich es ernsthaft. Seine Herangehensweise an wissenschaftliche Fragen und die Diskussion bei der Formulierung neuer Ideen (Ist diese Idee überhaupt sinnvoll und umsetzbar? Kann es das Wissen signifikant erweitern? Wenn ja, wie kann sie für die Menschen brauchbar sein?) haben mich sehr beeinflusst. Sein Projekt, „Calciumregulierung von Ang-(1-7) auf Mas“, hat mich gut darin geschult, die grundlegenden Calciumwege zu verstehen und selbstständig an diesem Thema zu arbeiten.

Besonders möchte ich Dr. Stefan Kubick dafür danken, dass er die Grundidee der Calcium-Imaging bei der zellfreien Proteinsynthese formuliert und die notwendigen Ressourcen und Materialien zur Verfügung gestellt hat, um neue Forschungsansätze zu testen. Er war immer tatkräftig, dynamisch, zielstrebig und hatte das Motiv, Studenten zu erlauben, neue Ideen bis zu einem gewissen Grad auf der Grundlage ihrer bisherigen Erfahrungen auszuprobieren.

Ein besonderer Dank geht auch an Dr. Noushafarin Khajavi in der Gruppe von PD. Dr. Stefan Mergler für ihre Unterstützung bei den Methoden, insbesondere bei der Einweisung der komplexen Software zur Auswertung von Ionenkanalmessungen.

Ich möchte auch Dr. Srujan Dondapati danken, insbesondere für das Korrekturlesen des Manuskripts und die Durchführung von Revisionsexperimenten während des Veröffentlichungsprozesses. Ich danke ihm auch für die Beratung bei der Beantragung des Aufenthaltstitels bei der Ausländerbehörde und anderen behördlichen Angelegenheiten in Potsdam während meines Einsatzes am Fraunhofer-Institut für Zelltherapie und Immunologie, Potsdam-Golm. Ein weiterer Dank geht an alle Mitglieder der Forschungsgruppe von Dr. Stefan Kubick, die mir in den verschiedenen Phasen des Projekts, wie z.B. bei der Formulierung von Ideen, der Laborarbeit und dem Veröffentlichungsprozess, sehr geholfen haben.

Mein besonderer Dank gilt auch meinen Deutschlehrern an den vom BAMF geförderten Schulen in Berlin, die mir geholfen haben, während dieser Pandemie, das C1-Niveau in Deutsch zu erreichen.

Schließlich möchte ich mich bei meinem Mann bedanken, der mich geistig und finanziell beim Deutschlernen unterstützt hat und zu mir stand, besonders in den schwierigen Zeiten.

6. Publikationsliste

Erste Autor:

1. **Priyavathi Dhandapani**, Srujan Kumar Dondapati, Anne Zemella, Dennis Bräuer, Doreen Anja Wüstenhagen, Stefan Mergler, and Stefan Kubick. "Targeted Esterase-Induced Dye (TED) Loading Supports Direct Calcium Imaging in Eukaryotic Cell-Free Systems." *RSC Advances* 11, no. 27 (April 30, 2021): 16285–96. <https://doi.org/10.1039/DORA08397F>
2. Mordhorst, Alexander*, **Priyavathi Dhandapani***, Susann Matthes, Valentina Mosienko, Michael Rothe, Mihail Todiras, Julie Self, Wolf-Hagen Schunck, Anja Schütz, Michael Bader and Natalia Alenina. "Phenylalanine Hydroxylase Contributes to Serotonin Synthesis in Mice." *The FASEB Journal* 35, no. 6 (2021): e21648. <https://doi.org/10.1096/fj.202100366R> (*-shared first authorship)
3. **Priyavathi Sureshkumar**, Robson Augusto Souza Dos Santos, Natalia Alenina, Stefan Mergler, und Michael Bader. „Angiotensin-(1-7) Mediated Calcium Signalling by MAS". *Peptides* 165 (Juli 2023): 171010. <https://doi.org/10.1016/j.peptides.2023.171010>

Mittel Autor:

1. Lucius, Alexander, Noushafarin Khajavi, Peter S. Reinach, Josef Köhrle, **Priyavathi Dhandapani**, Philipp Huimann, Nina Ljubojevic, Carsten Grötzing, and Stefan Mergler. "3-Iodothyronamine Increases Transient Receptor Potential Melastatin Channel 8 (TRPM8) Activity in Immortalized Human Corneal Epithelial Cells." *Cellular Signalling* 28, no. 3 (March 2016): 136–47. <https://doi.org/10.1016/j.cellsig.2015.12.005>
2. Fabian Garreis, Antje Schröder, Peter S. Reinach, Stefanie Zoll, Noushafarin Khajavi, **Priyavathi Dhandapani**, Alexander Lucius, Uwe Pleyer, Friedrich. Paulsen, and Stefan. Mergler. "Upregulation of Transient Receptor Potential Vanilloid Type-1 Channel Activity and Ca²⁺ Influx Dysfunction in Human Pterygial Cells." *Investigative Ophthalmology & Visual Science*, 2016. <https://doi.org/10.1167/iovs.16-19170>.
3. Lia Walcher, Clara Budde, Arina Böhm1, Peter S. Reinach, **Priyavathi Dhandapani**, Nina Ljubojevic, Markus W. Schweiger, Henriette von der Waydbrink, Ilka Reimers, Josef Köhrle, Stefan Mergler. "TRPM8 Activation via 3-Iodothyronamine Blunts VEGF-Induced Transactivation of TRPV1 in Human Uveal Melanoma Cells." *Front. Pharmacol.*, 2018. <https://doi.org/10.3389/fphar.2018.01234>
4. Tatiana Wojciechowicz, Maria Billert, **Priyavathi Dhandapani**, Dawid Szczepankiewicz, Oskar Wasielewski, Mathias Z. Strowski, Krzysztof W. Nowak and Marek Skrzypski. "Neuropeptide B Promotes Proliferation and Differentiation of Rat Brown Primary Preadipocytes." *FEBS Open Bio*, 2021. <https://doi.org/10.1002/2211-5463.13128>

5. Mirjana Ziemer, Beate Weidenthaler-Barth, Philipp Gussek, Maja Pfeiffer, Johannes Kleemann, Katrin Bankov, Peter J. Wild, Silke Seibold, **Priyavathi Sureshkumar**, Patricia Nickel, Anton Strobel, Markus Werner and Stephan Grabbe „Analytical Validation of an Immunohistochemical 7-Biomarker Prognostic Assay (Immunoprint®) for Early-Stage Cutaneous Melanoma in Archival Tissue of Patients with AJCC v8 T2–T3 Disease “, *Diagnostics* 13, Nr. 19 (Januar 2023): 3096.
<https://doi.org/10.3390/diagnostics13193096>

Tagungsbericht-Verlag:

1. Julika Lietzow, **Priyavathi Dhandapani**, Wenke Jonas, and Joseph Köhrle. “Effects of the Thyroid Hormone Metabolite 3,5-T₂ on Murine Heart Tissue and the Cardiomyocyte Cell Line H9C2.” *Experimental and Clinical Endocrinology & Diabetes* 123, no. 03 (March 2015): P12_09.
<https://doi.org/10.1055/s-0035-1547743>
2. Julika Lietzow, **Priyavathi Dhandapani**, Wenke Jonas, and Josef Kohrle. “3,5-T₂ Might Play a Crucial Role in the Rodent Heart.” *Endocrine Abstracts* 37 (May 1, 2015).
<https://doi.org/10.1530/endoabs.37.OC6.1>
3. Ekatarina Zaitseva, Srujan. Dondapati, Jeffrey Schloßhauer, Anne. Zemella, **Priyavathi Dhandapani**, Stefan Kubick, and Gerhard Baaken. “Functional Characterization of Ion Channels Expressed in Eukaryotic Cell-Free Systems Using Lipid Bilayer Arrays,” 2020.
<https://doi.org/10.1016/j.bpj.2019.11.3176>.

7. Eidestattliche Erklärung

Hiermit versichere ich an Eides statt, dass meine hinsichtlich der früheren Teilnahme an Promotionsverfahren gemachten Angaben richtig sind und, dass die eingereichte Arbeit oder wesentliche Teile derselben in keinem anderen Verfahren zur Erlangung eines akademischen Grades vorgelegt worden sind.

Ich versichere darüber hinaus, dass bei der Anfertigung der Dissertation die Grundsätze zur Sicherung guter wissenschaftlicher Praxis der DFG eingehalten wurden, die Dissertationselbständig und ohne fremde Hilfe, insbesondere für die allgemeine Einleitung und Diskussion, verfasst wurde, andere als die von mir angegebenen Quellen und Hilfsmittel nicht benutzt worden sind und die den benutzten Werken wörtlich oder sinngemäß entnommenen Stellen als kenntlich gemacht wurden.

Potsdam, den 25.09.2023

Unterschrift

ELSEVIER LICENSE TERMS AND CONDITIONS

Nov 27, 2022

This Agreement between Mrs. Priyavathi Sureshkumar ("You") and Elsevier ("Elsevier") consists of your license details and the terms and conditions provided by Elsevier and Copyright Clearance Center.

License Number	5437091494788
License date	Nov 27, 2022
Licensed Content Publisher	Elsevier
Licensed Content Publication	Journal of Microbiology, Immunology and Infection
Licensed Content Title	Role of calcium channels in cellular antituberculosis effects: Potential of voltage-gated calcium-channel blockers in tuberculosis therapy
Licensed Content Author	Lele Song,Ruina Cui,Yourong Yang,Xueqiong Wu
Licensed Content Date	Oct 1, 2015
Licensed Content Volume	48
Licensed Content Issue	5
Licensed Content Pages	6
Start Page	471
End Page	476
Type of Use	reuse in a thesis/dissertation
Portion	figures/tables/illustrations
Number of figures/tables /illustrations	1
Format	both print and electronic
Are you the author of this Elsevier article?	No
Will you be translating?	No
Title	Establishment of calcium imaging in cell-free protein synthesis platform
Institution name	University of Potsdam
Expected presentation date	Jan 2023
Portions	1
Requestor Location	Mrs. Priyavathi Sureshkumar Richard Strauss strasse 29
Publisher Tax ID	Munich, 81677 Germany Attn: University of Potsdam GB 494 6272 12
Total	0.00 USD
Terms and Conditions	INTRODUCTION 1. The publisher for this copyrighted material is Elsevier. By clicking "accept" in connection with completing this licensing transaction, you agree that the following terms and conditions apply to this transaction (along with the Billing and Payment terms and conditions established by Copyright Clearance Center, Inc. ("CCC"), at the time that you opened your Rightslink account and

that are available at any time at <http://myaccount.copyright.com>).

GENERAL TERMS

2. Elsevier hereby grants you permission to reproduce the aforementioned material subject to the terms and conditions indicated.
3. Acknowledgement: If any part of the material to be used (for example, figures) has appeared in our publication with credit or acknowledgement to another source, permission must also be sought from that source. If such permission is not obtained then that material may not be included in your publication/copies. Suitable acknowledgement to the source must be made, either as a footnote or in a reference list at the end of your publication, as follows:
"Reprinted from Publication title, Vol /edition number, Author(s), Title of article / title of chapter, Pages No., Copyright (Year), with permission from Elsevier [OR APPLICABLE SOCIETY COPYRIGHT OWNER]." Also Lancet special credit - "Reprinted from The Lancet, Vol. number, Author(s), Title of article, Pages No., Copyright (Year), with permission from Elsevier."
4. Reproduction of this material is confined to the purpose and/or media for which permission is hereby given.
5. Altering/Modifying Material: Not Permitted. However figures and illustrations may be altered/adapted minimally to serve your work. Any other abbreviations, additions, deletions and/or any other alterations shall be made only with prior written authorization of Elsevier Ltd. (Please contact Elsevier's permissions helpdesk [here](#)). No modifications can be made to any Lancet figures/tables and they must be reproduced in full.
6. If the permission fee for the requested use of our material is waived in this instance, please be advised that your future requests for Elsevier materials may attract a fee.
7. Reservation of Rights: Publisher reserves all rights not specifically granted in the combination of (i) the license details provided by you and accepted in the course of this licensing transaction, (ii) these terms and conditions and (iii) CCC's Billing and Payment terms and conditions.
8. License Contingent Upon Payment: While you may exercise the rights licensed immediately upon issuance of the license at the end of the licensing process for the transaction, provided that you have disclosed complete and accurate details of your proposed use, no license is finally effective unless and until full payment is received from you (either by publisher or by CCC) as provided in CCC's Billing and Payment terms and conditions. If full payment is not received on a timely basis, then any license preliminarily granted shall be deemed automatically revoked and shall be void as if never granted. Further, in the event that you breach any of these terms and conditions or any of CCC's Billing and Payment terms and conditions, the license is automatically revoked and shall be void as if never granted. Use of materials as described in a revoked license, as well as any use of the materials beyond the scope of an unrevoked license, may constitute copyright infringement and publisher reserves the right to take any and all action to protect its copyright in the materials.
9. Warranties: Publisher makes no representations or warranties with respect to the licensed material.
10. Indemnity: You hereby indemnify and agree to hold harmless publisher and CCC, and their respective officers, directors, employees and agents, from and against any and all claims arising out of your use of the licensed material other than as specifically authorized pursuant to this license.
11. No Transfer of License: This license is personal to you and may not be sublicensed, assigned, or transferred by you to any other person without publisher's written permission.
12. No Amendment Except in Writing: This license may not be amended except in a writing signed by both parties (or, in the case of publisher, by CCC on publisher's behalf).
13. Objection to Contrary Terms: Publisher hereby objects to any terms contained in any purchase order, acknowledgment, check endorsement or other writing prepared by you, which terms are inconsistent with these terms and conditions or CCC's Billing and Payment terms and conditions. These terms and conditions, together with CCC's Billing and Payment terms and conditions (which are incorporated herein), comprise the entire agreement between you and publisher (and CCC) concerning this licensing transaction. In the event of any conflict between your obligations established by these terms and conditions and those established by CCC's Billing and Payment terms and conditions, these terms and conditions shall control.
14. Revocation: Elsevier or Copyright Clearance Center may deny the permissions described in this License at their sole discretion, for any reason or no reason, with a full refund payable to you. Notice of such denial will be made using the contact information provided by you. Failure to receive such notice will not alter or invalidate the denial. In no event will Elsevier or Copyright Clearance Center be responsible or liable for any costs, expenses or damage incurred by you as a result of a denial of your permission request, other than a refund of the amount(s) paid by you to Elsevier and/or Copyright Clearance Center for denied permissions.

LIMITED LICENSE

The following terms and conditions apply only to specific license types:

15. **Translation:** This permission is granted for non-exclusive word **English** rights only unless your license was granted for translation rights. If you licensed translation rights you may only translate this content into the languages you requested. A professional translator must perform all translations and reproduce the content word for word preserving the integrity of the article.
16. **Posting licensed content on any Website:** The following terms and conditions apply as follows: Licensing material from an Elsevier journal: All content posted to the web site must maintain the copyright information line on the bottom of each image; A hyper-text must be included to the Homepage of the journal from which you are licensing at <http://www.sciencedirect.com/science/journal/xxxxx> or the Elsevier homepage for books at <http://www.elsevier.com>; Central Storage: This license does not include permission for a scanned version of the material to be stored in a central repository such as that provided by Heron/XanEdu.

Licensing material from an Elsevier book: A hyper-text link must be included to the Elsevier homepage at <http://www.elsevier.com>. All content posted to the web site must maintain the copyright information line on the bottom of each image.

Posting licensed content on Electronic reserve: In addition to the above the following clauses are applicable: The web site must be password-protected and made available only to bona fide students registered on a relevant course. This permission is granted for 1 year only. You may obtain a new license for future website posting.

17. For journal authors: the following clauses are applicable in addition to the above:

Preprints:

A preprint is an author's own write-up of research results and analysis, it has not been peer-reviewed, nor has it had any other value added to it by a publisher (such as formatting, copyright, technical enhancement etc.).

Authors can share their preprints anywhere at any time. Preprints should not be added to or enhanced in any way in order to appear more like, or to substitute for, the final versions of articles however authors can update their preprints on arXiv or RePEc with their Accepted Author Manuscript (see below).

If accepted for publication, we encourage authors to link from the preprint to their formal publication via its DOI. Millions of researchers have access to the formal publications on ScienceDirect, and so links will help users to find, access, cite and use the best available version. Please note that Cell Press, The Lancet and some society-owned have different preprint policies.

Information on these policies is available on the journal homepage.

Accepted Author Manuscripts: An accepted author manuscript is the manuscript of an article that has been accepted for publication and which typically includes author-incorporated changes suggested during submission, peer review and editor-author communications.

Authors can share their accepted author manuscript:

- immediately
 - via their non-commercial person homepage or blog
 - by updating a preprint in arXiv or RePEc with the accepted manuscript
 - via their research institute or institutional repository for internal institutional uses or as part of an invitation-only research collaboration work-group
 - directly by providing copies to their students or to research collaborators for their personal use
 - for private scholarly sharing as part of an invitation-only work group on commercial sites with which Elsevier has an agreement
- After the embargo period
 - via non-commercial hosting platforms such as their institutional repository
 - via commercial sites with which Elsevier has an agreement

In all cases accepted manuscripts should:

- link to the formal publication via its DOI
- bear a CC-BY-NC-ND license - this is easy to do
- if aggregated with other manuscripts, for example in a repository or other site, be shared in alignment with our hosting policy not be added to or enhanced in any way to appear more like, or to substitute for, the published journal article.

Published journal article (PJA): A published journal article (PJA) is the definitive final record of published research that appears or will appear in the journal and embodies all value-adding publishing activities including peer review co-ordination, copy-editing, formatting, (if relevant) pagination and online enrichment.

Policies for sharing publishing journal articles differ for subscription and gold open access articles:

Subscription Articles: If you are an author, please share a link to your article rather than the full-text. Millions of researchers have access to the formal publications on ScienceDirect, and so links will help your users to find, access, cite, and use the best available version.

Theses and dissertations which contain embedded PJAs as part of the formal submission can be posted publicly by the awarding institution with DOI links back to the formal publications on ScienceDirect.

If you are affiliated with a library that subscribes to ScienceDirect you have additional private sharing rights for others' research accessed under that agreement. This includes use for classroom teaching and internal training at the institution (including use in course packs and courseware programs), and inclusion of the article for grant funding purposes.

Gold Open Access Articles: May be shared according to the author-selected end-user license and should contain a [CrossMark logo](#), the end user license, and a DOI link to the formal publication on ScienceDirect.

Please refer to Elsevier's [posting policy](#) for further information.

18. For book authors the following clauses are applicable in addition to the above: Authors are permitted to place a brief summary of their work online only. You are not allowed to download and post the published electronic version of your chapter, nor may you scan the printed edition to create an electronic version. **Posting to a repository:** Authors are permitted to post a summary of their chapter only in their institution's repository.

19. Thesis/Dissertation: If your license is for use in a thesis/dissertation your thesis may be submitted to your institution in either print or electronic form. Should your thesis be published commercially, please reapply for permission. These requirements include permission for the Library and Archives of Canada to supply single copies, on demand, of the complete thesis and include permission for Proquest/UMI to supply single copies, on demand, of the complete thesis. Should your thesis be published commercially, please reapply for permission. Theses and dissertations which contain embedded PJAs as part of the formal submission can be posted publicly by the awarding institution with DOI links back to the formal publications on ScienceDirect.

Elsevier Open Access Terms and Conditions

You can publish open access with Elsevier in hundreds of open access journals or in nearly 2000 established subscription journals that support open access publishing. Permitted third party re-use of these open access articles is defined by the author's choice of Creative Commons user license. See our [open access license policy](#) for more information.

Terms & Conditions applicable to all Open Access articles published with Elsevier:

Any reuse of the article must not represent the author as endorsing the adaptation of the article nor should the article be modified in such a way as to damage the author's honour or reputation. If any changes have been made, such changes must be clearly indicated.

The author(s) must be appropriately credited and we ask that you include the end user license and a DOI link to the formal publication on ScienceDirect.

If any part of the material to be used (for example, figures) has appeared in our publication with credit or acknowledgement to another source it is the responsibility of the user to ensure their reuse complies with the terms and conditions determined by the rights holder.

Additional Terms & Conditions applicable to each Creative Commons user license:

CC BY: The CC-BY license allows users to copy, to create extracts, abstracts and new works from the Article, to alter and revise the Article and to make commercial use of the Article (including reuse and/or resale of the Article by commercial entities), provided the user gives appropriate credit (with a link to the formal publication through the relevant DOI), provides a link to the license, indicates if changes were made and the licensor is not represented as endorsing the use made of the work. The full details of the license are available at <http://creativecommons.org/licenses/by/4.0>.

CC BY NC SA: The CC BY-NC-SA license allows users to copy, to create extracts, abstracts and new works from the Article, to alter and revise the Article, provided this is not done for commercial purposes, and that the user gives appropriate credit (with a link to the formal publication through the relevant DOI), provides a link to the license, indicates if changes were made and the licensor is not represented as endorsing the use made of the work. Further, any new works must be made available on the same conditions. The full details of the license are available at <http://creativecommons.org/licenses/by-nc-sa/4.0>.

CC BY NC ND: The CC BY-NC-ND license allows users to copy and distribute the Article, provided this is not done for commercial purposes and further does not permit distribution of the Article if it is changed or edited in any way, and provided the user gives appropriate credit (with a link to the formal publication through the relevant DOI), provides a link to the license, and that the licensor is not represented as endorsing the use made of the work. The full details of the license are available at <http://creativecommons.org/licenses/by-nc-nd/4.0>. Any commercial reuse of Open Access articles published with a CC BY NC SA or CC BY NC ND license requires permission from Elsevier and will be subject to a fee.

Commercial reuse includes:

- Associating advertising with the full text of the Article
- Charging fees for document delivery or access
- Article aggregation
- Systematic distribution via e-mail lists or share buttons

Posting or linking by commercial companies for use by customers of those companies.

20. Other Conditions:

v1.10

Questions? customercare@copyright.com or +1-855-239-3415 (toll free in the US) or +1-978-646-2777.